Report
R-21-02
December 2022

Near-field radionuclide transport models for the post-closure safety assessment in the PSAR SFR

Per-Gustav Åstrand
Maria Rasmusson
Ola Wessely

SVENSK KÄRNBRÄNSLEHANTERING AB

SWEDISH NUCLEAR FUEL
AND WASTE MANAGEMENT CO

Box 3091, SE-169 03 Solna
Phone +46 8 459 84 00
skb.se

SVENSK KÄRNBRÄNSLEHANTERING

ISSN 1402-3091
SKB R-21-02
ID 1946738

December 2022

Near-field radionuclide transport models for the post-closure safety assessment in the PSAR SFR

Per-Gustav Åstrand, Maria Rasmusson, Ola Wessely
Svensk Kärnbränslehantering AB

This report is published on www.skb.se

Preface

This report describes the radionuclide transport models used to estimate radionuclide releases from the SFR repository for short-lived low- and intermediate-level waste in Forsmark. The report forms part of the preliminary safety analysis report (PSAR) for SFR, the repository for short-lived low- and intermediate-level radioactive waste in Forsmark in Östhammar municipality.

This report is authored by Per-Gustav Åstrand (SKB), Maria Rasmusson (SKB) and Ola Wessely (SKB). The report has been reviewed by Maria Lindgren (Kemakta Konsult AB) and Mike Thorne (Mike Thorne and Associates Ltd., UK). An informal review has also been performed by Jan Rosdahl (SKB) and Svante Hedström (SKB).

Abstract

This report presents radionuclide transport models for the near-field (repository) of SFR, the final repository for short-lived radioactive waste in Forsmark. The report forms part of the post-closure safety assessment in the PSAR SFR. The models are similar to those used in the previous safety assessment for SFR, SR-PSU. However, these models have been updated to adopt the most recent description of the existing and planned extension of SFR. Models have also to some extent been simplified to avoid overly detailed implementation of features that are of minor importance to the modelling results.

Transport of radionuclides from the waste is expected to take place with flowing groundwater, so-called advective transport, as well as by diffusive transport. To limit these releases, the waste vaults have been designed with transport barriers of various kinds, where the waste vaults that contain the highest levels of radioactivity have been provided with more advanced technical barriers, whereas in other waste vaults with low-level waste the barrier formed by the sub-sea siting, the host-rock and plugs has been considered sufficient.

The processes directly considered in the models are advection, diffusion, decay and in-growth of radionuclides. The model for the 1BRT vault also considers corrosion-controlled radionuclide release. Some supporting calculations also takes solubility limits into account.

The radionuclide transport models are built using the compartmental approach. In compartment modelling, the modelled system is divided into compartments with internally homogenous properties, where in each compartment the radionuclides are assumed to be fully mixed and the internal properties of the compartment is represented by sums or averages. The models have a detailed representation of the waste and barriers, corresponding to control volumes used in the hydrological calculations (Abarca et al. 2020). Results from probabilistic calculations obtained with these models are used in the post-closure safety assessment the PSAR SFR, see the **Radionuclide transport report** and the **Post-closure safety report** for further details.

Sammanfattning

Denna rapport presenterar radionuklidtransportmodeller för närzonen (förvaret) för SFR, slutförvaret för kortlivat avfall i Forsmark. Rapporten utgör en del av analysen av säkerheten efter förslutning PSAR SFR. Modellerna liknar de modeller som användes i den tidigare säkerhetsanalysen för SFR, SR-PSU. Modellerna har dock uppdaterats för att stämma överens med den senaste beskrivningen av befintligt SFR och den planerade utbyggnaden. Modellerna har också förenklats för att undvika alltför detaljerad implementering av funktioner som är av mindre betydelse för resultatet av modelleringen.

Uttransport av radionuklider från avfallet förväntas ske med flödande grundvatten så kallad advektiv transport, samt genom diffusiv transport. För att begränsa dessa utsläpp har förvarsdelarna utformats med transportbarriärer av olika slag där de förvarsdelar som innehåller högst radioaktivitet har försetts med mer sofistikerade tekniska barriärer medan det i andra förvarsdelar med lågaktivt avfall har bedömts vara tillräckligt att använda de barriärer som lokaliseringen under havet, det omgivande berget och pluggar utgör.

Processerna som direkt beaktas i modellerna är advektion, diffusion, sönderfall och inväxt av radionuklider. Modellen för 1BRT tar också hänsyn till korrosionsstyrd radionuklidfrigörelse. Vissa stödjande beräkningar tar också hänsyn till löslighetsbegränsningar.

Radionuklidtransportmodellerna är boxmodeller, där det modellerade systemet delas upp i boxar med internt homogena egenskaper. I varje box antas radionukliderna vara helt omblandade och de interna egenskaperna i boxen representeras av summor eller medelvärden över hela boxen. Modellerna har en detaljerad representation av avfallet och barriärerna, motsvarande de kontrollvolymer som används i de hydrologiska beräkningarna (Abarca et al. 2020). Resultat från probabilistiska beräkningar med dessa modeller används i säkerhetsanalysen PSAR SFR. De beräkningarna beskrivs i **Radionuklidtransportrapporten** (**Radionuclide transport report**) och **Huvudrapporten för säkerhet efter förslutning** (**Post-closure safety report**).

Contents

1 Introduction

The final repository for short-lived low- and intermediate-level radioactive waste, SFR, is located in Forsmark in northern Uppland, in the immediate vicinity of the Forsmark nuclear power plant (Figure 1-1). SFR is situated 60–130 metres below the Baltic seafloor and comprises four 160-metre-long waste vaults and one waste vault with a 50-metre-high concrete silo for the most radioactive waste. Two parallel kilometre-long access tunnels link the facility to the surface. SKB plans to extend this facility with a new part directly adjoining the existing facility. The extension consists of six waste vaults with a length of 240–275 metres each, located 120–140 metres below the Baltic seafloor. When the extension is complete, SFR will have room for about 200 000 cubic metres of waste, compared with about 63 000 cubic metres today.

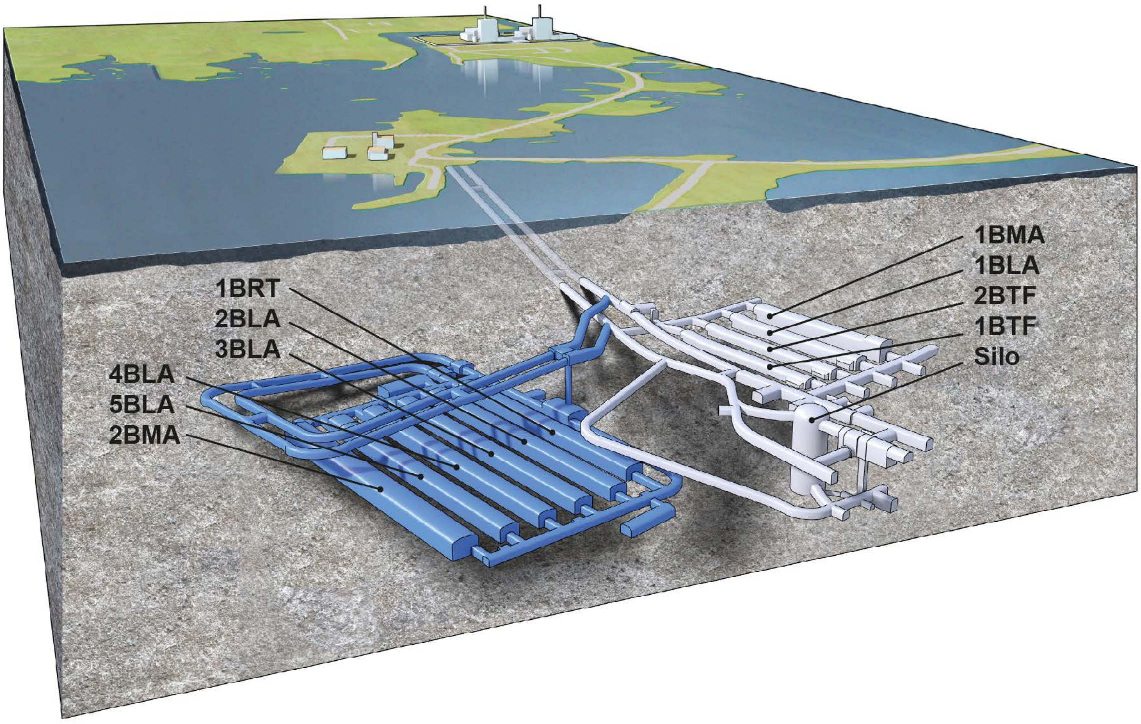

Figure 1-1. The existing SFR (SFR 1) in grey and the extension (SFR 3) in blue with access tunnels. The waste vaults in the figure are the silo for intermediate-level waste, 1–2BMA vaults for intermediate-level waste, 1–2BTF vaults for concrete tanks (and ash drums in 1BTF) with intermediate-level waste, 1BLA and 2–5BLA vaults for low-level waste and the 1BRT vault for reactor pressure vessels.

The present report utilizes information from the **Post-closure safety report** and main references to that report. These reports are listed and briefly described in Table 1-1, also including the abbreviated titles (in bold) by which they are identified in the text.

Table 1-1. Post-closure safety report and main references for the post-closure safety assessment.

Abbreviated title by which they are identified in this report Report number	**Content**
Post-closure safety report SKB TR-23-01	The main report of the PSAR post-closure safety assessment for SFR.
Initial state report SKB TR-23-02	Description of the expected conditions (state) of the repository at closure. The initial state is based on verified and documented properties of the repository and an assessment of its evolution during the period up to closure.
Waste process report SKB TR-23-03	Description of the current scientific understanding of the processes in the waste form and in the packaging that have been identified in the FEP processing as potentially relevant for the post-closure safety of the repository. Reasons are given as to why each process is handled in a particular way in the safety assessment.
Barrier process report SKB TR-23-04	Description of the current scientific understanding of the processes in the engineered barriers that have been identified in the FEP processing as potentially relevant for the post-closure safety of the repository. Reasons are given as to why each process is handled in a particular way in the safety assessment.
FHA report SKB TR-23-08	Description of the handling of inadvertent future human actions (FHA) that are defined as actions potentially resulting in changes to the barrier system, affecting, directly or indirectly, the rate of release of radionuclides, and/or contributing to radioactive waste being brought to the surface. Description of radiological consequences of FHAs that are analysed separately from the main scenario.
Radionuclide transport report SKB TR-23-09	Description of the radionuclide transport and dose calculations carried out for the purpose of demonstrating compliance with the radiological risk criterion.
Data report SKB TR-23-10	Description of how essential data for the post-closure safety assessment are selected, justified and qualified through traceable standardised procedures.
Model tools report SKB TR-23-11	Description of the model tool codes used in the safety assessment.

1.1 This report

The aim of this report is to describe the models for near-field radionuclide transport (RNT) that are used in the estimation of radiological risk for the post-closure safety assessment PSAR. This report describes in detail the models for radionuclide transport in the near-field of the extended SFR repository. Model configuration, use, and results for the calculations performed in the PSAR are presented in the **Radionuclide transport report.**

1.2 About the results presented in this report

The calculations presented in this report are mostly based on data from the *base case* in the PSAR safety assessment. However, the results are partly based on preliminary data. The purpose of the report is only to give a description of models and serve as documentation to ensure reproducibility of the results and that the near-field models are correctly implemented. Furthermore, this report presents results only from deterministic calculations. The final quantitative assessment of releases for the PSAR are presented in the **Radionuclide transport report**. Those calculations are done probabilistically and the releases are propagated to dose calculations.

The RNT calculations includes over 50 radionuclides. To increase the readability of the graphs presented in this report, the number of radionuclides shown is restricted so that only radionuclides with a maximum release rate of larger than 1 000 Bq a^{-1} are displayed. In addition to this, when there are many radionuclides with a release larger than 1 000 Bq a^{-1} only 10–15 of those, with the largest releases, are shown.

1.3 Models used in earlier assessments for SFR

This work is a continuation of a series of modelling efforts undertaken to assess the radionuclide releases from SFR. The three most recent modelling efforts are briefly presented below.

1.3.1 SAFE

The safety assessment conducted within the SAFE (Safety Assessment of Final Disposal of Operational Radioactive Waste) project was submitted to the regulatory authorities in 2001 (SKB 2001). The NUCFLOW code was used to represent the near-field at a very detailed level (Lindgren et al. 2001). This code allows for a representation of the near-field in three dimensions.

1.3.2 SAR-08

The safety assessment SAR-08 (SKB R-08-130) was submitted in 2008. In this study the assessment period for the quantitative analysis was extended to 100 000 years. The Amber software (Thomson et al. 2008) was used for the near-field transport calculations. The near-field models were essentially the same as the ones used in SAFE.

1.3.3 SR-PSU

The safety assessment SR-PSU (SKB TR-14-01) was submitted in 2014. This was the first assessment that also included the planned extension. Dedicated radionuclide transport models for each waste vault were developed in the Ecolego software (SKB TR-14-11). The models presented in the current report are a further development of the models used in SR-PSU.

1.4 Structure of the report

This report contains descriptions of models used for radionuclide transport calculations underpinning the post-closure safety assessment PSAR. The following is a brief description of the contents of the chapters in this report.

Chapter 1 – Introduction: This chapter gives the background and discusses the role of this report within the safety assessment PSAR.

Chapter 2 – Model description: This chapter contains a description of the modelling concept with compartment models.

Chapter 3 – Modelling tool: This chapter contains a brief description of the modelling tool Ecolego. The description is focused on concepts relevant for the models presented in this report.

Chapter 4 – Input data: This chapter contains a general description of the data used and the data handling in the modelling.

Chapter 5 – Waste packages: This chapter contains a description of the modelling of waste packages. Explicit modelling of waste packages is done in the models of the silo, 1–2BMA and 1–2BTF.

Chapter 6 – Silo model: This chapter contains a description of the silo model, and results for the *base case*.

Chapter 7 – 1BMA model: This chapter contains a description of the 1BMA model, and results for the *base case*.

Chapter 8 – 2BMA model: This chapter contains a description of the 2BMA model, and results for the *base case*.

Chapter 9 – 1BRT model: This chapter contains a description of the 1BRT model, and results for the *base case*.

Chapter 10 – BTF models: This chapter contains a description of the 1BTF and 2BTF models, and results for the *base case*.

Chapter 11 – BLA models: This chapter contains a description of the 1BLA and 2BLA models, and results for the *base case*. Note that the 2–5BLA models are identical, except for the water flow parameters, hence the discussion here is based on 2BLA only.

Chapter 12 – Summary: This chapter presents a summary of the near-field modelling work undertaken.

Appendix A – Input data files: This appendix describes details of the input data files used in the modelling.

Appendix B – Implementation details: This appendix describes details of the implementation of the RNT models.

Appendix C – Supporting calculations: This appendix presents supporting calculations done to illustrate different aspects of the modelling.

Appendix D – Comparison to SR-PSU: This appendix presents a comparison with results from the RNT models used in the previous safety assessment (SR-PSU).

1.5 Terms and abbreviations used in this report

Terms and abbreviations used in this report are listed in Table 1-2.

Table 1-2. Glossary of terms and explanations of abbreviations.

Term or abbreviation	Description
1BLA	Vault for low-level waste in SFR1
1BMA	Vault for intermediate-level waste in SFR1
1BRT	Vault for reactor pressure vessels in SFR3
1BTF	Vault for concrete tanks in SFR1
2BTF	Vault for concrete tanks in SFR1
2BLA	Vault for low-level waste in SFR3
2BMA	Vault for intermediate-level waste in SFR3
2–5BLA	Vaults for low-level waste in SFR3
AD	Anno Domini
AMBER	A compartmental computer code (Assisted Model Building with Energy Refinement)
Barrier	In the safety assessment context, a barrier is a physical feature, engineered or natural, which in one or several ways contributes to the containment and prevention or retention of dispersion of radioactive substances, either directly or indirectly by protecting other barriers
Base case	The base case constitutes the basis for the radionuclide transport and dose calculations. The present-day climate calculation case is selected as the base case for the analysis of the main scenario. Models built, and assumptions made, for the other calculation cases are only described if they deviate from the base case, and results from these cases are compared with those for the base case

Table 1-2. Continued.

Term or abbreviation	Description
Best estimate (BE)	A single value for a parameter, describing a property or a process, used in deterministic calculations. Best estimates are typically derived from site and/or literature data and often correspond to mean values of the underpinning datasets
Bulk density	The bulk density of a porous medium is defined as the mass of the solid particles that make up the medium divided by the total volume they occupy. The total volume includes particle volume, inter-particle void volume, and internal pore volume. (cf. ”particle density”)
Calculation case (CC)	Used for the quantitative assessment of the scenarios selected in the safety assessment, typically by calculating doses
Cautious	Indicates an expected overestimate of annual effective dose that follows from assumptions made, or models and parameter values selected, within the reasonably expected range of possibilities
Clab	Central interim storage facility for spent nuclear fuel in Simpevarp
COMSOL Multiphysics	Commercial software for finite element analysis, solver and multi-physics simulation software
Crushed rock	Mechanically crushed rock material with varying grain size distribution and hydraulic properties. The selected grain size distribution is dependent on the required properties. See also macadam
DarcyTools	A computer code developed by SKB for simulation of flow and transport in porous and/or fractured media
Data uncertainty	Uncertainties concerning all quantitative input data, that is parameter values, used in the assessment
Deterministic analysis	Analysis using single numerical values for parameters (taken to have a probability of one), which leads to a single value for the result
Geosphere	The bedrock, including groundwater, surrounding the repository, bounded upwards by the surface system
HCP	Hydrated cement paste
Initial state	The expected state of the repository and its environs at closure of the repository
Macadam	Crushed rock sieved in fractions 2–65 mm. Macadam has no or very little fine material (grain size < 2 mm). The fraction is given as intervals, for example “Macadam 16-32” is crushed rock comprising the fraction 16–32 mm
Model waste package	A simplified representation of waste used in the near-field models
Near-field	Typically used for the model domain representing the repository, which may contain part of the nearby bedrock to obtain boundary conditions
Packaging	The outer container, such as a mould, drum or ISO-container, protecting the waste form (synonymous with Waste packaging)
Particle density	The particle density of a porous medium is the intrinsic density of the solid particles that make up the medium, i.e. the density the medium would have if it had zero porosity. (cf. ”bulk density”)
PDF	Probability density function
Pessimistic	Indicates an expected overestimate of annual effective dose that follows from assumptions made, or models and parameter values selected, beyond the reasonably expected range of possibilities
PSAR	Preliminary Safety Analysis Report
PSU	Programme SFR extension
PWR	Pressurised water reactor
QA	Quality assurance
Radiotoxicity	The product of the activity of a radionuclide and it’s corresponding dose coefficient
Repository	The disposed waste packages, and the engineered barriers and other repository structures
Repository system	The repository, the bedrock, and the biosphere surrounding the repository. Synonymous with repository and its environs
RNT	Radionuclide transport
RPV	Reactor pressure vessel
RSL	Relative sea level

Table 1-2. Continued.

Term or abbreviation	Description
SAFE	Post-closure safety assessment for SFR1 reported to the regulatory authorities in 2001
Safety analysis	In the context of present safety assessment, the distinction is generally not viewed as important and therefore safety analysis and safety assessment are used interchangeably. However, if the distinction is important, safety analysis should be used as a documented process for the study of safety, and safety assessment should be used as a documented process for the evaluation of safety
Safety assessment	The safety assessment is the systematic process periodically carried out throughout the lifetime of the repository to ensure that all the relevant safety requirements are met, and entails evaluating the performance of the repository system and quantifying its potential radiological impact on human health and the environment. The safety assessment corresponds to the term safety analysis in the Swedish Radiation Safety Authority's regulations
SAR	Safety Analysis Report
SAR-08	Post-closure safety assessment for SFR1 reported to the regulatory authorities in 2008
Scenario	A description of a potential evolution of the repository and its environs, given an initial state and specified external conditions and their development, and how the protective capability of the repository is affected
SE-SFL	The evaluation of post-closure safety for a proposed repository concept for SFL evaluation
SFL	Final repository for long-lived radioactive waste
SFR	Final repository for short-lived radioactive waste at Forsmark
SFR1	The existing part of SFR
SFR3	The extension part of SFR
Silo	Cylindrical vault for intermediate-level waste (part of SFR1)
SKB	Swedish Nuclear Fuel and Waste Management Company
Sorption coefficient	Element-specific sorption coefficient, defined as the ratio between the elemental concentrations in the solid and liquid phases
SR-PSU	Post-closure safety assessment that was a reference to the F-PSAR for the extended SFR, reported to the regulatory authority in 2014
SRF	Sorption Reduction Factor (due to complexing agents)
SRF group	Group of radionuclides with analogous complexation properties and thus same SRF values
SVN	Subversion. A version handling system used for code and data in the PSAR SFR
Transition material	Component in earth dam plug e.g. 30/70 mixture bentonite and crushed rock. The role of the transition material is to hinder bentonite transport from the hydraulically tight section, to take up the load from bentonite swelling and transfer it to the backfill material
Waste domain	Part of waste vaults where waste is placed (inside the engineered barriers)
Waste form	Waste in its physical and chemical form after treatment and/or conditioning
Waste package	The waste (form) and its packaging
Waste packaging	The outer container, such as a mould, drum or ISO-container, protecting the waste form (synonymous with Packaging)
Waste type	SKB's systematic classification of wastes according to a developed code system
Waste vault	Part of repository where waste is stored

2 Model description

The layout of the extended SFR is shown in Figure 2-1. A radionuclide transport model has been developed for each of the 11 waste vaults.

The engineered concrete and bentonite barriers of the near-field limit the release of radionuclides by reducing the water flow (Section 4.3) through the waste packages and by introducing high radionuclide sorption capacity. These barriers are explicitly represented by several compartments in the radionuclide transport models.

The access tunnels and plugs are also of importance for post-closure safety. However, they are not explicitly represented in the radionuclide transport models. Instead, their impact on radionuclide transport is considered through their effect on water flow. As the plugs represent flow resistances, they affect the pre-calculated water flows used as input to the radionuclide transport calculations.

The details of the compartment models for each waste vault are described in Chapters 6 to 11.

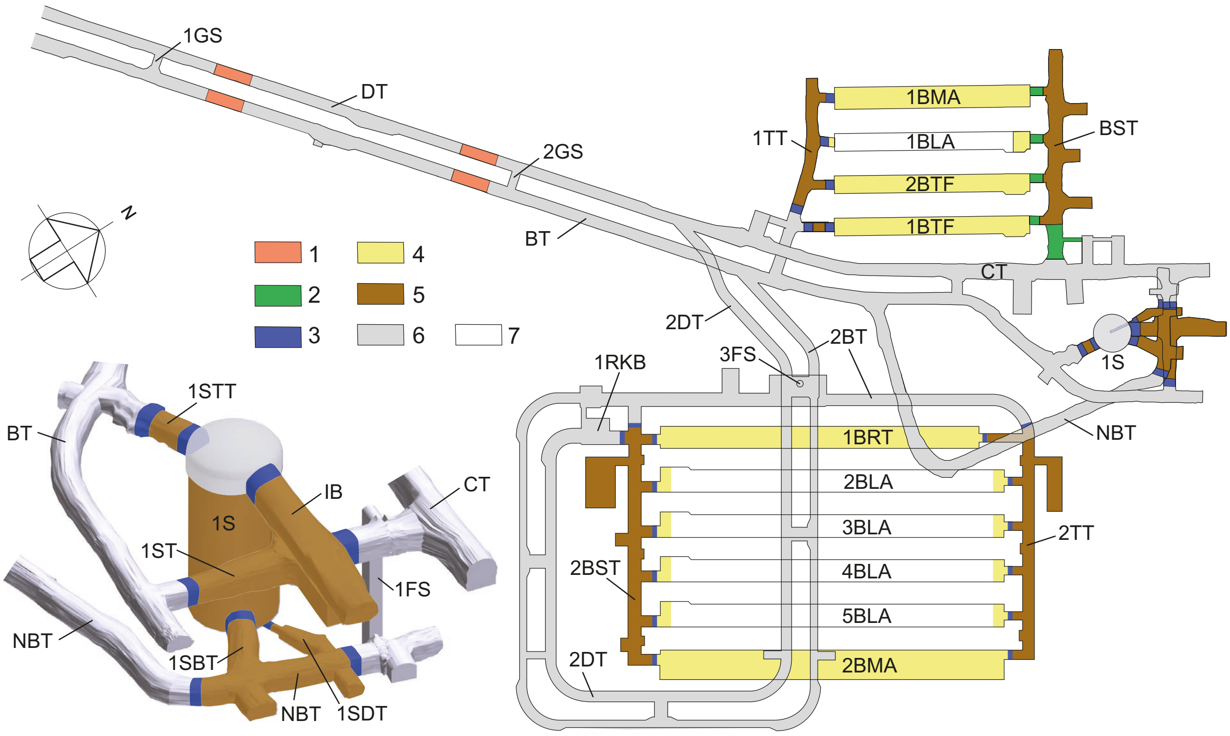

Figure 2-1. *Schematic plan of SFR 1 and SFR 3, with a detailed view of the silo. Key to numbering: 1) Plugs in access tunnels 2) Transition material 3) Mechanical constraint of concrete 4) Backfill material of macadam 5) Hydraulically tight section of bentonite 6) Backfill material in access tunnels and the central area of the tunnel system 7) Non-backfilled openings.*

2.1 Compartment models

The radionuclide transport models are built using the compartmental approach. In compartment modelling, the modelled system is divided into compartments with internally homogenous properties, where in each compartment the radionuclides are assumed to be uniformly mixed and the internal properties of the compartment are represented by sums or averages. This is a simplification that can be justified considering the uncertainties in the description of the system and its future evolution. The compartmental approach provides a simple and transparent model for the transport of radionuclides from the waste packages in the waste vaults, through the barriers, to the bedrock. However, the number and size of the compartments and connections between them must be chosen with care so that the representation is suitable (optimized such that the representation is sufficiently detailed while remaining computationally feasible) for the assessment context.

The transport properties are assumed to be spatially constant within each compartment. A region with homogenous properties can often be represented adequately by one single compartment. However, if the concentration of radionuclides within one such region cannot be assumed to be homogenous, the approach is instead to represent that region using several sub-compartments. The latter applies particularly to the concrete and bentonite barriers in the repository.

The state of a compartment in terms of the radionuclide inventory at a given time, depends on local processes (e.g. radioactive decay and in-growth) as well as exchange processes (e.g. advective and diffusive transport) between connected compartments.

2.2 Processes explicitly included in the models

A large number of physical and chemical processes have been identified and analysed for the near-field of SFR, see the **Waste process report** and the **Barrier process report**. However, only a few of them have a significant impact on radionuclide transport. The main near-field processes of relevance for radionuclide transport modelling are the following.

Radioactive decay and in-growth

Radioactive decay and in-growth are well-understood physical processes with accurate mathematical descriptions. These processes are explicitly modelled as decay and in-growth rates that are proportional to the inventory of the corresponding radionuclide (or its parent) at a given time and parameterised using decay constants and branching ratios (Equation 2-1).

Speciation

Speciation of radionuclides is implicitly included in near-field models as pre-calculated, time-dependent sorption coefficients and diffusivities. These coefficients are determined based on chemical and physical conditions that will change with time, as external and internal processes drive the evolution of the near-field hydrogeochemical conditions. This is modelled with a time-dependence evaluated individually for each vault.

Advection

Advection is explicitly included in the RNT modelling (Equation 2-3). The water flow rates between control volumes obtained from near-field hydrological model simulations are used, together with volumes and sorption data for waste vaults, to calculate the retention and advective transport of radionuclides in the RNT model. The water flow representation is briefly described in Section 4.3 and a more detailed description can be found in Abarca et al. (2020). A possible future occurrence of water flow localised to larger cracks in the concrete barriers of 1–2BMA and 1BRT is also considered in the models, by redirecting the advective transfer directly through the cracks, without taking sorption on the surface of the cracks into account (Section 2.3).

Diffusion

Diffusion is explicitly included in the model equations (Equation 2-4). The model considers the material-specific effective diffusivities of radionuclides, as well as the porosities and compartmental geometries (transport lengths and cross section areas) of the waste packages and barriers. The effective diffusivities for concrete are increased over time to describe a gradual degradation of the concrete barriers. Diffusive resistance is, pessimistically, neglected for bitumen-solidified wastes. Diffusion from the near-field into the surrounding host rock is accounted for in the silo model. Diffusion from the vault to bedrock is not accounted for in the other vault models, because transport from the near-field to the geosphere is dominated by advection due to the highly conductive backfill in those vaults.

Dispersion

Dispersion, as discussed here, refers to dispersive effects caused by the pore- and crack-structure of the material. In contrast to diffusion, dispersion is not represented explicitly in the model. A compartment model, representing transport through e.g. a concrete wall gives rise to a certain degree of numerical dispersion in the modelling result. This numerical dispersion depends on the degree of compartmentalisation and can be estimated in terms of a dispersion length as half the length that one compartment represents. Dispersion lengths for porous media vary over several orders of magnitudes. For a transport distance of 1 m in a natural porous medium Holzbecher (2007) reports dispersion lengths in the range of 0.001 m to 0.1 m. As Holzbecher (2007) indicates that the numerical dispersion is of the same order or higher than the real mechanical dispersion in the barriers, it is considered as not appropriate to include additional, explicit dispersion in the near-field model. Further it should be noted that the dispersion, as discussed above, has little, if any, effect on the main result of the radionuclide transport calculations, i.e. the estimate of the total (combined) releases from the whole repository. These releases originate from different waste vaults with dimensions in the order of hundreds of meters, with different shapes and properties of barriers and waste packages. The dispersive effect introduced by these factors will overshadow the issue of numerical and mechanical dispersion on the barrier thickness scale.

Sorption

Sorption on an immobile solid phase has a retarding effect on transport of radionuclides. Sorption is here used to describe the combined effect of all attachment to solid surfaces, including adsorption, absorption and ion-exchange. Sorption on near-field materials, mainly cement but also crushed rock and bentonite in the silo, is explicitly included in the radionuclide transport modelling using a linear approach, based on K_d values specific to the chemical species (Equation 2-2). K_d is also dependent on the solid material properties and chemical conditions in the system, both of which are assumed to vary over time (these variations are neglected for bentonite and crushed rock by choosing pessimistic K_d values). Relevant condition parameters include redox potential, pH (which relate to changes in the cement mineralogical properties, represented with four different degradation states), complexing-agent concentrations (see below), and chemical speciation of radionuclides.

Complexation

Organic complexing agents present in the repository tend to associate with cationic radionuclides, forming soluble coordination complexes (Section 6.2.8 in the **Post-closure safety report**). This decreases the effective sorption coefficient of these radionuclides. Hence, due to the presence of complexing agents in the repository, the K_d values of several radionuclides are divided by a unitless sorption reduction factor (SRF) before application in the transport calculations (Equation 2-2). The SRF is a dynamic parameter that changes over time, as it is dependent on variations in the concentration of complexing agents. An SRF value of unity corresponds to fully intact sorption, unaffected by complexing agents.

Corrosion-controlled radionuclide release

The steel in the reactor pressure vessels in the 1BRT vault contains radionuclides produced as a result of neutron activation of the steel during the operation of the reactor. During this time, the vessel surfaces are also contaminated by radionuclides present in the reactor water. The surface contamination is assumed to dissolve in the surrounding pore water directly after closure of the repository, whereas the fraction of the radionuclides that originates from neutron activation is assumed to be released congruently with the corrosion products as the steel corrodes. The corrosion rate of the steel in the reactor pressure vessels changes with time. The change with time is determined by the expected evolution of pH and redox conditions in the vault. This process is explicitly included in the model as described in Equation 2-10.

Solubility

Solubility limits represent an upper bound on the concentration of a species in solution. For a radionuclide, this limits the fraction that is available for transport. Under SFR conditions, solubility limits are relevant for a handful of radionuclides but are, pessimistically, not considered in the calculation cases in the PSAR. However, this report presents some supporting calculations done to illustrate the effect of solubility limits, as described in Appendix C.

2.3 Modelling of transport through cracked concrete

Advective transport through concrete barriers is modelled in two ways, either as transport through a homogenous porous medium or a cracked medium (possible future cracking of the concrete barriers is described in Chapters 6 and 7 in the **Post-closure safety report**). The latter approach applies for cases when degradation has caused cracks in the concrete, and the water flow can be expected to be localised to a few larger cracks.

For the radionuclides transported by advection in cracks, the sorbing surface will be smaller (per water volume) for a few larger than for many smaller cracks. This will limit the validity of a homogenous representation in the model. An analysis of the conditions under which modelling of the concrete barriers as homogenous media is valid can be found in Appendix B in the **Radionuclide transport report.** The conclusions is drawn that it is appropriate to model the concrete in the barriers as a porous medium for intact and moderately degraded concrete. For severely and completely degraded concrete on the other hand, it was decided to model the barrier as a cracked medium. In the crack model, advection through the barriers is modelled by redirecting the advective transfer directly through the cracks, without taking sorption on the surface of the cracks into account, while diffusion and sorption are assumed to remain in the intact parts of the concrete barriers.

2.4 Mathematical model description

Activity transport equation

The concepts “transfer (or transfer rate)” and “transfer coefficient” are used in the compartment model to describe the exchange processes between compartments, defined as:

Transfer N_{jk}^{i} (Bq a^{-1}): The transfer rate of species (radionuclide) i from the source compartment j to the target compartment k.

Transfer coefficient μ_{jk}^{i} (a^{-1}): The rate coefficient, i.e., the factor of proportionality between the transfer rate N_{jk}^{i} and the radionuclide inventory $\mathbb{A}_{j}^{i}$ of the source compartment j. The transfer coefficient can be applied for transfers depending linearly on the inventory of the source compartment, i.e., $N_{jk}^{i} = \mu_{jk}^{i} \mathbb{A}_{j}^{i}$. The linear model is applied for most transfer processes. One exception is solubility limited transport.

The rate of change of a compartment’s inventory can be described by the following equation[1].

[1] Note that the radionuclide inventory is expressed in (Bq) in Equation 2-1. This affects the form of the in-growth term. Considering that the in-growth, expressed in number of nuclei per time unit of the decay product, is given by $\frac{d}{dt}M^i = Br_p^i \lambda^p M^p$ (where M denotes the number of atoms), and by definition $\mathbb{A} \equiv \lambda M$, the time derivate of the radionuclide inventory is given by $\frac{d}{dt}\mathbb{A}^i \equiv \lambda^i \frac{d}{dt}M^i = \lambda^i Br_p^i \lambda^p M^p \equiv \lambda^i Br_p^i \mathbb{A}^p$.

$$\frac{d}{dt}\mathbb{A}_j^i = \sum_{k \in n_j} (\overbrace{\mu_{kj}^i \mathbb{A}_k^i}^{N_{kj}^i} - \overbrace{\mu_{jk}^i \mathbb{A}_j^i}^{N_{jk}^i}) + \sum_{p \in P_i} \lambda^i Br_p^i \mathbb{A}_j^p - \lambda^i \mathbb{A}_j^i + r_j^i \qquad \text{Equation 2-1}$$

Where:

$\mathbb{A}_j^i$: inventory of radionuclide *i* in compartment *j*, (Bq),

n_j: set of indices of transfers connected to compartment *j*, (-),

N_{jk}^i: transfer rate of radionuclide *i* from compartment *j* to *k*, (Bq a^{-1}),

μ_{jk}^i: transfer coefficient of radionuclide *i* from compartment *j* to *k*, (a^{-1}),

P_i: set of indices of parents of radionuclide *i*, (-),

λ^i: decay rate of radionuclide *i* (a^{-1}),

Br_p^i: branching ratio from parent radionuclide *p* to radionuclide *i*, (-),

r_j^i: sink/source term (representing external connections) for radionuclide *i* in compartment *j*, (-).

The transfer coefficients used to represent transport processes in the models are presented below.

Radioactive decay and in-growth

The mathematical description of decay and in-growth of radionuclides is shown in Equation 2-1.

These processes are modelled in each compartment in the model.

Capacity

The sorption of radionuclides is dependent on several physical and chemical processes described in the process reports for the PSAR (**Waste process report** and **Barrier process report**). These processes are represented by a simplified linear model for the partitioning of radionuclides dissolved in the water and sorbed to the matrix of the porous medium. In this model, the sorption coefficient, K_d, is defined as the ratio of the quantity of the radionuclide sorbed per unit mass of porous medium to the amount remaining in solution at equilibrium.

The concept of capacity (m^3) has been used in this work to condense the mathematical expressions used in the models and report. The capacity can be interpreted as a fictive volume consisting of the pore volume plus the effective volume of sorption sites. Hence, the pore-water concentration of a radionuclide in a compartment is obtained by dividing the total amount of the radionuclides in the compartment with the capacity of the compartment.

The capacity, Cap_j^i (m^3), of a compartment *j* to store radionuclide *i* is defined as:

$$\mathrm{Cap}_j^i = V_j \left(\phi + (1-\phi) f_m \rho_c \frac{K_d^i}{SRF_j^i} \right) \qquad \text{Equation 2-2}$$

where:

V_j: volume of the compartment *j* (m^3),

ϕ: porosity of the medium in the compartment (-),

f_m: mass fraction of the sorbing media in the solid media in the compartment (-),

ρ_c: particle density of the (total) solid medium in the compartment (kg m^{-3}),

K_d^i: sorption coefficient for radionuclide i in the sorbing media (m^3 kg^{-1}).

SRF_j^i: sorption reduction factor for radionuclide *i* in compartment *j* (-).

The mixing fraction (f_m) is less than one for both concrete and sand/bentonite mix. However, for both bentonite and crushed rock backfill $f_m = 1$.

Advection

The advective transfer coefficient between compartments is expressed as:

$$\mu^{i}_{\mathrm{adv},jk} = \frac{Q_{jk}}{Cap^{i}_{j}} \qquad \text{Equation 2-3}$$

where:

$\mu^{i}_{adv,jk}$: Advective transfer coefficient for radionuclide i from compartment j to k (a^{-1}),

Q_{jk}: Water flow from compartment j to compartment k ($m^3\ a^{-1}$),

Cap^{i}_{j}: Capacity of compartment j to store radionuclide i (m^3).

The model is implemented with advective transfer in or out over selected compartment surfaces. At a given time, only unidirectional transfer over a surface is considered, but the direction can change with time. This arrangement makes it possible to consider changes in the direction of water-flow over time.

Diffusion

The total diffusive transfer between compartments is expressed as a combination of a forward and a backward diffusive transfer, each expressed as:

$$\mu^{i}_{\mathrm{diff},jk} = \frac{1}{0.5\left(R_j + R_k\right)Cap^{i}_{j}} \qquad \text{Equation 2-4}$$

Where:

$\mu^{i}_{diff,jk}$: Diffusive transfer coefficient for radionuclide i from compartment j to k (a^{-1}),

R_j: Diffusive resistance in the direction of diffusion in compartment j ($a\ m^{-3}$),

Cap^{i}_{j}: Capacity of compartment j to store radionuclide i. (m^3).

Diffusive resistance in a particular direction for a compartment is defined as:

$$R_j = \frac{L_j}{A_j D_{\mathrm{e}}} \qquad \text{Equation 2-5}$$

where:

L_j: Length of compartment in the direction of diffusion (m),

A_j: Diffusion area i.e. cross-sectional area of the compartment perpendicular to the direction of diffusion (m^2),

D_e: Effective diffusivity in the porous medium in the compartment ($m^2\ a^{-1}$).

Note that R_j refers to the diffusive resistance of the full length of the compartment. The transport between two adjacent compartments experience on average half of the diffusive resistance of each of the compartments, hence the factor 0.5 in the denominator in Equation 2-4.

The diffusive net transfer rate $N^{\mathrm{diff,net}}_{jk}$(Bq a^{-1}) from compartment j to k is driven by the difference in concentration of a particular radionuclide between the compartments:

$$N^{\mathrm{diff,net}}_{jk} = \frac{1}{0.5\left(R_j + R_k\right)}\left(\frac{\mathbb{A}_j}{Cap_j} - \frac{\mathbb{A}_k}{Cap_k}\right) \qquad \text{Equation 2-6}$$

A waste compartment in a near-field model can represent multiple physical waste packages in the repository. The concept used here is like parallel coupling of equal resistances in electronic circuits. In this case the expression for the diffusive resistance of the model compartment becomes:

$$R = \frac{L}{nA_s D_\mathrm{e}} \qquad \text{Equation 2-7}$$

where:

n: the actual number of waste packages represented by the compartment (-),

A_s: the surface area of one waste package (m^2),

L: the diffusion length (typically the thickness of a mould wall) (m).

Diffusion into bedrock

The diffusive transport of radionuclides from the silo bentonite into the bedrock that occurs from bentonite compartments in contact with slowly moving water in the bedrock is represented by the *equivalent water flow*, Q_eq (Neretnieks et al. 1987). For other vaults, diffusion to bedrock is not accounted for because the transport from the near-field to the geosphere is dominated by advection due to the highly conductive backfill in those vaults.

The Q_eq flow transports dissolved radionuclides, with concentrations equal to the concentrations in the compartment from where releases to the bedrock take place. The value of Q_eq ($m^3\ a^{-1}$) depends on the size of the contact area, the water flux (Darcy velocity), the flow porosity in the bedrock and the diffusivity as follows:

$$\mathrm{Q_{eq}} = A_w \varepsilon_\mathrm{rock} \sqrt{\frac{4D_\mathrm{w}}{\pi t_\mathrm{res}}} \qquad \text{Equation 2-8}$$

where:

A_w: Contact area between the compartment and rock (m^2),

$\varepsilon_\mathrm{rock}$: Flow porosity in rock (-),

D_w: Diffusivity of radionuclides in water ($m^2\ a^{-1}$),

t_res: Residence time of the water in contact with the compartment (a).

$$t_\mathrm{res} = \frac{\varepsilon_\mathrm{rock} L}{q} \qquad \text{Equation 2-9}$$

where:

L: The distance (length scale) over which flowing water is in contact with the compartment (m),

q: The Darcy velocity of water in the rock ($m\ a^{-1}$).

Corrosion-controlled radionuclide release

Irradiation-induced radionuclides in the steel in the reactor pressure vessels are released congruently with corrosion products as the metal corrodes. The following expressions describe the yearly release of radionuclides from steel with a rate corresponding to the amount of radionuclides in a thin layer of the steel corroding each year. The transfer is modelled with expressions given in Equation 2-10 and Equation 2-11.

$$\mu_{\mathrm{corr}} = \begin{cases} \dfrac{1}{\max\left(1, t_{\mathrm{corr}_1} - t\right)} & ;\ t < t_0 \text{ , alkaline} \\[2ex] \dfrac{1}{\max\left(1, t_{\mathrm{corr}_2} + \left(1 - \dfrac{t_{\mathrm{corr}_2}}{t_{\mathrm{corr}_1}}\right) t_0 - t\right)} & ;\ t \geq t_0 \text{ , near-neutral} \end{cases} \qquad \text{Equation 2-10}$$

$$\begin{cases} t_{\mathrm{corr}_1} = \dfrac{d_{\mathrm{steel}}}{2k_{\mathrm{corr}_1}} & \text{; alkaline conditions} \\[2ex] t_{\mathrm{corr}_2} = \dfrac{d_{\mathrm{steel}}}{2k_{\mathrm{corr}_2}} & \text{; near-neutral conditions} \end{cases} \qquad \text{Equation 2-11}$$

where:

μ_{corr}: transfer coefficient for corrosion (a^{-1}),

d_{steel}: steel thickness (m),

k_{corr1}: corrosion rate for alkaline conditions (m a^{-1}),

k_{corr2}: corrosion rate for non-alkaline conditions (m a^{-1}),

t_0: time when conditions change from alkaline to near-neutral (a),

t_{corr1}: time for complete corrosion of a steel piece under alkaline conditions (a),

t_{corr2}: time for complete corrosion of a steel piece under near-neutral conditions (a).

When the steel is fully corroded the denominator in Equation 2-10 is set to 1. This is done to prevent errors in the calculation resulting from division by zero or negative transfer coefficients. The steel from the reactor pressure vessels is assumed to corrode from both sides, hence the steel thickness is divided by two in Equation 2-11.

Solubility limited release

It is expected that some radionuclides may be subject to solubility limitations. Since the calculations performed in most calculation cases do not take this into account, the release of some radionuclides may be overestimated. To assess the effect of solubility limitations, the effect of this process is studied in supporting calculations (Appendix C). The mathematical approach used for calculations with solubility limitations is described below.

Equation 2-12 and Equation 2-13 shows how solubility limited transfer rates for advection and diffusion are implemented in the model. The difference from Equation 2-3 and Equation 2-4 is the definition of available activity $\mathbb{A}_j^{if}$.

The advective transfer rate between compartments is expressed as:

$$N_{\mathrm{adv},jk}^{i} = \mu_{\mathrm{adv},jk}^{i} \mathbb{A}_j^{if} = \frac{\mathrm{Q}_{jk}}{\mathrm{Cap}_j^i} \mathbb{A}_j^{if} \qquad \text{Equation 2-12}$$

The diffusive transfer rate between compartments is expressed as:

$$N_{\mathrm{diff},jk}^{i} = \mu_{\mathrm{diff},jk}^{i} \mathbb{A}_j^{if} = \frac{1}{0.5\left(R_j + R_k\right)\mathrm{Cap}_j^i} \mathbb{A}_j^{if} \qquad \text{Equation 2-13}$$

Where:

$\mathbb{A}_j^{if}$: Activity of dissolved or sorbed radionuclide i in compartment j (Bq), defined as:

$$\mathbb{A}_j^{if} = \begin{cases} \mathbb{A}_j^i & ; \; c_{\mathrm{tot},j}^{\mathrm{elm}} < c_{\mathrm{sat}}^{\mathrm{elm}} \\ Cap_j^i \lambda^i N_A c_{\mathrm{sat}}^{\mathrm{elm}} \dfrac{n_j^i}{\sum_{i \in E} n_j^i} = \dfrac{c_{\mathrm{sat}}^{\mathrm{elm}}}{c_{\mathrm{tot},j}^{\mathrm{elm}}} \mathbb{A}_j^i & ; \; c_{\mathrm{tot},j}^{\mathrm{elm}} \geq c_{\mathrm{sat}}^{\mathrm{elm}} \end{cases} \qquad \text{Equation 2-14}$$

$$c_{\mathrm{tot},j}^{\mathrm{elm}} = \frac{n_j^{\mathrm{elm}}}{Cap_j^i} \quad ; i \in E$$

Where:

$\Sigma_{\mathrm{elm} \in E}\, n_j^{\mathrm{elm}}$: Total amount of isotopes of the same element in compartment j (mol).

$\mathbb{A}_j^i$: Activity of radionuclide i in compartment j (Bq).

n_j^i : Amount of substance of radionuclide i in compartment j (mol).

n_j^{elm} : Amount of substance of element *elm* in compartment j (mol).

$c_{\mathrm{sat}}^{\mathrm{elm}}$: Concentration saturation limit for element *elm* (mol m^{-3}).

$c_{\mathrm{tot},j}^{\mathrm{elm}}$: Total concentration of all nuclides of the same element *elm* in compartment j (mol m^{-3}).

N_A : Avogadro's number 6.022×10^{23} (mol^{-1}).

E : Set of all isotopes of element elm.

2.5 Coupling to the geosphere model

In all near-field models, except the silo model, the only transport process considered from near-field to bedrock is the advective flow. Diffusion to bedrock is not accounted for in these models as the transport from the near-field to the geosphere is dominated by advection due to the permeable backfill in those vaults. For the silo, diffusion is a significant transport process from the bentonite to the bedrock, modelled with the equivalent water flow concept (Equation 2-8).

3 Modelling tool

This chapter contains a description of Ecolego (**Model tools report**), the software used for radionuclide transport modelling. The description is focused on concepts relevant for the models presented in this report. All calculations for this report are performed with models implemented in Ecolego version 6.5. A programmatic approach is implemented to build models and perform calculations, as described in Appendix B.

3.1 Ecolego

Ecolego is a software tool for creating compartment models (see Figure 3-1) and performing deterministic and probabilistic simulations, as well as sensitivity analyses. The graphical user interface of Ecolego allows the user to define a model as an interaction matrix in several hierarchical levels, which simplifies the handling of large complex models. Upon execution, Ecolego translates the model representation to Java source code that is compiled and run automatically[2].

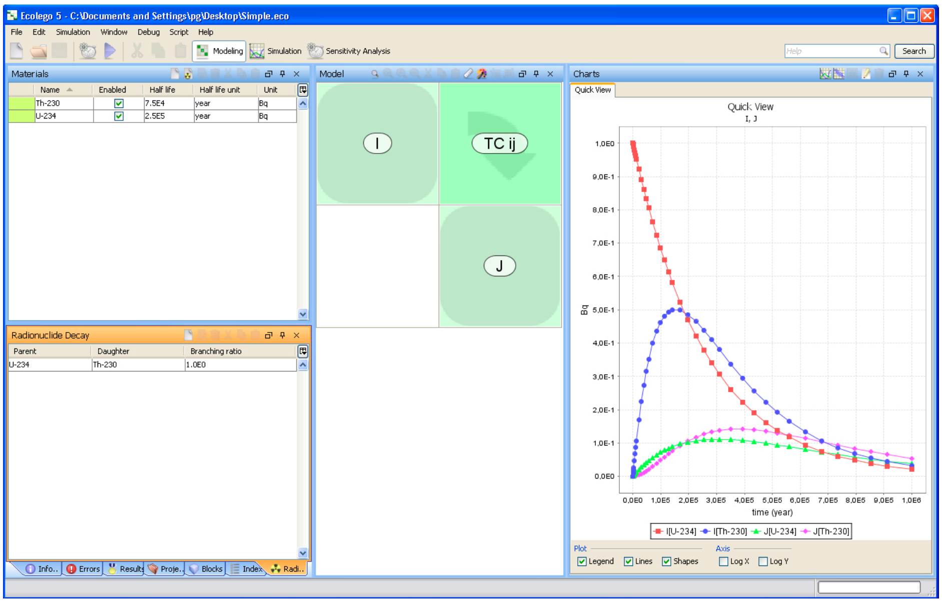

Figure 3-1. *The Ecolego tool showing a simple model consisting of two compartments (I and J) and a transfer between them implemented with a transfer coefficient TC_ij.*

[2] The numerical solvers make use of libraries written in other programming languages to enhance the performance of the numerical algorithms.

Figure 3-2 shows a graphical representation of how compartments of the model interact via transfer processes. It shows a simple example model (graphically represented in the Ecolego matrix form) for advection and diffusion in a system with waste, a concrete barrier, a permeable backfill and an external system (geosphere). The convention used for the models presented in this report is to use blue and yellow colours to identify advective and diffusive transfer coefficients, respectively.

The compartments (or subsystems with several compartments) are placed on the diagonal positions of the matrix and the transfer processes are displayed on the off-diagonal positions. The matrix is read clockwise so that a transfer from the compartment at position 1,1 to the compartment at position 2,2 are displayed in the off-diagonal position 1,2.

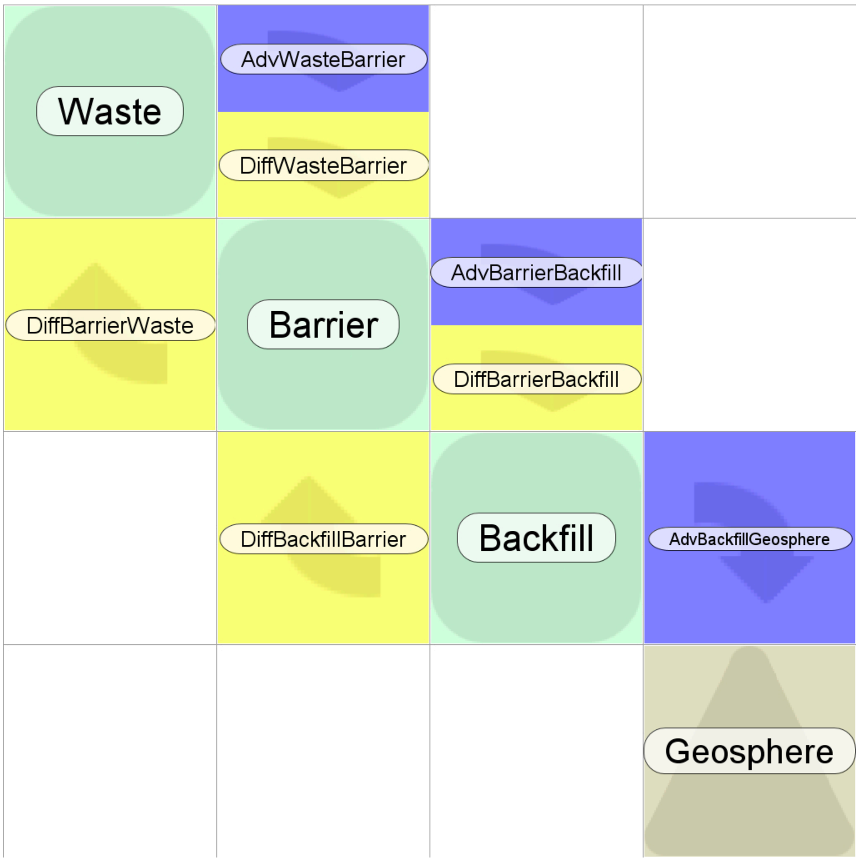

Figure 3-2. *The visual presentation of advection and diffusion in an example Ecolego model. The convention used for the models presented in this report is to use blue and yellow colours to identify advective and diffusive transfer coefficients, respectively.*

3.2 Blocks

Block is the Ecolego name for the components or building-blocks used in the construction of the radionuclide transport model. The most used Ecolego blocks are described below.

Compartment

A compartment is a block that acts as an integrator (over time) of quantities of the radionuclides in a model. The quantity held within this block is calculated with a differential equation, where the input and output rates are defined by transfer blocks.

Transfer

The transfer block represents the transfer of radionuclides between compartments. It defines the quantity of radionuclides transferred per unit time from a source/sink or compartment block to a destination compartment or source/sink block, i.e. the transfer blocks constitute the time derivatives of the differential equation.

Parameter

Parameters are blocks that hold values and are used in other blocks of the model, for instance in transfers and expressions. The value of a parameter remains constant through a simulation and is given either as a single (deterministic) value or a probability density function.

Expression

The expression block can be used to specify an arbitrary function consisting of values defined by other blocks in the model.

Lookup table

Lookup tables are like parameters, but the lookup table value can change as a function of the simulation time. The time-dependent value of a lookup table is deterministic but may be multiplied with a probabilistic parameter to obtain a probabilistic time-dependent value.

Source/Sink

A source/sink is a special type of compartment, with either unlimited quantity of the modelled radionuclides, from which any quantity can be subtracted and then added to other compartments, or an infinite well to which any quantity can be added from another compartment. In short, source/sink blocks represent objects outside of the model that either feed or pull radionuclides to or from compartments inside the model.

Transport block

The transport block facilitates handling of several compartments, transfers and other blocks as described in Section 3.4.

3.3 Subsystems and groups

Ecolego offers two ways to arrange blocks in a hierarchical structure; subsystems and groups. The difference between them is that subsystems control both the visual presentation and the unique identity (ID) of the contained blocks, whereas groups are only related to the visual presentation of the contained blocks. The ID is important when it comes to handling parameters and expressions in the model.

The ID of a block in the model is defined by its name and the "path" of subsystems in which it is contained, where each level is separated with a dot. This simplifies handling of large models. E.g. a model could have two parameters named "Kd", if one of them is located in a subsystem called "NearField" it would have the ID "NearField.Kd" whereas another K_d parameter in a subsystem called "Geosphere" would have the ID "Geosphere.Kd". The safe and correct handling of parameters and expressions read from input data files relies on the uniqueness of this ID.

3.4 The transport block

For parts of the modelled system that need to be represented by several compartments it is sometimes practical to use the transport block available in Ecolego. The transport block is a subsystem with extra functionality to automatically generate compartments and transfers when the model is run. This makes it useful for one-dimensional transport, through parts of the model-domain that require fine discretisation, e.g. concrete walls.

Figure 3-3 shows the use of the Ecolego transport block. The "Barrier" is represented by a transport block visualised as a subsystem containing the two compartments "Begin" and "End".

The transport is defined by connecting the "Begin" and "End" blocks with transfer blocks. The "Begin" block will be duplicated (N−1) times. The number N is set in an expression contained in the transport block. Most transport blocks used in the near-field models presented in this report represent five compartments, i.e. N = 5. This number of compartments has been considered a reasonable compromise between accuracy and computing time (Appendix F in Quintessa 2011).

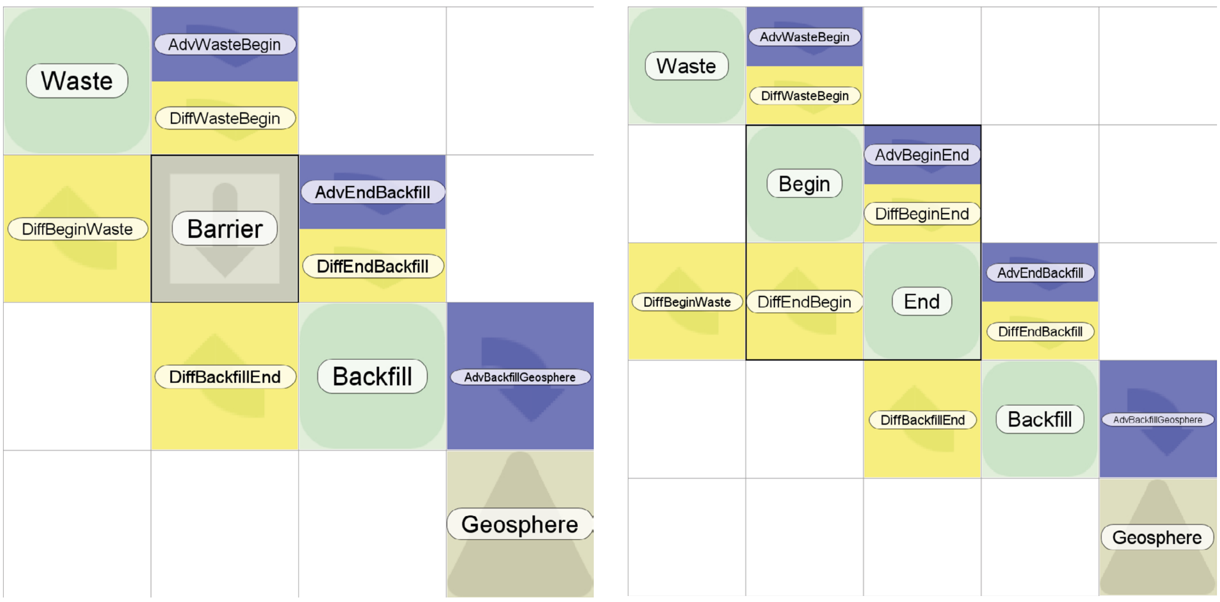

Figure 3-3. An example model including the transport block as used in the Ecolego models for the near-field.

3.5 Index-lists

Index-lists is an Ecolego feature that facilitates the use of multidimensional data. An index-list contains a set of named indices. Ecolego has several predefined index-lists that are automatically updated when the model is built and edited. In addition to the predefined index-lists the user can define new index-lists useful for a specific model.

When index-lists are used in an expression in Ecolego, a notation with square brackets, e.g. "Kd[Concrete][Ni]", is used to select a specific index value. Here, the K_d value for Nickel in concrete is specified, assuming K_d is a "2-dimensional" parameter that depends on 2 index-lists, Media and Species, where Concrete is one of the indices in the Media index-list and Ni is one of the indices in the Species index-list. The predefined index-lists are described below.

Materials – this index-list is automatically synchronized with the list of materials in the model and is used for blocks with a material dependence. This list can be used for all blocks. (Note: the naming of this index-list may cause some confusion; this index-list contains the modelled contaminants (radionuclides or stable solutes). Bulk materials such as concrete, bentonite etc are contained in the user-defined index-list *Media* in the PSAR models as described in Appendix B).

Radionuclides – a sub-set of the materials index list, which only has indices for the radionuclides included in the model. This list can be used for all blocks.

Elements – a mapped index list, which has indices for each atomic element of the radionuclides in the model. This list can be used for all blocks. (Note: there are some limitations with this index-list. Hence, in the PSAR models a user defined index-list, *Species*, is defined for a similar purpose.)

Compartments – this index-list has indices for each compartment of the model. This list can contain indices for parameters, expressions etc whose values are compartment dependent.

Transfers – this index-list has indices for each transfer of the model. This list can be used as indices for parameters, expressions etc whose values are transfer dependent.

In the modelling described in this report several additional index-lists have been defined to facilitate the handling of data. These index-lists are described in Appendix B.

The index-lists can be related to each other in two different ways, 1) one index-list can be a subset of another index-list; this is mainly for aesthetic reasons to remove unnecessary indices from data where these indices are not needed, or, 2) an index-list can be mapped to another index-list; this facilitates handling of data that are common to several indices in one index-list. Examples of such mappings used in the present analysis are mappings from radionuclides to species and mappings from compartments to media (see Appendix B1 for details).

4 Input data

The handling of models and data represents a challenge in terms of quality assurance. The data management must be automated to avoid handling errors as far as possible. The approach used in the PSAR has been to deliver and store input data to the radionuclide transport model in a machine-readable format, in a revision control system. The input data used in the radionuclide transport modelling are stored together with relevant metadata (authorship, date of change, revision number and source) in spreadsheets and text-files to facilitate input, review and quality assurance by modellers as well as the data suppliers (subject experts). These data files are automatically read by the modelling tool. Intermediate and final versions of the data files are stored in a revision control system with a central-server-based data repository using the software “Subversion” (https://subversion.apache.org/). This handling simplifies data access and quality assurance, including traceability of data.

This chapter highlights some key data and aspects of the handling of data. Further details and links to data files are available in Appendix A.

4.1 Radionuclide inventory

The inventory of each radionuclide in each waste type is used as input in the transport calculations. Those values are used in the models to transform the data to represent the amounts of each radionuclide in each *model waste type* and each section of the models. The results presented in this report are from deterministic calculations using the best-estimate values of the inventory presented in Appendix E in SKB (R-18-07) (in Swedish).

Note that the inventory of C-14 is divided into three parts, with different transport properties. These are inorganic C-14 (C-14-inorg) which is relatively strongly sorbing, organic C-14 which is very weakly sorbing and induced C-14 which is considered non sorbing. The corresponding species are called C-inorg, C-org and C-ind in this report.

The models for 1–5BLA have no detailed representation of the waste packages and hence the total initial radionuclide inventory is used in the calculations. In the 1BRT model, each *real waste type* is represented explicitly in the model. For the silo, 1–2BMA and 1–2BTF the distribution of the radionuclide inventory in the vaults is defined by the assignment of the number of waste packages of the given *real waste types* to compartments of the waste domain. The distribution of the radionuclide inventory is then calculated in the RNT model. The input data for this calculation are the number of waste packages of each type and the estimated initial amounts of radionuclide inventory per waste type (TIA). Hence the input data files contain the number of waste packages of each real waste type (NRWP) and the estimated initial amounts per waste type. The radionuclide inventory for each waste vault and *model waste type* is presented in Chapter 6 to Chapter 11.

4.2 Dimensions

Dimensional data is used to calculate volumes, diffusion-lengths and diffusion-areas for the compartments in the model. Pre-processing of data is avoided as far as possible in the modelling. Hence, the calculations of volumes and diffusion-lengths/areas are done in the RNT models. The parameters used for these calculations are given in the **Initial state report**.

4.3 Water flow

The hydrological calculations analyse the groundwater flow field around and within the SFR vaults. The flowchart in Figure 4-1 sketches the main data flows between the hydrological modelling tasks and the radionuclide transport modelling.

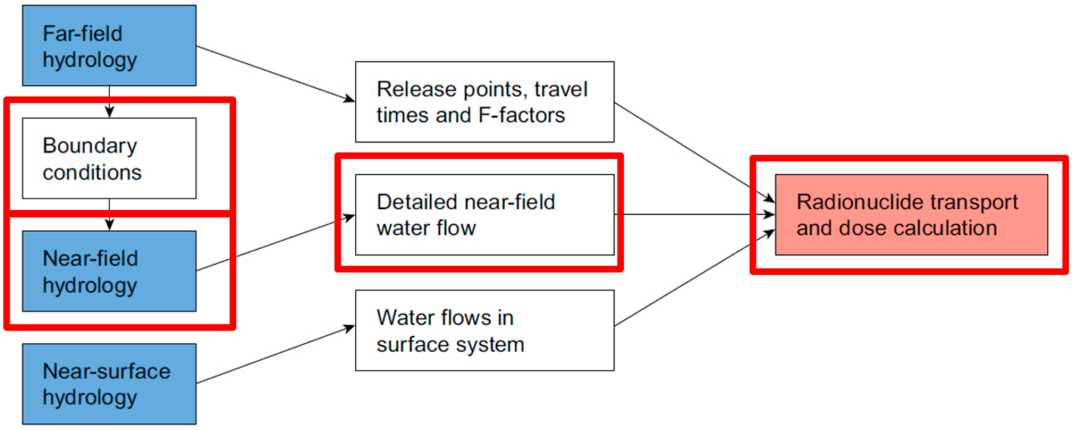

Figure 4-1. *Schematic overview of the hydrological modelling process preceding radionuclide transport calculations. Processes pertaining to the near-field are contained within red borders.*

4.3.1 Uncertainty factors

In the PSAR the uncertainties of vault flow (and geosphere water-flow parameters) are derived from variations between three bedrock fracture realisations that are considered to be representative, covering the range of uncertainty in bedrock parametrisation as described in Appendix A in the **Radionuclide transport report**.

This affects the flow used both in the deterministic calculations (used in this report) and the probabilistic uncertainty factors used in the probabilistic calculations presented in the **Radionuclide transport report**. The resulting point value uncertainty factors used in the deterministic calculations presented in this report are shown in Table 4-1.

The point values are based on the geometric mean of the three bedrock realisations (low, base, high). This is further described in the **Radionuclide transport report**.

Table 4-1. Uncertainty factors (-) applied to rescale the water flow in the deterministic models presented in this report.

Time	Silo	1BMA	2BMA	1BRT	1BTF	2BTF	1BLA	2BLA
2000 AD	1.53	2.04	1.16	0.95	1.72	1.34	1.0	0.98
2100 AD	1.58	1.77	1.24	0.95	1.43	1.12	0.87	1.0
2250 AD	1.20	1.37	1.51	1.01	1.19	0.91	0.7	0.89
2500 AD	0.90	1.27	2.20	1.08	1.16	0.81	0.62	0.95
2750 AD	0.72	1.19	1.72	0.99	1.42	1.10	0.73	0.96
3000 AD	0.68	1.23	1.53	0.96	1.24	1.12	0.73	0.98
3500 AD	0.69	1.27	1.65	0.94	1.17	1.09	0.72	0.94
5000 AD	0.71	1.27	1.63	0.92	1.14	1.08	0.72	0.92
9000 AD	0.71	1.27	1.63	0.91	1.14	1.07	0.71	0.92

4.3.2 Near-field flow calculations

Calculations of water flow in the near-field have been performed on the geometry depicted in Figure 4-2. Near-field water flow is calculated using repository-scale models implemented in COMSOL Multiphysics (COMSOL 2017). The COMSOL Multiphysics software uses a finite-element discretisation method to calculate near-field steady-state flows through barriers and waste. The calculated water flows through barriers and waste are used in the radionuclide transport models as input data.

To take shoreline regression and degradation of barriers into account in the RNT calculations, there is a need to use results from several hydrological calculations as input to one RNT calculation. The water flow rates corresponding to four different shoreline positions (representing the hydrological conditions for a submerged repository, a repository located near the shoreline, and a repository located above sea level at two different distances from the shoreline) are calculated at 2000 AD, 2500 AD, 3500 AD and 5000 AD, respectively (Abarca et al. 2020). The boundary conditions used are obtained from DarcyTools (Svensson et al. 2010) models (Öhman and Odén 2018). Between these time points the flow rates for the RNT calculations are obtained by linear interpolation. Near-field water flows for intact concrete and three different concrete degradation states (moderately degraded, severely degraded and completely degraded) are calculated for each shoreline position (Abarca et al. 2020). The RNT modelling is thus impacted by the gradual cement degradation in terms of altered flow. A short concrete degradation transition time of 100 years is assumed in the RNT calculations, as exact estimates of the transition times have not been determined. A summary of the vault and waste flow rates are shown for each vault in Chapters 6 to 11.

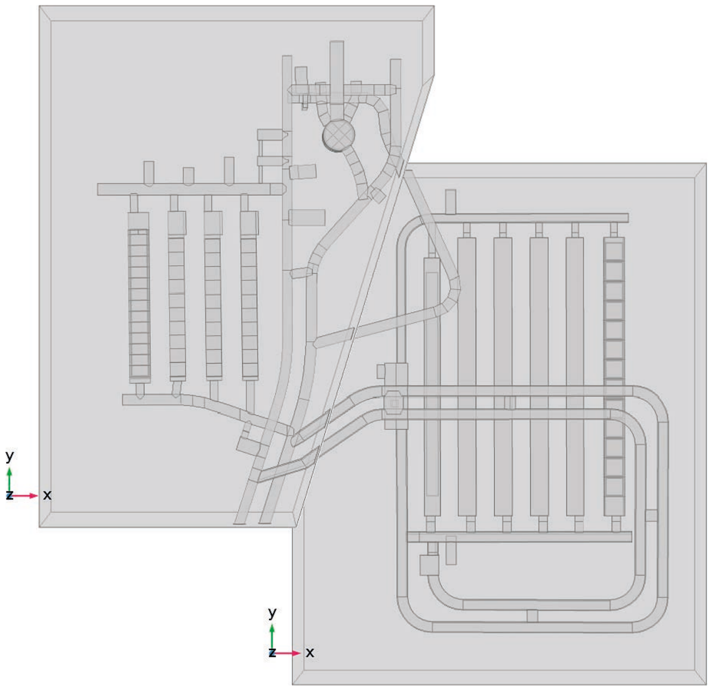

Figure 4-2. *Geometry of SFR1 (on the upper left) and SFR3 (on the lower right) as imported into the hydrological model. (Abarca et al. 2020).*

4.3.3 Control volumes

In the near-field flow modelling, the vaults are divided into control volumes (Abarca et al. 2013, 2020), model-specific entities that allow evaluation of the annual vault-water balance, including calculation of (directional) annual water flows through bounding surfaces (faces) of the control volumes. The control volumes and their faces are mapped to compartments or groups of compartments in the RNT model as described in Figure 4-3. Hence, control volumes are used to facilitate transfer of results from the hydrological models to the RNT models.

A control volume representing backfill is represented by one compartment in the RNT model. Barriers are not represented by their own control volumes in the hydrological model, instead the control volumes are arranged so that their faces coincide with a barrier, those barriers are normally represented with a transport block (five compartments) in the RNT model. The water flow through one such barrier is taken from the corresponding control-volume face, which is the only parameter taken from the hydrological to the RNT model. Thus, there is no need to keep track of which of two adjacent control volumes the barrier "belonged" to, since all dimensions are provided separately to the RNT model, not via the hydrological model.

In the near-field hydrological model, the waste packages are not resolved in detail, but rather the interior of the waste domain is assumed to be homogeneous. Conversely, in the near-field radionuclide transport model the waste packages, in some of the vaults, are represented with more detail, with several model compartments.

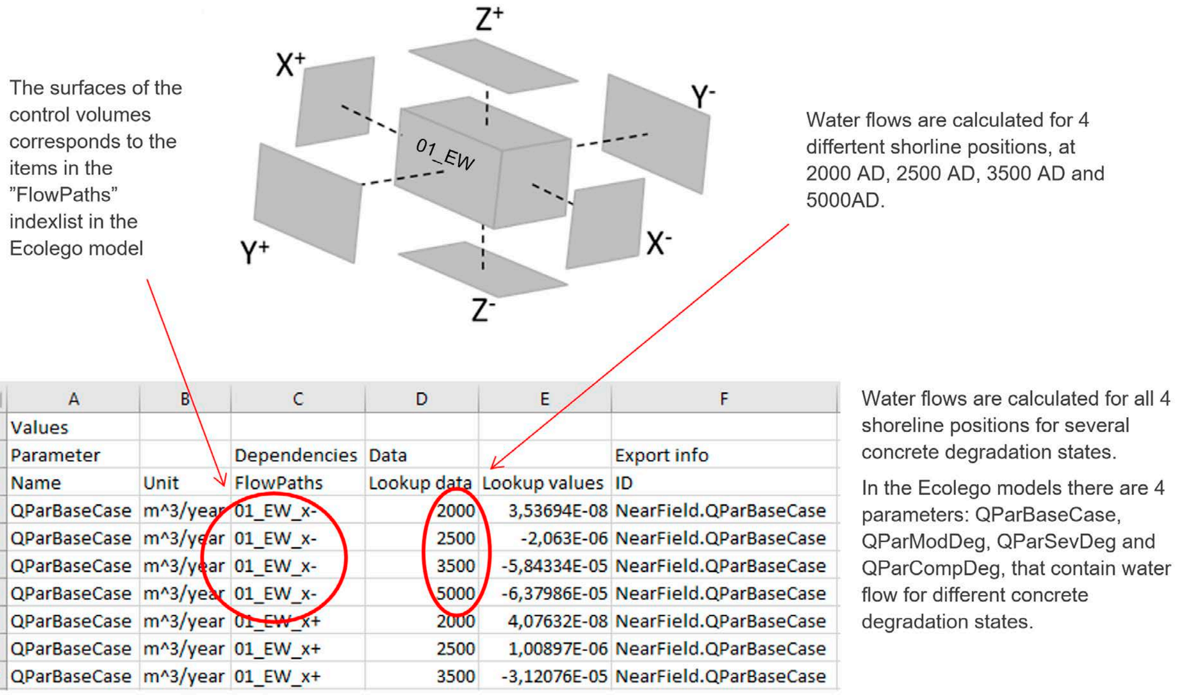

	A	B	C	D	E	F
1	Values					
2	Parameter		Dependencies	Data		Export info
3	Name	Unit	FlowPaths	Lookup data	Lookup values	ID
4	QParBaseCase	m^3/year	01_EW_x-	2000	3,53694E-08	NearField.QParBaseCase
5	QParBaseCase	m^3/year	01_EW_x-	2500	-2,063E-06	NearField.QParBaseCase
6	QParBaseCase	m^3/year	01_EW_x-	3500	-5,84334E-05	NearField.QParBaseCase
7	QParBaseCase	m^3/year	01_EW_x-	5000	-6,37986E-05	NearField.QParBaseCase
8	QParBaseCase	m^3/year	01_EW_x+	2000	4,07632E-08	NearField.QParBaseCase
9	QParBaseCase	m^3/year	01_EW_x+	2500	1,00897E-06	NearField.QParBaseCase
10	QParBaseCase	m^3/year	01_EW_x+	3500	-3,12076E-05	NearField.QParBaseCase

__Figure 4-3.__ Relationship between near-field hydrological data and parameters in the RNT models.

4.4 Sorption data

Sorption coefficients (K_d values) for cement paste are given for four time periods (cement degradation states). Initially all cementitious materials are in chemical degradation state I, characterised by dissolution of sodium and potassium hydroxides and a pH > 12.5. Thereafter follows degradation state II (dissolution of portlandite, pH ≈ 12.5), degradation state IIIa (incongruent dissolution of C-S-H phases, presence of Ca-aluminates, pH ≈ 12) and degradation state IIIb (incongruent dissolution of C-S-H phases, absence of Ca-aluminates, pH ≈ 10.5).

The duration of each state may vary between different waste vaults since the cement degradation rate varies between vaults. K_d values for each state are given in Figure 4-4. The time periods for each vault are given in Chapters 6 to 11.

Only a single K_d value is defined for each element for sorption on bentonite (Figure 4-5) since the bentonite is not assumed to degrade. The same assumption is made for sorption on crushed rock (Figure 4-6). The pH dependency for sorption on bentonite and crushed rock is neglected by choosing pessimistic K_d values.

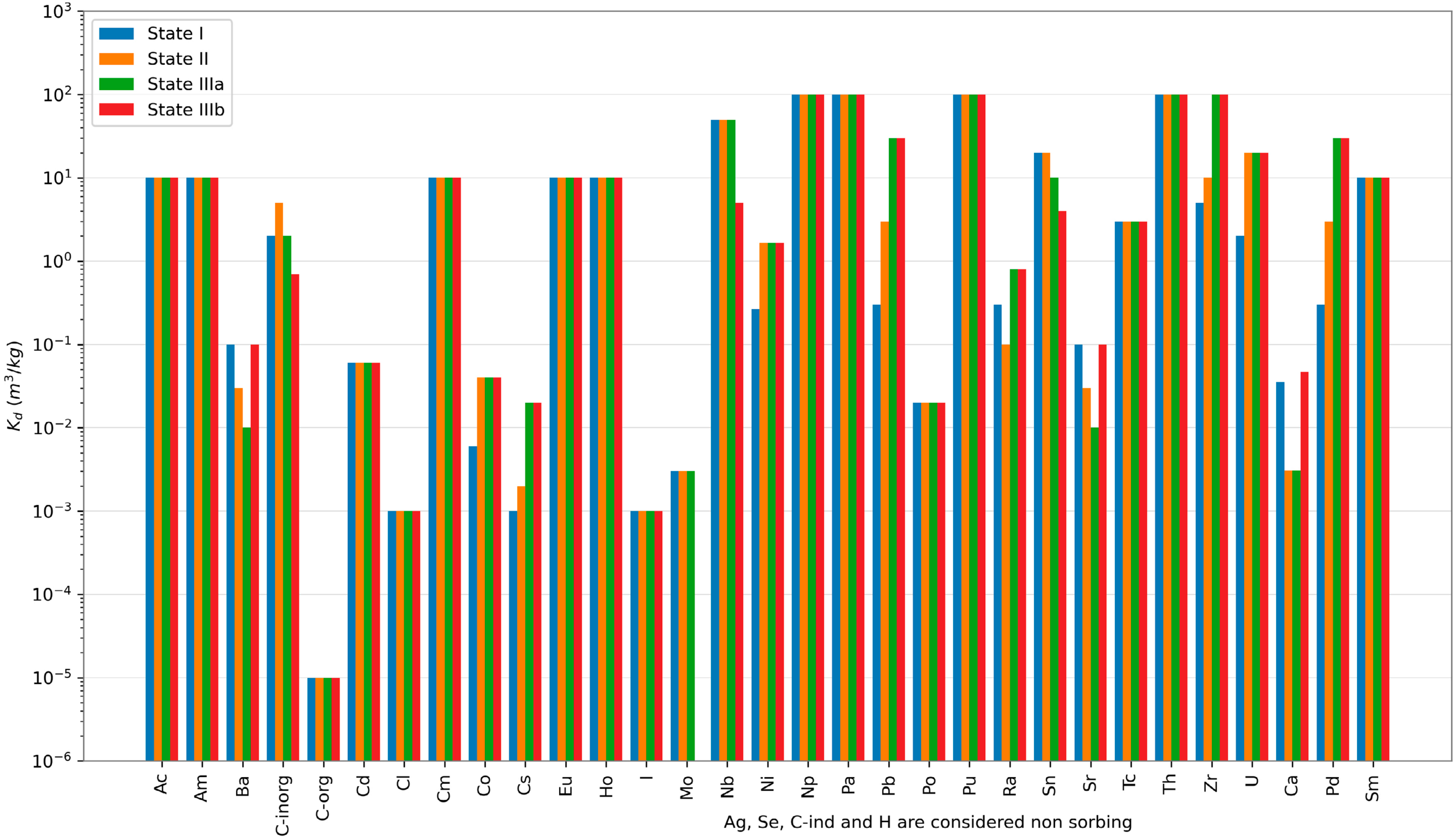

Figure 4-4. *Sorption coefficients for cement paste in the four degradation states (**Data report**).*

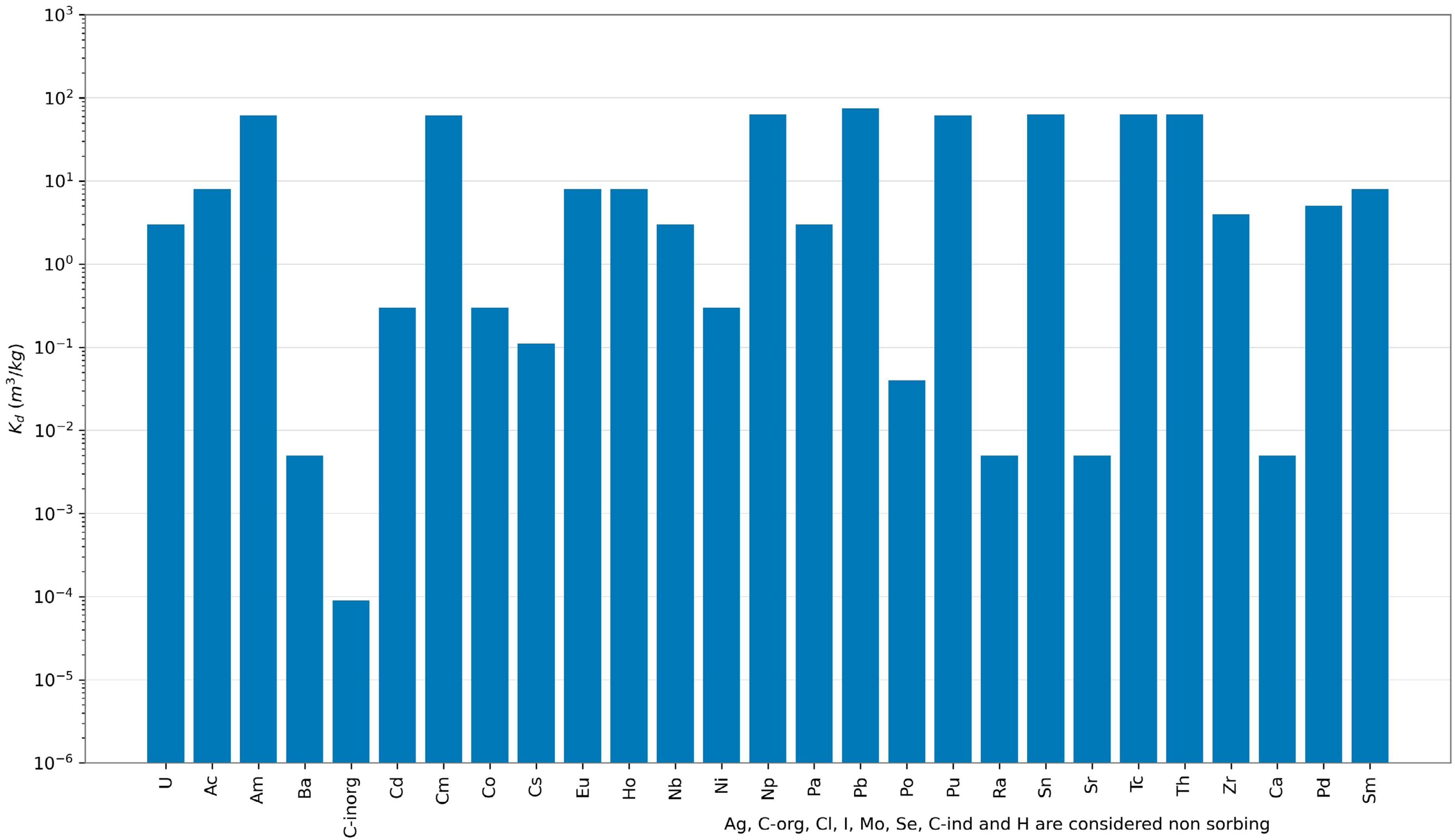

Figure 4-5. *Sorption coefficients for bentonite (**Data report**).*

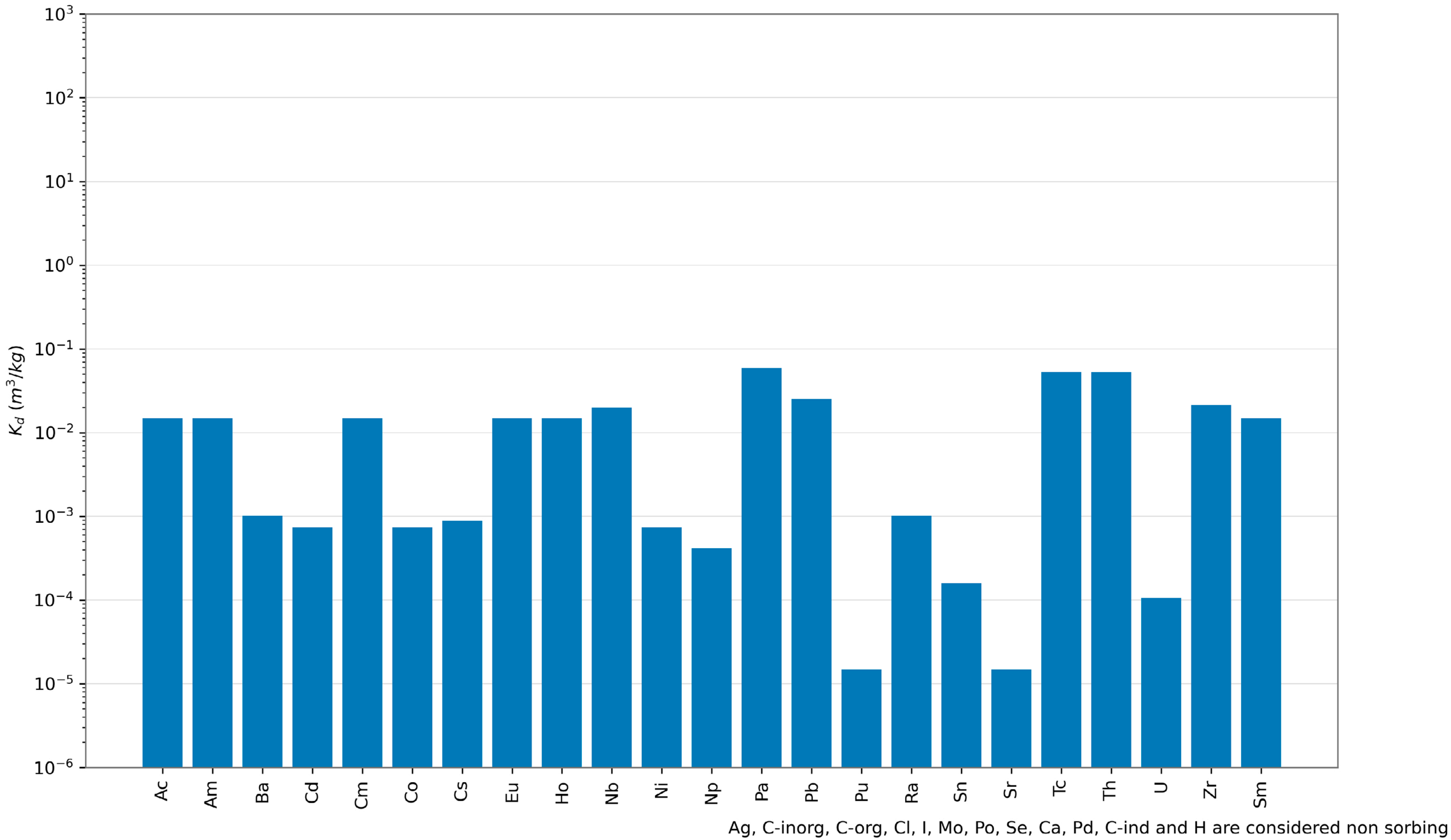

Figure 4-6. *Sorption coefficients for crushed rock backfill (**Data report**).*

4.4.1 Sorption reduction factors

Due to the expected presence of complexing agents in the repository, effective K_d values are calculated by means of sorption reduction factors (SRF). In the RNT modelling it is assumed that complexing agents reduce sorption on crushed rock backfill and bentonite in the silo in a similar way as it reduces sorption on cement. However, the SRFs are lower for bentonite/crushed rock than for cement, as the concentration of complexing agents in these parts are assumed to be lower than in the inner parts. The assumption here is that complexation is a solution-phase process, little influenced by the solid phase.

SRF values are defined for five groups of species (SRF Groups) with assumed analogous complexation properties within each group (Table 4-2). Note that only the SRF value is necessarily identical within an SRF Group, whereas other properties such as the K_d value are not (Tables 7-4 to 7-7 in the **Data report**). The SRF values are dependent on the concentration of complexing agents and hence they differ for each waste vault. The actual values for SRFs in each vault are discussed in Chapters 6 to 11.

Table 4-2. Radionuclides grouped by assumed analogous complexation properties and thus SRF values. Denoted by their oxidation states and relevant isotopes, respectively. Note that some oxidation states are assumed to not be relevant and thus are not included in the transport calculations.

SRF Group	Elements by oxidation state	Relevant isotopes in the RNT modelling
Group 1	Ac(III), Eu(III), Am(III), Cm(III), Ho(III), Pu(III), Sm(III), Po(IV), Np(V), Pu(V)	Ac-227, Am-241, Am-242m, Am-243, Cm-243, Cm-244, Cm-245, Cm-246, Eu-152, Ho-166m, Po-210, Sm-151
Group 2	Pb(II), Pd(II)	Pb-210, Pd-107
Group 3	Th(IV), Np(IV), U(IV), Pa(IV), Tc(IV), Zr(IV), Sn(IV), Nb(V), Pa(V)	Np-237, Pa-231, Sn-126, Tc-99, Th-229, Th-230, Zr-93
Group 4	Pu(IV)	Pu-238, Pu-239, Pu-240, Pu-241, Pu-242
Group 5	U(VI), Pu(VI)	U-232, U-233, U-234, U-235, U-236, U-238
Other	Species assumed not affected by complexing agents	Ag-108m, Ba-133, C-14-ind, C-14-inorg, C-14-org, Ca-41, Cd-113m, Cl-36, Co-60, Cs-135, Cs-137, H-3, I-129, Mo-93, Nb-93m, Nb-94, Ni-59, Ni-63, Ra-226, Se-79, Sr-90

4.5 Effective diffusivity and porosity

The development in time of diffusivity and porosity in the concrete barriers varies between the vaults. Values for each vault are given in Chapters 6 to 11. For other materials, the diffusivities are assumed to be the same for all vaults and are given in Table 4-3.

Table 4-3. Effective diffusivity (D_e) and porosity (ϕ) in different materials and at different points in time (Data report, Initial state report).

Material	Time period (AD)	Elements	Assumed speciation	D_e (m²/s)	ϕ (-)
Bentonite	2000–102 000	Mo, Cl, I, Se, C-inorg	anion	4×10^{-11}	0.24
Bentonite	2000–102 000	C-ind, Tc	neutral	4×10^{-10}	0.61
Bentonite	2000–102 000		cations and uncertain	7.5×10^{-10}	0.61
Bitumen	2000–102 000			2×10^{-9}	0.1[a]
Crushed rock	2000–102 000			6×10^{-10}	0.3
Sand-bentonite mix[b]	2000–102 000	Mo, Cl, I, Se, C-inorg	anion	5.44×10^{-10}	0.25
Sand-bentonite mix[b]	2000–102 000	C-ind, Tc	neutral	5.8×10^{-10}	0.25
Sand-bentonite mix[b]	2000–102 000		cations and uncertain	6.15×10^{-10}	0.25
Waste cement	2000–2100			3×10^{-10}	0.4
Waste cement	2100–2500			3.5×10^{-10}	0.4
Waste cement	2500–3000			5×10^{-10}	0.4
Waste cement	3000–102 000			1×10^{-9}	0.4
Waste concrete	2000–2100			3×10^{-10}	0.4
Waste concrete	2100–2500			3.5×10^{-10}	0.4
Waste concrete	2500–3000			5×10^{-10}	0.4
Waste concrete	3000–102 000			1×10^{-9}	0.4
Water	2000–102 000			2×10^{-9}	1
Waste, 2–5BLA	2000–102 000			2×10^{-9}	0.76
Waste, 1BLA	2000–102 000			2×10^{-9}	0.77

[a] Void volume in bitumen waste packages.
[b] Combined De for 90 % crushed rock and 10 % bentonite.

5 Waste packages

All waste types disposed in SFR have an approved waste type description (**Initial state report**). These waste type descriptions are also the basis for the estimation of material amounts and radionuclide inventory in the RNT models.

In the following text the terms *real waste type* (or waste type) refer to all the different actual waste types deposited in SFR. The term *model waste type* is used to refer to the simplified representation of waste used in the RNT models. When packages of a certain type are referred to they are called *real waste package* (or waste package) and *model waste package*, respectively.

The approach to modelling of the waste differs between the vaults as described below.

The waste domain in the models of 1–5BLA consists of one single section, modelled as a stirred tank, i.e. waste packages are not explicitly modelled.

For the silo, 1BRT, 1–2BMA and 1–2BTF, the waste packages are represented in some detail, although still in a simplified way. There are more than 50 waste types, which would be difficult and unnecessary in the present context to represent separately. However, as many of the waste types are similar, the chosen approach is to group similar package types into one group and represent each such group with one representative *model waste type*. The representation of waste packages is described below.

5.1 Description of model waste types

Below is a brief description of the *modelled waste types*. A more detailed description of the radionuclide inventory and the *real waste types* can be found in SKB (R-18-07, Chapter 2 (in Swedish)) for the reference inventory at year 2016 and SKB (R-15-15, Chapter 2 (in English)) for the reference inventory at year 2013.

5.1.1 Cement-solidified and concrete-embedded waste in concrete moulds

These two *model waste types* (CM_Ce and CM_Co) are represented using two compartments, one for the interior with cement-solidified or concrete-embedded waste and one for the concrete mould. These *model waste types* are used to represent cement-solidified ion-exchange resins and sludge in concrete moulds (1–2BMA and silo), concrete-embedded trash and scrap metal in concrete moulds (1–2BMA and silo) and cement-solidified evaporate concentrate in concrete moulds (1–2BMA) from operational waste, and concrete-embedded trash and scrap metal in concrete moulds (1–2BMA) from decommissioning waste.

5.1.2 Cement-solidified and concrete-embedded waste in steel moulds

These two *model waste types* (SM_Ce and SM_Co) are represented with only one compartment for the interior with cement-solidified or concrete-embedded waste. The steel packaging is not accounted for in the modelling. These *model waste types* are used to represent operational waste in the form of cement-solidified sludge and ion-exchange resins in steel moulds (silo), cement-solidified ion-exchange resins in steel moulds (1–2BMA and silo) and concrete-embedded trash and scrap metal in steel moulds (1–2BMA and silo). These *model waste types* are used also to represent decommissioning waste in the form of cement-solidified ion-exchange resins in steel moulds (silo), concrete-embedded trash and scrap metal in steel moulds (1–2BMA) and concrete-embedded trash and scrap metal.

5.1.3 Dual moulds

This *model waste type* (DualMould) is represented with only one compartment for the interior with concrete-embedded waste. The steel packaging is not accounted for in the modelling. This *model waste type* is used to represent decommissioning waste in the form of concrete and sand in dual-moulds in 2BMA.

5.1.4 Cement-solidified and concrete-embedded waste in steel drums

These two *model waste types* (DrumCe and DrumCo) are represented with only one compartment for the interior with cement-solidified or concrete-embedded waste. These *model waste types* are used to represent cement-solidified ion-exchange resins in steel drums (silo), trash and scrap metal in steel drums (1–2BMA) from operational waste, and concrete-embedded ashes in steel drums (1–2BMA) from decommissioning waste.

5.1.5 Ashes in steel drums

This *model waste type* (DrumAsh) is represented with two compartments, one for the interior with ashes and one for the outer concrete (the ashes are placed in an inner drum surrounded by concrete); the steel packaging is not accounted for in the modelling. This *model waste type* is used to represent concrete-embedded ashes and is used only in 1BTF.

5.1.6 Bitumen-solidified waste in steel moulds

This *model waste type* (SM_Bi) is represented with only one compartment for the interior with bitumen-solidified waste; the steel packaging is not accounted for in the modelling. No transport-limiting effects are accounted for in this waste type. This *model waste type* is used to represent bitumen-solidified ion-exchange resins in steel moulds (1–2BMA and silo) from operational and decommissioning waste.

5.1.7 Bitumen-solidified waste in steel drums

This *model waste type* (DrumBi) is represented with only one compartment for the interior with bitumen-solidified waste; the steel packaging is not accounted for in the modelling. No transport-limiting effects are accounted for in this waste type. This *model waste type* is used to represent bitumen-solidified ion-exchange resins in steel drums (1–2BMA and silo) from operational waste.

5.1.8 Concrete tanks with dewatered ion exchange resins

This *model waste type* (ConcreteTank) is represented with two compartments, one for the interior with ion-exchange resins and one for the concrete tank walls. This *model waste type* is used only to represent the de-watered ion-exchange resins in concrete tanks (1–2BTF) from operational waste.

5.1.9 Steel boxes

This *model waste type* (SteelBox) represents a waste type that is only present in 2BTF. It consists of miscellaneous waste in the form of steam separators in steel boxes. Outer dimensions are the same as for the concrete tanks, but the packaging is made of steel. The model waste type is represented with only one compartment.

5.1.10 Cortén boxes

This *model waste type* (CortenBox) represents a waste type that is only present in 1BTF. It consists of fractured concrete moulds in steel boxes. The model waste type is represented with only one compartment.

5.1.11 Steel from reactor pressure vessels and reactor tank lids

The waste packages with steel from reactor pressure vessels (TankA, TankB12, TankF123, TankO123 and TankR1) are represented by one compartment each in the model (1BRT) and the transport of irradiation-induced radionuclides is modelled with transfers corresponding to the rate governed by the corrosion rate during alkaline (initially) and non-alkaline conditions (after the cement is sufficiently degraded). Also, the reactor tank lids (LidR2 and LidR34) are modeled with one single compartment each and the release of induced radionuclides is modeled with a transfer rate corresponding to corrosion. However, for the reactor tank lids the corrosion rate is pessimistically set to an extremely high value, corresponding to a time of 100 years for the steel to become completely corroded. This is done to avoid imposing any constraints on the chemical environment for the reactor tank lids. The reactor pressure vessels and tank lids also contain radionuclides in surface contamination, and this fraction of radionuclides is assumed to be immediately released to the surrounding grout.

5.1.12 Summary of model waste types

The waste in 1–2BMA, 1–2BTF and silo is modelled using different *model waste types* that represent all waste types disposed in SFR. A summary of the different *model waste types* is given in Table 5-1. The mapping between *real waste types* and *model waste types* for each vault is given in Chapters 6 to 11. The 1–5BLA vaults are modelled as stirred tanks, hence no *model waste types* are used in these models. Also, 1BRT is modelled with another approach, where each waste type is modelled with one compartment each. The dimensions for the *model waste types* are given in Table 5-2.

Table 5-1. Description of model waste types.

Model waste type	Waste description	Occurs in
DrumBi	Bitumen-solidified waste in drum	1BMA and silo
DrumCo	Concrete-embedded waste in drum	2BMA
DrumCe	Cement-solidified waste in drum	1BMA
SM_Bi	Bitumen-solidified waste in steel mould	1–2BMA and silo
SM_Co	Concrete-embedded waste in steel mould	1–2BMA and silo
SM_Ce	Cement-solidified waste in steel mould	1–2BMA and silo
CM_Co	Concrete-embedded waste in concrete mould	1–2BMA and silo
CM_Ce	Cement-solidified waste in concrete mould	1–2BMA and silo
DrumAsh	Ashes in drum with outer concrete	1BTF
ConcreteTank	Concrete tank	1–2BTF
SteelBox	Steel box with same outer dimensions as concrete tank	2BTF
CortenBox	Concrete-embedded waste in steel box	1BTF
TankA, TankB12, TankF123, TankO123 and TankR1	Dual moulds with steel from reactor pressure vessels	1BRT
LidR2 and LidR34	Reactor tank lids	1BRT
DualMould	Concrete-embedded waste in large steel mould	2BMA

Table 5-2. Dimensions for model waste types (Table 5-1) (values marked "-" are not used in the model) (SKB R-18-07).

Model waste type	Height, Width, Length (m)	Wall thickness (m)	Outer volume (m^3)	Inner volume (m^3)
SM_Ce, SM_Bi and SM_Co	-	-	-	1.7
CM_Ce and CM_Co	1.2, 1.2, 1.2	0.1	1.73	1.0
DrumCe, DrumBi and DrumCo	-	-	-	0.2
DrumAsh	0.84, 0.57 (diam.)	0.05	0.2	0.1
ConcreteTank	2.3, 1.3, 3.3	0.15	9.87	6.0
SteelBox	-	-	-	6.82
CortenBox	-	-	-	3.31
DualMould	-	-	-	2.87

5.2 Water flow and diffusion in waste packages

5.2.1 Water flow

Due to the lack of detailed water flow data for the interior of the waste domains, a simplified approach is taken to estimate the water flow through the waste packages. For waste packages in 1–2BTF, silo and 1–2BMA all the water flowing into the waste domain is pessimistically also assumed to flow through all the *model waste packages*.

5.2.2 Diffusive resistance in waste packages

In the transport from waste packages to the surrounding water or grout only the diffusive resistance in the waste is taken into account.

Diffusive resistance in waste is calculated according to Equation 2-7. To calculate diffusive resistance the L/A quota is first calculated. This ratio is then divided by the effective diffusivity and the number of *real waste packages* represented by the *model waste package*. The values for L/A, calculated from values in Table 5-2, are given in Table 5-3. The values in the table corresponds to one waste package. L is the wall thickness and A is pessimistically chosen to be the outer area of the waste package.

Table 5-3. L/A for waste packages.

Waste compartment	L/A (m^{-1})
Mould wall	0.01
Matrix in concrete moulds	*
Matrix in steel moulds	*
Drums	*
Ash drums concrete	0.025
Ash drums inner	*
Concrete tank wall	0.004
Concrete tank waste	*
Steel tank	*

* Artificial small value (1×10^{-5}) used to effectively neglect diffusive resistance.

5.3 Sorption data for cementitious waste materials

As the concrete degrades, its sorption capability is also affected, due to the pH evolution associated with cement leaching. Therefore, different K_d values are used for different time periods. The evolution of K_d values for waste packages is assumed to follow the evolution of K_d values for the barriers in the respective repository (as described in Chapters 6 to 11). Due to the expected presence of complexing agents the effective sorption in the cementitious materials is expected to be reduced. This is represented by means of sorption reduction factors (SRF) (Keith-Roach et al. 2021). The same SRF values are applied for the waste packages as for the barrier materials in the corresponding vaults (see Chapters 6 to 11).

The cement fraction for packaging concrete (0.219 kg/kg) is given directly in the input data (**Data report**). The average cement fraction in cement-solidified waste (0.6 kg/kg) and concrete-embedded waste (0.1 kg/kg) is estimated as a representative average for the waste packages as described in Appendix A in the **Radionuclide transport report**. The total amount of cement in packaging concrete (mould walls) decreases over time as the porosity increases. This is considered in the modelling, while the porosities of cement-solidified and concrete-embedded waste are assumed to be constant over time and thus also the amount of cement is constant in these wastes.

6 Silo model

The silo contains most of the activity in SFR and therefore has the most advanced barriers.

Figure 6-1 shows an illustration of the silo. The silo consists of a cylindrical vault within which a cylinder of reinforced concrete has been built. Inside this concrete cylinder are several shafts separated by concrete walls. These shafts are filled with waste and are thereafter grouted. The outer wall of the silo is surrounded by bentonite, creating a watertight barrier between the silo and the bedrock. The lower part of the silo consists of a slab of reinforced concrete founded on a bed of sand mixed with bentonite. The top of the silo also consists of a slab of concrete covered with a layer of sand-bentonite mixture. The empty space above the silo will be filled with crushed rock. A detailed description of the silo is given in the **Initial state report**.

6.1 Radionuclide inventory

Figure 6-2 shows the best estimate (deterministic value) of the total initial radionuclide inventory in the silo compared with the total inventory in SFR. Figure 6-3 shows the distribution over *model waste types* for the initial radionuclide inventory in the silo.

Figure 6-1. *Illustration of the silo during the operational period.*

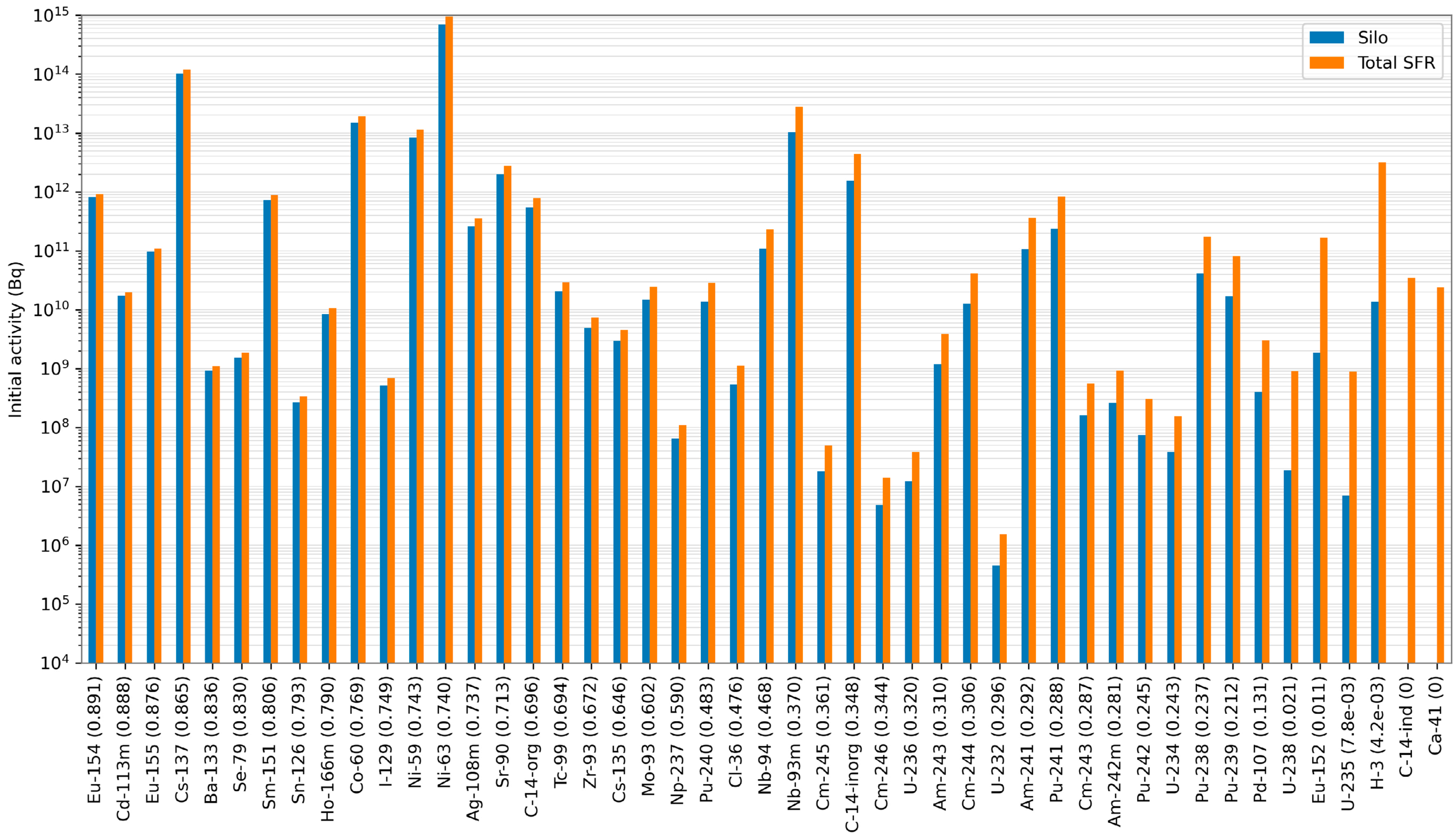

Figure 6-2. *Radionuclide inventory in the silo. The figure shows the inventory in the silo (blue bars) and the total inventory in SFR (orange bars). The bars are ordered so that the radionuclides with the largest fractions are shown to the left. The fraction is shown within parentheses after the radionuclide name.*

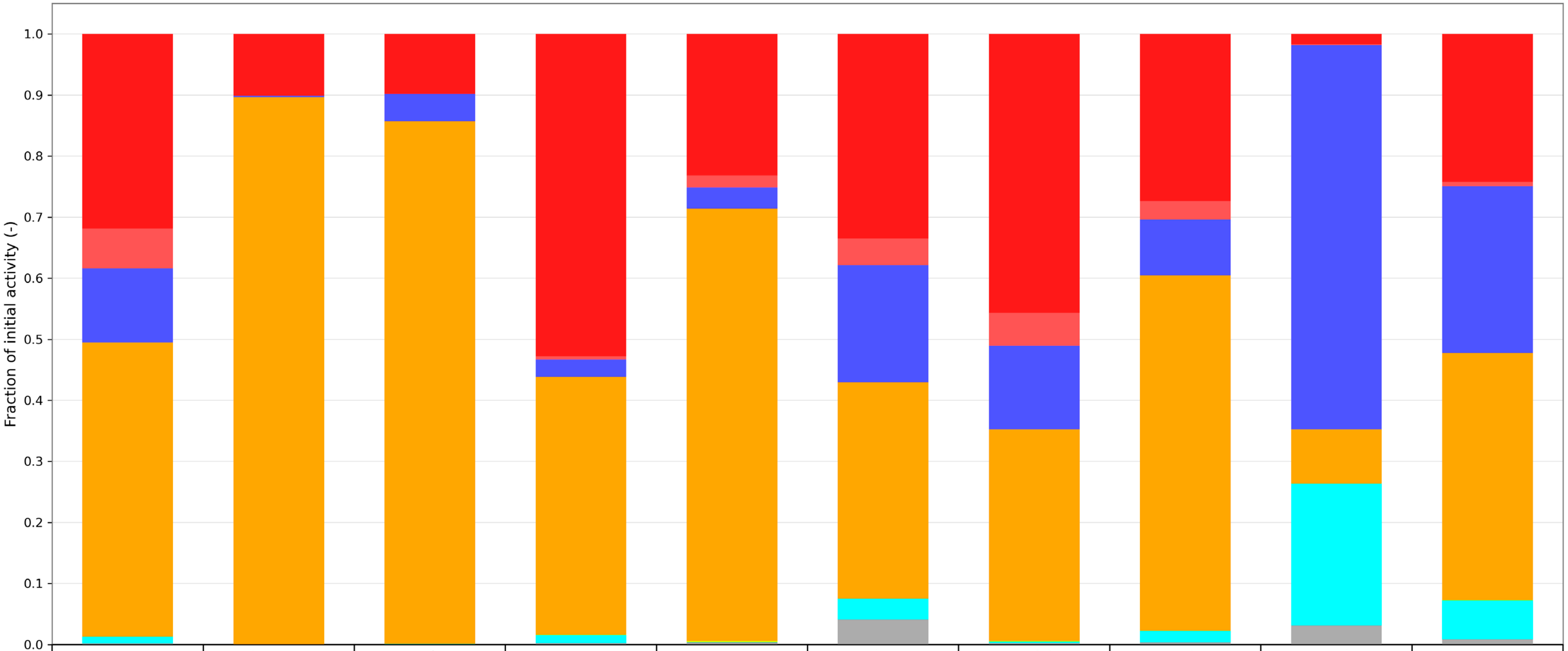

	Mo-93	C-14-org	C-14-inorg	Ni-59	Cs-135	Cl-36	I-129	Tc-99	U-235	U-238
CM_Ce	0.319	0.101	0.098	0.528	0.231	0.335	0.457	0.274	0.017	0.242
CM_Co	0.065	0.000	0.000	0.005	0.020	0.043	0.054	0.030	0.001	0.007
SM_Bi	0.121	0.002	0.045	0.029	0.035	0.192	0.137	0.092	0.630	0.273
SM_Ce	0.482	0.896	0.856	0.422	0.708	0.354	0.347	0.582	0.089	0.405
SM_Co	0.000	0.000	0.000	0.000	0.002	0.000	0.001	0.000	0.000	0.000
DrumBi	0.011	0.000	0.000	0.013	0.001	0.034	0.003	0.018	0.232	0.064
DrumCe	0.002	0.000	0.001	0.002	0.004	0.041	0.002	0.004	0.031	0.009

Figure 6-3. *Fraction of radionuclide inventory per model waste type in the silo. See Table 5-1 for an explanation of the names of the model waste types. The figure shows a subset of the radionuclides that are expected to be of largest importance in the safety assessment.*

6.2 Handling of waste

Table 6-1 shows the number of waste packages in the silo. The number of waste packages, together with waste package data on cement and radionuclide content, are used in the model to calculate total amount of cement and initial amounts of radionuclides in the waste. The mapping between *real waste types* and *model waste types* in the silo model is given in Table 6-2. An explanation of the abbreviations used for *real waste types* can be found in SKB (R-18-07, Chapter 2 (in Swedish); R-15-15, Chapter 2 (in English)).

Table 6-1. Number of waste packages in the silo model. The waste is evenly distributed vertically over the five layers of waste in the model shown in Figure 6-4.

Model waste type	Number of packages in inner (9) shafts	Number of packages in outer shafts
CM_Ce	108	3717
SM_Ce	0	3368
CM_Co	0	307
SM_Co	0	187
DrumCe	752	1039
DrumBi	1776	0
SM_Bi	863	0

Table 6-2. Mapping of real waste types to model waste types (Table 5-1) in the silo model.

Real waste type	Model waste type
C.24:00_20, C.24:00_29, E.24:00_33_RINGHALS, V.24:00_33	CM_Co
B.04:00_205, B.04:D_205, S.04:00_206, S.04:00_206_Svafo, S.04:00_210	DrumCe
E.24:00_53_RINGHALS	SM_Co
F.18:00_51, F.18:D_51	SM_Bi (inner shafts)
R.02:09_23, O.02:09_30	CM_Ce (inner shafts)
B.04:00_205, S.04:00_206_Svafo, S.04:00_206	DrumCe (inner shafts)
C.02:00_30, O.02:00_30_CLAB, O.02:00_30, O.02:09_0, O.02:09_20, O.02:09_30, O.02:09_30_CLAB, R.02:00_30, R.02:09_13, R.02:09_23	CM_Ce
B.06:00_205	DrumBi (inner shafts)
C.16:D_50, O.16:D_50, R.16:00_50, R.16:D_50, S.11:00_50_Svafo, R.24:00_10, R.24:00_30	SM_Ce

6.3 Compartment structure

The silo model is built as a 2-dimensional axisymmetric model, i.e., radionuclide transport is modelled in the radial and axial directions as shown in Figure 6-4. For the silo, a level of detail for control volumes has been chosen where the vertical shafts are grouped into inner and outer control volumes. Vertically, the silo is divided in ten layers: five layers representing the waste domain (inner and outer), one layer each for sand/bentonite at the top and bottom, one layer each for the concrete lid and slab, and one layer of backfill at the top of the silo.

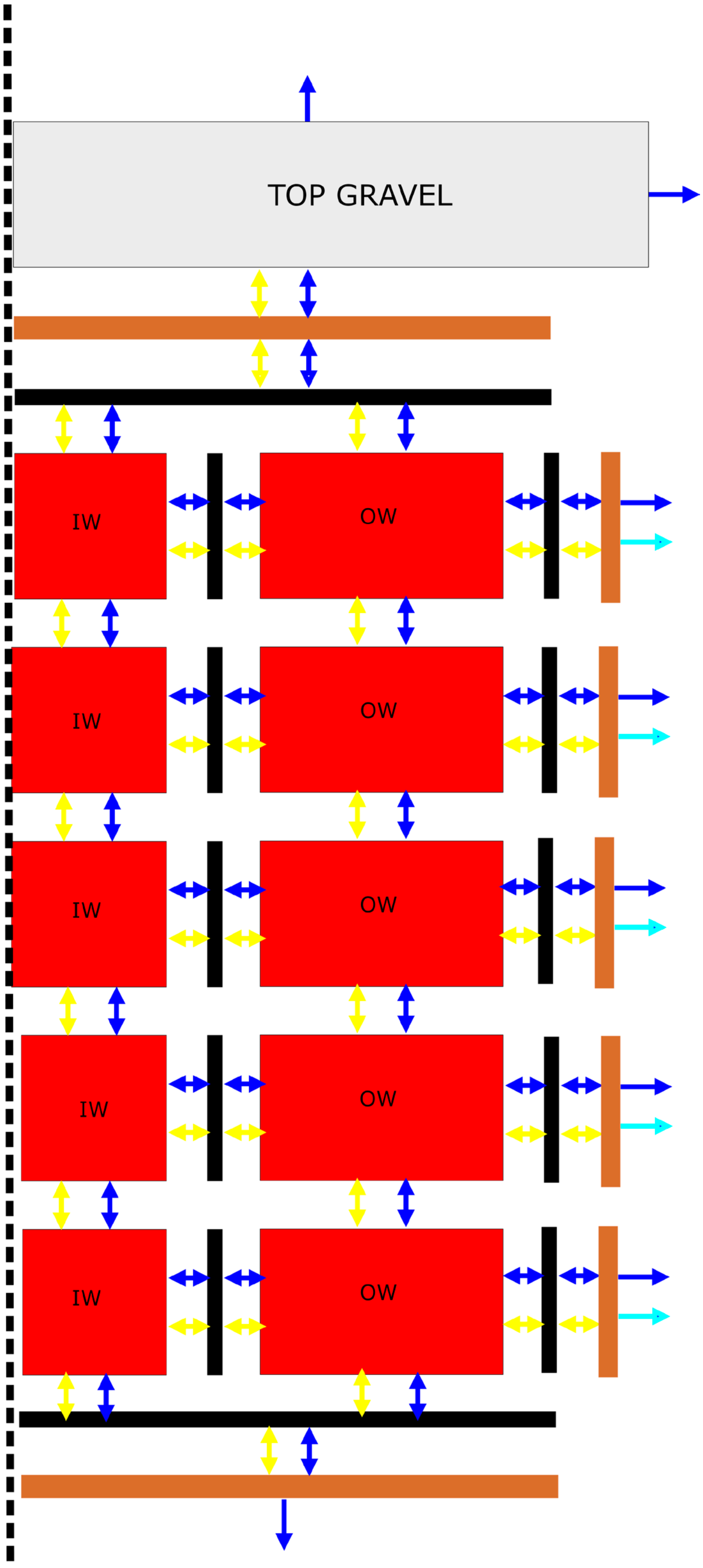

Figure 6-4. Conceptual illustration of the compartment model for the silo. From the top down the parts are: the top crushed rock backfill (grey), the top sand-bentonite layer (brown), the concrete lid (black), the five (identical) vertical layers of the waste (red), the concrete bottom slab (black) and the bottom sand-bentonite layer (brown). From left to right (radial direction) the parts are: inner waste (red), wall between inner and outer waste (black), outer waste (red), concrete wall (black) and bentonite (brown). Between each part there are advective (blue arrows) and diffusive transfers (yellow arrows). From the top and bottom there are advective transfers to the bedrock. From the silo mantle there is assumed to be both advective and diffusive transfers to the bedrock. The diffusive transfers (cyan arrows) are modelled with the Qeq concept (Equation 2-8).

Each of the five layers of the waste domain is divided in two parts, an inner and an outer part (Figure 6-5). The inner part (upper left) represents the nine inner shafts of the silo, where mainly bituminised waste is disposed. The outer part (lower right) represents all the other shafts. Transport of radionuclides from the waste takes place by advection (blue arrows) and diffusion (yellow arrows). The advection is cautiously only accounted for in the direction out from the waste.

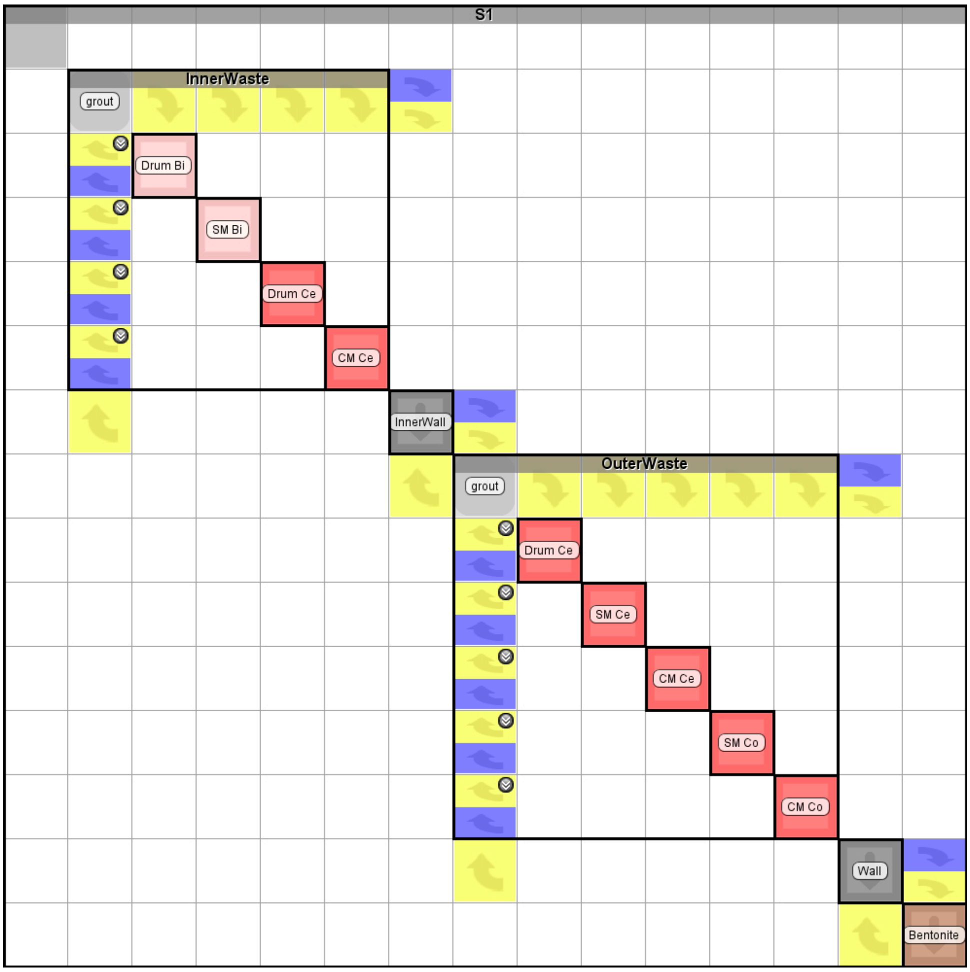

Figure 6-5. *The figure shows a representation of one of the five equal waste layers in the silo model in Ecolego. The picture shows the bitumen- and cement-solidified waste packages in the inner nine shafts (InnerWaste), the shaft walls surrounding the inner waste (InnerWall) and various cement/concrete conditioned waste packages in the outer shafts (OuterWaste). The inner wall as well as the outer wall and bentonite are divided into five compartments each. The represented waste packages are: Bituminised waste in drums (Drum Bi), Bituminised waste in steel moulds (SM Bi), cement-solidified waste in steel drums (Drum Ce), cement-solidified waste in steel containers (SM Ce), cement-solidified waste in concrete moulds (Cm Ce), concrete-embedded waste in steel moulds (SM Co) and concrete-embedded waste in concrete moulds. See Section 5.1 for further description of the model waste types.*

6.4 Dimensions

Table 6-3 shows the dimensional parameters used in the silo model.

Table 6-3. Parameters for dimensions in the silo model.

Name	Value (m)	Description
bentonite_zone_height	1.5	Thickness of sand/bentonite layers (same value for top and bottom)
concrete_wall_radius	13.8	Concrete wall radius
shaft_height	51.3	Shaft height
shaft_zone_radius	13.0	Shaft zone radius
silo_structure_radius	14.7	Silo structure radius
thickness_reinforced_floor	0.9	Thickness of reinforced bottom slab
thickness_shaft_walls	0.2	Thickness shaft walls
top_lid_thickness	1.0	Top lid thickness
shaft_side_length	2.55	Shaft side length
gravel_height	8.4	Crushed rock height in top above the silo

Table 6-4 shows the L/A values as calculated in the silo model. The values are shown for each section and for the radial (R) and vertical (V) directions. The L/A values are further divided with effective diffusivities in the model to calculate diffusive resistances as described in Equation 2-5.

Table 6-4. L/A values for the silo model.

Section	Part	Direction	Area (m^2)	Length (m)	Number of comp.	L/A (m^{-1} per comp.)
Top	Bentonite	V	679 ($\pi \times 14.7^2$)	1.5	1	0.0022
Top	Lid	V	679 ($\pi \times 14.7^2$)	1.0	5	0.0003
1–5	Inner Grout	V	59 ($2.55^2 \times 9$)	10.3 (51.3/5)	1	0.1437
1–5	Inner Grout	R	-	-	1	0*
1–5	Inner Wall	R	314 ($2.55 \times 12 \times 51.3/5$)	0.20	5	0.0001
1–5	Outer Grout	V	620 (679-59)	10.3 (51.3/5)	1	0.0223
1–5	Outer Grout	R	-	-	1	0*
1–5	Outer Wall	R	890 ($2 \times \pi \times 13.8 \times 51.3/5$)	0.8	5	0.0002
1–5	Bentonite	R	890 ($2 \times \pi \times 13.8 \times 51.3/5$)	0.9	5	0.0002
Bottom	Slab	V	679 ($\pi \times 14.7^2$)	0.9	5	0.0003
Bottom	Bentonite	V	679 ($\pi \times 14.7^2$)	1.5	1	0.0022

* No diffusive resistance in grout is accounted for in the radial direction.

6.5 Sorption data

Initially all cementitious materials in the silo are in chemical degradation state I, which persists until 34 000 AD after which degradation state II applies for the rest of the assessment period. K_d values for the different degradation states are given in Figure 4-4. The structural concrete in the silo contains a cement fraction of 0.219 (kg/kg) and the grout contains a cement fraction of 0.267 (kg/kg) (**Data report**). The sorption in the silo is reduced by complexing agents expected to be present in the vault. This is modelled by means of sorption reduction factors (Keith-Roach et al. 2021). The radionuclides are divided into five groups depending on how much they are influenced by complexing agents (Table 4-2). In the silo it is assumed that complexing agents reduce sorption on bentonite in a similar way as they reduce sorption on cement, however, to a lesser extent as the concentration of complexing agents is lower in the bentonite. The SRFs for most groups are unity at all times except for group 3 and group 4. The evolution over time for the SRFs in Group 3 and Group 4 is shown in Table 6-5.

Table 6-5. Sorption reduction factors (SRF) used in the silo model.[a]

Media	SRF Group[b]					
	Group 3			Group 4		
	Start value[c]	End value[c]	End time[c] (AD)	Start value	End value	End time (AD)
Bentonite	53	1	17 450	49	1	17 450
Cement	179	1	22 450	98	1	22 450

[a] SRF Groups 1, 2 and 5 have SRF = 1 in the silo throughout the assessment period.

[b] The radionuclides contained in each SRF Group are given in Table 4-2.

[c] The SRF value varies linearly between the given start and end value and becomes constant (= end value) after the given end time.

6.6 Physical transport parameters

Figure 6-6 (upper panel) shows the total water flow through the silo and the flow through the waste domain. The initial rise in flow is due to the increase in hydraulic gradient as the shoreline passes the repository due to shoreline regression. The figure shows the total flow as calculated in the RNT model, interpolated from values taken from Abarca et al. (2020) with uncertainty factors from Table 4-1 applied. Note that the physical degradation state indicated by the blue colour-bar in Figure 6-6 only affects the concrete in the silo. The bentonite, which is the main flow barrier, is assumed to be intact during the whole assessment period.

Figure 6-6 also shows the effective diffusivities (middle panel) of radionuclides and porosities (bottom panel) of the materials in the silo model. These time-dependent values are used in the calculations of capacity and diffusive resistances as described in Equation 2-2 and Equation 2-5.

6.6.1 Data for equivalent water flow

The parameters for Q_{eq} (Equation 2-8) that governs the diffusion from the silo bentonite into the bedrock are shown in Table 6-6 and described in Abarca et al. (2014, Appendix E).

Table 6-6. Parameter values for calculation of the equivalent flow Q_{eq}.

Parameter	Value (unit)	Description
A_w	5×10^3 (m^2)	Area of interface between bentonite and rock
ε_{rock}	2.3×10^{-5} (-)	Flow porosity averaged from hydrogeological data
D_w	2×10^{-9} ($m^2\ s^{-1}$)	Diffusivity in water
L	50 (m)	Approximate path-length for water seeping along the silo

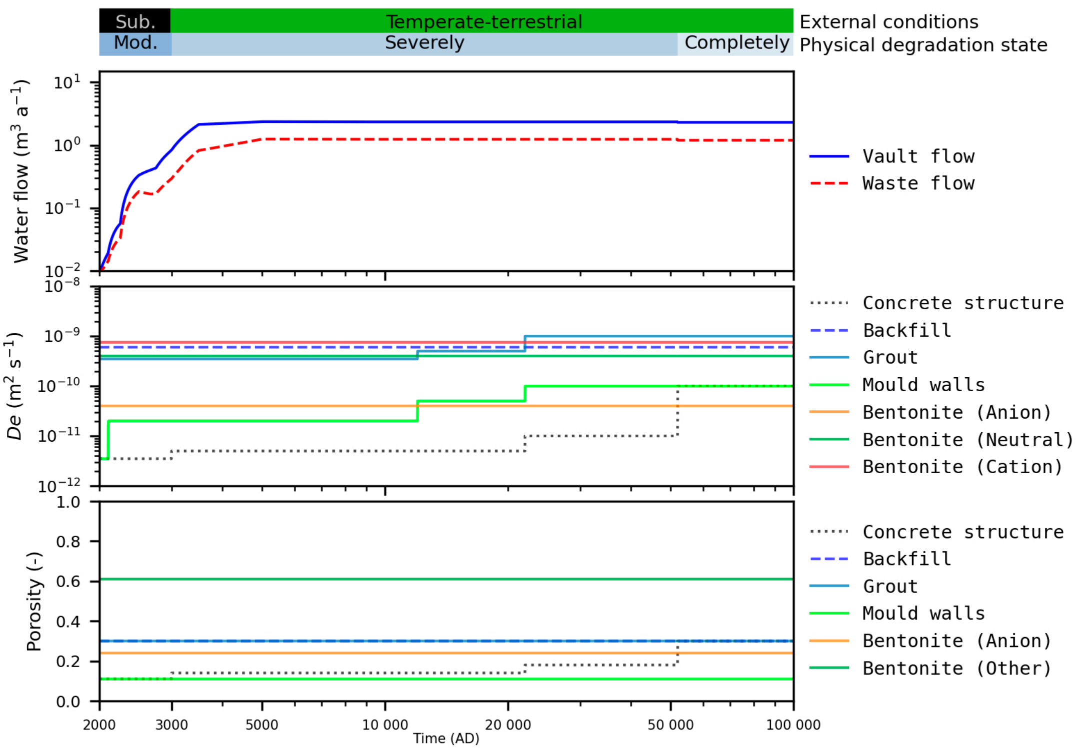

Figure 6-6. *Upper panel: Water flow through the whole silo vault (Vault flow) and through the waste domain (Waste flow). Middle and bottom panels show effective diffusivity and porosity as a function of time for the materials in the silo.*

6.7 Releases in the base case

Figure 6-7 shows the radionuclide releases from the silo in the *base case* compared with the total releases from SFR. The release from the silo gives a large contribution to the total releases from SFR for non-sorbing or weakly sorbing radionuclides such as Se-79, I-129, C-14-org, Mo-93 and Ag-108m. On the other hand, for strongly sorbing radionuclides, such as the actinides, the barriers of the silo are very effective and those radionuclides do not reach significant release levels.

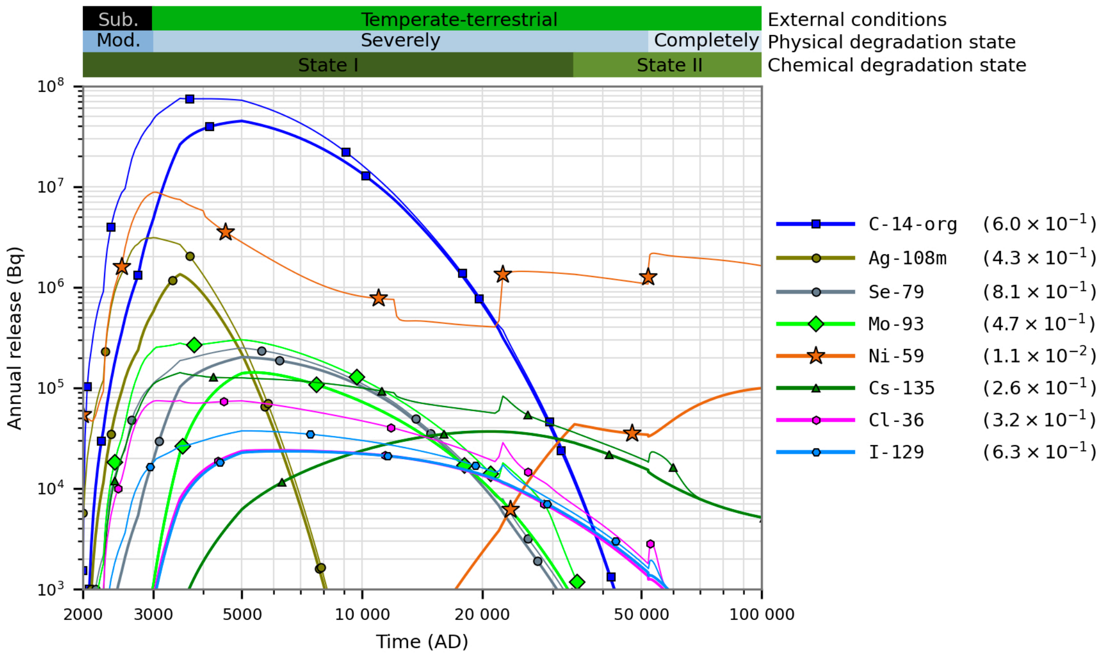

Figure 6-7. *Releases from the silo (thick lines) compared with releases from the whole SFR (thin lines). The colour bars in the upper part of the figure show the evolution of the external conditions and of the concrete physical and chemical degradation, respectively. It should be noted that the physical and chemical degradation states shown in the coloured bar only affects the cementitious materials in the silo, the bentonite is assumed to retain its initial properties over the whole assessment period. The evolution of water flow, diffusivity and porosity are shown in Figure 6-6. The values in parentheses show the ratio of the maximum silo release to the maximum of the total release from SFR.*

7 1BMA model

The existing waste vault for intermediate-level waste (1BMA) consists of a concrete structure with 15 sections (13 large and 2 small ones) separated by concrete walls. Each section contains several waste packages. At closure, the concrete structure will be covered with a lid and concrete slabs, so that the waste will be completely encased in concrete barriers. The space between waste packages will be left empty.

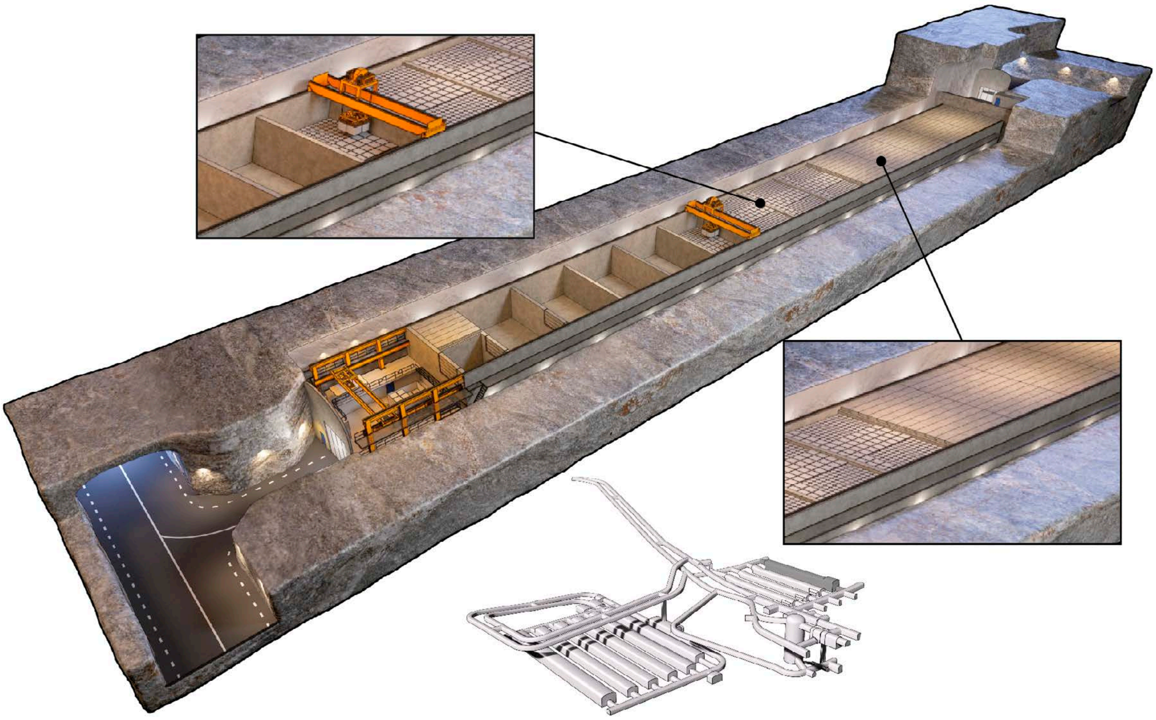

Figure 7-1. *Illustration of 1BMA during the operational period. The upper detail shows the emplacement of waste packages, the lower detail shows the concrete lid. In addition, there is a view of SFR with the position of 1BMA highlighted.*

When the operational period is complete, an additional concrete structure is planned to be cast around the existing 1BMA concrete structure, see Figure 7-2. A detailed description of 1BMA is given in the **Initial state report.**

For the 1BMA model, a discretisation has been chosen to allow each of the 13 large sections to be represented separately, whereas the two small sections are represented by one section in the compartment model. For each section, the model also includes four compartments for the crushed rock backfill. The backfill in each end of the vault is also represented in the model by one compartment each. Figure 7-3 shows the control volumes for 1BMA used in the hydrological and RNT calculations. The outer parts (walls, lid and bottom) of the concrete structure have been discretised into 5 compartments each. In the concrete structure only transport *through* the walls is considered, i.e., no lateral transport inside the wall is included.

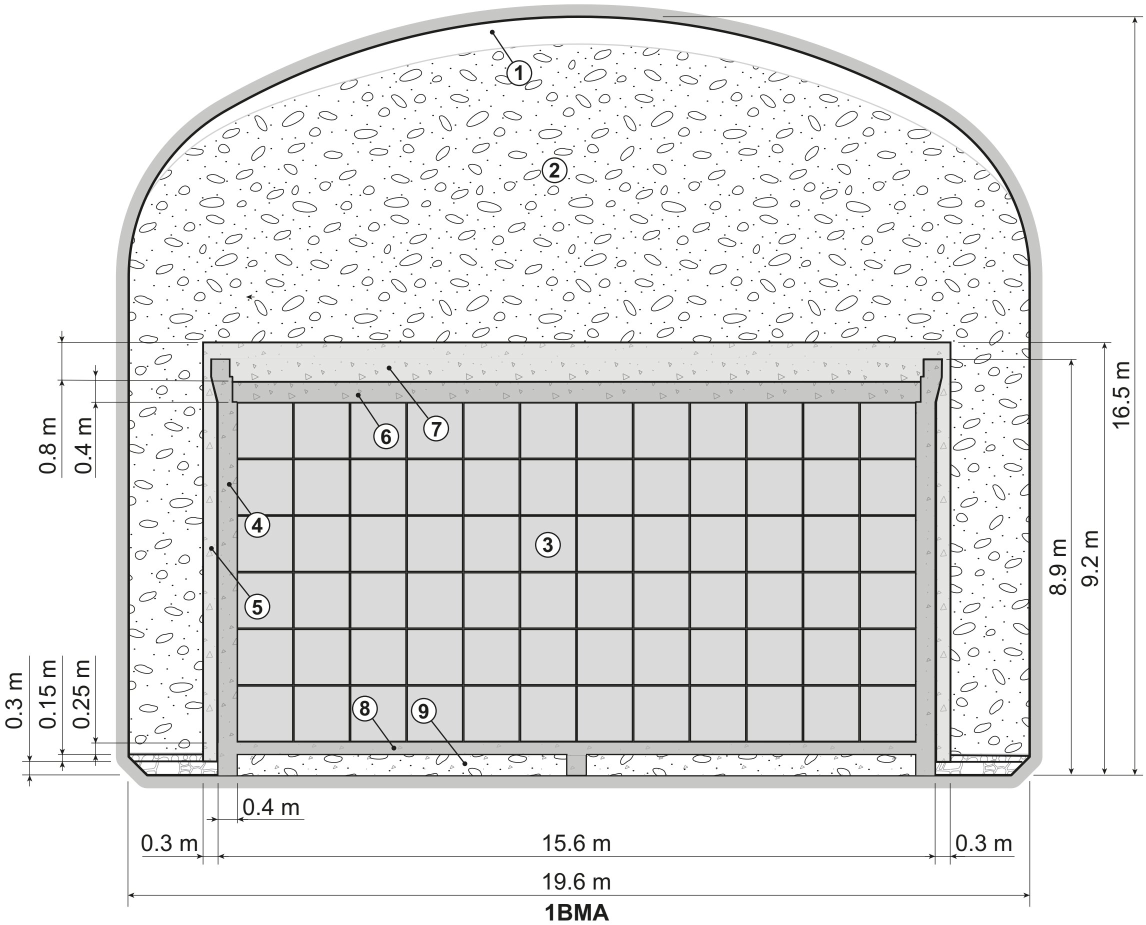

Figure 7-2. *Cross section of the 1BMA vault showing the present concrete structure surrounded by the planned additional concrete structure and the crushed rock backfill. Key to numbering: 1) Void 2) Macadam backfill 3) Waste domain 4) Existing outer wall 5) New outer wall 6) Pre-fabricated concrete element 7) New concrete lid 8) Slab 9) Crushed rock.*

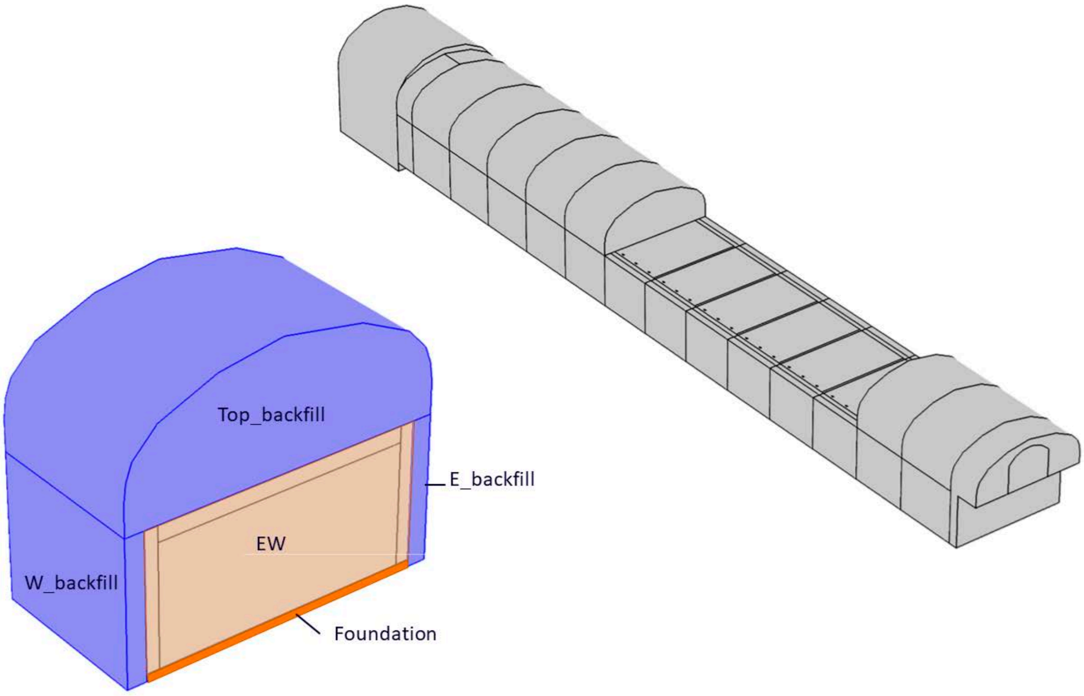

Figure 7-3. *Control volumes for 1BMA in the hydrological model (Abarca et al. 2020).*

7.1 Radionuclide inventory

Figure 7-4 shows the total initial radionuclide inventory (best estimate) in 1BMA compared with the total radionuclide inventory in SFR. Figure 7-5 shows the distribution over *model waste types* for the initial radionuclide inventory in 1BMA.

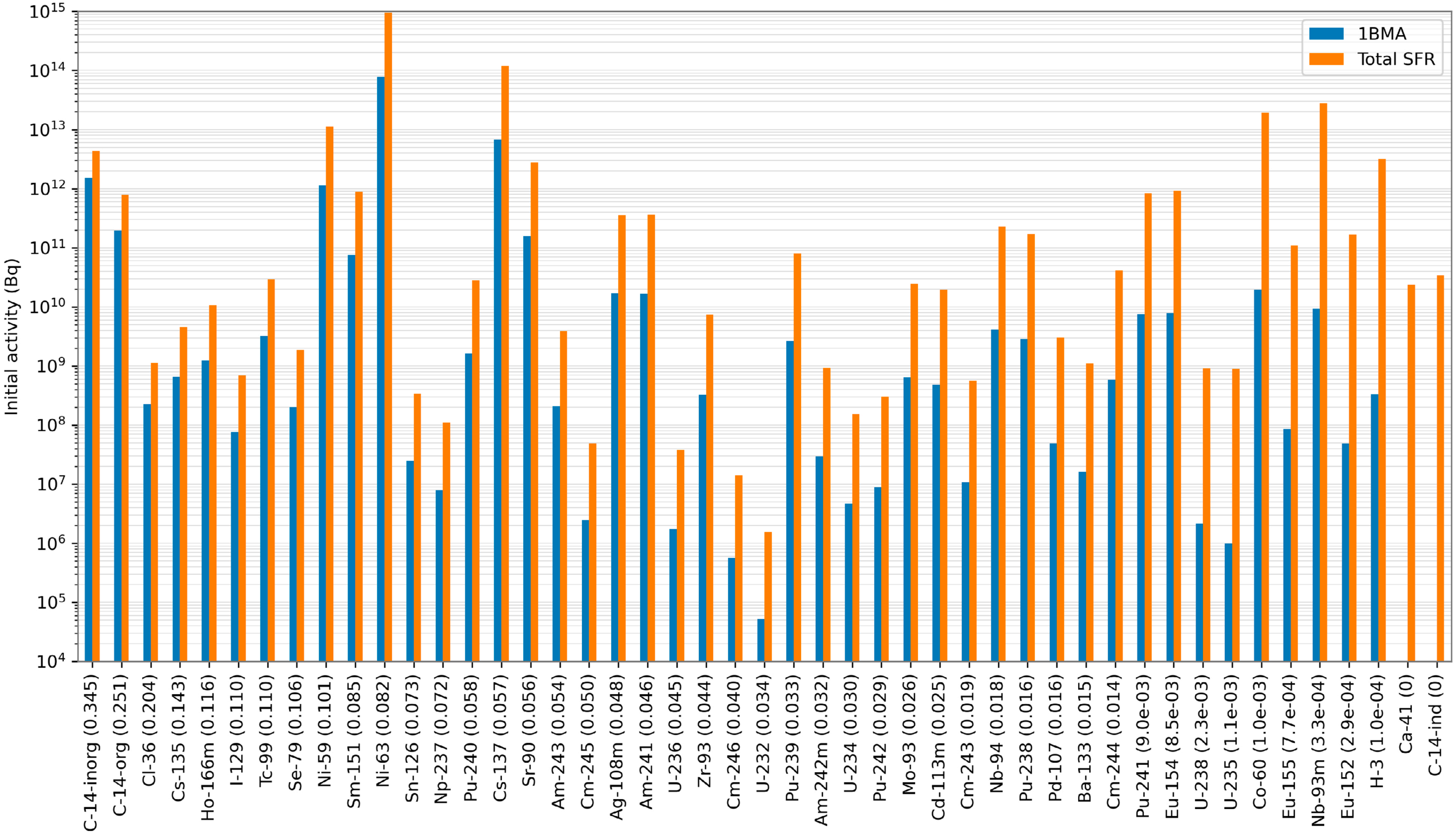

Figure 7-4. *Inventory of radionuclides in 1BMA. The figure shows the inventory in 1BMA (blue bars) and the total inventory in SFR (orange bars). The bars are ordered so that the radionuclides with the largest fractions are shown to the left. The fraction is shown within parentheses after the radionuclide name.*

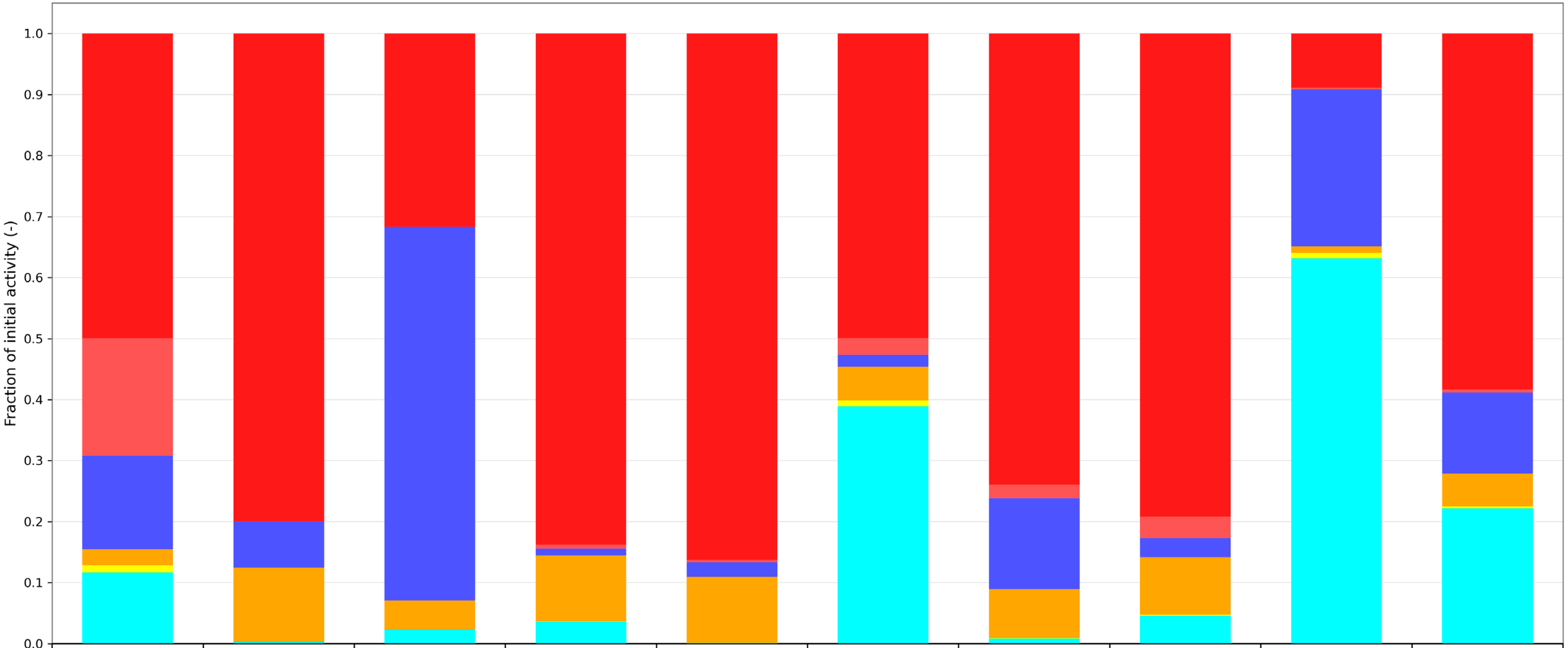

	Mo-93	C-14-org	C-14-inorg	Ni-59	Cs-135	Cl-36	I-129	Tc-99	U-235	U-238
CM_Ce	0.499	0.800	0.317	0.838	0.863	0.499	0.739	0.792	0.089	0.583
CM_Co	0.193	0.000	0.000	0.006	0.004	0.028	0.022	0.035	0.002	0.005
SM_Bi	0.153	0.076	0.613	0.011	0.024	0.020	0.149	0.031	0.257	0.133
SM_Ce	0.026	0.122	0.048	0.108	0.108	0.054	0.080	0.094	0.011	0.054
SM_Co	0.012	0.000	0.000	0.001	0.000	0.010	0.001	0.002	0.008	0.003
DrumBi	0.117	0.003	0.023	0.036	0.001	0.389	0.008	0.045	0.632	0.222
DrumCe	0.000	0.000	0.000	0.000	0.000	0.000	0.000	0.000	0.000	0.000

Figure 7-5. *Fraction of radionuclide inventory per model waste package type in 1BMA. See Table 5-1 for an explanation of the model waste types. The figure shows a subset of the radionuclides that are expected to be of largest importance in the safety assessment.*

7.2 Handling of waste

Table 7-1 shows the number of waste packages in 1BMA. The number of waste packages, together with waste package data on cement and radionuclide content, are used in the model to calculate total amount of cement and initial amounts of radionuclides in the waste. The mapping between *real waste types* and *model waste types* in the 1BMA model is given in Table 7-2. An explanation of the abbreviations used for *real waste types* can be found in SKB (R-18-07, Chapter 2 (in Swedish); R-15-15, Chapter 2 (in English)).

Table 7-1. Number of waste packages in 1BMA.

Model waste type	Section	Number of packages	Model waste type	Section	Number of packages
CM_Ce	S1	576	SM_Bi	S13	42
CM_Ce	S2	148	SM_Bi	S14	163
CM_Ce	S3	144	SM_Ce	S1–S3	0
CM_Ce	S4	344	SM_Ce	S4	132
CM_Ce	S5	144	SM_Ce	S5	0
CM_Ce	S6	144	SM_Ce	S6	3
CM_Ce	S7	528	SM_Ce	S7	0
CM_Ce	S8	258	SM_Ce	S8	80
CM_Ce	S9	393	SM_Ce	S9	16
CM_Ce	S10	205	SM_Ce	S10	0
CM_Ce	S11	48	SM_Ce	S11	113
CM_Ce	S12	12	SM_Ce	S12–S14	0
CM_Ce	S13–S14	0	SM_Co	S1–S3	0
CM_Co	S1–S3	0	SM_Co	S4	15
CM_Co	S4	85	SM_Co	S5–S6	0
CM_Co	S5–S6	0	SM_Co	S7	10
CM_Co	S7	38	SM_Co	S8	88
CM_Co	S8	150	SM_Co	S9	0
CM_Co	S9	167	SM_Co	S10	61
CM_Co	S10	156	SM_Co	S11	32
CM_Co	S11	103	SM_Co	S12–S14	0
CM_Co	S12–S14	0	DrumBi	S1	0
SM_Bi	S1–S2	0	DrumBi	S2	2094
SM_Bi	S3	144	DrumBi	S3	1438
SM_Bi	S4	0	DrumBi	S4	0
SM_Bi	S5	28	DrumBi	S5	2096
SM_Bi	S6	259	DrumBi	S6	336
SM_Bi	S7–S9	0	DrumBi	S7–S14	0
SM_Bi	S10	144	DrumCe	S1–S5	0
SM_Bi	S11	9	DrumCe	S6	2
SM_Bi	S12	42	DrumCe	S7–S14	0

Table 7-2. Mapping of real waste types to model waste types in the 1BMA model.

Real waste type	Model waste type
F.23:00_50	SM_Co
O.01:09_20, O.01:09_30_CLAB, O.01:09_30, R.01:00_30, R.01:09_13, R.01:09_20, R.01:09_23, R.01:09_30, R.10:00_10, R.10:00_13, R.10:00_20, R.10:00_23, R.10:00_30, R.29:00_30, R.23:00_10, R.23:00_13, R.23:00_20, R.23:00_23, R.23:00_24, R.23:00_29, R.23:00_30, B.23:00_32	CM_Ce
C.23:00_20, F.23:00_10, F.23:00_20, O.23:00_0, O.23:00_20_CLAB, O.23:00_20, O.23:09_0, O.23:09_10, O.23:09_20	CM_Co
B.05:09_205, B.05:02_205, B.05:00_205, F.05:02_205, F.05:01_205	DrumBi
F.17:00_50, F.17:00_51, F.17:01_50, F.17:01_51, F.17:02_51, R.99:02_28	SM_Bi
B.23:00_52, R.23:00_52, F.15:00_50, R.15:00_50	SM_Ce
F.99:01_50	DrumCe

7.3 Compartment structure

Figure 7-6 shows the Ecolego model for 1BMA. The left panel shows an overview of the whole model which is subdivided into 14 subsystems for the waste domain and one subsystem each for the south and north end. The right panel shows one section of the waste domain in 1BMA. The section contains a compartment for the inner wall connecting to one of the neighbouring sections and transport blocks (see Section 3.4) for the outer concrete barriers i.e. the lid, the two side walls and the slab. The backfill at the top, the sides and the bottom is represented with one compartment each.

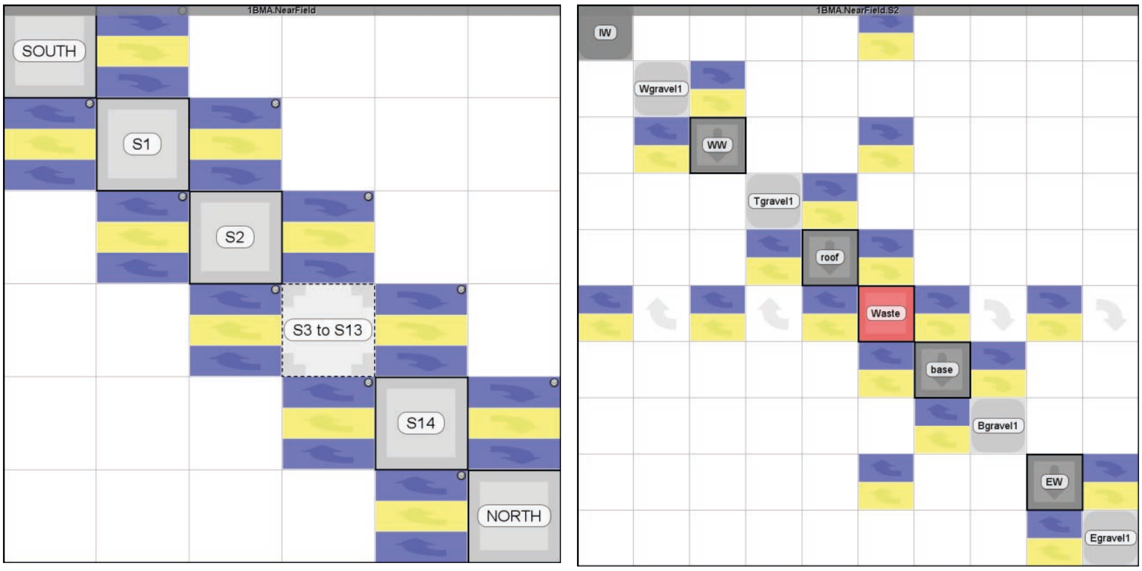

Figure 7-6. Left panel: The Ecolego model for the near-field of 1BMA. The figure shows the subsystem for the backfill in the south end of the 1BMA vault the 14 sections/subsystems and the subsystem for the backfill in the north end (reloading zone). The subsystems S3 to S13 are grouped using the group block in Ecolego (see Section 3.3). Right panel: One section of the 1BMA model in Ecolego with inner wall (IW) connecting to the next section, crushed rock backfill on the west side (Wgravel1), concrete wall on west side (WW), crushed rock backfill on top (Tgravel1), prefabricated lid and cast lid (roof), area with waste packages (waste) shown in more detail in Figure 7-7, concrete slab (base), crushed rock foundation (Bgravel1), concrete wall on east side (EW), crushed rock backfill on east side (Egravel1). The blue squares with arrows represent advective transfer, the yellow squares with arrows represent diffusive transfer and the white squares with arrows represent transfer via flow through cracks in the barrier.

Figure 7-7 shows a more detailed view of the waste packages in one section. Eight different types of model waste packages are represented in the model. In addition to the waste packages, a compartment representing the water in the void in the waste domain is included.

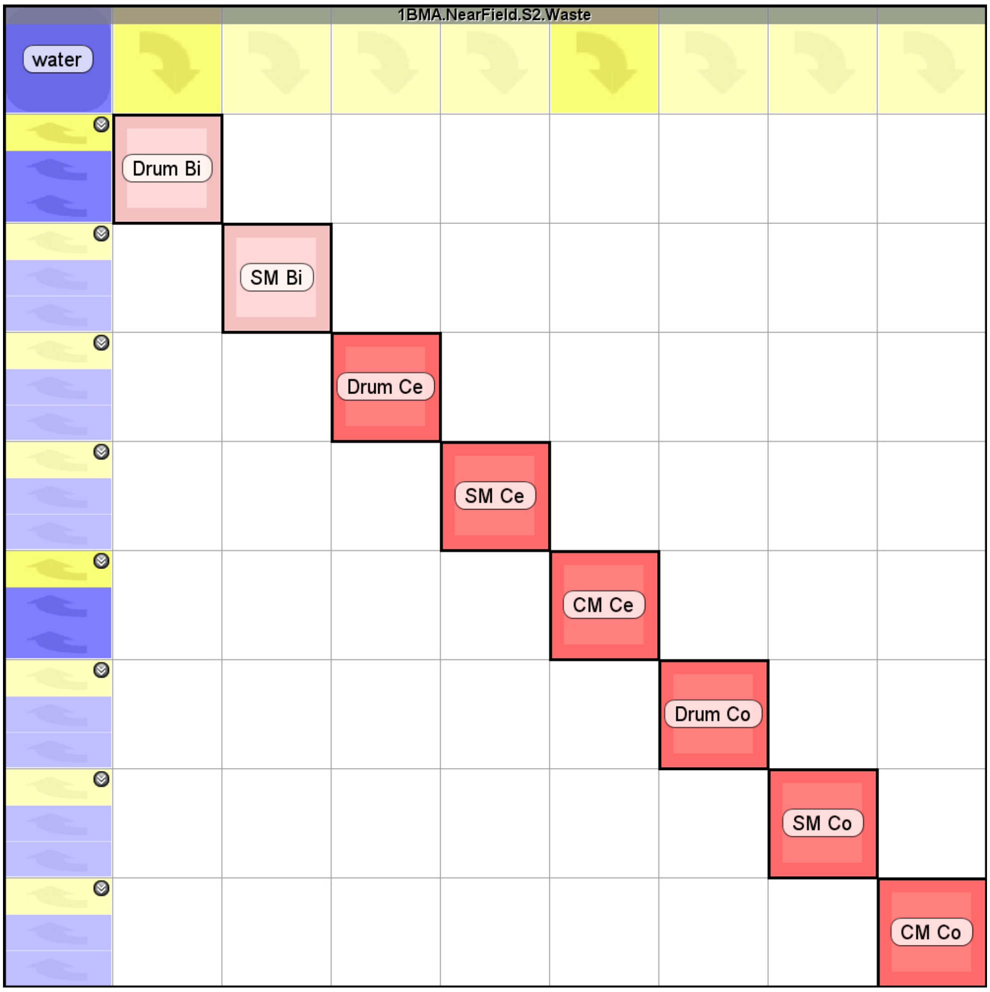

Figure 7-7. *One waste section in Ecolego*[3] *with a compartment representing the water that fills the void in the waste domain after saturation (water)), drums with bituminised waste (Drum_Bi), steel moulds with bituminised waste (SM_Bi), drums with cement-solidified waste (Drum_Ce), steel moulds with cement-solidified waste (SM_Ce), concrete moulds with cement-solidified waste (CM_Ce), drums with concrete-embedded waste (Drum_Co), steel moulds with concrete-embedded waste (SM_Co), concrete moulds with concrete-embedded waste (CM_Co). Note that the model allows all 8 types of waste packages to be modelled in all sections. However, most sections contain only a few types. The transfers for package types that are not present in the actual section are disabled in the model and are shown with a lighter tone in the figure. See Section 5.1 for further description of the model waste types (this approach is used only in the 1BMA model).*

[3] Note that the water flow for e.g. the waste packages is given in three dimensions, advective transfers for each direction are represented separately in the model. Hence, there are six blue arrows connecting the waste packages to the water. However, Ecolego shows a limited number of arrows on the of diagonal element in the matrix. When there are more transfers a downward pointing arrow is shown in the upper right corner of the matrix element to indicate that there are more transfers than shown in the matrix.

7.4 Dimensions

Table 7-3 shows the dimensional parameters used in the 1BMA model.

Table 7-3. Parameters for dimensions in the 1BMA model.

Name	Value (m)	Description
bottom_gravel_height	0.45	Thickness of crushed rock in bottom
bottom_thickness	0.25	Thickness of bottom concrete slab
cs_height	8.75	Concrete structure height
cs_width	16.22	Concrete structure width
lid_thickness	1.2	Thickness of concrete structure on top
long_compartment_length	9.9	Inner length of each section number 1–13
north_gravel_length	14.9	Length of crushed rock backfill in north end, facing vault BST
short_compartment_length	4.95	Inner length of section number 14/15
south_gravel_length	4.65	Length of crushed rock backfill in south end, facing vault 1TT
wall_thickness	0.7	Thickness of the walls on sides and ends (except north wall)
vault_height	15.3	Mean vault height
vault_width	19.6	Width of the vault
north_wall_thickness	0.9	North wall thickness
i_wall_thickness	0.4	Thickness of inner walls (also applicable for the old side walls)

L/A values used for the concrete structure are given in Table 7-4. The table also gives the number of compartments used in the model to represent each part of the barrier. The outer concrete walls are represented by 5 compartments each. The inner walls between the sections are represented by only one compartment each. The L/A values are further divided with effective diffusivities in the model to calculate diffusive resistances as described in Equation 2-5.

Table 7-4. L/A values for the concrete structures in the 1BMA model.

Section	Part	Area (m^2)	Length (m)	Number of comp.	L/A (m^{-1} per comp.)
1	South wall	142 (8.75 × 16.22)	0.7	5	0.001
1–13	Roof	161 (9.9 × 16.22)	1.2	5	0.001
1–13	East wall	87 (9.9 × 8.75)	0.7	5	0.002
1–13	West wall	87 (9.9 × 8.75)	0.7	5	0.002
1–13	Slab	161 (9.9 × 16.22)	0.25	5	0.0003
1–13	Inner wall	142 (8.75 × 16.22)	0.4	1	0.003
14	Roof	80 (4.95 × 16.22)	1.2	5	0.003
14	East wall	43 (4.95 × 8.75)	0.7	5	0.003
14	West wall	43 (4.95 × 8.75)	0.7	5	0.003
14	Slab	80 (4.95 × 16.22)	0.25	5	0.001
14	North wall	142 (8.75 × 16.22)	0.9	5	0.001

For most of the parts of the backfill, transport is considered in several directions. L/A values for the backfill are given in Table 7-5. To designate the different directions, the following terms are used. "H" is the direction across the vault, "V" is the vertical direction, "L" is the direction along the long side of the vault. In Table 7-5, L in L/A refers to length in the considered direction and A refers to area across this direction. Only the L/A values used in the calculation are listed in the table. All the backfill compartments are represented by one compartment each.

Table 7-5. L/A values for the backfill in the 1BMA model.

Section	Part	Direction	Area (m^2)	Length (m)	L/A (m^{-1})
SOUTH	SBF[a]	L	300 (15.3 × 19.6)	4.65	0.02
1–13	Roof	V	194 (19.6 × 9.9)	6.1	0.03
1–13	Roof	L	120 (19.6 × (15.3 − 8.75 − 0.45))	9.9	0.08
1–13	East	H	87 (8.75 × 9.9)	1.7	0.02
1–13	East	L	14.8 (8.75 × (19.6 − 16.22)/2)	9.9	0.67
1–13	West	H	87 (8.75 × 9.9)	1.7	0.02
1–13	West	L	14.8 (8.75 × (19.6 − 16.22)/2)	9.9	0.67
1–13	Bottom	V	160.6 (16.22 × 9.9)	0.45	0.003
1–13	Bottom	L	7.3 (16.22 × 0.45)	9.9	1.36
14–15	Roof	V	97 (19.6 × 4.95)	6.1	0.06
14–15	Roof	L	120 (19.6 × (15.3 − 8.75 − 0.45))	4.95	0.04
14–15	East	H	43.3 (8.75 × 4.95)	1.7	0.04
14–15	East	L	14.8 (8.75 × (19.6 − 16.22)/2)	4.95	0.34
14–15	West	H	43.3 (8.75 × 4.95)	1.7	0.04
14–15	West	L	14.8 (8.75 × (19.6 − 16.22)/2)	4.95	0.34
14–15	Bottom	V	80.3 (16.22 × 4.95)	0.45	0.01
14–15	Bottom	L	7.3 (16.22 × 0.45)	4.95	0.68
NORTH	LZ[b]	L	300 (15.3 × 19.6)	14.9	0.05

[a] South tunnel end
[b] North tunnel end (loading zone)

7.5 Sorption data

Initially all cementitious materials in 1BMA are in chemical degradation state I until 12 000 AD when degradation state II is initiated, which remains the degradation state for the rest of the assessment time. K_d values for the different degradation states are given in Figure 4-4. The structural concrete in 1BMA contains a cement fraction of 0.182 (kg/kg) (**Data report**). The cement fraction for the existing structure is pessimistically used also for the enhancement. For the concrete in the planned enhancement the cement fraction is 0.197 (kg/kg). However, the new and old part of the concrete structure are not represented separately in the RNT model and thus the lower value is used for the whole structure, to not overestimate its sorption capacity. The sorption in 1BMA is reduced by complexing agents expected to be present in the vault. Individual SRFs have been defined for the 14 sections of the 1BMA model as shown in Table 7-6 (Keith-Roach et al. 2021).

Table 7-6 SRF values (-) used for different groups of radionuclides and sections in 1BMA in the base case.

Section	SRF Group[ac]							
	1	2	3 Linear function[b]			4 Linear function[b]		
			Start value	End value	End time (AD)	Start value	End value	End time (AD)
S1	1	1	1	1	-	1	1	-
S2	1	100	1	1	-	1	1	-
S3	1	100	653	1	11 100	141	1	11 100
S4	1.3	100	842	4	11 400	158	3	11 400
S5	1	1	20	1	5900	18	1	5900
S6	1	1	1 661	1	12 500	233	1	12 500
S7	1	100	1	1	-	1	1	-
S8	2	100	32	17	6950	29	16	6950
S9	2.4	100	60	14	8550	56	13	8550
S10	2	100	455	17	10 700	123	15	10 700
S11	4	100	36	36	-	33	33	-
S12	1	1	7.4	1	4200	6.9	1	4200
S13	1	1	1	1	-	1	1	-
S14	1	1	32	1	6950	30.1	1	6950

[a] SRF Group 5 has SRF = 1 in 1BMA throughout the assessment period.
[b] The SRF value varies linearly between the given start and end value, and becomes constant (= end value) after given end time.
[c] The radionuclides contained in each SRF Group are given in Table 4-2.

7.6 Physical transport parameters

Figure 7-8 (upper panel) shows the water flow through the 1BMA vault and waste. The figure shows the total flow as calculated in the RNT model, interpolated from values taken from Abarca et al. (2020) with uncertainty factors from Table 4-1 applied. In the beginning during submerged conditions the hydraulic gradients in the surrounding bedrock are extremely low and thus the water flow rates are very low. As the shoreline passes over the repository the gradients and flow increase until relatively stationary conditions are reached around 5000 AD. At the beginning the hydraulic conductivity of the concrete structure is low compared with that of the backfill and thus the water flows mainly through the backfill. However, at the end when the concrete is assumed to be degraded and to have the same hydraulic conductivity as the backfill a larger fraction flows through the waste.

Figure 7-8 also shows the effective diffusivities (middle panel) of radionuclides and porosities (bottom panel) in concrete barriers in the 1BMA model. These time-dependent values are used in the calculations of capacity and diffusive resistances as described in Equation 2-2 and Equation 2-5.

It should be noted that in addition to the cracks in all concrete structures appearing at 22 000 AD (symbolised with the hatched area in the bar at the top of the upper panel in Figure 7-8) cracks in the concrete slab are assumed from the start in the modelling.

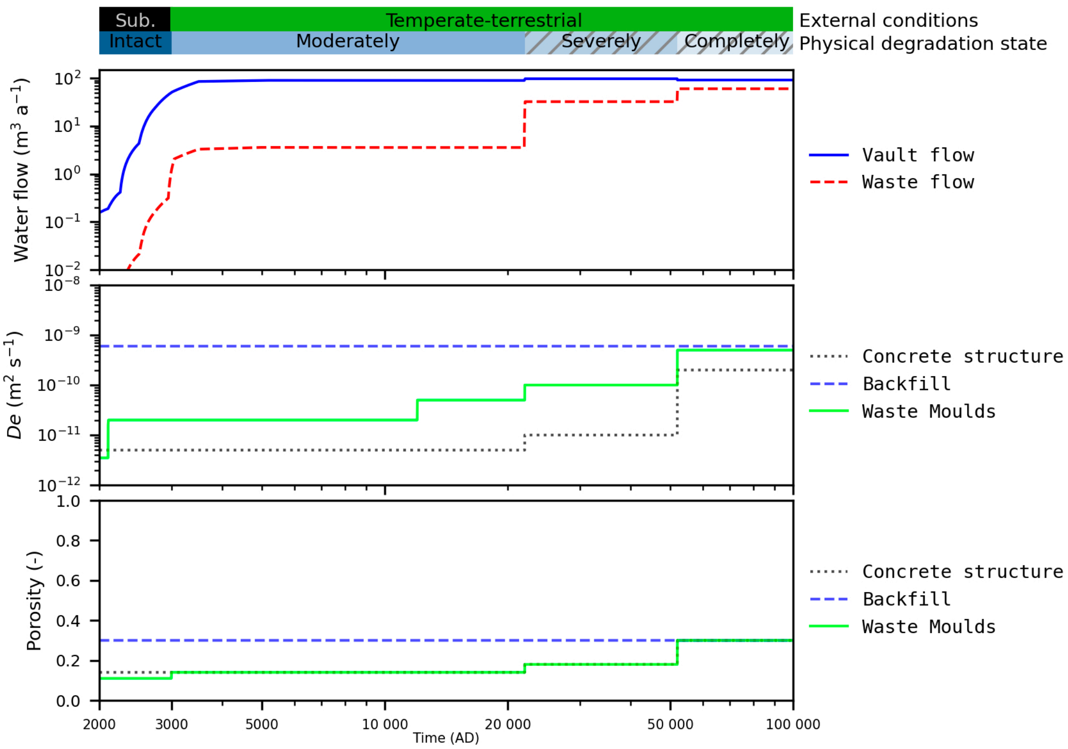

Figure 7-8. *Upper panel: Water flow through the 1BMA vault (Vault flow) and through the waste domain (Waste flow). Middle and bottom panel show effective diffusivity and porosity as a function of time for the materials in 1BMA.*

7.7 Releases in the base case

Figure 7-9 shows the radionuclide releases from 1BMA in the *base case* (thick lines) compared with the total releases from SFR (thin lines). The release from 1BMA gives a significant contribution to the total radionuclide releases from SFR, especially for C-14-org and C-14-inorg. The large release of the strongly sorbing C-14-inorg is due to the cracked slab in combination with the large fraction of C-14-inorg in bituminised (none sorbing) waste packages (Figure 7-5).

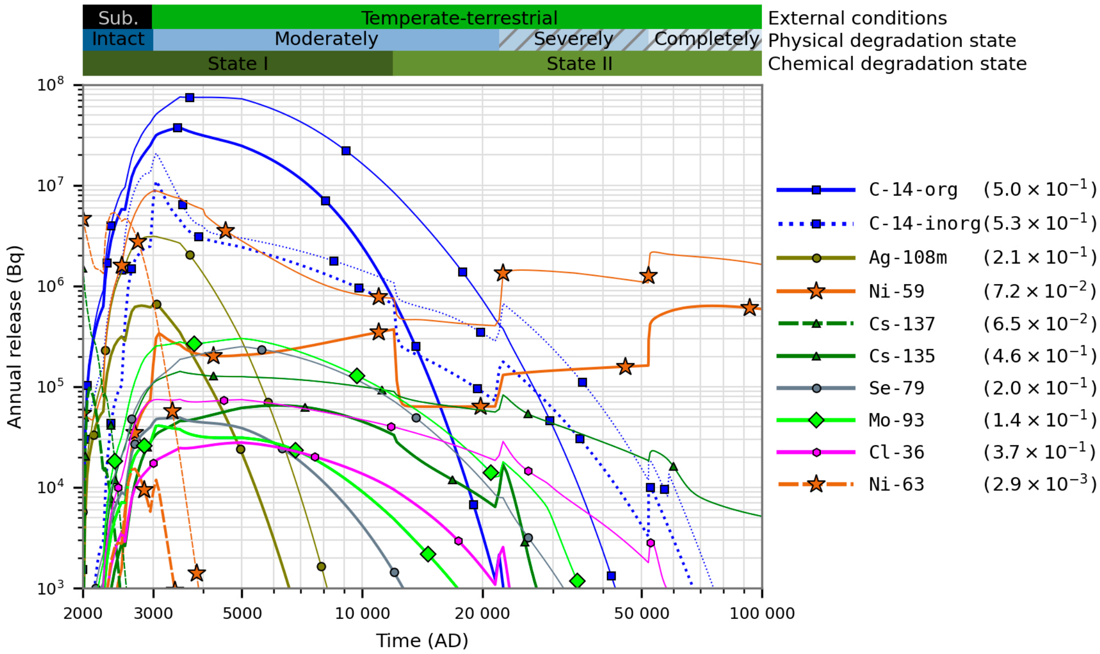

Figure 7-9. *Releases from 1BMA (thick lines) and the whole SFR (thin lines). The colour bars in the upper part of the figure show the evolution of the external conditions and of the concrete physical and chemical degradation, respectively, hatched pattern indicates explicitly modelled barrier crack flow. The evolution of water flow, diffusivity and porosity are shown in Figure 7-8. The values in parentheses show the ratio of the maximum 1BMA release and the maximum of the total release from SFR.*

8 2BMA model

Figure 8-1 shows an illustration of 2BMA during the operational period. In 2BMA, the radioactive waste is stored in 13 free-standing concrete caissons. These will be filled with waste packages. The space between waste packages will be left empty. As the caissons are filled up with waste, they are closed with a concrete lid. The space outside the caissons is backfilled with crushed rock. A more detailed description of 2BMA is given in the **Initial state report**.

In the RNT model, a discretisation where the 13 caissons are represented separately has been chosen. For each caisson, the model also includes compartments representing the crushed rock backfill surrounding the caisson. The crushed rock backfill in the reloading zone of the vault is also represented by one compartment. Figure 8-2 shows the control volumes of 2BMA used in the water-flow calculations. 2BMA has a system for release of gas shown in Figure 8-2 (labelled GEC1-GEC6). The hydrological calculations include calculation of water flow through each of the gas evacuation channels. The gas evacuation channels are also explicitly represented in the RNT model.

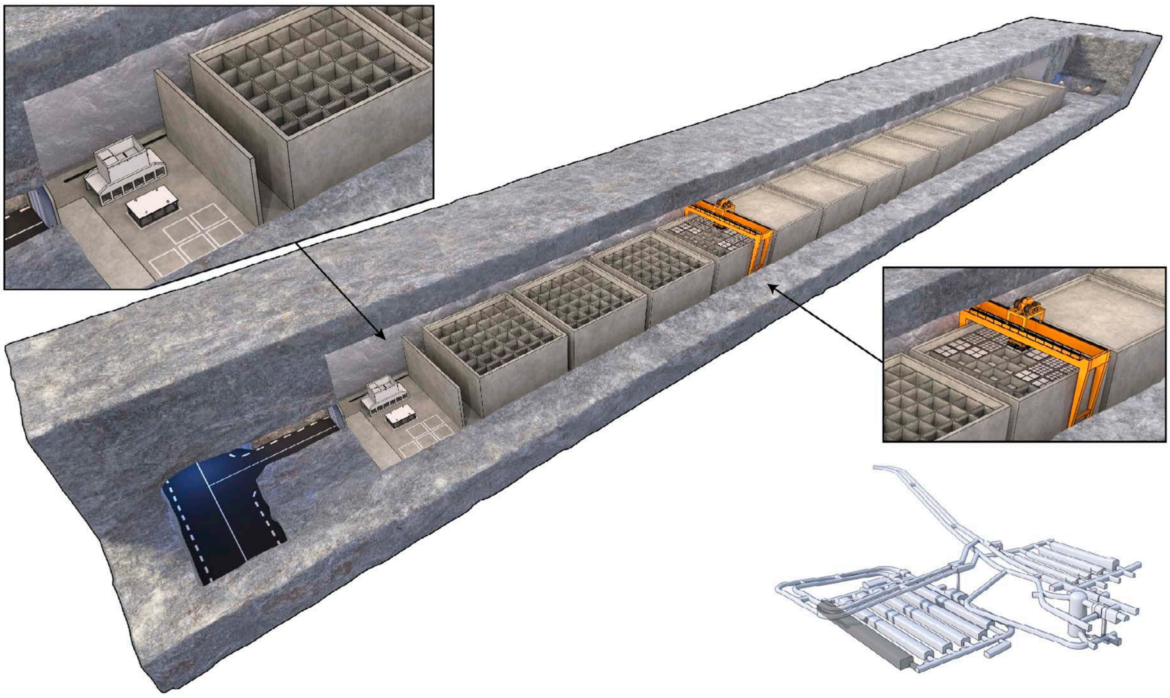

Figure 8-1. *Illustration of 2BMA during the operational period. The upper inset shows the reloading zone the lower inset shows the emplacement of waste packages. In addition, there is a view of SFR with the position of 2BMA highlighted in dark grey.*

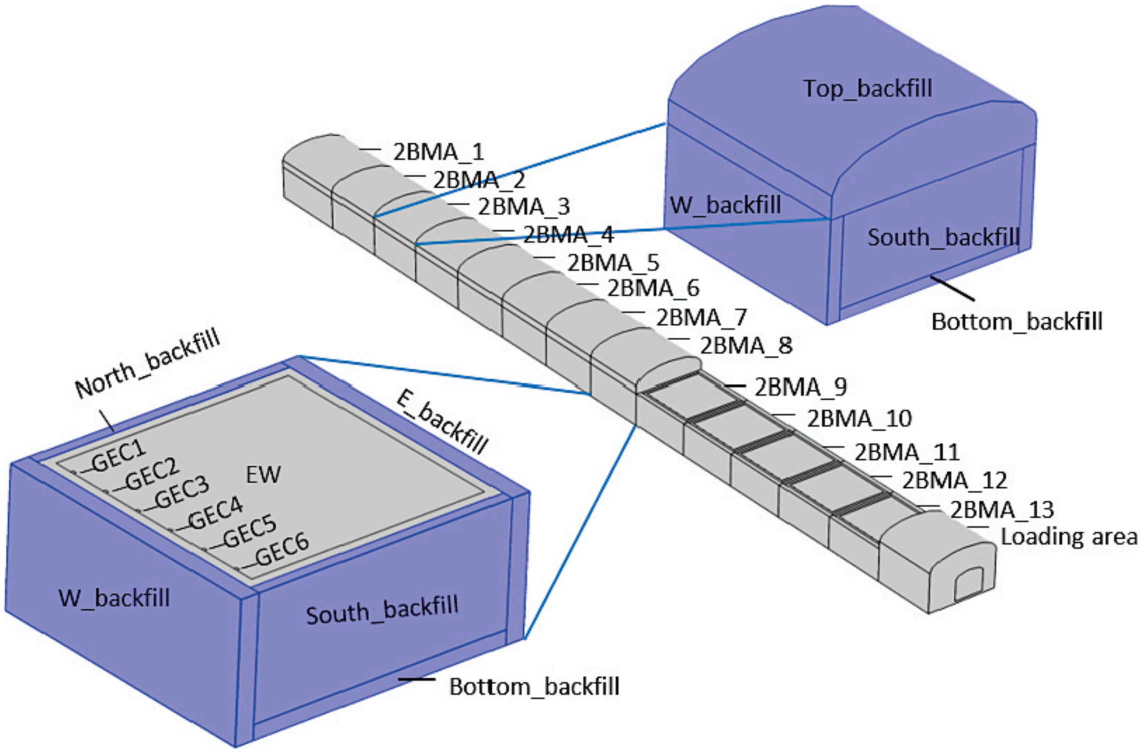

Figure 8-2. *The control volumes used in the hydrological 2BMA model (Abarca et al. 2020).*

8.1 Radionuclide inventory

Figure 8-3 shows the total initial radionuclide inventory (best estimate) in 2BMA compared with the total initial inventory in SFR. Figure 8-4 shows the distribution over *model waste types* for the initial radionuclide inventory in 2BMA.

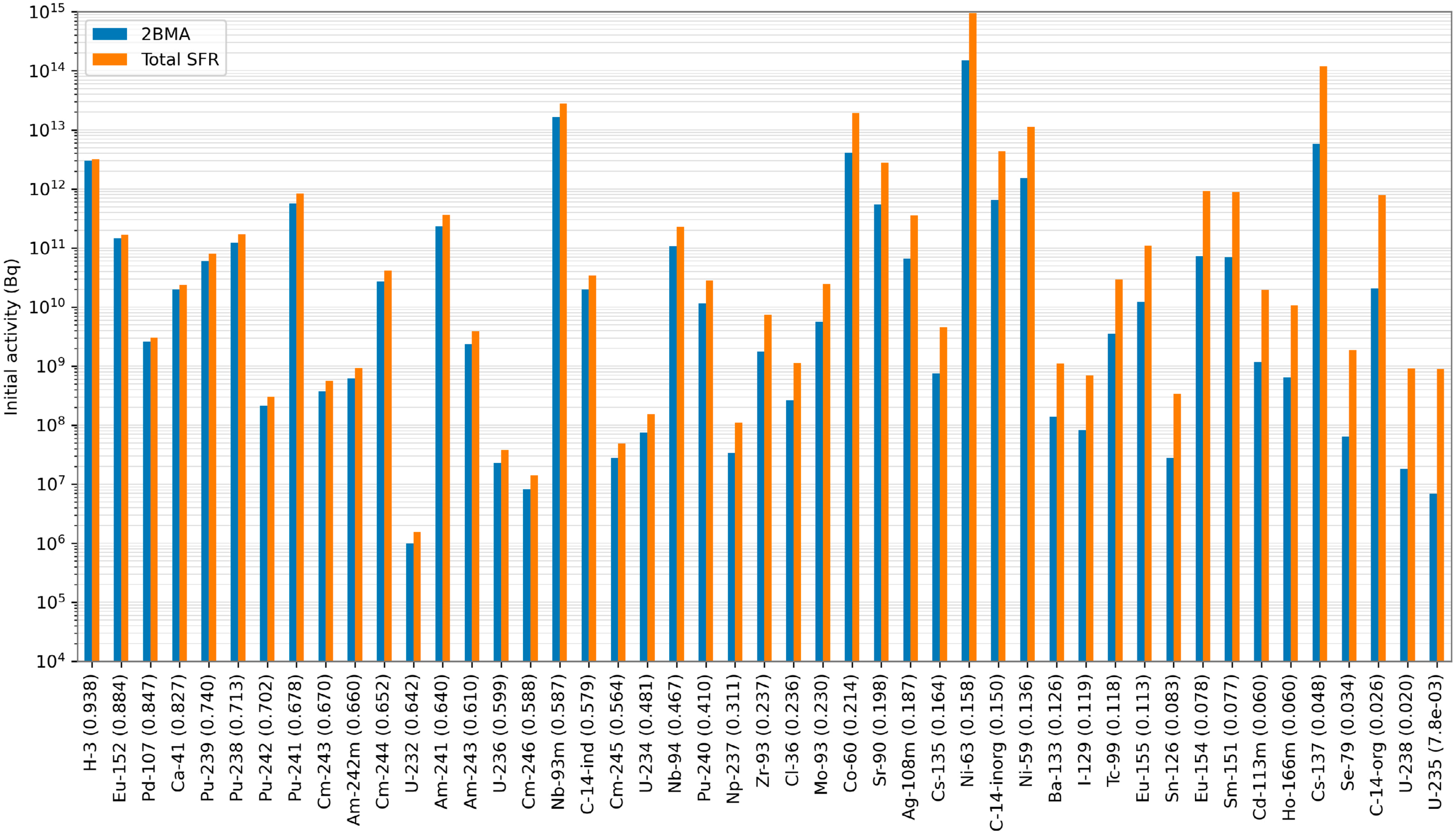

Figure 8-3. *Radionuclide inventory in 2BMA. The figure shows the inventory in 2BMA (blue bars) and the total inventory in SFR (orange bars). The bars are ordered so that the radionuclides with the largest 2BMA fractions are shown to the left. The fraction value is given within parentheses after the radionuclide name on the x-axis.*

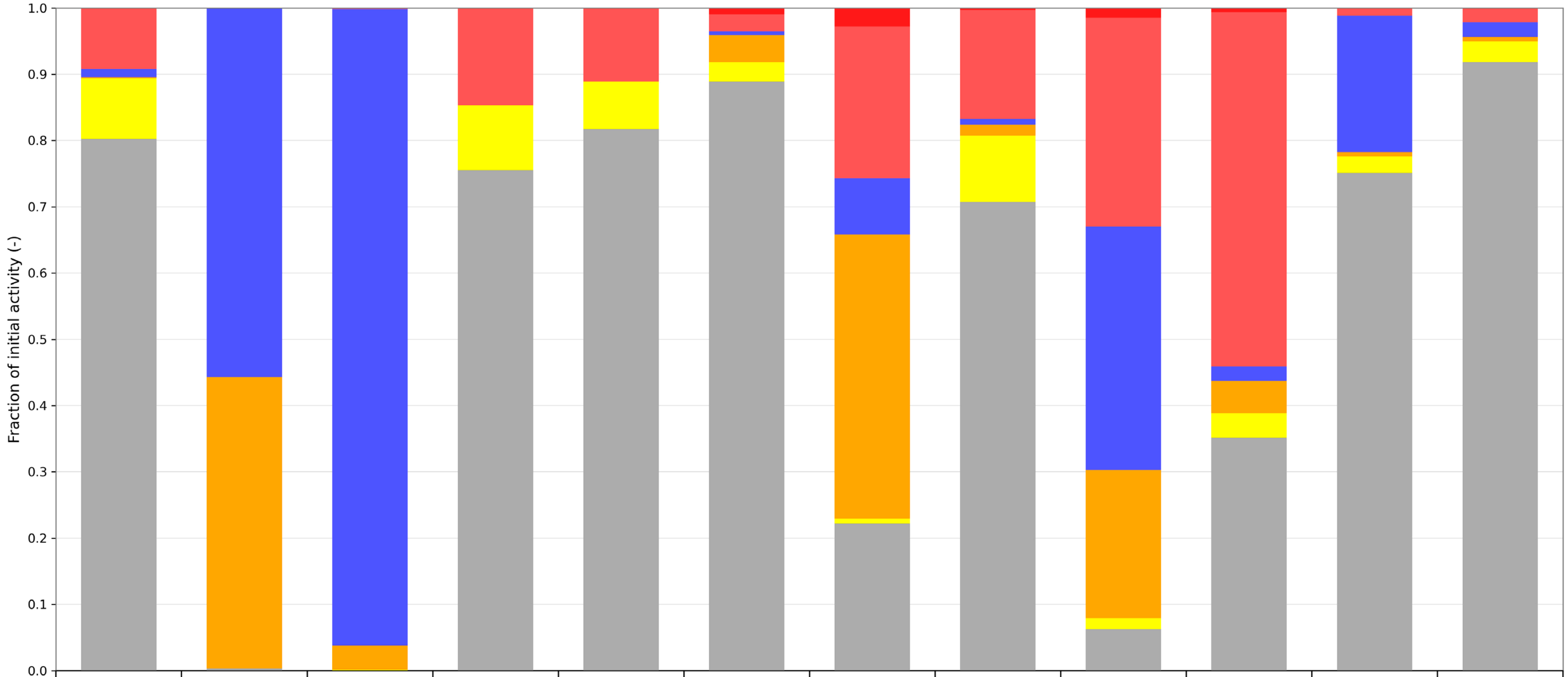

	Mo-93	C-14-org	C-14-inorg	C-14-ind	Ca-41	Ni-59	Cs-135	Cl-36	I-129	Tc-99	U-235	U-238
CM_Ce	0.000	0.000	0.000	0.000	0.000	0.010	0.028	0.003	0.015	0.006	0.000	0.000
CM_Co	0.092	0.000	0.002	0.147	0.111	0.026	0.229	0.164	0.315	0.535	0.011	0.021
SM_Bi	0.012	0.557	0.960	0.000	0.000	0.006	0.085	0.009	0.367	0.022	0.206	0.022
SM_Ce	0.001	0.440	0.037	0.000	0.000	0.041	0.429	0.016	0.224	0.049	0.007	0.007
SM_Co	0.091	0.000	0.001	0.098	0.072	0.029	0.007	0.100	0.017	0.037	0.025	0.031
DualMould	0.803	0.003	0.000	0.755	0.817	0.889	0.222	0.707	0.062	0.351	0.751	0.918

Figure 8-4. *Fraction of radionuclide inventory per model waste package type in 2BMA. See Table 5-1 for an explanation of the model waste names. The figure shows a subset of the radionuclides that are expected to be of largest importance in the safety assessment.*

8.2 Handling of waste

Table 8-1 shows the number of waste packages in 2BMA. The waste is evenly distributed over the 13 caissons. The number of waste packages, together with waste package data on cement and radionuclide content, are used in the model to calculate total amount of cement and initial amounts of radionuclides in the waste. The mapping between *real waste types* and *model waste types* in the 2BMA model is given in Table 8-2. An explanation of the abbreviations used for *real waste types* can be found in SKB (R-18-07, Chapter 2 (in Swedish); R-15-15, Chapter 2 (in English)).

Table 8-1. Number of waste packages in 2BMA (uniformly distributed over the 13 sections).

Model waste type	Section	Number of waste packages[a]
DualMould	S1–S13	276.2
CM_Ce	S1–S13	6.5
SM_Ce	S1–S13	23.8
CM_Co	S1–S13	23.5
SM_Co	S1–S13	51.7
DrumCo	S1–S13	84.6
SM_Bi	S1–S13	40.4

[a] Note that the model waste packages are a pure mathematical construct and hence the number can become a fractional value when they are uniformly spread out over the 13 sections.

Table 8-2. Mapping of real waste types to model waste types in the 2BMA model.

Real waste type	Model waste type
B.23:D_52, E.23:00_53_STUDSVIK, F.23:00_50, E.23:00_53, R.23:D_52, V.23:D_52	SM_Co
R.23:00_24, R.10:00_30, R.29:00_30	CM_Ce
C.23:00_20, O.23:00_20, V.23:00_33, V.23:D_33	CM_Co
F.17:00_51	SM_Bi
R.15:00_50, R.23:00_52	SM_Ce
B.23:D_65, C.23:D_65, F.23:D_65, F.23C:D_65, O.23:D_65, O.23C:D_65, O.23S:D_65, R.23:D_65, R.23C:D_65, S.23:D_65, Å.23:D_65, Å.23C:D_65	DualMould
S.09:00_206, S.21:D_214, V.09:00_206	DrumCo

8.3 Compartment structure

Figure 8-5 (left) shows an overview of the whole Ecolego model for 2BMA, which is subdivided into 13 subsystems for the waste domain and one subsystem for the reloading zone in the south end[4]. Figure 8-5 (right) shows the subsystem for one caisson in 2BMA. The model contains transport blocks for the outer concrete barriers, i.e., the six sides of the caisson. The model also contains compartments for the crushed rock backfill outside the caisson, one at each of the six sides.

Figure 8-6 shows a detailed view of the waste packages in one caisson. Seven different *model waste types* are represented in the model. In addition, the model contains a compartment representing the water that will fill the void in the waste domain after closure of the repository and a compartment representing the inner shaft walls, as shown in the figure.

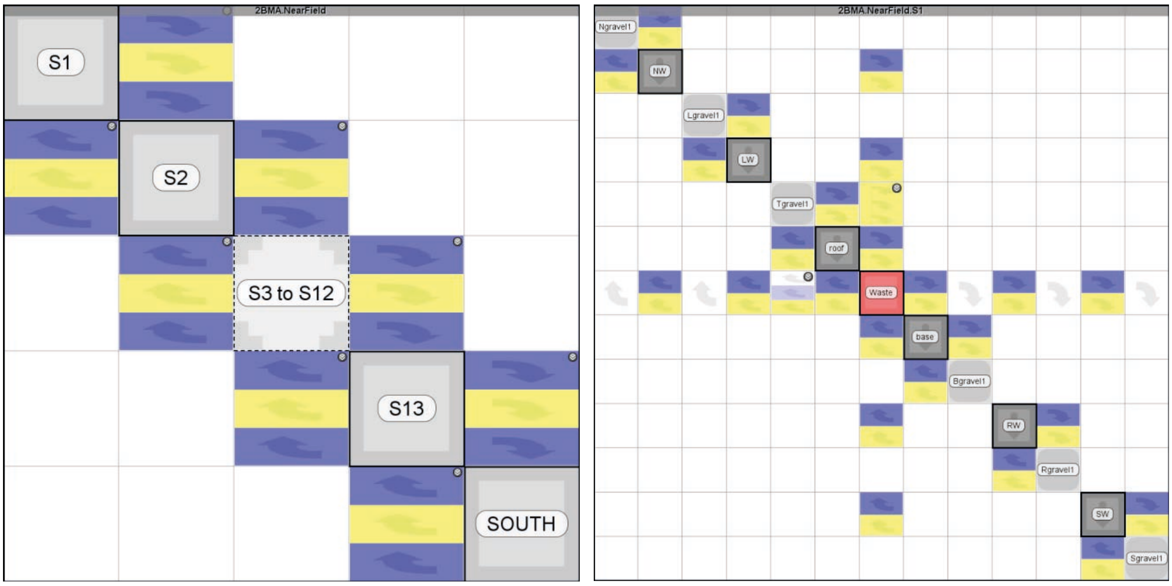

Figure 8-5. *The Ecolego model for the near-field of 2BMA. The left panel shows the subsystems for the 13 caissons and the subsystem for the backfill in the south end (Loading zone). The subsystems S3 to S12 are grouped with the group block in Ecolego (see Section 3.3). The right panel shows one section of the 2BMA model with crushed rock backfill on north side (Ngravel1), concrete wall on north side (NW), crushed rock backfill on west side (Lgravel1), concrete wall on west side (LW), crushed rock backfill on top (Tgravel1), concrete lid of the caisson (roof), area with waste packages (Waste) shown in more detail in Figure 8-6, concrete caisson slab (base), crushed rock foundation (Bgravel1), concrete wall on east side (RW), crushed rock backfill on east side (Rgravel1), concrete wall on south side (SW), crushed rock backfill on south side (Sgravel1). The blue squares with arrows represent advective transfer, the yellow squares with arrows represent diffusive transfer, the white squares with arrows represent flow in cracks through the barrier and light blue squares with arrows represent advective transfer through gas evacuation channels.*

[4] Note that the smaller amount of backfill in the north end does not have its own control volume in the model, instead it is included in the NGravel compartment in the S1 section of the model. This approach is taken both in the hydrological model and the RNT model.

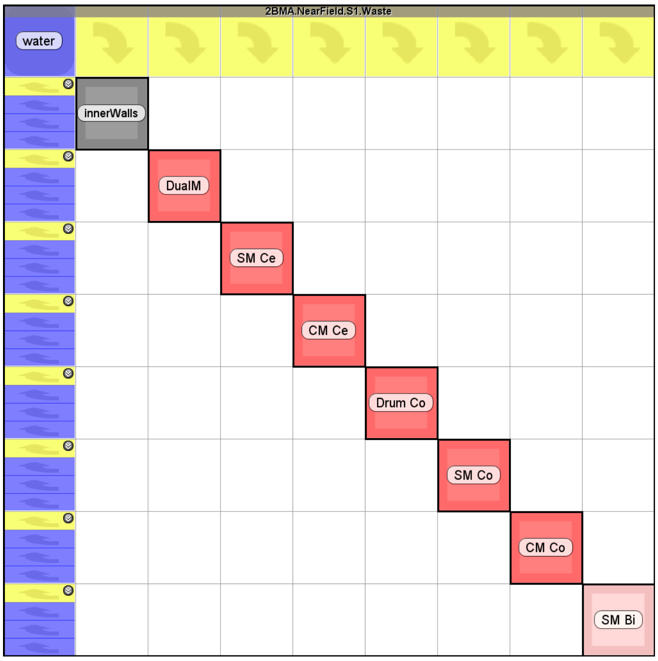

Figure 8-6. Detailed view of the waste in one caisson in Ecolego with water filling the void between the waste compartments after saturation (water), the shaft walls (innerWalls), dual moulds (DualM), steel moulds with cement-solidified waste (SM_Ce), concrete moulds with cement-solidified waste (CM_Ce), drums with concrete-embedded waste (Drum_Co), steel moulds with waste grouted with concrete (SM_Co), concrete moulds with concrete-embedded waste (CM_Co), steel moulds with bituminised waste (SM_Bi). Note that the waste configuration is identical in all 13 caissons. See Section 5.1 for further description of the model waste types.

8.4 Dimensions

Table 8-3 shows the dimensions used in the 2BMA model. Note that for the inner walls the total volume is given in the indata file, this value is only used for calculation of sorption capacity, no diffusive resistance is considered for the inner walls.

Table 8-3. Dimension parameters in the 2BMA model.

Name	Value (m)	Description
caisson_bottom_thickness	0.6	Caisson slab thickness
caisson_side_length	18.12	Caisson side wall length
caisson_lid_thickness	1.14	Caisson lid thickness
caisson_wall_thickness	0.68	Caisson wall thickness
caisson_height	9.0	Caisson height
inner_wall_volume	3 834 (m^3)	Volume of inner walls
bottom_gravel_height	1.0	Thickness of crushed rock layer in bottom
north_gravel_length	2	Length of crushed rock backfill in north end, facing tunnel 2TT (Represented by the NGravel compartment in S1 (Figure 8-5))
south_gravel_length	19.44	Length of crushed rock backfill in south end, facing tunnel 2BST (loading zone)
space_between_caissons	1.5	Distance between the caissons
vault_height	17.8	Mean vault height
vault_width	23.5	Width of the vault
gec_side1	0.2	One side of a gas evacuation channel
gec_side2	0.25	One side of a gas evacuation channel
gec_height	0.64	The height of (the grout in) a gas evacuation channel

Table 8-4 shows the L/A values and number of compartments used for the caisson walls in the 2BMA model. Table 8-5 shows the L/A values used for the backfill in the 2BMA model. All the backfill compartments are represented by one compartment each. The L/A values are further divided with effective diffusivities in the model to calculate diffusive resistances as described in Equation 2-5.

Table 8-4. L/A values for the caisson walls in the 2BMA model.

Section	Part	Area (m^2)	Length (m)	$N_{compartments}$	L/A (m^{-1} per comp.)
1–13	Roof	328 (18.12^2)	1.14	5	7×10^{-4}
1–13	South wall	163 (9 × 18.12)	0.68	5	8×10^{-4}
1–13	East wall	163 (9 × 18.12)	0.68	5	8×10^{-4}
1–13	West wall	163 (9 × 18.12)	0.68	5	8×10^{-4}
1–13	North wall	163 (9 × 18.12)	0.68	5	8×10^{-4}
1–13	Caisson slab	328 (18.12^2)	0.60	5	4×10^{-4}

Table 8-5. L/A values for backfill in the 2BMA model.

Section	Part	Direction	Area (m^2)	Length (m)	L/A (m^{-1})
1–13	Top Gravel	L	183 ((17.8 − 10) × 23.5)	19.6	0.107
1–13	Top Gravel	V	461 (23.5 × 19.62)	7.8	0.017
1–13	East Gravel	H	177 (19.62 × 9)	2.69	0.015
1–13	West Gravel	H	177 (19.62 × 9)	2.69	0.015
1–13	East Gravel	L	24 ((23.5 − 18.12)/2 × 9)	19.6	0.81
1–13	West Gravel	L	24 ((23.5 − 18.12)/2 × 9)	19.6	0.81
1–13	Bottom Gravel	V	356 (19.62 × 18.12)	1.0	0.003
1–13	Bottom Gravel	L	18.12 (1 × 18.12)	19.6	1.08
SOUTH	LZ[a]	L	418 (17.8 × 23.5)	19.4	0.046

[a] South tunnel end (loading zone)

8.5 Sorption data

Initially all cementitious materials in 2BMA are in chemical degradation state I, until 12 000 AD when degradation state II starts and remains applicable for the rest of the assessment time. K_d values for the different degradation states are given in Figure 4-4. The inner walls (structural concrete) in 2BMA contains a cement fraction of 0.219 (kg/kg) and the outer barriers (Limestone concrete) contain a cement fraction of 0.197 (**Data report**). In the *base case* there is no effect of complexing agents in 2BMA, so no sorption reduction factors needs to be defined here.

8.6 Physical transport parameters

Figure 8-7 (top) shows the water flow through the 2BMA vault and waste. The figure shows the total flow as calculated in the RNT model interpolated from values taken from Abarca et al. (2020) with flow factors from Table 4-1 applied. At the beginning the hydraulic conductivity of the concrete structure is low compared with that of the crushed rock backfill and thus the water flows mainly through the crushed rock. However, as the concrete degrades and is assigned the same hydraulic conductivity as the backfill a larger fraction flows through the waste. In the beginning during submerged conditions the hydraulic gradients and thus the waterflows in the surrounding bedrock are extremely low. As the shoreline passes over the repository the gradients and flow increase until relatively stationary conditions are reached around 5000 AD. The water flow through the waste (waste flow) in Figure 8-7 is downscaled with the number of caissons (13) to approximate the flow through each caisson. (The total waste flow would become larger than the vault flow for completely degraded concrete as water that leaves one caisson can enter another caisson). Figure 8-7 (middle and bottom) shows the effective diffusivities of radionuclides and porosities in concrete barriers in the 2BMA model. These time-dependent values are used in the calculations of the capacity and the diffusive resistances as described in Equation 2-2 and Equation 2-5.

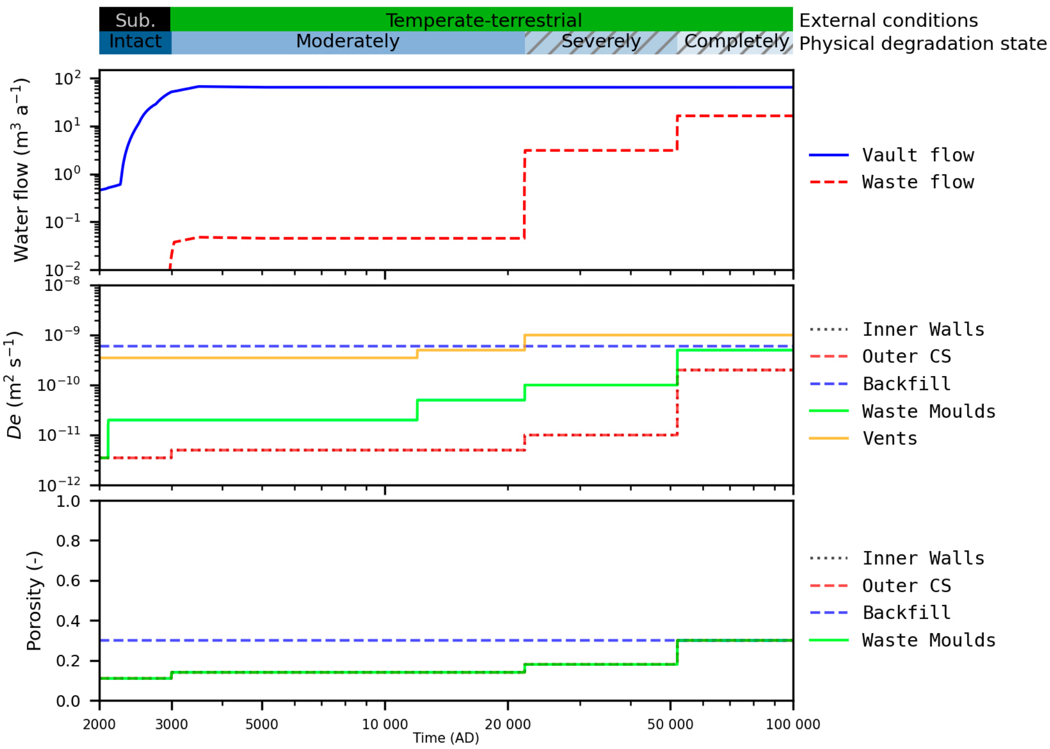

Figure 8-7. *Upper panel: Water flow through the 2BMA vault (Vault flow) and through each caisson (Waste flow). Middle and bottom panel show effective diffusivity and porosity as a function of time for the materials in 2BMA. Outer CS is short for the outer concrete sructures, i.e the caisson walls. Vents denotes the grout in the gas evacuation channels.*

8.7 Releases in the base case

Figure 8-8 shows the radionuclide releases from 2BMA in the *base case* compared with the total releases from SFR. The release from 2BMA dominates the total release of Ca-41 from SFR after 12 000 AD (the thin and thick lines coincide). 2BMA also gives a significant contribution to the release of Ni-59 during the later period with cracked concrete.

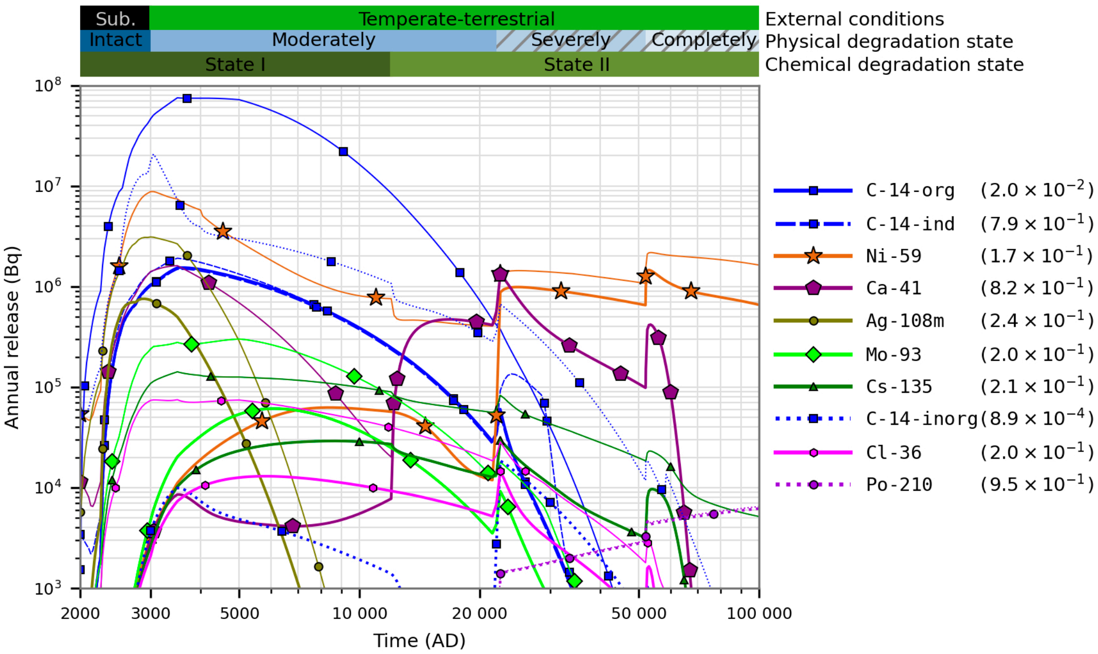

***Figure 8-8.** Releases from 2BMA (thick lines) and the whole SFR (thin lines). The colour bars in the upper part of the figure show the evolution of the external conditions and of the concrete physical and chemical degradation, respectively, hatched pattern indicates explicitly modelled barrier crack flow. The evolution of water flow, diffusivity and porosity are shown in Figure 8-7. The values in parentheses show the ratio of the maximum 2BMA release and the maximum of the total release from SFR.*

9 1BRT model

The waste vault for reactor pressure vessels (1BRT; Figure 9-1) will contain segmented reactor pressure vessels (RPV) arising from the decommissioning of Swedish nuclear reactors. 1BRT will also contain three reactor tank lids. The pressure vessels will be cut into segments, placed in double moulds and embedded in concrete. The waste packages will be placed in a concrete structure. The space between the waste packages will be filled with self-compacting concrete, so that a network of load-bearing structures is formed and a low corrosion rate is ensured. A more detailed description of 1BRT is given in the **Initial state report**.

9.1 Radionuclide inventory

Figure 9-2 shows the total initial radionuclide inventory (best estimate) in 1BRT compared with the total radionuclide inventory in SFR. Figure 9-3 shows the fractions of surface contamination and irradiation-induced radionuclide inventories in 1BRT.

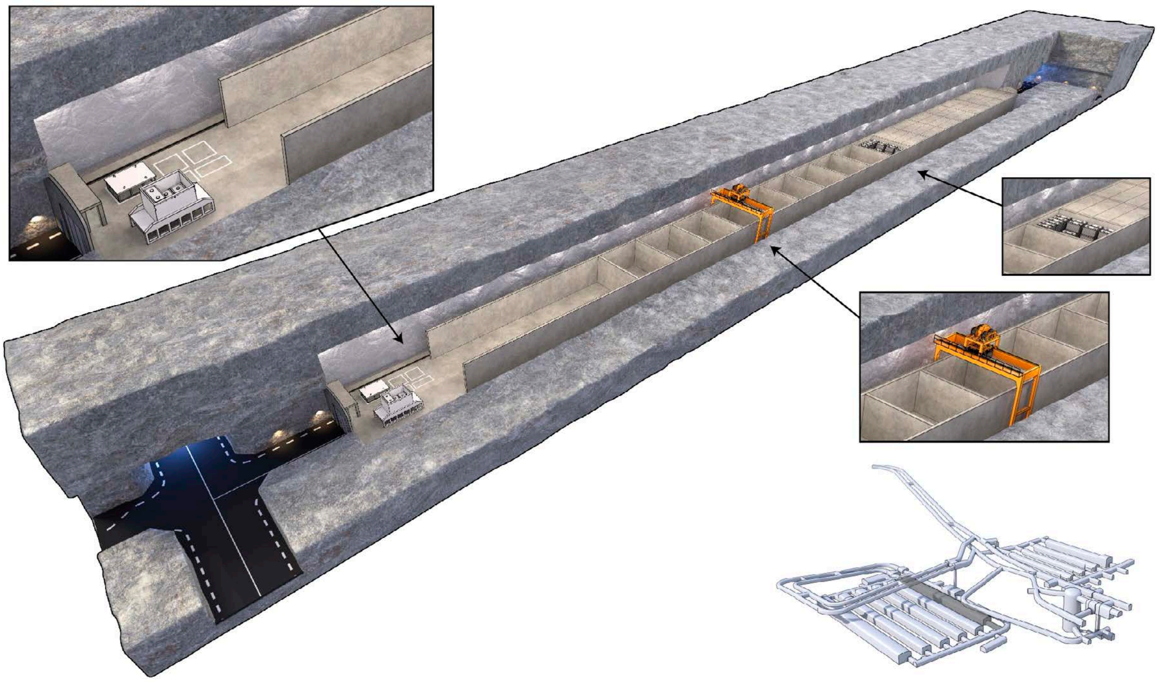

***Figure 9-1.** Illustration of 1BRT during the operational period. The lower detail shows SFR with the position of 1BRT in dark grey.*

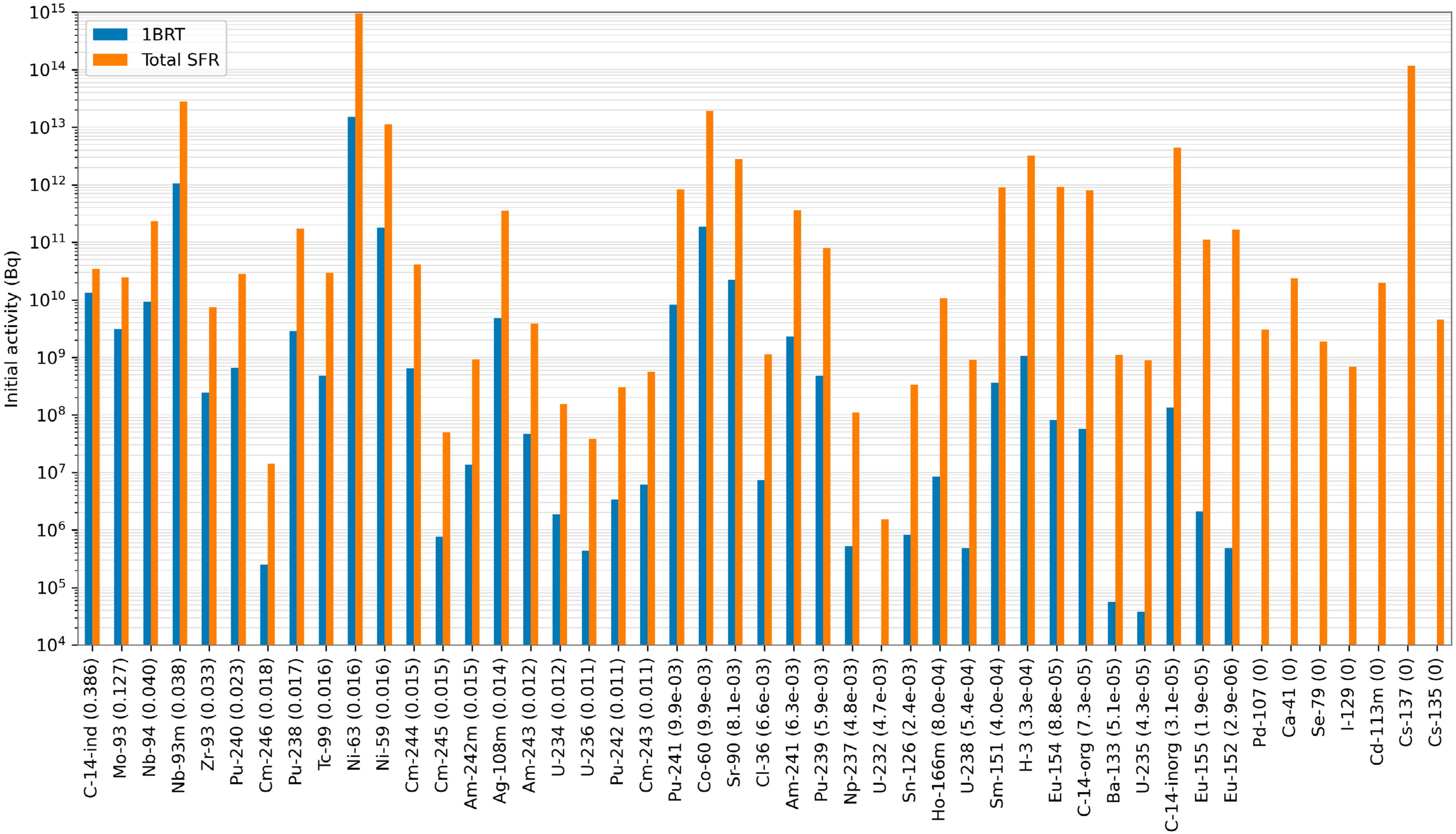

Figure 9-2. *Radionuclide inventory in 1BRT. The figure shows the inventory in 1BRT (blue bars) and the total inventory in SFR (orange bars). The bars are ordered so that the radionuclides with the largest 1BRT fractions are shown to the left. The fraction value is shown within parentheses after the radionuclide name.*

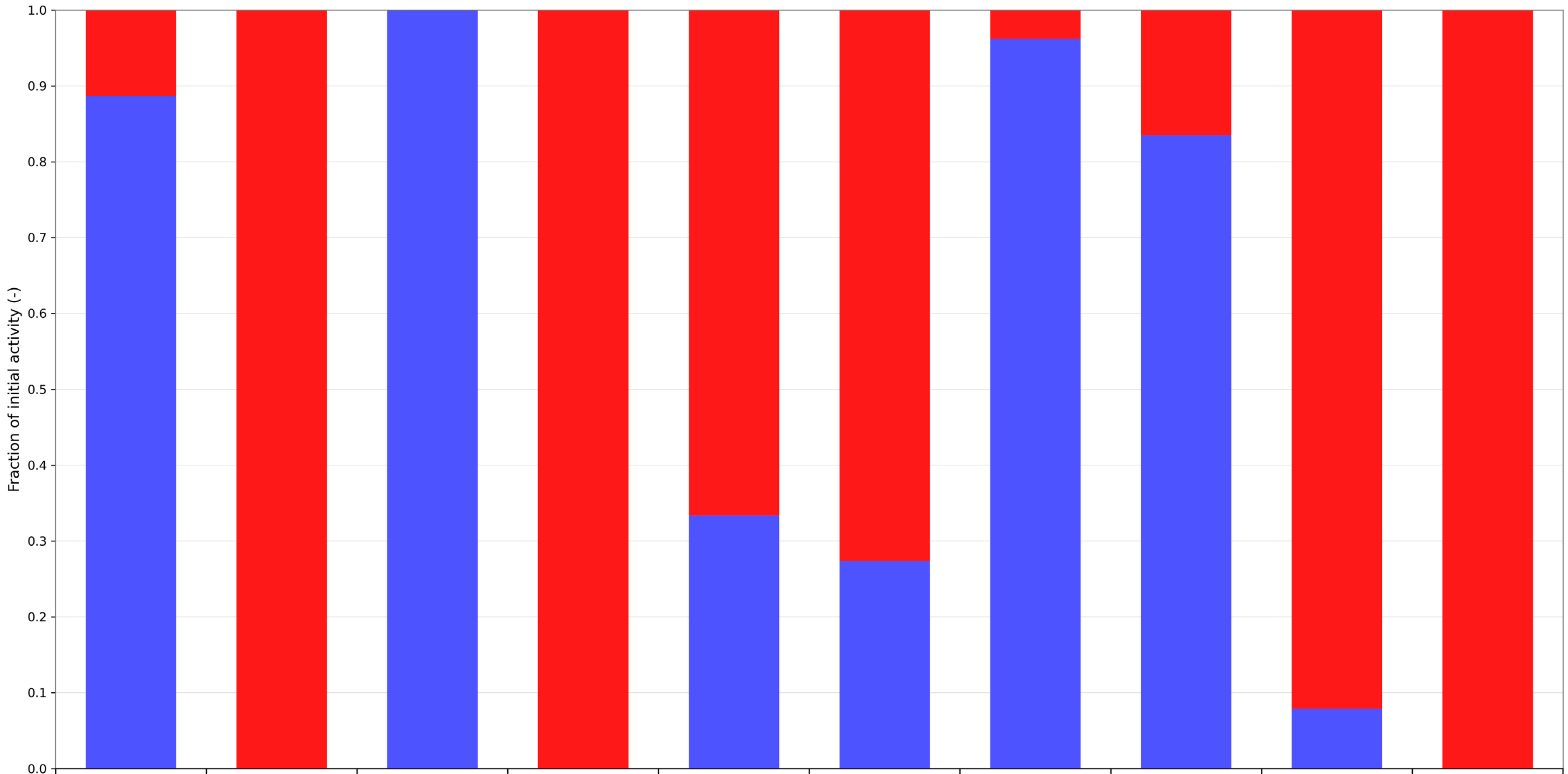

	Mo-93	C-14-org	C-14-ind	Ag-108m	Ni-59	Ni-63	Cl-36	Tc-99	Nb-94	Zr-93
Surface	0.113	1.000	0.000	1.000	0.666	0.726	0.038	0.165	0.921	1.000
Induced	0.887	0.000	1.000	0.000	0.334	0.274	0.962	0.835	0.079	0.000

Figure 9-3. *Fraction of surface contamination and irradiation-induced radionuclide inventories in 1BRT. The figure shows a subset of the radionuclides that are expected to be of largest importance in the safety assessment.*

9.2 Handling of waste

Table 9-1 shows the number of waste packages in the 1BRT model. The number of waste packages, together with waste package data on cement and radionuclide content, are used in the model to calculate total amount of cement and initial amounts of radionuclides in the waste. Note that in 1BRT each *real waste type* is represented with a corresponding model waste type.

Table 9-1. Number of waste packages in 1BRT (SKB R-18-07).

Waste type	Packaging (code)	Waste producer	Number of waste packages	Model waste type
B.40	Double mould (65)	Barsebäck	398	TankB12
F.40	Double mould (65)	Forsmark	814	TankF123
O.40	Double mould (65)	Oskarshamn	639	TankO123
R.40	Double mould (65)	Ringhals	297	TankR1
R.99:01	Other (990)	Ringhals	1	LidR2
R.99:06	Other (990)	Ringhals	2	LidR34
Å.40	Double mould (65)	Ågesta	50	TankA

9.3 Compartment structure

Figure 9-4 shows the 1BRT model in Ecolego. Waste packages containing waste from the RPVs are represented by one compartment per RPV type and shown in red in the figure. The compartments contain packages with steel from the RPV from Ågesta (TankA), packages with steel from the two vessels from Barsebäck (TankB12), packages with steel from the three vessels from Forsmark (TankF123), packages with steel from the three vessels from Oskarshamn (TankO123), packages with steel from the boiling water reactor pressure vessel from Ringhals (TankR1) and reactor tank lids (LidR2 and LidR34). In addition, there is a transport block (five compartments) in the model representing the concrete structure (Walls) surrounding the waste domain, one compartment representing the vault backfill and one compartment representing the grout inside the concrete structure.

Release of irradiation-induced radionuclides from the reactor pressure vessels takes place via steel corrosion. The transfers due to corrosion are represented by purple-colored arrows in the figure. Both corrosion during alkaline and non-alkaline conditions are considered in the model. Hence there are two transfers from each vessel in the model, one representing corrosion during alkaline conditions and one representing corrosion during non-alkaline conditions (Equation 2-10). The release to grout from the reactor tank lids is assumed to be instantaneous in the present calculations, however the model allows for a slower release rate for the induced fraction of radionuclides in the lids (Thus the transfers from LidR2 and LidR34 to Grout are not used in the present calculations, instead the whole radionuclide inventory in the lids is pessimistically handled as surface contamination immediately released to the grout).

The surface contamination is assumed to dissolve (and be released to the surrounding grout) immediately as the vault is saturated. In the model this is handled by assigning the whole inventory of surface contamination to the grout compartment at the start of the simulation.

The advective transfer of radionuclides from the concrete structure to the backfill can take place in intact[5] concrete (blue colored squares with arrows in figure) or via larger cracks modelled explicitly (white square with arrow), see also Section 2.3. Diffusive transfer is modelled between grout, walls and backfill (yellow colored squares with arrows).

[5] The model can handle advective transfer through the concrete both with the homogenous porous media representation or as a flow through cracks in the concrete. However, the configuration of the model in the PSAR is such that only the flow through cracks is used, as the concrete walls of 1BRT are assumed to be cracked already from the start of the modelling.

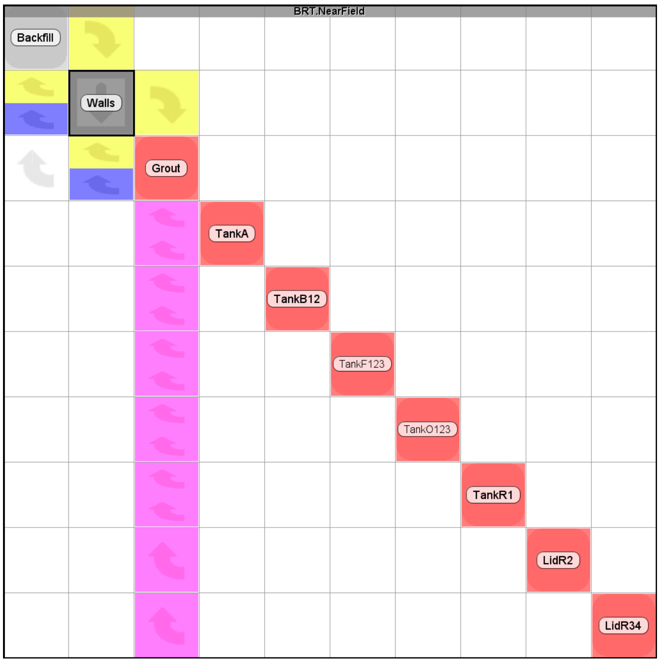

Figure 9-4. *The Ecolego near-field radionuclide transport model for the 1BRT vault. Each waste type is represented by one compartment. The figure shows packages with steel from the RPV from Ågesta (TankA), packages with steel from the two RPVs from Barsebäck (TankB12), packages with steel from the three RPVs from Forsmark (TankF123), packages with steel from the three RPVs from Oskarshamn (TankO123), packages with steel from the RPV from Ringhals (TankR1), packages with steel from reactor tank lids (LidR2 and LidR34), the walls (Walls) modelled with a transport block (representing five compartments), and the grout (Grout) and backfill (Backfill) represented by one compartment each. The purple arrows represent corrosion limited transfers, the blue arrows represent advective transfers, the yellow arrows represent diffusive transfers and the white arrow represents flow through cracks in the concrete walls.*

9.4 Dimensions

The 1BRT model is built as a one-dimensional model. The diffusive resistance in the waste domain and backfill is neglected as its value is insignificant in comparison with the diffusive resistance of the concrete barrier. Hence there is only one L/A value used in the 1BRT model.

Table 9-2 shows the dimensions used in the 1BRT model and Table 9-3 shows the L/A values used for the wall in the 1BRT model. The wall is modelled with a transport block, representing five compartments. The L/A values are further divided with effective diffusivities in the model to calculate diffusive resistances as described in Equation 2-5.

Table 9-2. Dimension parameters in the 1BRT model.

Name	Value (m)	Description
vault_width	17.7	Vault width
vault_height	14.5	Vault height (average)
north_gravel_length	10	Length of vault part without waste in north end
south_gravel_length	20.6	Length of vault part without waste in south end
waste_domain_length	224.4	Length of vault part where waste will be stored
waste_domain_width	11.5	Waste domain width (including walls)
waste_domain_height	6.4	Waste domain height (including lid and (inner) slab)
wall_thickness	0.5	Thickness of outer walls, slab and lid

Table 9-3. L/A values for concrete structural walls in the 1BRT model.

Section	Part	Area (m^2)	Length (m)	Number of compartments	L/A (m^{-1} per comp.)
-	Wall	8181*	0.50	5	1.2×10^{-5}

* Area calculated as: 2 × (224.4 × 11.5 + 224.4 × 6.4 + 11.5 × 6.4).

9.5 Sorption data

Initially all cementitious materials in 1BRT are in chemical degradation state I until at 4000 AD degradation state II begins. This persists until 22 000 AD when degradation state IIIa begins. Degradation state IIIb commences at 87 000 AD and continues for the rest of the assessment time. K_d values for the different degradation states are given in Figure 4-4. The structural concrete in 1BRT contains a cement fraction of 0.219 (kg/kg) and the grout contains a cement fraction of 0.174 (kg/kg) (**Data report**). In the *base case* there is no effect of complexing agents in 1BRT.

9.6 Physical transport parameters

Figure 9-5 (upper panel) shows the water flow through the 1BRT vault and waste. The figure shows the total flow as calculated in the RNT model, interpolated from values from Abarca et al. (2020) with flow factors from Table 4-1 applied. The concrete structure is pessimistically assumed to be severely degraded with cracks present already from start. Hence, the water flow is relatively high through the waste. At the beginning (during submerged conditions) the hydraulic gradient and thus water flow in the surrounding bedrock is very low. As the shoreline passes over the repository the gradient and flow increase until relatively stationary conditions are reached around 5000 AD. Figure 9-5 (middle and bottom panels) shows the effective diffusivities of radionuclides and porosities in concrete barriers in the 1BRT model. These time-dependent values are used in the calculations of the capacity and the diffusive resistances as described in Equation 2-2 and Equation 2-5.

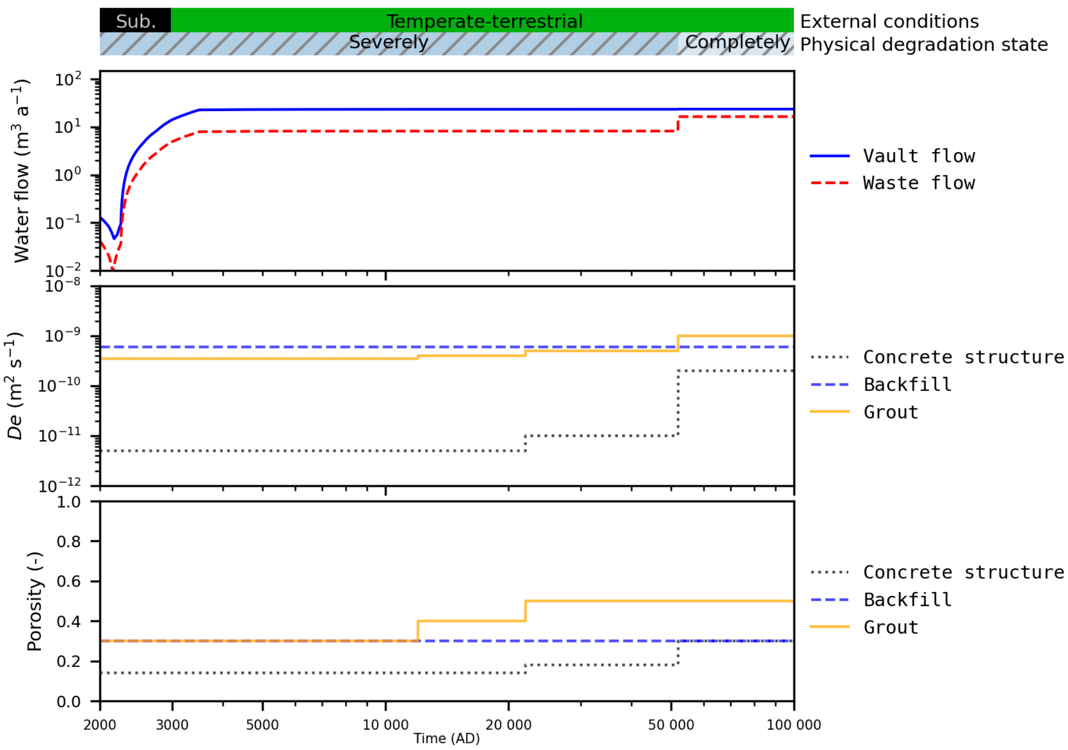

Figure 9-5. *Upper panel: Water flow through vault and waste in 1BRT. Middle and bottom panels show the evolution over time of effective diffusivity and porosity of the outer concrete structure, the crushed rock backfill (Backfill) and the grout in the waste domain (Grout) in the 1BRT model.*

9.7 Corrosion-controlled release

The release of radionuclides from the steel to the surrounding grout is calculated using Equation 2-10. Figure 9-6 shows the corrosion-controlled release of C-14-ind, Mo-93 and Ni-59 from the steel to the surrounding grout. In the period up until 22 000 AD with high pH, the corrosion rate is low (2.5×10^{-8} m/a, Chapter 5 in the **Data report**). At 22 000 AD the corrosion rate increases significantly (1.0×10^{-5} m/a). The abrupt stop of the release (at ca 30 000 AD) occurs when all steel is corroded.

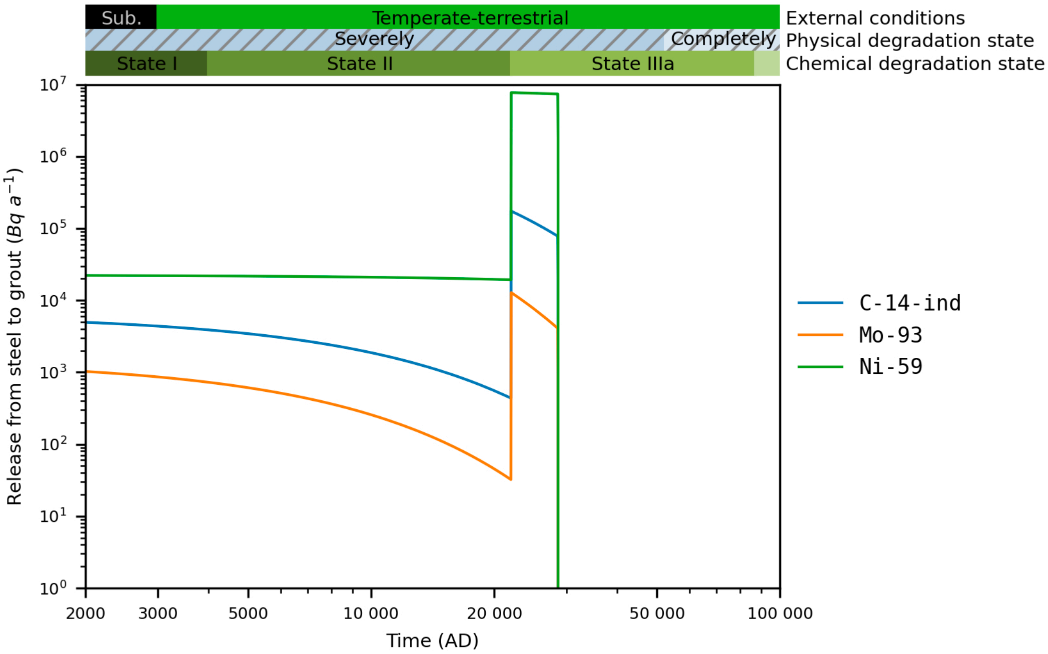

Figure 9-6. *Release of irradiation-induced radionuclides from the steel in 1BRT to the grout.*

9.8 Releases in the base case

Figure 9-7 shows the radionuclide releases from 1BRT in the *base case* compared with the total releases from SFR. The release of Mo-93, Ag-108m and Ni-59 from 1BRT contributes notably to the total release from SFR. Between ca 22 000 AD and ca 30 000 AD the total release of C-14 is dominated by release of irradiation-induced C-14 from 1BRT, but C-14 has decayed to insignificant levels at this time.

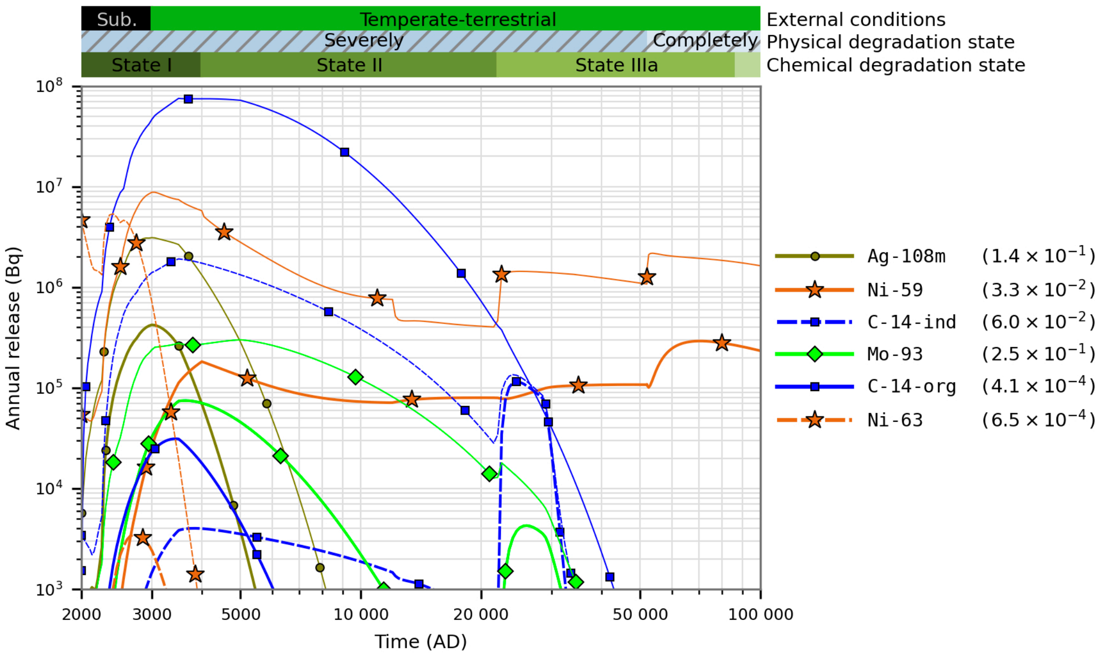

Figure 9-7. *Releases from 1BRT (thick lines) and the whole SFR (thin lines). The colour bars in the upper part of the figure show the evolution of the external conditions and of the concrete physical and chemical degradation, respectively, hatched pattern indicates explicitly modelled barrier crack flow. The evolution of water flow, diffusivity and porosity are shown in Figure 9-5. The values in parentheses show the ratio of the maximum 1BRT release and the maximum of the total release from SFR.*

10 BTF models

Figure 10-1 and Figure 10-2 show the 1BTF and 2BTF vaults during the operational period. Both 1BTF and 2BTF contain concrete tanks with dewatered ion-exchange resins. 1BTF also contains waste drums with ashes, Cortén boxes and supporting walls built with concrete tanks (along the vault) and concrete moulds (across). 2BTF also contains 18 steel boxes. Lids of concrete are placed on top of the waste. The space between the waste packages.is grouted and the space between concrete tanks and rock wall is filled with cementitious backfill. The remaining empty space is backfilled with crushed rock.

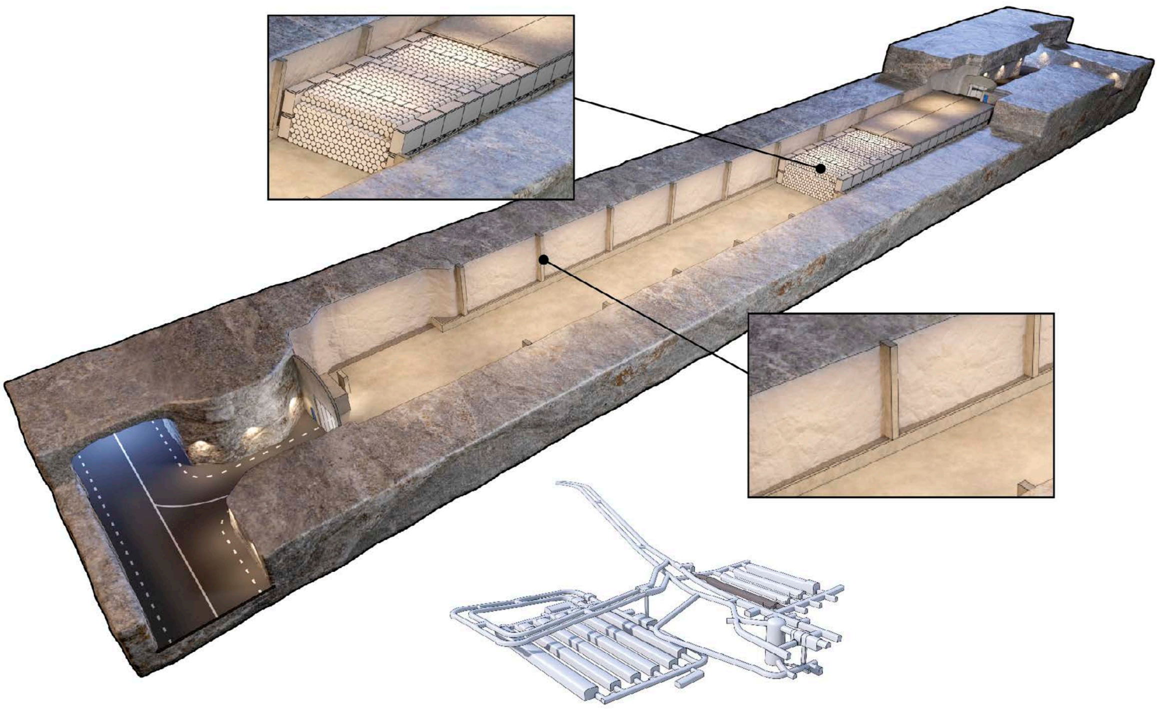

__Figure 10-1.__ Illustration of 1BTF during the operational period. The upper detail shows the emplacement of the ash drums between concrete tanks, the lower detail shows the skirting and concrete pillars. In addition, there is a view of SFR with the position of 1BTF highlighted in dark grey.

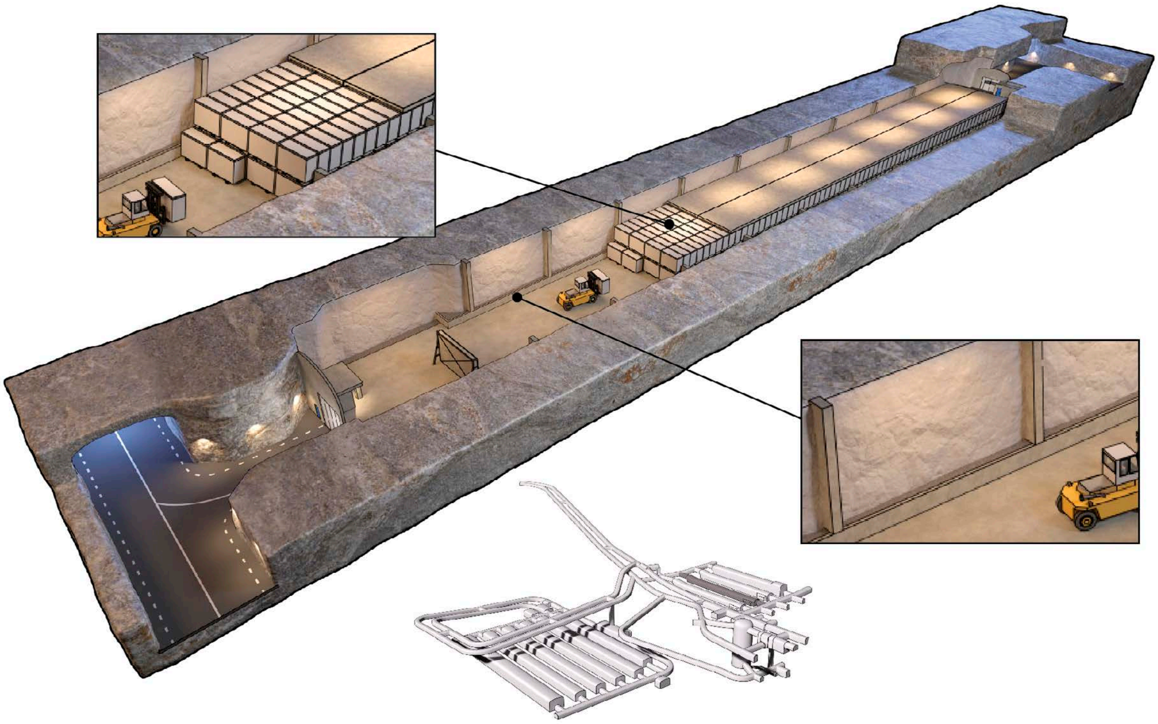

Figure 10-2. Illustration of 2BTF during the operational period. The upper detail shows the emplacement of concrete tanks, the lower detail shows the skirting and concrete pillars. In addition, a view of SFR is shown with the position of 2BTF highlighted in dark grey.

10.1 Radionuclide inventory

Figure 10-3 shows the total initial radionuclide inventory in 1BTF compared with the total initial radionuclide inventory in SFR. Figure 10-4 shows the distribution over *model waste types* for the initial radionuclide inventory in 1BTF.

Figure 10-5 shows the total initial radionuclide inventory in 2BTF compared with the total initial radionuclide inventory in SFR. Figure 10-6 shows the distribution over *model waste types* for the initial radionuclide inventory in 2BTF.

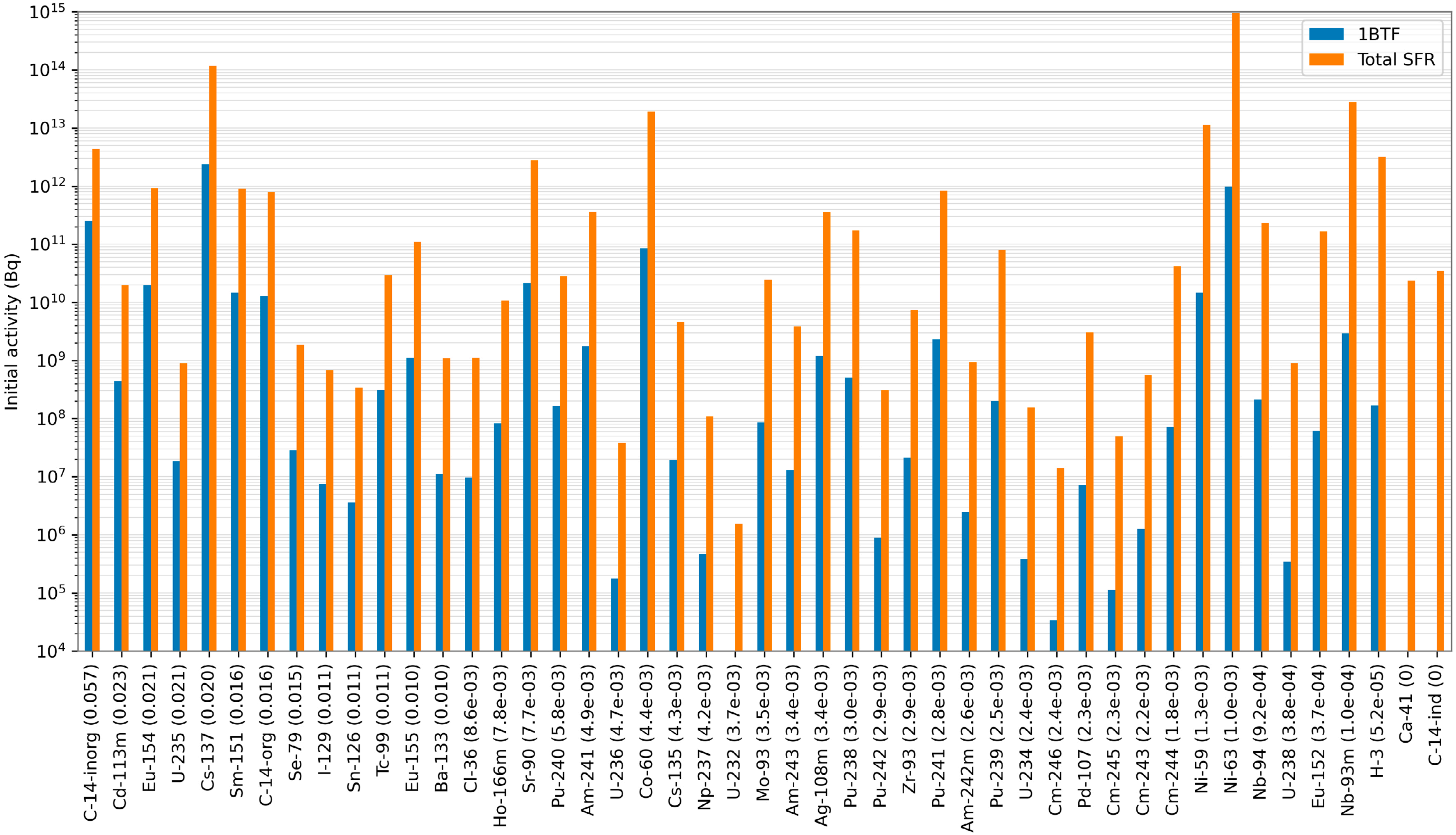

Figure 10-3. *Radionuclide inventory in 1BTF. The figure shows the inventory in 1BTF (blue bars) and the total inventory in SFR (orange bars). The radionuclides are ordered from largest to smallest 1BTF fractions, shown within parentheses after the radionuclide name.*

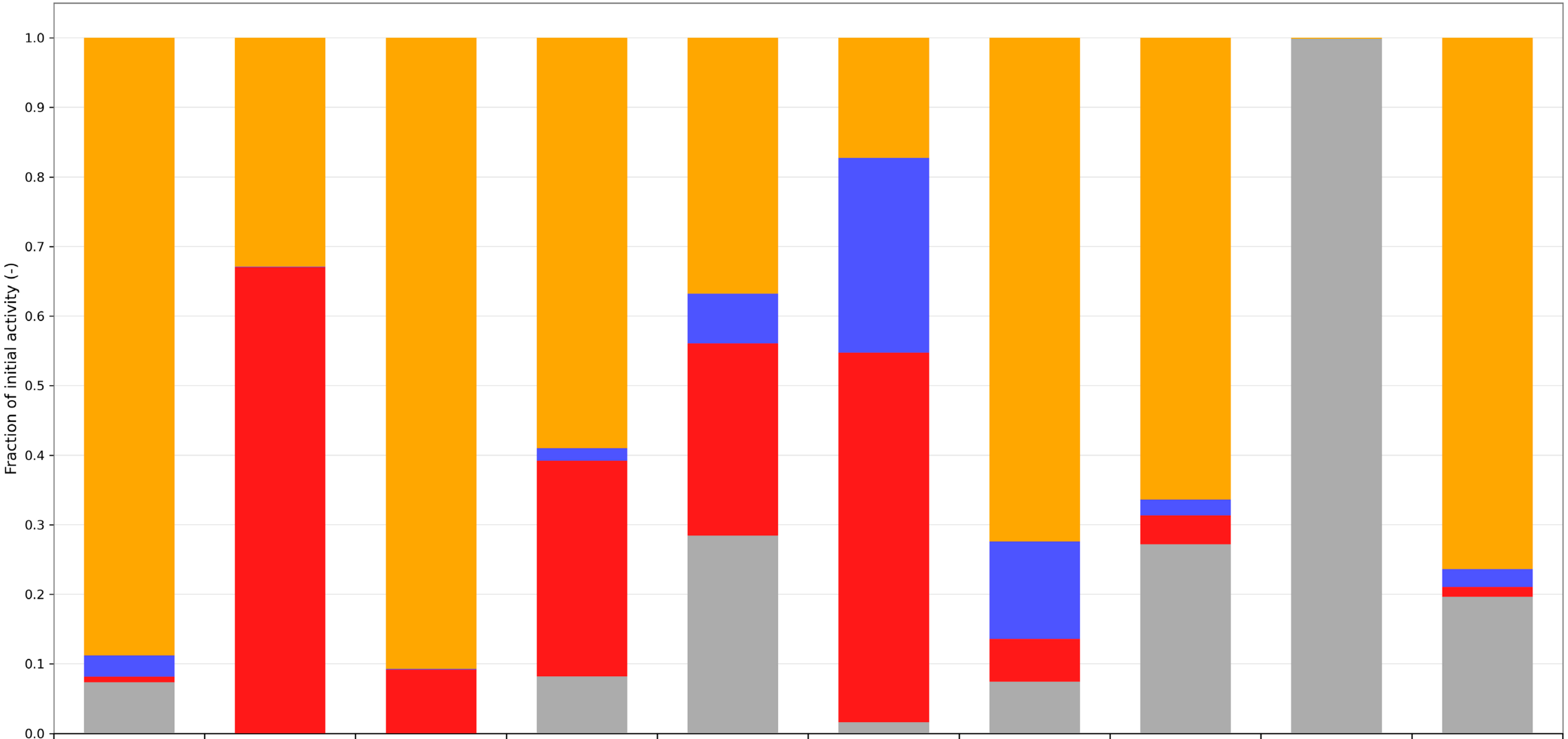

	Mo-93	C-14-org	C-14-inorg	Ni-59	Cs-135	Cl-36	I-129	Tc-99	U-235	U-238
ConcreteTank	0.888	0.329	0.907	0.590	0.368	0.173	0.724	0.664	0.001	0.764
CortenBox	0.030	0.001	0.001	0.018	0.071	0.280	0.140	0.023	0.000	0.026
CM_Ce	0.008	0.670	0.092	0.310	0.277	0.531	0.062	0.041	0.000	0.014
DrumAsh	0.074	0.000	0.000	0.082	0.284	0.016	0.074	0.272	0.999	0.197

Figure 10-4. *Fraction of radionuclide inventory per model waste package type in 1BTF. See Table 5-1 for an explanation of the model waste names. The figure shows a subset of the radionuclides that are expected to be of largest importance in the safety assessment.*

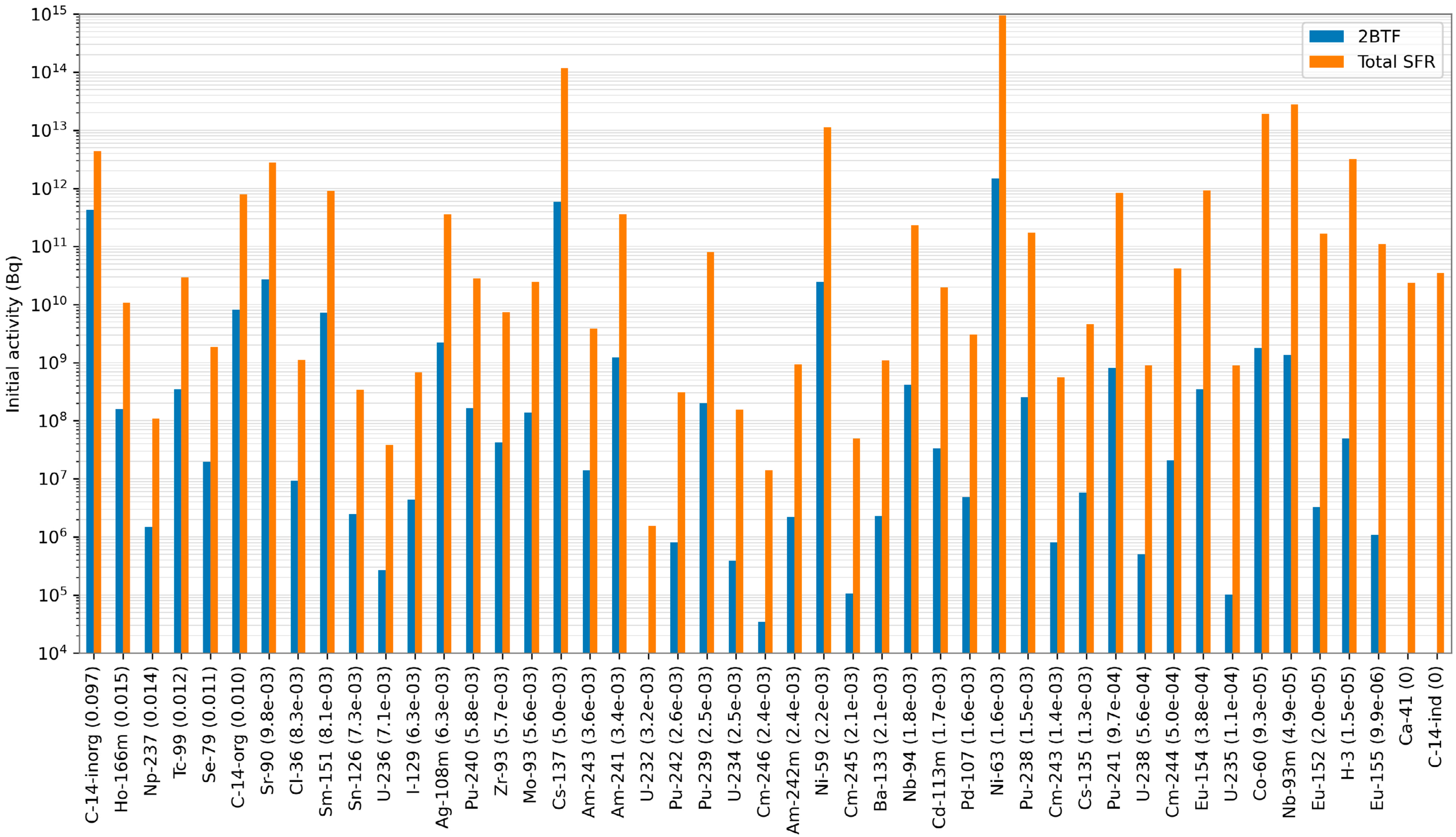

Figure 10-5. *Radionuclide inventory in 2BTF. The figure shows the inventory in 2BTF (blue bars) and the total inventory in SFR (orange bars). The radionuclides are ordered from largest to smallest 1BTF fractions, shown within parentheses after the radionuclide name.*

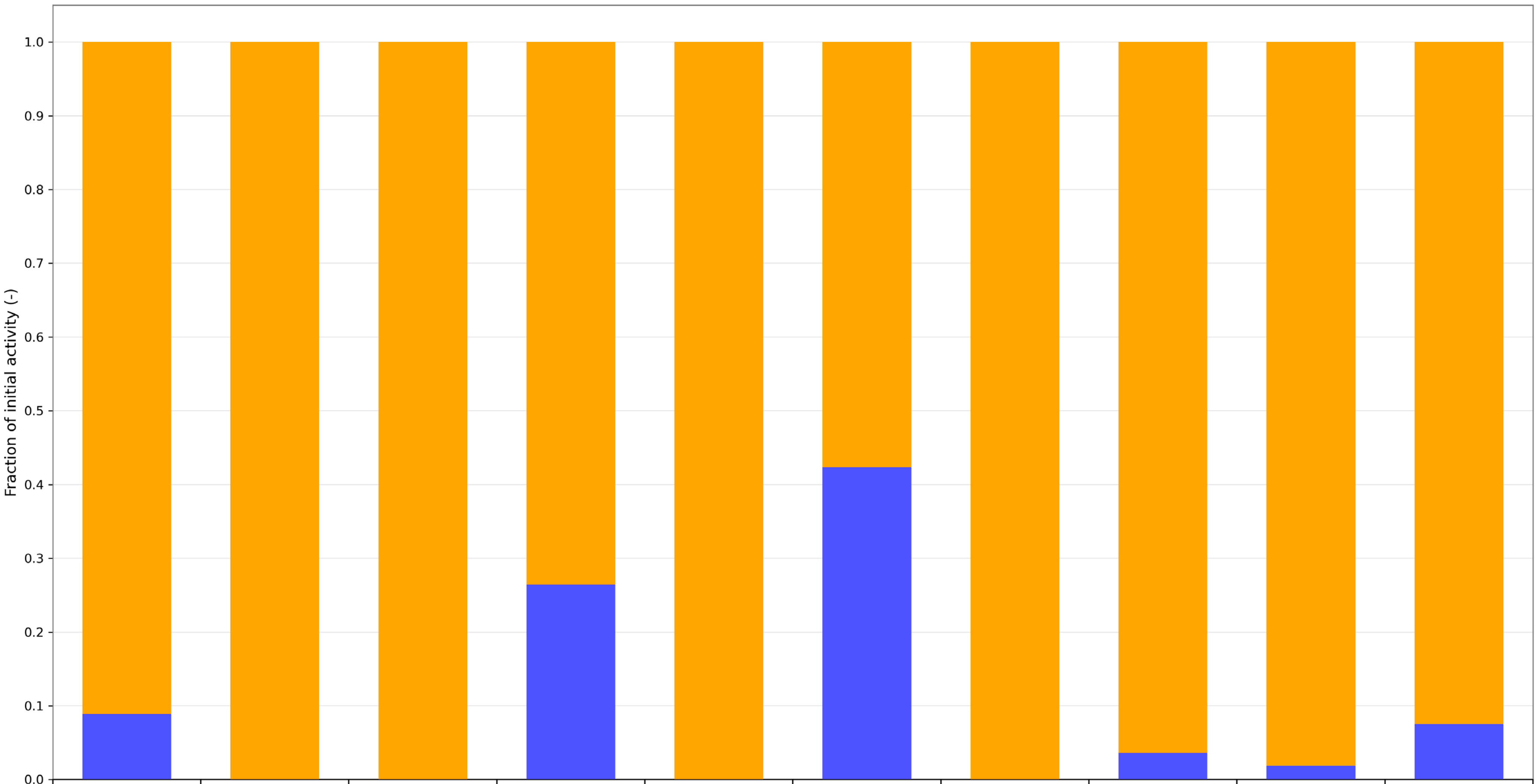

	Mo-93	C-14-org	C-14-inorg	Ni-59	Cs-135	Cl-36	I-129	Tc-99	U-235	U-238
ConcreteTank	0.911	1.000	1.000	0.736	1.000	0.576	1.000	0.964	0.981	0.925
SteelBox	0.089	0.000	0.000	0.264	0.000	0.424	0.000	0.036	0.019	0.075

Figure 10-6. *Fraction of radionuclide inventory per model waste package type in 2BTF. See Table 5-1 for an explanation of the model waste names. The figure shows a subset of the radionuclides that are expected to be of largest importance in the safety assessment.*

10.2 Handling of waste

Table 10-1 shows the number of *model waste packages* in the 1BTF model and Table 10-2 shows the number of *model waste packages* in the 2BTF model (Since the *model waste packages* are a pure mathematical construct they can represent a fractional number of *real waste packages*). The number of waste packages, together with waste package data on cement and radionuclide content, are used in the model to calculate total amount of cement and initial amounts of radionuclides in the waste. The mapping between *real waste types* and *model waste types* in the 1–2BTF models are given in Table 10-3. An explanation of the abbreviations used for *real waste types* can be found in SKB (R-18-07, Chapter 2 (in Swedish); R-15-15, Chapter 2 (in English)).

Table 10-1. Number of waste packages in each section of the 1BTF model.

Model waste type	Section	Number of packages
ConcreteTank	S1–S4	14.5
ConcreteTank	S5–S10	54.2
DrumAsh	S1–S4	1222.8
DrumAsh	S5–S10	0
CM_Ce	S1–S4	36
CM_Ce	S5–S10	0
CortenBox	S1–S4	0
CortenBox	S5–S10	6.7

Table 10-2. Number of waste packages in each section of the 2BTF model.

Model waste type	Section	Number of packages
ConcreteTank	S1–S10	75
SteelBox	S1–S10	1.8

Table 10-3. Mapping of real waste types to model waste types in the BTF models.

Real waste type	Model waste type
O.99:01_22	CortenBox
B.07:00_100, B.07:01_100, B.07:09_100, O.07:00_100, O.07:09_100	ConcreteTank
O.01:09_20, R.01:00_30, R.01:09_13, R.01:09_20, R.01:09_23, R.01:09_30, R.10:00_20, R.10:00_30, R.23:00_20, R.23:00_23, R.23:00_24, R.23:00_29, R.23:00_30	CM_Ce
S.13:00_210_FORSMARK, S.13:00_210_OSKARSHAMN, S.13:00_210_RINGHALS, S.13:00_214_BARSEBÄCK, S.13:00_214_Cyclife, S.13:00_214_FORSMARK, S.13:00_214_OSKARSHAMN, S.13:00_214_RINGHALS, S.13:00_214, S.13:00_214_Svafo	DrumAsh
F.99:02_990	SteelBox

10.3 Compartment structure

In the near-field hydrological model, the waste domain is divided into 10 waste sections. Each section consists of three control volumes, one for the bottom, the waste and the top crushed rock domains, respectively. The hydrological model also contains control volumes for the reloading zone (N) and the inner zone (S) as illustrated in Figure 10-7.

A graphical illustration of the radionuclide transport models for 1–2BTF is shown in Figure 10-8. Blue arrows represent advective transport and yellow arrows diffusive transport. Grey boxes represent crushed rock or grout, whereas black bars represent concrete structures. The red boxes represent the waste domain with grout and waste packages (shown in more detail in Figure 10-10. Note that in the RNT model a finer discretisation is done (compared with the hydrological model) as also the grout on the sides is represented by separate compartments.

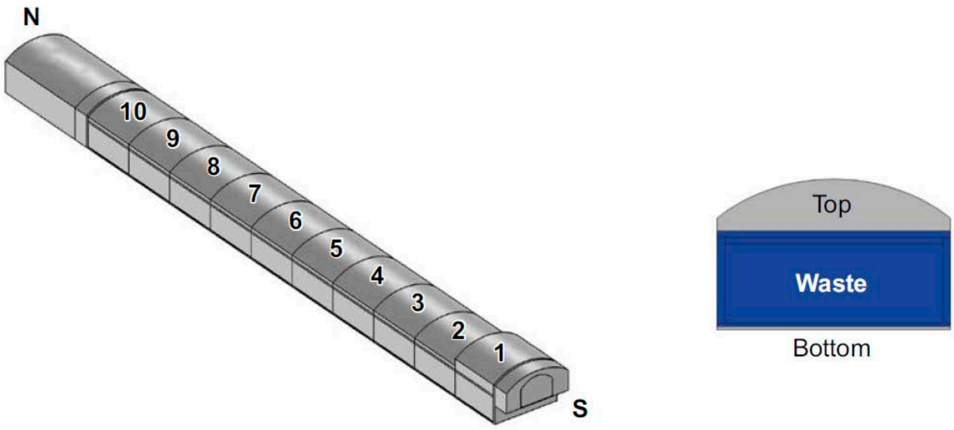

Figure 10-7. *Control volumes for the BTF vaults (Abarca et al. 2020).*

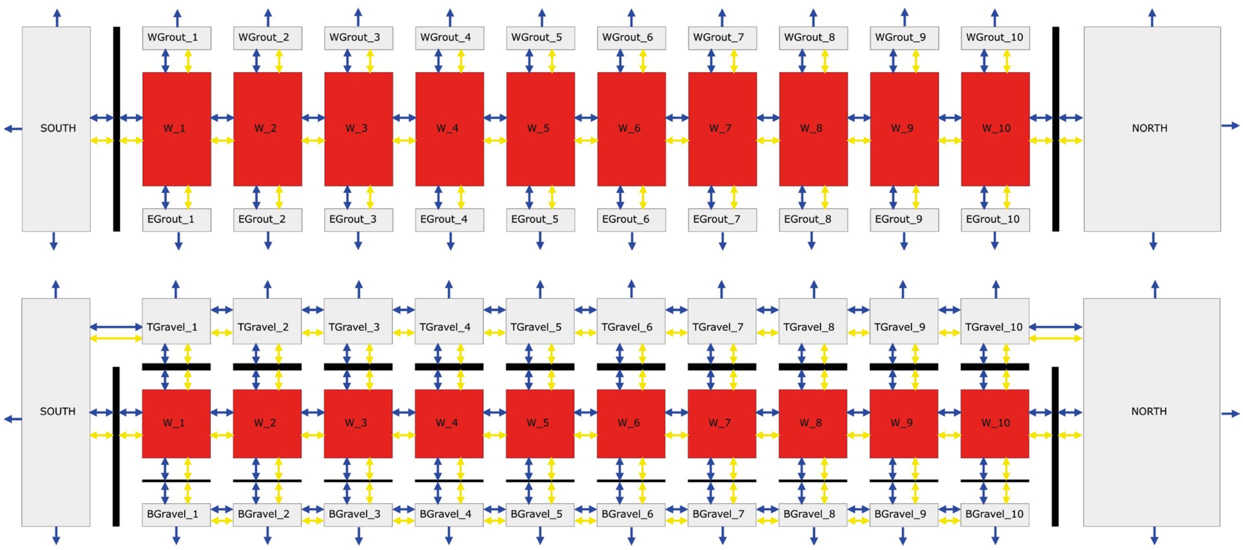

Figure 10-8. *Schematic view of the radionuclide transport model for 1BTF or 2BTF. The upper figure shows a horizontal cross section of the model (top view) and the lower figure shows a vertical cross section (side view). Blue arrows represent advective transport and yellow arrows represent diffusive transport. The grey boxes in the ends (SOUTH, NORTH) represents backfill in the tunnel ends. The grey boxes in the upper figure (WGrout, EGrout) represent the porous concrete backfill at the sides. The grey boxes in the lower figure (TGravel, BGravel) represents crushed rock backfill. Each red box represents several waste packages in the model as shown in Figure 10-10.*

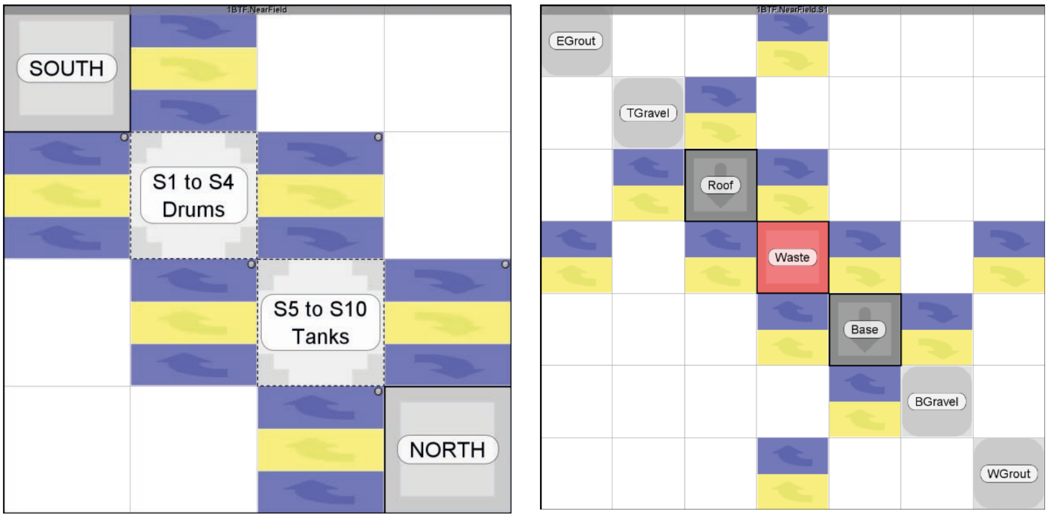

Figure 10-9. *The left panel shows the Ecolego model for the near-field of 1BTF (with transfers directed along the vault). The figure shows the subsystem for the crushed rock backfill in the south end of the vault (South), the four sections with ash-drums (S1 to S4 Drums), the six sections with tanks (S5 to S10 Tanks) and the subsystem for the crushed rock backfill in the north end (reloading zone) (North). The sections S1 to S4 (with ash drums) and S5 to S10 (with concrete tanks) are grouped using the group block in Ecolego (see Section 3.3). The right panel shows one section of the 1BTF/2BTF models in Ecolego (with transfers directed across the vault) with grout backfill on the east side (EGrout), crushed rock backfill on top (TGravel), concrete lid (Roof), waste domain (Waste) (shown in more detail in Figure 10-10, concrete slab (Base), crushed rock foundation (BGravel) and grout backfill on west side (WGrout). The blue arrows represent advective transfer and the yellow arrows represent diffusive transfer.*

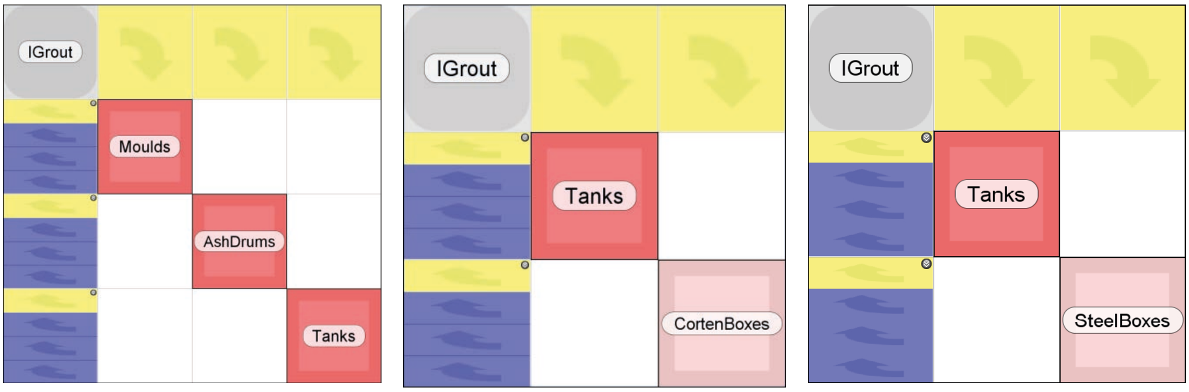

Figure 10-10. *Left panel: One of the (Drums) waste sections of 1BTF with grouting between the waste packages (IGrout), concrete moulds with mainly cement-solidified waste (Moulds), ash drums (AshDrums) concrete tanks (Tanks). Midle panel: One of the (Tanks) waste sections in 1BTF with grouting between the waste packages (IGrout), concrete tanks (Tanks) and Corten boxes (CortenBoxes). Right panel: One of the (ten identical) waste sections of 2BTF with grouting between the waste packages (IGrout), concrete tanks (Tanks) and steel boxes (SteelBoxes). See Section 5.1 for further description of the model waste types.*

10.4 Dimensions

Table 10-4 shows the dimensions used in the BTF models. Table 10-5 shows the L/A values used for the BTF models. The values are shown for each section and for the direction along the vault (L), horizontal direction across the vault (H) and vertical direction (V). The L/A values are further divided with effective diffusivities in the model to calculate diffusive resistances as described in Equation 2-5. The table also gives the number of compartments used to represent each part of the barrier in the model. The roof and slab (base) are the only substantial concrete structures and are expected to act as an important barrier between the waste and backfill, hence they are given a finer discretisation.

Table 10-4. Dimensions used in the BTF models.

Name	Value (m)	Description
bottom_gravel_height	0.45	Height (thickness) of crushed rock layer in bottom
bottom_thickness	0.25	Bottom concrete plate thickness
lid_thickness	0.8	Thickness of prefabricated and cast lid
vault_width	14.7	Vault width
vault_height	8.8	Vault height (mean)
north_gravel_length	25.8	Length of vault part without waste in north end (reloading zone)
south_gravel_length	3.6	Length of vault part without waste in south end
waste_domain_length	130.0	Length where waste will be stored
waste_domain_width	13.7	Width of waste domain
waste_domain_height	4.9	Height of waste domain

Table 10-5. L/A values for the BTF models.

Section	Part	Direction	Area (m^2)	Length (m)	Number of comp.	L/A (m^{-1} per comp.)
North	Backfill	L	129 (14.7 × 8.8)	25.80	1	0.1994
South	Backfill	L	129 (14.7 × 8.8)	3.60	1	0.0278
S1–S10	Grout[a]	L	67 (13.7 × 4.9)	13.00	1	0.1937
S1–S10	EGrout	H	64 (130 × 4.9/10)	0.50	1	0.0078
S1–S10	WGrout	H	64 (130 × 4.9/10)	0.50	1	0.0078
S1–S10	TopGravel	V	191 (130 × 14.7/10)	3.45	1	0.0181
S1–S10	TopGravel	L	51 (14.7 × (8.8−0.45−4.9))	13.00	1	0.2563
S1–S10	BottomGravel	V	191 (130 × 14.7/10)	0.45	1	0.0024
S1–S10	BottomGravel	L	7 (14.7 × 0.45)	13.00	1	1.9652
S1–S10	Roof	V	178 (130 × 13.7/10)	0.80	5	0.0009
S1–S10	Base	V	178 (130 × 13.7/10)	0.25	5	0.0003

[a] Represents inner grout and waste packages (this leads to a cautious simplification of the diffusive resistance as the waste packages are assumed to have a higher diffusive resistance than grout).

10.5 Sorption data

Initially all cementitious materials in 1–2BTF are in chemical degradation state I. Thereafter at 4000 AD follows degradation state II, degradation state IIIa begins at 22 000 AD and degradation state IIIb begins at 87 000 AD persisting for the rest of the assessment time. K_d values for the different degradation states are given in Figure 4-4. The structural concrete in 1–2BTF contains a cement fraction of 0.219 (kg/kg) and the grout contains a cement fraction of 0.171–0.235 (kg/kg) (**Data report**). The sorption in 1–2BTF is reduced by complexing agents expected to be present in the vault. This is modelled by means of sorption reduction factors (Keith-Roach et al. 2021). The radionuclides are divided into five groups depending on how much they are influenced by complexing agents. SRFs for most groups are unity at all times except for group 3 and group 4. The evolution over time for the SRFs in 1–2BTF is shown in Table 10-6.

Table 10-6. Sorption reduction factors (SRF) used in 1–2BTF for different groups of radionuclides in the base case.[a]

Vault	SRF Group[b]					
	Group 3 Linear function[c]			Group 4 Linear function[c]		
	Start value	End value	End time (AD)	Start value	End value	End time (AD)
1BTF	9	1	2850	8	1	2850
2BTF	6673	1	7600	688	1	7600

[a] SRF Groups 1, 2 and 5 have SRF = 1 in 1–2BTF throughout the assessment period.

[b] The radionuclides contained in each SRF Group are given in Table 4-2.

[c] The SRF value varies linearly with time between the given start and end values, and becomes constant (= end value) after the given end time.

10.6 Physical transport parameters

Figure 10-11 (upper panel) shows the water flow in vault and waste for the BTF models. The initial rise in flow is due to the increase in hydraulic gradient as the shoreline passes the repository due to shoreline regression. At 12 000 AD there is an additional increase in the flow through the waste due to the transition from severely degraded to completely degraded concrete in the model. The figure shows the total flow through the waste and vault used in the RNT model interpolated from values in Abarca et al. (2020) with flow factors from Table 4-1 applied. Figure 10-11 (middle and bottom panels) show the effective diffusivities of radionuclides and porosities of materials used in the BTF models. These time-dependent values are used in the calculations of capacity and diffusive resistances as described in Equation 2-2 and Equation 2-5.

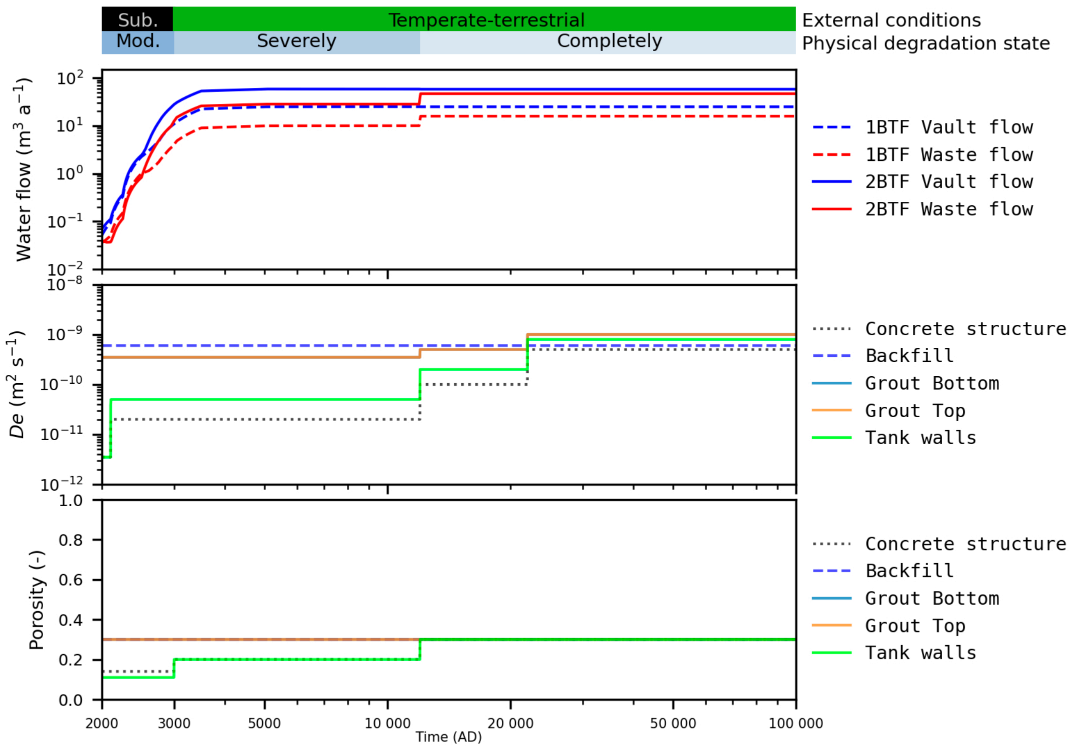

Figure 10-11. *Upper panel: Time-dependent total water flow in vault and waste for the 1–2BTF models. Middle and bottom panel show the evolution over time of the effective diffusivity and porosity of radionuclides in the materials of 1–2BTF. Note that the values for grout bottom and grout top overlap in effective diffusivity. Concrete Structure here refers to the concrete lid and base (slab). Note that for porosity the values for Concrete Structure and tank walls overlap. Also the values for backfill and grout overlap.*

10.7 Releases in the base case

Figure 10-12 shows the radionuclide releases from 1–2BTF in the *base case* compared with the total releases from SFR. The release from 1–2BTF gives a small contribution to the total radionuclide releases from SFR for most radionuclides. The high release of Tc-99 and Zr-93 from 2BTF is due to the high concentrations of complexing agents in 2BTF (Table 10-6).

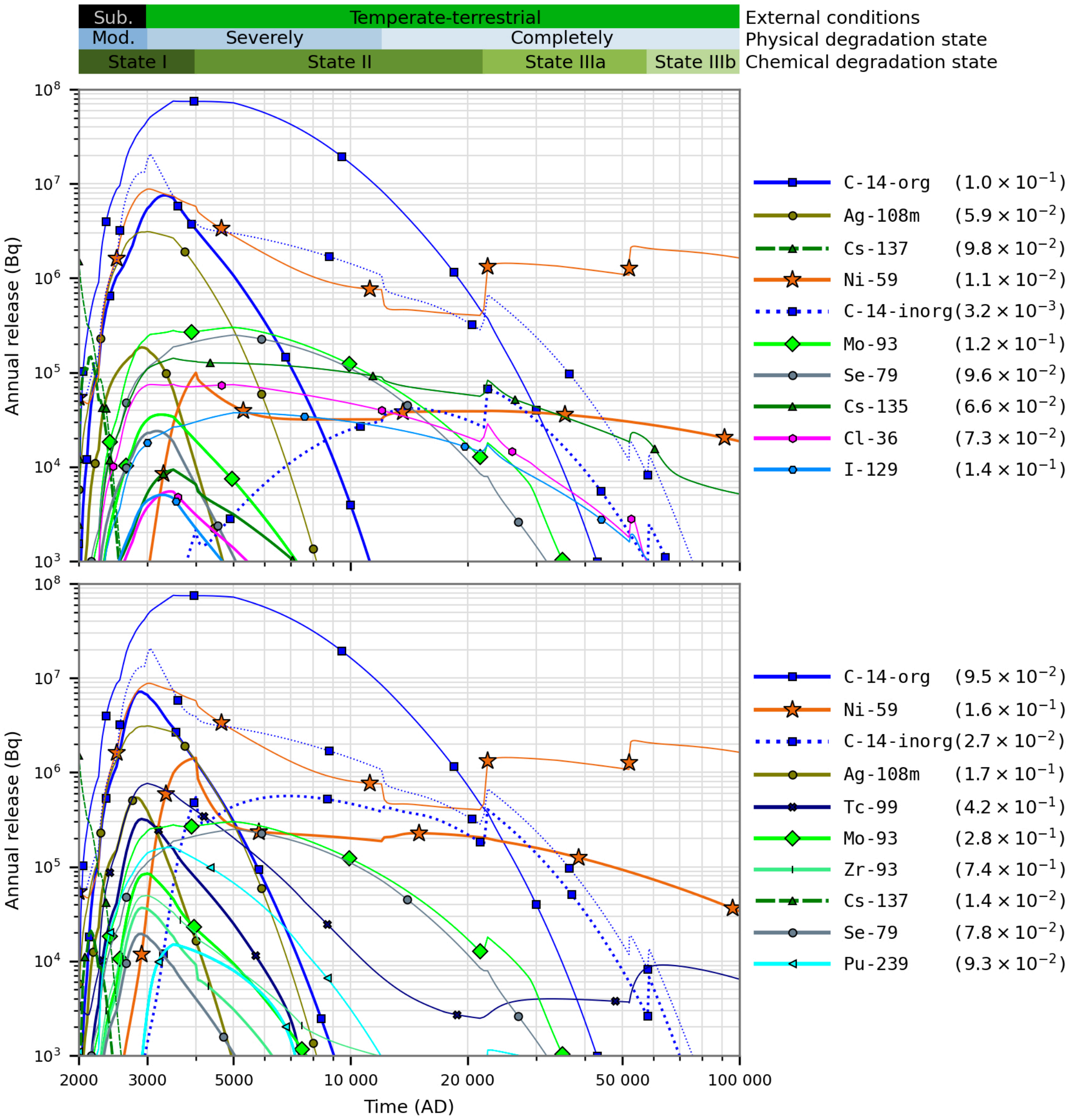

Figure 10-12. *Releases from 1BTF (upper panel) and 2BTF (lower panel) (thick lines) compared with the same radionuclide releases from SFR as a whole (thin lines). The colour bars in the upper part of the figure show the evolution of the external conditions and of the concrete physical and chemical degradation respectively. The evolution of water flow, diffusivities and porosities are shown in Figure 10-11. The values in parentheses show the ratio of the maximum 1–2BTF release and the maximum of the total release from SFR.*

11 BLA models

Figure 11-1 shows the 1BLA and 2–5BLA vaults during the operational period. In the BLA vaults, the waste is emplaced in ISO-containers that are placed directly on a concrete slab. No backfilling or grouting is planned to be used in the BLA vaults.

11.1 Radionuclide inventory

Figure 11-2 and Figure 11-3 show the total initial radionuclide inventory in 1BLA and 2–5BLA (total for all four vaults) compared with the total initial radionuclide inventory in SFR.

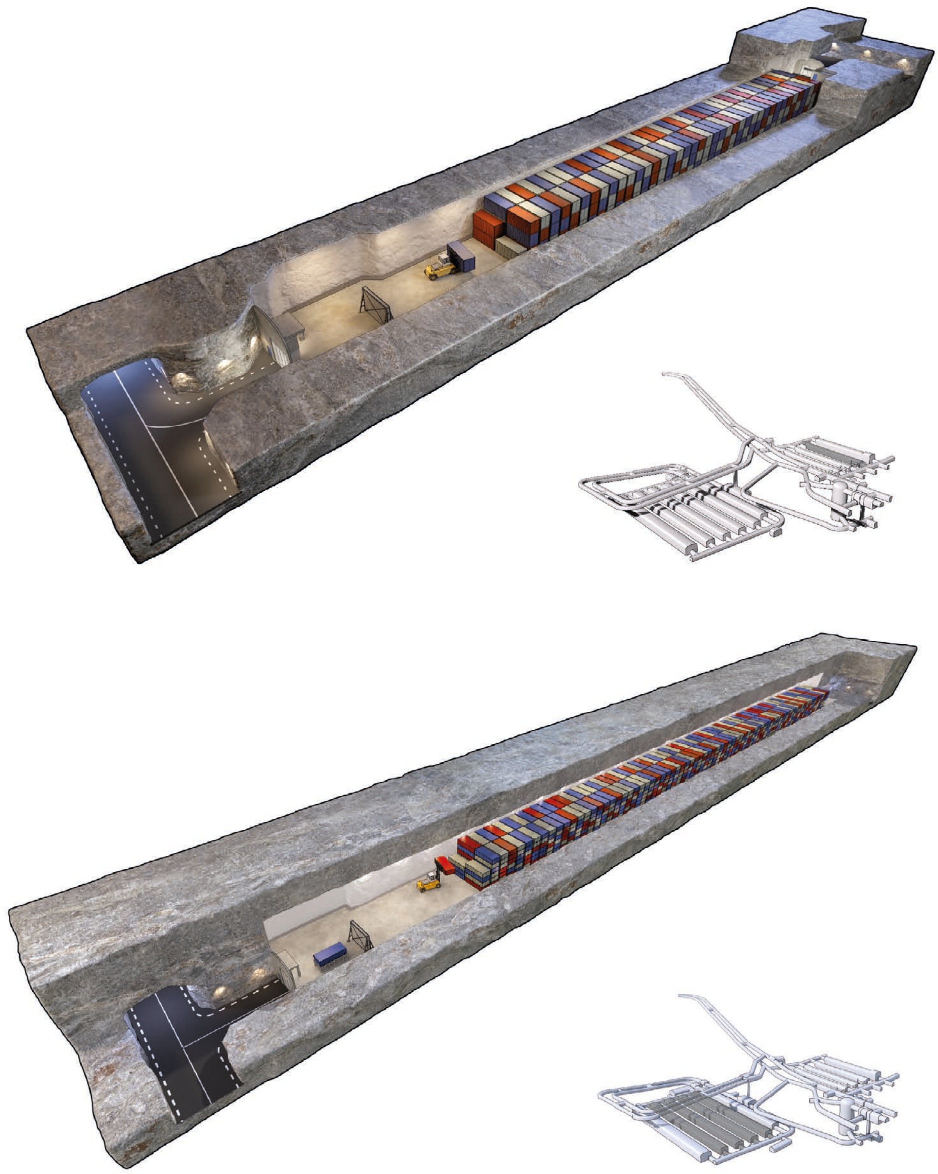

Figure 11-1. *Illustration of 1BLA (upper panel) and 2–5BLA (lower panel) during the operational period. The insets show the position in SFR of respective vaults highlighted in dark grey.*

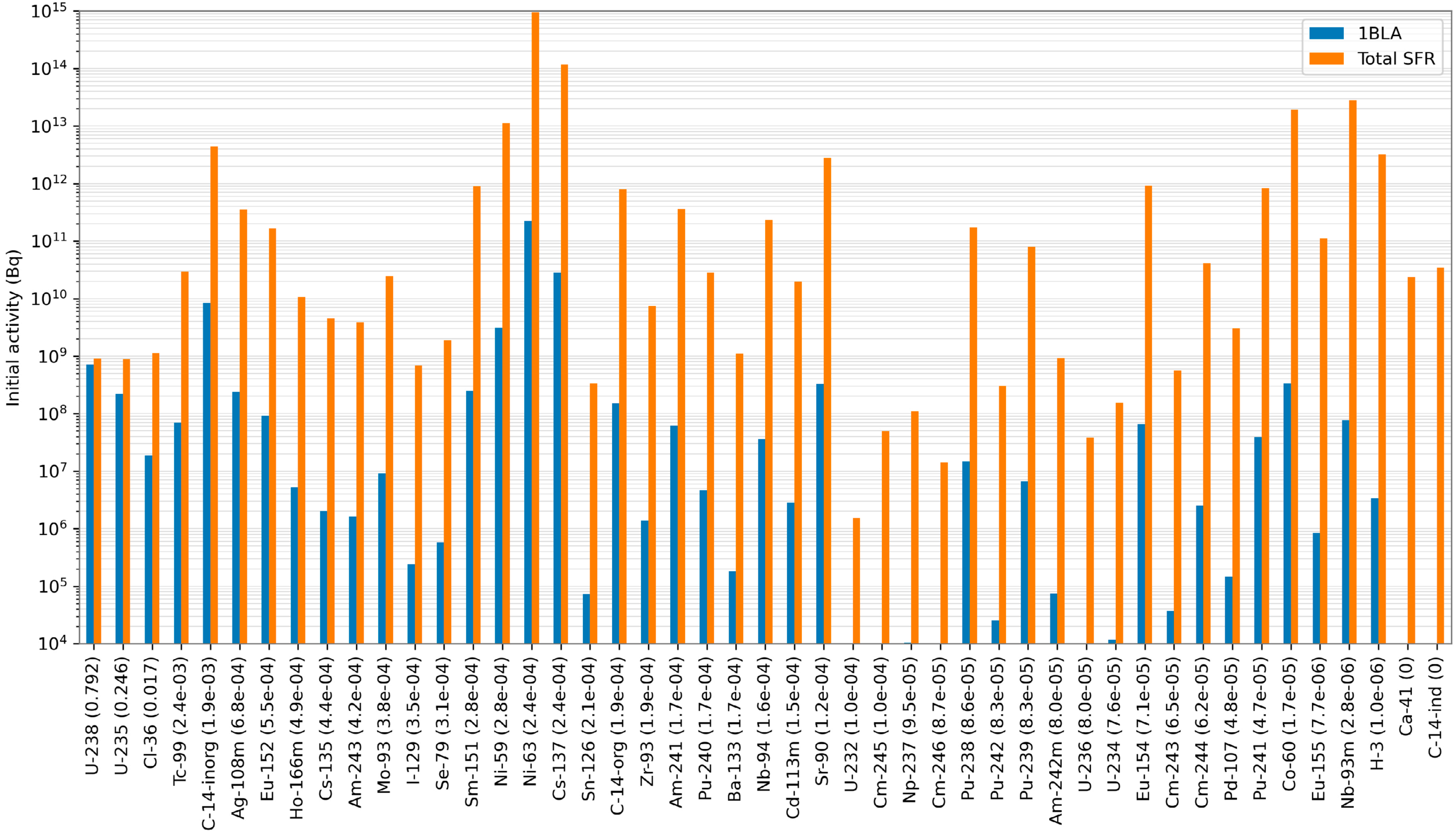

Figure 11-2. *Radionuclide inventory in 1BLA. The figure shows the inventory in 1BLA (blue bars) and the total inventory in SFR (orange bars). The bars are ordered so that the radionuclides with the largest fractions are shown to the left. The fraction is shown within parentheses after the radionuclide name.*

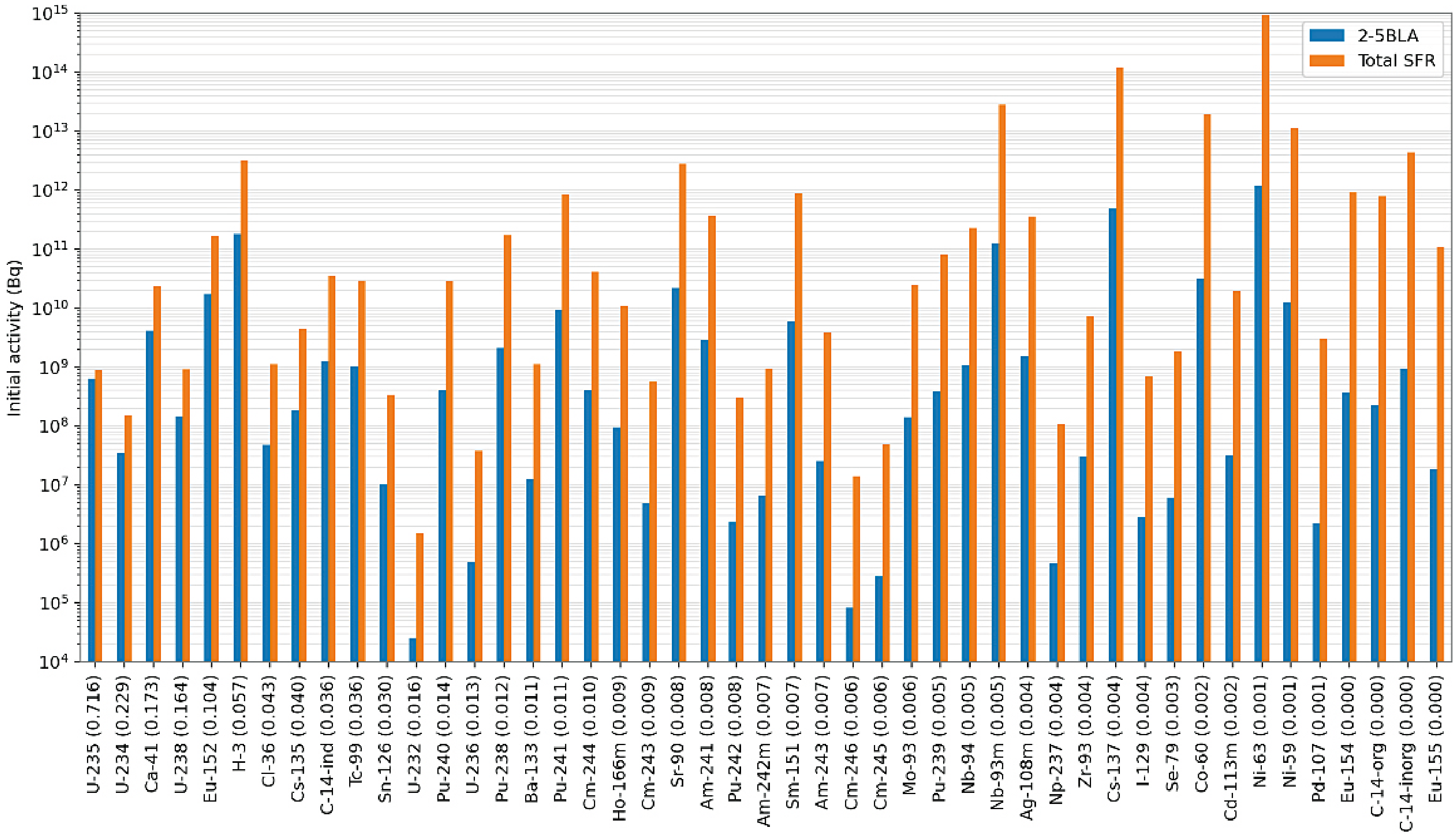

Figure 11-3. *Radionuclide inventory in 2–5BLA (total for all four vaults). The figure shows sum of the inventory in 2–5BLA (blue bars) and the total inventory in SFR (orange bars). The bars are ordered so that the radionuclides with the largest fractions are shown to the left. The fraction is shown within parentheses after the radionuclide name.*

11.2 Handling of waste

The waste domains in the BLA vaults are each modelled as stirred tanks, i.e. represented by only one compartment. Hence, the waste packages are not explicitly represented in the model.

11.3 Compartment structure

The compartment structures of the radionuclide transport models for 1BLA and 2BLA are shown in Figure 11-4. In 1BLA the waste domain is represented by one compartment and the crushed rock backfills in the vault ends are also represented by one compartment each. The models of the 2–5BLA vaults consist of only one single section, modelled as a stirred tank. Possible sorption that could occur in, for example, the concrete slab or concrete waste is not included in the radionuclide transport modelling.

The models of the 2–5BLA vaults are conceptually identical, though they differ with respect to the parameterisation of transfers due to slightly different flows obtained from the hydrological model.

As the models for 2–5BLA are identical, only the 2BLA model is further described in this report.

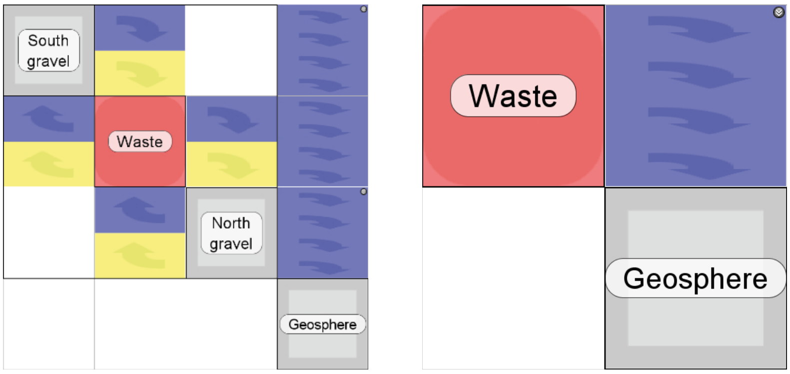

Figure 11-4. *Compartment structures for 1BLA (left) and 2–5BLA (right) in Ecolego.*

11.4 Dimensions

Table 11-1 shows the dimensions used in the BLA models.

Table 11-1. Dimensions for the BLA models.

Name	1BLA (m)	2–5BLA (m)	Description
waste_domain_length	146.3	243.0	Length of waste storage domain
north_gravel_length	10.0	8.2	Length of vault section with crushed rock backfill in the north end (loading zone in 1BLA)
south_gravel_length	3.7	23.8	Length of vault section with crushed rock backfill in the south end (loading zone in 2–5BLA)
vault_width	14.7	17.9	Vault width
vault_height	11.8	13.0	Vault height

Table 11-2 shows the L/A values used for the waste-domain and end-zones in the 1BLA model. Note that the 2–5BLA models do not have separate control-volumes/compartments for the end zones. Instead, the properties (porosity) of the 2–5BLA compartment are calculated as an average over the whole tunnel length. As the 1BLA model is divided in three compartments the diffusion along the tunnel is included to achieve appropriate mixing during periods with very low water flow. The approach taken for the 2–5BLA vaults would be appropriate also for 1BLA as the effect of the finer discretisation in 1BLA is negligible. However, to avoid tampering with the water flow data the RNT model discretisation for 1BLA follows the control-volumes used in the hydrological model.

Table 11-2. L/A values for the 1BLA model.

Section	Part	Direction	Area (m^2)	Length (m)	L/A (m^{-1})
SOUTH	SBF	L	173 (14.7 × 11.8)	3.7	0.021
Waste	Waste	L	173 (14.7 × 11.8)	146.3	0.843
NORTH	LZ	L	173 (14.7 × 11.8)	10.0	0.058

11.5 Water flow

Figure 11-5 shows the water flow in vault and waste for the 1BLA and 2BLA model. The initial increase in flow is caused by the increase in hydraulic gradient as the shoreline passes the repository due to shoreline regression. The figure shows the total flow through the waste and vault used in the RNT model, i.e. flows obtained from Abarca et al. (2020) with uncertainty factors from Table 4-1. As mentioned in Section 11.3 3–5BLA will not be discussed here as the results from these vaults are very similar to 2BLA, with only small differences in water flow (Abarca et al. 2020).

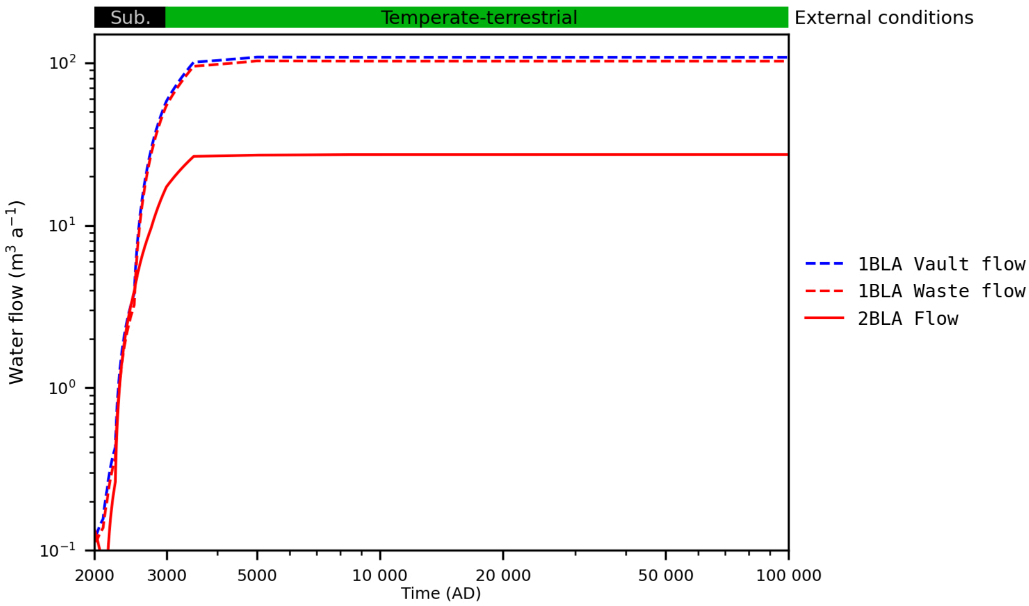

Figure 11-5. *Water flow through 1BLA and 2BLA (in 2BLA there is only one compartment i.e. tunnel and waste flow are the same).*

11.6 Releases in the base case

Figure 11-6 (upper panel) shows the radionuclide releases from 1BLA in the *base case* compared with the total releases from SFR. The 1BLA vault gives the dominating contribution to the U-238 release from SFR and a significant contribution to the release of U-235 during the initial period. Figure 11-6 (bottom panel) shows the radionuclide releases from 2BLA in the *base case* compared with the total releases from SFR. The 2BLA vault contributes significantly to the release of Ca-41 from SFR during the initial period. Considering that the releases from 2–5BLA are very similar it can be concluded that the initial release of Ca-41 and several other radionuclides (with fraction 0.25 in the lower panel in Figure 11-6) is dominated by the contributions from 2–5BLA. At later times 2BMA dominates the releases of Ca-41, as shown in Figure 8-8.

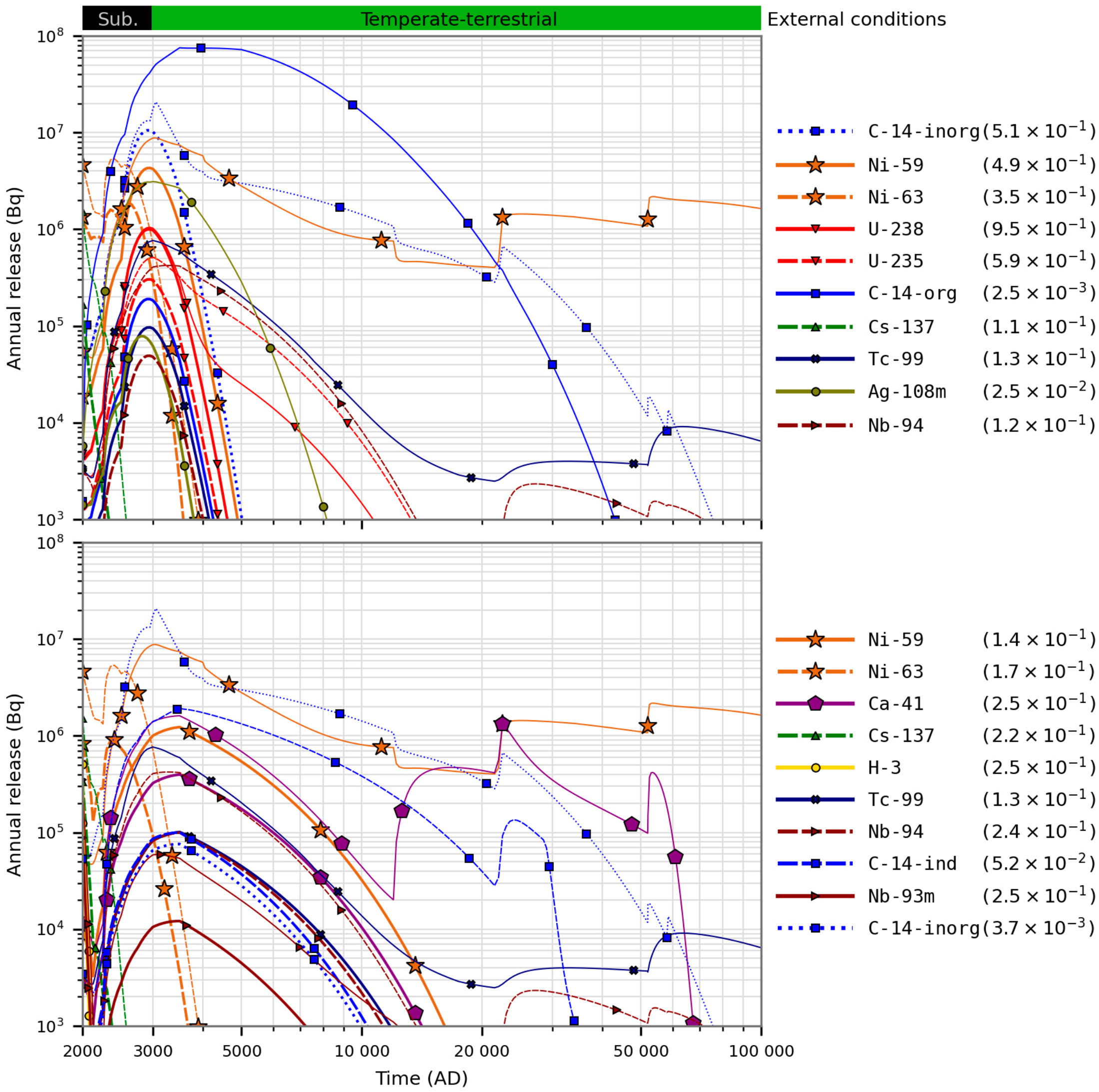

Figure 11-6. *Releases from 1BLA (upper panel) and 2BLA (bottom panel) (thick lines) compared with releases of the same radionuclides from SFR as a whole (thin lines). The colour bar in the upper part of the figure shows the evolution of the external conditions.*

12 Summary

12.1 Modelling and results

This report presents radionuclide transport models for the near-field (repository) of the existing and extended SFR. The models are developed in the compartment modelling tool Ecolego. The models are like the models used in SR-PSU, the previous safety assessment for SFR. However, the models have been updated to adopt the updated description of the existing and planned extension of SFR. Models have also to some extent been simplified to avoid overly detailed implementation of features that are of minor importance to the overall performance of the repository. This applies in particular to the simplified discretisation of the silo model. There have also been updates of input data which in some cases gives significant changes in modelling results compared with those obtained in SR-PSU. A comparison with results from SR-PSU is made in Appendix D.

The most significant releases are obtained for organic C-14, I-129 and Mo-93 at early time points and Ni-59 at later times. The releases of organic C-14, I-129 and Mo-93 are dominated by the releases from the silo and 1BMA. The release of Ni-59 has more evenly shared fractions from several vaults (1–2BMA, 1–2BTF and 1BRT), as shown in Chapters 7 to 10.

Releases in this report are presented mainly as activity releases. An alternative release measure (used only in Figure 12-1 in this report) is radiotoxicity release. Radiotoxicity release is obtained by multiplying the activity release (Bq) by the dose factor for ingestion (Sv Bq^{-1}) for each individual radionuclide. The dose factors used are discussed in Appendix A in the **Radionuclide transport report**. The advantage of presenting the release in this way is that the potential severity of different radionuclide releases can be more easily compared. In addition, radiotoxicity can be summed to a total release in a way that is meaningful, since summing activity releases of different radionuclides is not.

The ability for different vaults to contain their initial radiotoxicity is shown in Figure 12-1. It should be noted that the main part of the initial radiotoxicity remains or decays in the vaults. An exception to this is the BLA vaults where no sorption is taken into account. Note that as calculated in Figure 12-1 the released fraction continues to decay and ingrowth can take place, hence the radiotoxicity released from the BLA vaults continues to grow even after the vaults are depleted as the release contains a large fraction of U-235 and U-238 which decay to more toxic radionuclides.

It should be noted that the relative contributions of specific radionuclides and by different waste vaults to the total radionuclide release from the repository depend on several factors. These factors are influenced by the degree of pessimism in the modelling assumptions made concerning processes and parameter values. The assumptions may differ between vaults and radionuclides depending on their (expected) relative importance. Hence, the calculations should be seen as valid only for the purpose to show compliance with regulatory limits, i.e. they do not necessarily show a precise ranking of the actual contributions from individual vaults and radionuclides. One such assumption is the pessimistic handling of the BLA vaults where no sorption is taken into account. Another pessimistic assumption in the modelling is the omission of solubility limits, e.g. U-238 and U-235 in the BLA vaults may be subject to solubility limits, as discussed in Appendix C.

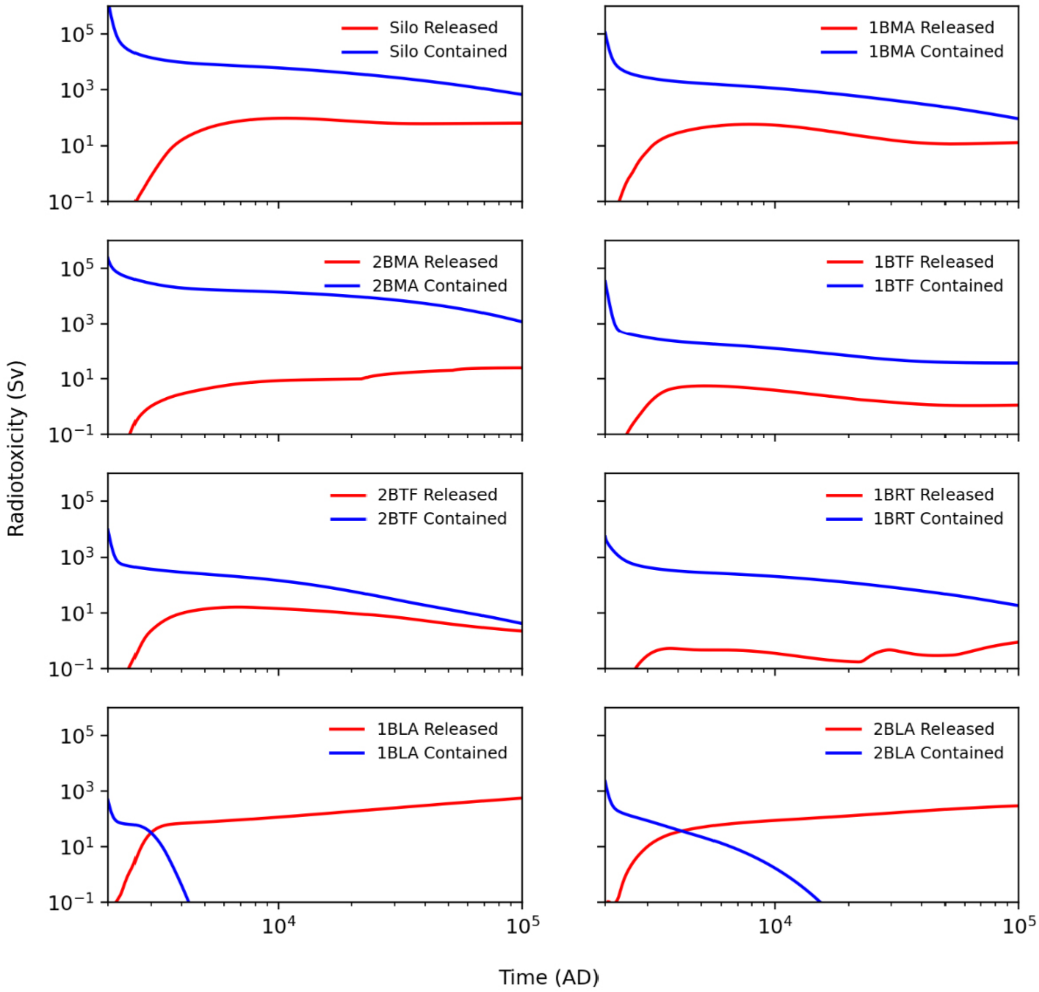

Figure 12-1. *Released and contained radiotoxicity over time for the vaults in SFR.*

12.2 Practical issues

Some of the models used in the PSAR consist of a relatively large number of compartments. The largest models contain several hundreds of compartments and parameters, and results for over fifty radionuclides are calculated. The handling of models and data represents a challenge in terms of quality assurance. The data management has been automated to avoid handling errors as far as possible.

This work has been carried out with a compartment-modelling approach, but since a very detailed discretisation becomes unpractical to handle in a compartment-based tool, other modelling tools such as finite element-based tools (e.g. Comsol Multiphysics) might be a good choice for deterministic supporting calculations. However, a simplified compartment model remains a good complement for probabilistic calculations, due to the lower demands for computing power with compartment models.

References

SKB's (Svensk Kärnbränslehantering AB) publications can be found at www.skb.com/publications.

References with abbreviated names

Post-closure safety report, 2023. Post-closure safety for SFR, the final repository for short-lived radioactive waste at Forsmark. Main report, the PSAR version. SKB TR-23-01, Svensk Kärnbränslehantering AB.

Barrier process report, 2023. Post-closure safety for SFR, the final repository for short-lived radioactive waste at Forsmark. Engineered barrier process report, the PSAR version. SKB TR-23-04, Svensk Kärnbränslehantering AB.

Data report, 2023. Post-closure safety for SFR, the final repository for short-lived radioactive waste at Forsmark. Data report, the PSAR version. SKB TR-23-10, Svensk Kärnbränslehantering AB.

FHA report, 2023. Post-closure safety for SFR, the final repository for short-lived radioactive waste at Forsmark. Handling of future human actions, the PSAR version. SKB TR-23-08, Svensk Kärnbränslehantering AB.

Initial state report, 2023. Post-closure safety for SFR, the final repository for short-lived radioactive waste at Forsmark. Initial state of the repository, the PSAR version. SKB TR-23-02, Svensk Kärnbränslehantering AB.

Model tools report, 2023. Post-closure safety for SFR, the final repository for short-lived radioactive waste at Forsmark. Model tools summary report, the PSAR version. SKB TR-23-11, Svensk Kärnbränslehantering AB.

Radionuclide transport report, 2023. Post-closure safety for SFR, the final repository for short-lived radioactive waste at Forsmark. Radionuclide transport and dose calculations, the PSAR version. SKB TR-23-09, Svensk Kärnbränslehantering AB.

Waste process report, 2023. Post-closure safety for SFR, the final repository for short-lived radioactive waste at Forsmark. Waste form and packaging process report, the PSAR version. SKB TR-23-03, Svensk Kärnbränslehantering AB.

Other references

Abarca E, Idiart A, de Vries L M, Silva O, Molinero J, von Schenk H, 2013. Flow modelling on the repository scale for the safety assessment SR-PSU. SKB TR-13-08, Svensk Kärnbränslehantering AB.

Abarca E, Silva O, Idiart A, Nardi A, Font J, Molinero J, 2014. Flow and transport modelling on the vault scale. Supporting calculations for the safety assessment SR-PSU. SKB R-14-14, Svensk Kärnbränslehantering AB.

Abarca E, Sampietro D, Sanglas J, Molinero J, 2020. Flow modelling at the near-field for the safety assessment SR-PSU (PSAR). SKB R-19-20, Svensk Kärnbränslehantering AB.

Bruno J, González-Siso M R, Duro L, Gaona X, Altmaier M, 2018. Key master variables affecting the mobility of Ni, Pu, Tc and U in the near field of the SFR repository. Main experimental findings and PA implications of the PhD thesis. SKB TR-18-01, Svensk Kärnbränslehantering AB.

COMSOL, 2017. COMSOL Multiphysics® v. 5.3. COMSOL AB, Stockholm, Sweden.

Holzbecher E, 2007. Environmental modelling: using Matlab. Berlin: Springer.

Keith-Roach M, Lindgren M, Källström K, 2014. Assessment of complexing agent concentrations in SFR. SKB R-14-03, Svensk Kärnbränslehantering AB.

Keith-Roach M, Lindgren M, Källström K, 2021. Assessment of complexing agent concentrations for the post-closure safety assessment in the PSAR SFR. SKB R-20-04, Svensk Kärnbränslehantering AB.

Lindgren M, Pettersson M, Karlsson S, Moreno L, 2001. Project SAFE. Radionuclide release and dose from the SFR repository. SKB R-01-18, Svensk Kärnbränslehantering AB.

Neretnieks I, Arve S, Moreno L, Rasmuson A, Zhu M, 1987. Degradation of concrete and transport of radionuclides from SFR-repository for low- and intermediate-level nuclear waste. SKB SFR 87-11, Svensk Kärnbränslehantering AB.

Quintessa, 2011. Postclosure safety assessment: analysis of the normal evolution scenario. NWMO DGR-TR-2011-26, Quintessa Ltd.

SKB, 2001. SFR 1. Slutförvar för radioaktivt driftavfall. Slutlig säkerhetsrapport, version 1.0. Svensk Kärnbränslehantering AB. (In Swedish.)

SKB R-08-130. SKB 2008. Safety analysis SFR 1. Long-term safety. Svensk Kärnbränslehantering AB.

SKB R-15-15. SKB 2015. Low- and intermediate-level waste in SFR. Reference inventory for waste 2013. Svensk Kärnbränslehantering AB.

SKB R-18-07. SKB 2019. Låg- och medelaktivt avfall i SFR. Referensinventarium för avfall 2016. Svensk Kärnbränslehantering AB. (In Swedish.)

SKB TR-10-50. SKB 2010. Radionuclide transport report for the safety assessment SR-Site. Svensk Kärnbränslehantering AB.

SKB TR-14-01. SKB 2015. Safety analysis for SFR. Long-term safety. Main report for the safety assessment SR-PSU. Revised version. Svensk Kärnbränslehantering AB.

SKB TR-14-09. SKB 2015. Radionuclide transport and dose calculations for the safety assessment SR-PSU. Revised edition. Svensk Kärnbränslehantering AB.

SKB TR-14-10. SKB 2014. Data report for the safety assessment SR-PSU. Svensk Kärnbränslehantering AB.

SKB TR-14-11. SKB 2014. Model summary report for the safety assessment SR-PSU. Svensk Kärnbränslehantering AB.

Svensson U, Ferry M, Kuylenstierna H-O, 2010. DarcyTools version 3.4 – Concepts, methods and equations. SKB R-07-38, Svensk Kärnbränslehantering AB.

Thomson G, Herben M, Lloyd P, Rose D, Smith C, Barraclough I, 2008. Implementation of project Safe in AMBER. Verification study for SFR 1 SAR-08. SKB R-08-13, Svensk Kärnbränslehantering AB.

Öhman J, Odén M, 2018. SR-PSU (PSAR) Bedrock hydrogeology. TD18 – Temperate climate conditions. SKB P-18-02, Svensk Kärnbränslehantering AB.

Appendix A

Input data files

A1 Version handling

The input data and script code for the PSAR is stored in the version handling system Subversion (SVN). A good overview of SVN in general can be found at: http://svnbook.red-bean.com/ A user friendly SVN client for windows can be downloaded from: https://tortoisesvn.net/downloads.html

The URL of the SVN repositories for the PSAR is: svn://svn.skb.se/PSU/. Input data files are stored in the folder: svn://svn.skb.se/PSU/PSAR/RNT-Data.

Results files are stored in the folder: svn://svn.skb.se/PSU/PSAR/RNT-Results.

A2 Ecolego Excel-file format for parameters

Most of the parameters used for the RNT modelling in the PSAR are stored in Excel spreadsheets.

The parameters used in the near-field models can be found in SVN in the directory:
svn://svn.skb.se/PSU/PSAR/RNT-Data/Near-field

Each spreadsheet of the Excel file can contain values of one or more parameters. The Excel file contains (at least) two spreadsheets. These two spreadsheets ("Definitions" and "Parameters") contain data that are read automatically into Ecolego. Hence, the data in these spreadsheets must follow a format described here. It should be noted that Ecolego accepts data to be organised in numerous ways in the Excel spreadsheets. The aim of this appendix is only to explain how the spreadsheets are organised and used.

A2.1 The "Definitions" spreadsheet

The definitions spreadsheet has several optional columns, but should contain at least the following columns:

- **Name** – The name of the parameter.
- **Dependencies** – The name(s) of the index list(s) for the parameters. If the parameters have multiple dimensions the names are comma separated. If the parameter is a scalar this column is left empty.
- **Unit** – The unit of the parameter.
- **Full name** – The full name of the parameter (may be empty).
- **Description** – A description of the parameter.

An alternative format (also used in the PSAR) for the dependencies is to use two columns instead of the Dependencies column:

- **Index list-1** – The first index list of the parameter (may be empty).
- **Index list-2** – The second index list of the parameter (may be empty).

A2.2 The "Parameters" spreadsheet

The "Parameters" spreadsheet contains the actual values of the parameter(s). The content is grouped as follows:

"Parameter" fields (two columns)

- **Name** – The name of the parameter (must be exactly as listed in the "Definitions" spreadsheet).
- **Unit** – The unit of the parameter (as listed on the "Definitions" spreadsheet).

“Dependencies” fields

These columns are used for indices of the value. The number and name(s) of columns depend on the dependencies of each parameter as listed in the definition section.

“Data” fields

Data – This group of columns is differently organised depending on whether the data is in the format of a parameter or a lookup table (time series).

For parameters:

- **Value** – The deterministic (best estimate) value of a parameter.

For lookup tables:

- **Lookup data** – The “x” value of a lookup table, typically time.
- **Values** – The “y”-values of a lookup table.
- **Cyclic** – Indicates whether the time series is cyclic or not (TRUE or FALSE).
- **Interpolation** – Interpolation method used (needs only to be assigned to the first entry for each name).

“Distribution” fields

This group of columns is needed only if any of the parameters has a distribution.

- **PDF** – The distribution, defined with a name and formal arguments.

The rest of the columns in the “Distribution” fields contain actual arguments to the distribution with column names depending on the distribution.

“References” fields (two columns)

- **References** – Literature references.
- **Comment** – A comment to the parameter entry.

“Export info” fields (one column)

- **ID** – The full path to the parameter in the model.

QA fields

The “Responsible persons” fields and the “QA status” are not read by Ecolego but exist only for the purpose of QA. More details about the QA can be found in the **Radionuclide transport report**, Appendix A.

A3 Input data file locations

The actual input data files used in the simulation can be found on SVN.

Files used in this report are dated before 2021-06-16.

A3.1 Input data files common to several models

Near-field K_d parameters can be found on SVN in the files:

svn://svn.skb.se/PSU/PSAR/RNT-Data/Near-field/Kd.xlsm

svn://svn.skb.se/PSU/PSAR/RNT-Data/Near-field/KdGravel.xlsm

For bentonite and crushed rock the diffusivities,porosities and densities are assumed to be constant in time and the same for all vaults. The (particle) densities are also assumed to be constant in time for all concrete materials. These parameter files can be found on SVN in the files:

svn://svn.skb.se/PSU/PSAR/RNT-Data/Near-field/De.xlsm

svn://svn.skb.se/PSU/PSAR/RNT-Data/Near-field/Porosity.xlsm

svn://svn.skb.se/PSU/PSAR/RNT-Data/Near-field/Rho.xlsm

Note that the development of diffusivities in concrete materials allows for seven different degradation states. The time points for changes between these states are given in the file:

svn://svn.skb.se/PSU/PSAR/RNT-Data/Near-field/DeSelector.xlsm

Note that this file is common for all vaults and the differences between vaults are instead determined by the data in the files for concrete porosity and concrete diffusivity given in the sections below.

A3.2 Input data files for the silo model (Chapter 6)

Water flow rates:
svn://svn.skb.se/PSU/PSAR/RNT-Data/Near-field /Silo/Silo_WaterFluxes.xlsx

Qeq flow rates:
svn://svn.skb.se/PSU/PSAR/RNT-Data/Near-field /Silo/Silo_QeqParameter.xlsx

Time points for changes in water flow:
svn://svn.skb.se/PSU/PSAR/RNT-Data/Near-field/Silo/Silo_BarrierFailure.xlsm

Time points for changes in K_d values:
svn://svn.skb.se/PSU/PSAR/RNT-Data/Near-field/Silo/Silo_KdSelector.xlsm

Typical (average) initial radionuclide amount per waste package:
svn://svn.skb.se/PSU/PSAR/RNT-Data/Near-field /RawdataDeliveries/LOMA/mc_tia_Silo.csv

Number of waste packages:
svn://svn.skb.se/PSU/PSAR/RNT-Data/Near-field /Silo/Silo_NRWP.xlsm

Sorption reduction factors:
svn://svn.skb.se/PSU/PSAR/RNT-Data/Near-field /Silo/Silo_SRF.xlsm
svn://svn.skb.se/PSU/PSAR/RNT-Data/Near-field /Silo/Silo_SRFTiming.xlsm

Diffusivities:
svn://svn.skb.se/PSU/PSAR/RNT-Data/Near-field /Silo/Silo_De.xlsm

Porosities:
svn://svn.skb.se/PSU/PSAR/RNT-Data/Near-field /Silo/Silo_ConcretePorosity.xlsm

Dimensions:
svn://svn.skb.se/PSU/PSAR/RNT-Data/Near-field/Silo/Silo_Dimensions.xlsm

A3.3 Input data files for the 1BMA model (Chapter 7)

Water flow rates:
svn://svn.skb.se/PSU/PSAR/RNT-Data/Near-field/BMA1/BMA1_WaterFluxes_Partial_Repair.xlsx

Time points for changes in water flow:
svn://svn.skb.se/PSU/PSAR/RNT-Data/Near-field/BMA1/BMA1_BarrierFailure.xlsm

Time points for changes in K_d values:
svn://svn.skb.se/PSU/PSAR/RNT-Data/Near-field/BMA1/BMA1_KdSelector.xlsm

Typical (average) initial radionuclide amount per waste package:
svn://svn.skb.se/PSU/PSAR/RNT-Data/Near-field/RawdataDeliveries/LOMA/mc_tia_1BMA.csv

Number of waste packages:
svn://svn.skb.se/PSU/PSAR/RNT-Data/Near-field /BMA1/BMA1_NRWP.xlsm

Sorption reduction factors:
svn://svn.skb.se/PSU/PSAR/RNT-Data/Near-field/BMA1/BMA1_SRF.xlsm
svn://svn.skb.se/PSU/PSAR/RNT-Data/Near-field/BMA1/BMA1_SRFTiming.xlsm

Diffusivities:
svn://svn.skb.se/PSU/PSAR/RNT-Data/Near-field/BMA1/BMA1_De.xlsm

Porosities:
svn://svn.skb.se/PSU/PSAR/RNT-Data/Near-field /BMA1/BMA1_ConcretePorosity.xlsm

Dimensions:
svn://svn.skb.se/PSU/PSAR/RNT-Data/Near-field/BMA1/BMA1_Dimensions_Partial_Repair.xlsm

A3.4 Input data files for the 2BMA model (Chapter 8)

Water flow rates:
svn://svn.skb.se/PSU/PSAR/RNT-Data/Near-field/BMA2/BMA2_WaterFluxes.xlsx

Time points for changes in water flow:
svn://svn.skb.se/PSU/PSAR/RNT-Data/Near-field/BMA2/BMA2_BarrierFailure.xlsm

Time points for changes in K_d values:
svn://svn.skb.se/PSU/PSAR/RNT-Data/Near-field/BMA2/BMA2_KdSelector.xlsm

Typical (average) initial radionuclide amount per waste package:
svn://svn.skb.se/PSU/PSAR/RNT-Data/Near-field/RawdataDeliveries/LOMA/mc_tia_2BMA.csv

Number of waste packages:
svn://svn.skb.se/PSU/PSAR/RNT-Data/Near-field /BMA2/BMA2_NRWP.xlsm

Diffusivities:
svn://svn.skb.se/PSU/PSAR/RNT-Data/Near-field/BMA2/BMA2_De.xlsm

Porosities:
svn://svn.skb.se/PSU/PSAR/RNT-Data/Near-field /BMA2/BMA2_ConcretePorosity.xlsm

Dimensions:
svn://svn.skb.se/PSU/PSAR/RNT-Data/Near-field/BMA2/BMA2_Dimensions.xlsm

A3.5 Input data files for the 1BRT model (Chapter 9)

Water flow rates:
svn://svn.skb.se/PSU/PSAR/RNT-Data/Near-field/BRT/BRT_WaterFluxes.xlsx

Time points for changes in water flow:
svn://svn.skb.se/PSU/PSAR/RNT-Data/Near-field/BRT/BRT_BarrierFailure.xlsm

Time points for changes in K_d values:
svn://svn.skb.se/PSU/PSAR/RNT-Data/Near-field/BRT/BRT_KdSelector.xlsm

Typical (average) initial radionuclide amount per waste package:
svn://svn.skb.se/PSU/PSAR/RNT-Data/Near-field/RawdataDeliveries/LOMA/mc_tia_BRT.csv

Number of waste packages:
svn://svn.skb.se/PSU/PSAR/RNT-Data/Near-field /BRT/BRT_NRWP.xlsm

Diffusivities:
svn://svn.skb.se/PSU/PSAR/RNT-Data/Near-field/BRT/BRT_De.xlsm

Porosities:
svn://svn.skb.se/PSU/PSAR/RNT-Data/Near-field /BRT/BRT_ConcretePorosity.xlsm

Dimensions:
svn://svn.skb.se/PSU/PSAR/RNT-Data/Near-field/BRT/BRT_Dimensions.xlsm

A3.6 Input data files for the 1–2BTF models (Chapter 10)

Water flow rates:
svn://svn.skb.se/PSU/PSAR/RNT-Data/Near-field/BTF1/BTF1_WaterFluxes.xlsx
svn://svn.skb.se/PSU/PSAR/RNT-Data/Near-field/BTF2/BTF2_WaterFluxes.xlsx

Time points for changes in water flow:
svn://svn.skb.se/PSU/PSAR/RNT-Data/Near-field/BTF/BTF_BarrierFailure.xlsm

Time points for changes in K_d values:
svn://svn.skb.se/PSU/PSAR/RNT-Data/Near-field/BTF/BTF_KdSelector.xlsm

Typical (average) initial radionuclide amount per waste package:
svn://svn.skb.se/PSU/PSAR/RNT-Data/Near-field/RawdataDeliveries/LOMA/mc_tia_1BTF.csv
svn://svn.skb.se/PSU/PSAR/RNT-Data/Near-field/RawdataDeliveries/LOMA/mc_tia_2BTF.csv

Number of waste packages:
svn://svn.skb.se/PSU/PSAR/RNT-Data/Near-field /BTF1/BTF1_NRWP.xlsm
svn://svn.skb.se/PSU/PSAR/RNT-Data/Near-field /BTF2/BTF2_NRWP.xlsm

Diffusivities:
svn://svn.skb.se/PSU/PSAR/RNT-Data/Near-field/BTF/BTF_De.xlsm

Porosities:
svn://svn.skb.se/PSU/PSAR/RNT-Data/Near-field /BTF/BTF_ConcretePorosity.xlsm

Sorption reduction factors:
svn://svn.skb.se/PSU/PSAR/RNT-Data/Near-field/BTF1/BTF1_SRF.xlsm
svn://svn.skb.se/PSU/PSAR/RNT-Data/Near-field/BTF1/BTF1_SRFTiming.xlsm
svn://svn.skb.se/PSU/PSAR/RNT-Data/Near-field/BTF2/BTF2_SRF.xlsm
svn://svn.skb.se/PSU/PSAR/RNT-Data/Near-field/BTF2/BTF2_SRFTiming.xlsm

Dimensions (common for 1BTF and 2BTF):
svn://svn.skb.se/PSU/PSAR/RNT-Data/Near-field/BTF/BTF_Dimensions.xlsm

A3.7 Input data files for the 1–5BLA models (Chapter 11)

Water flow rates:
svn://svn.skb.se/PSU/PSAR/RNT-Data/Near-field/BLA1/BLA1_WaterFluxes.xlsx
svn://svn.skb.se/PSU/PSAR/RNT-Data/Near-field/BLA2-5/BLA2_WaterFluxes.xlsx
svn://svn.skb.se/PSU/PSAR/RNT-Data/Near-field/BLA2-5/BLA3_WaterFluxes.xlsx
svn://svn.skb.se/PSU/PSAR/RNT-Data/Near-field/BLA2-5/BLA4_WaterFluxes.xlsx
svn://svn.skb.se/PSU/PSAR/RNT-Data/Near-field/BLA2-5/BLA5_WaterFluxes.xlsx

Typical (average) initial radionuclide amount per waste package:
svn://svn.skb.se/PSU/PSAR/RNT-Data/Near-field/RawdataDeliveries/LOMA/mc_tia_1BLA.csv
svn://svn.skb.se/PSU/PSAR/RNT-Data/Near-field/RawdataDeliveries/LOMA/mc_tia_2-5BLA.csv

Number of waste packages:
svn://svn.skb.se/PSU/PSAR/RNT-Data/Near-field /BLA1/BLA1_NRWP.xlsm
svn://svn.skb.se/PSU/PSAR/RNT-Data/Near-field /BLA2-5/BLA2-5_NRWP.xlsm

Dimensions:
svn://svn.skb.se/PSU/PSAR/RNT-Data/Near-field/BLA1/BLA1_Dimensions.xlsm
svn://svn.skb.se/PSU/PSAR/RNT-Data/Near-field/BLA2-5/BLA2-5_Dimensions.xlsm

Appendix B

Implementation details

There are two possible approaches to building models and handling assessments in Ecolego; using a graphical user interface to manually build models and perform assessments or using a programmatic approach where the models are built and handled with scripts.

In the PSAR assessment the programmatic approach has been used as far as possible. Reasons for using this approach, i.e., programmatically created models, are that it facilitates consistency among multiple models and model variants, it eases reproducibility, and eases revision and adjustment without having to repeat lengthy, tedious and error-prone procedures in a graphical user interface.

Scripts for Ecolego are written using the Java programming language. Scripts can be written in any text editor (e.g. Notepad), but it is advised to write the code in a development tool suited for Java programming, such as Eclipse (https://www.eclipse.org), which has been used here.

The handling of various processes in the model is described on a conceptual level in Sections 2.2 to 2.4. However, more technical details of the implementation of the models are presented here.

B1 User defined index-lists

As mentioned in Section 3.5, Ecolego allows the user to use vectorised data based on index-lists to facilitate the handling of data in the models. In addition to the predefined index-lists in Ecolego, several user-defined index-lists have been used in the near-field models.

The user-defined index-lists are described below;

Species – This is a mapped index-list, which has indices for each species of the radionuclides in the model. This list is similar to the pre-defined Elements index-list but allows several entries for one radionuclide; this is useful for handling of parameters for several species of one radionuclide e.g. the three forms of C-14 used.

Sections – This index-list is used to simplify the calculation of the amount of waste in different sections of the model. The index-list is used by the parameter NRWP (Number of Real Waste Packages) and the expression NMWP (Number of Model Waste Packages).

WasteCompartments – this index-list is a sub-set of the Compartments index list used to facilitate the handling of the initial radionuclide inventory and the dimensions of compartments representing waste.

BarrierCompartments – this index-list is a sub-set of the Compartments index list used to facilitate the handling of dimensions for compartments representing barriers and backfill.

ModelWasteTypes – this index-list contains indices for all model waste types in a model. This index-list is used by the expression NMWP (Number of Model Waste Packages).

RealWasteTypes – this index-list contains indices for all real waste types that are used in the model. This index-list is used by the parameter TIA (Typical Initial Amount) and the parameter NRWP (Number of Real Waste Packages). TIA and NRWP (and NMWP) are used to calculate the total amounts of radionuclides in different sections of the model.

Parts – this index-list is used to avoid direct dependencies between compartments and parameters in respect of dimensions. This is useful when various parts are discretised for numerical reasons, but dimensions are calculated for the whole part. This is useful specifically for parts that are represented by transport blocks.

Media – this index-list is mapped to the Compartments index-list. The index-list contains the media (materials) in each compartment such as concrete, bentonite etc. The index-list is used to facilitate the handling of medium-dependent data such as diffusivities, sorption coefficients, porosities, densities etc.

MixedMedia – this index-list contains media that are mixes of other media for which sorption properties are defined.

FlowPaths – this index-list facilitates the mapping of the results from the hydrological modelling to the RNT model (as described in Section B4).

AdvectiveTransfers – this index-list is a sub-set of the Transfers index list and has indices for each advective transfer in the model. This facilitates the handling of the water flow rates in the model.

DiffusiveTransfers – this index-list is a sub-set of the Transfers index list and has indices for each diffusive transfer in the model.

B2 Radionuclide inventory and waste materials

B2.1 BLA and 1BRT

For the BLA and 1BRT models, the parameters for the radionuclide inventory needs no pre-processing in the RNT model. The parameters are directly imported to the models from data files stored on SVN.

B2.2 BMA, BTF and the silo

For BMA, BTF and the silo, the amounts of radionuclides and cementitious materials related to the waste packages are calculated in the Ecolego models.

The parameters and expressions used to calculate the amounts of radionuclides and materials related to the waste packages in different sections of the models are:

- **TIA**: This parameter is used to specify the typical (average) initial amount (TIA) of radionuclides in all types of waste packages in SFR. The parameter has two dependencies, the **Radionuclides** and **RealWasteTypes** index-lists.
- **NRWP**: This is a parameter used to specify the number of (real) waste packages in the model. In some cases (1BMA, 1BTF and the silo) NRWP also contains information on the emplacement of waste in different sections of the model. The parameter has one or two dependencies; the **RealWasteTypes** index-list and also the **Sections** index-list in the cases when the parameter also contains information on the emplacement of waste.
- **NRWPExpr**: This is an expression used in 1–2BTF, 2BMA and the silo to specify the number of (real) waste packages in different sections of the model. The parameter has two dependencies, the **RealWasteTypes** and **Sections** index-lists. For 2BTF and 2BMA, the distribution of waste is simply done by dividing NRWP by the number of sections in the model (i.e. the activity is assumed to be evenly distributed over all sections of the model). For the silo, the NRWP parameter contains information of the distribution of waste between the inner and outer parts of the silo, thus NRWPExpr for the silo is used only to provide an even distribution of waste between the five vertical (model) sections in the silo. For 1BTF, the NRWP parameter contains information of the distribution of waste between the part of the vault where drums are stored and the part where concrete tanks are stored. Thus, NRWPExpr for 1BTF is used only to provide an even distribution of waste within these two parts of the vault.
- **NMWP**: This is an expression used to calculate the number of model waste packages in different sections of the model. The expression has two dependencies, the **ModelWasteTypes** and **Sections** index-lists. The calculation is based on the mapping between real waste types and model waste types provided in Chapter 5.
- **InitialAmount**: This is an expression used to calculate the initial amounts of radionuclides in each model waste package in the model. The expression has two dependencies, the **Radionuclides** and **WasteCompartments** index-lists.

B3 Dimensions and diffusive resistances

Key dimensions of the repository parts are provided as parameters to the Ecolego models. Expressions in the Ecolego models are used to derive the dimensions for individual compartments from these parameters.

Compartment dimensions are defined in three spatial dimensions for all vaults except the silo which is defined in two directions (axial and radial) and 1BRT which is one-dimensional. The expressions used in the three-dimensional case is defined as follows:

- **ldir**: dimension in direction of vault.
- **vdir**: dimension in the vertical direction.
- **hdir**: dimension across vault.

The quantities above are used to calculate the quantity length per cross-section area L/A in all directions as

- **la_ldir** = dim_ldir / (dim_vdir · dim_hdir): L/A in the direction along the vault.
- **la_vdir** = dim_vdir / (dim_ldir · dim_hdir): L/A in the vertical direction.
- **la_hdir** = dim_hdir / (dim_ldir · dim_vdir): L/A across the vault.

In some cases, a transport block is used to represent a part of the repository, in such cases the value above is divided by the number of compartments represented by the transport block (*nCompsInBarriers*).

B3.1 Diffusive resistances

Diffusive resistances are calculated according to Equation 2-5 as:

- **res_ldir** = la_ldir / DeExpr : diffusive resistance in the direction along the vault.
- **res_vdir** = la_vdir / DeExpr : diffusive resistance in the vertical direction.
- **res_hdir** = la_hdir / DeExpr : diffusive resistance across the vault.

The diffusive resistance for compartments representing waste packages is described with a single value (i.e. the waste is handled with a simplified one-dimensional approach).

- **res_waste** = la_waste/(DeExpr · NMWP[“Model waste type”][“Section_ID”])

The L/A values for waste packages are presented in Table 5-3.

B4 Water flow

The water flow used in an advective transfer (Equation 2-3) is represented by the expression *Q* in the model.

The value for an entry in *Q* is on the form:

Q = switch_flow · **flowOut**[“flow path”]

or

Q = switch_flow · **flowIn**[“flow path”]

Where “flow path” is a member of the *FlowPaths* index-list. The indices in the *FlowPaths* index-list correspond to the surfaces of the control volumes. The choice between *flowOut* and *flowIn* is dependent on if the transfer using the *Q* value is directed out from or into the control volume through the surface in question. This corresponds to flows out from a control volume or flows into a control volume. The expression *switch_flow* can be used to scale the waterflows or to completely stop the advective fluxes during periods when there is no water flow (e.g. during permafrost).

flowOut and **flowIn** have the form:

flowOut = if(**QParExpr**>=0.0,**QParExpr**,0.0)

and

flowIn = if(**QParExpr**<0.0,-**QParExpr**,0.0)

Where **QParExpr** is an expression used to select water flow for the current time point in the simulation. (The physical degradation of the concrete structures affects water flow, porosity and diffusivity. The handling of diffusivity and porosity is discussed in Section B5)

Here the conditional expression in Ecolego is used. The form of the conditional expression is:
if(condition, "value if condition is true", "value if condition is false")

The **QParExpr** has the form:

QParExpr=QParBaseCase·BarrierDegradation0+QParModDeg·BarrierDegradation1+QParSevDeg·BarrierDegradation2+QParCompDeg·BarrierDegradation3

i.e. **QParExpr** selects between (up to four) parameter sets from the hydrological modelling corresponding to water flow for different physical degradation states.

BarrierDegradation0, BarrierDegradation1, BarrierDegradation2 and BarrierDegradation3 are "switches", active one at a time.

B5 Diffusivity and porosity

The value for effective diffusivity D_e in Equation 2-5 is implemented with an expression called **DeExpr** in the Ecolego models.

DeExpr is used to select D_e values for the current physical degradation state (for the current time-point), and to convert the unit to m^2a^{-1}.

DeExpr has the following form:

$$\begin{cases} \mathrm{DeExpr}(t) = \displaystyle\sum_{i=1}^{7} \mathrm{DeDS}(i)\mathrm{DeSEL}(i,t) \\ \displaystyle\sum_{i=1}^{7} \mathrm{DeSEL}(i,t) = 1\,; \mathrm{DeSEL}(i,t) \geq 0 \end{cases}$$

where:

DeSEL1–DeSEL7 are lookup tables that selects one time-window each.

DeDS1–DeDS7 are the D_e values for different physical degradation states.

The value for porosity of different media in Equation 2-2 is implemented with an expression called porosityExpr in the RNT models. The expression porosityExpr is used to select porosity values for each of the media for the current physical degradation state (at a given time *t*).

porosityExpr has the following form:

$$\begin{cases} \mathrm{porosityExpr}(t) = \displaystyle\sum_{i=1}^{7} \mathrm{PorDS}(i)\mathrm{DeSEL}(i,t) \\ \displaystyle\sum_{i=1}^{7} \mathrm{DeSEL}(i,t) = 1\,; \mathrm{DeSEL}(i,t) \geq 0 \end{cases}$$

where:

PorDS1–PorDS7 are the porosity values for different physical degradation states.

DeSEL1–DeSEL7 are the switches for diffusivity, which are also used for the porosity.

B6 Sorption

KdExpr selects K_d values for the current chemical degradation state (at a given time t), applies sorption reduction factors and scales K_d for cement contents.

KdExpr has the following form (for cementitious materials):

$$\begin{cases} \mathrm{KdExpr}(t) = \sum_{i=1}^{4} \mathrm{KdDS}(i)\ \mathrm{KdSEL}(i,t)\ \mathrm{FracCem(m)}\ /\ \mathrm{SRFExpr(t)} \\ \qquad\qquad\quad \sum_{i=1}^{4} \mathrm{KdSEL}(i,t) = 1\,;\mathrm{KdSEL}(i,t) \geq 0 \end{cases}$$

where:

KdDS1, KdDS2, KdDS3_first_part and KdDS3_second_part are the K_d values for pure cement for different chemical degradation states (I, II, IIIa and IIIb).

KdSEL1, KdSEL2, KdSEL3_first_part and KdSEL3_second_part are lookup tables that selects one time-window each.

SRFExpr is an expression used to apply time-dependent sorption reduction factors due to complexing agents.

Where:

FracCem(m) is a parameter for the cement fraction in the cementitious medium m.

Appendix C

Supporting calculations

Several supporting calculations are performed to illustrate different aspects of the models and to ensure that the models are correctly implemented. Some of the calculations have similarities with calculation cases in the PSAR (**Post-closure safety report**). However, the results here are from deterministic calculations based on preliminary data and are intended only for the verification of the models and not for evaluation of the performance of SFR.

C1 No sorption

The objective of this calculation is to illustrate the importance of sorption, which is dominated by sorption on cementitious materials. However, for some radionuclides sorption on bentonite (in the silo) is also of significance. In this calculation case all K_d values are set to zero.

As can be seen in Figure C-1 to Figure C-5 releases of Ni-59, Ni-63 and C-14-inorg become the dominating if no sorption is taken into account. The release of C-14-inorg and Ni-63 in the *base case* are generally too low to be visible in the figures (i.e. the thin line is missing in the figure as the maximum release in the *base case* is below 1 000 Bq).

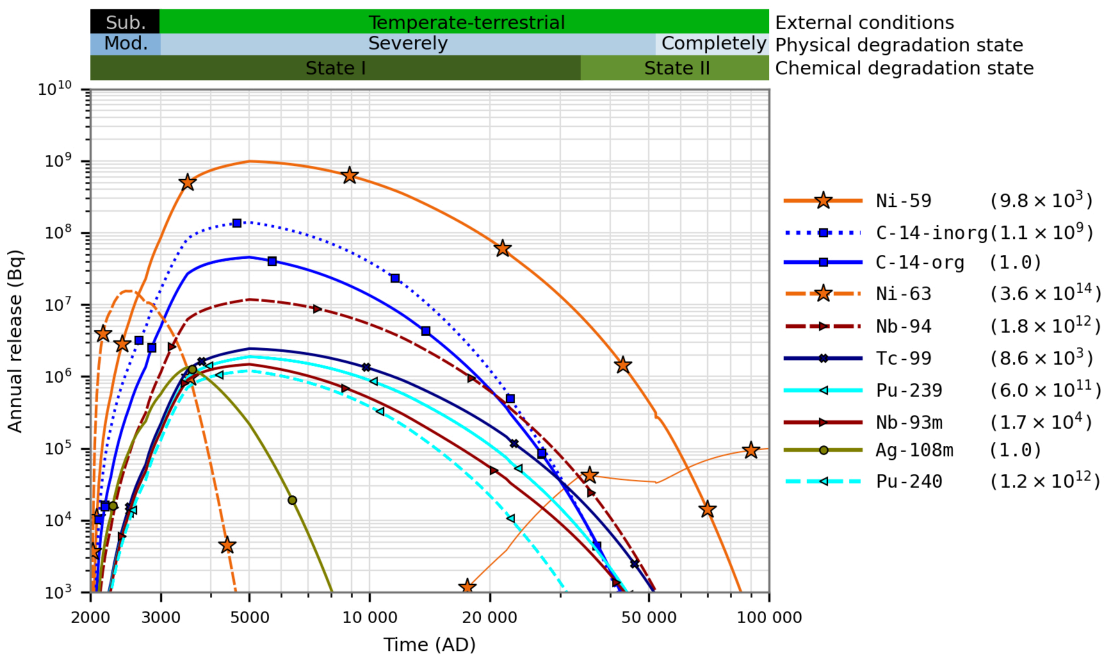

Figure C-1. *Comparison of releases from the silo without sorption (thick lines) and for the base case (thin lines). The values in parentheses show the ratio between the maximum release in the present case and the base case.*

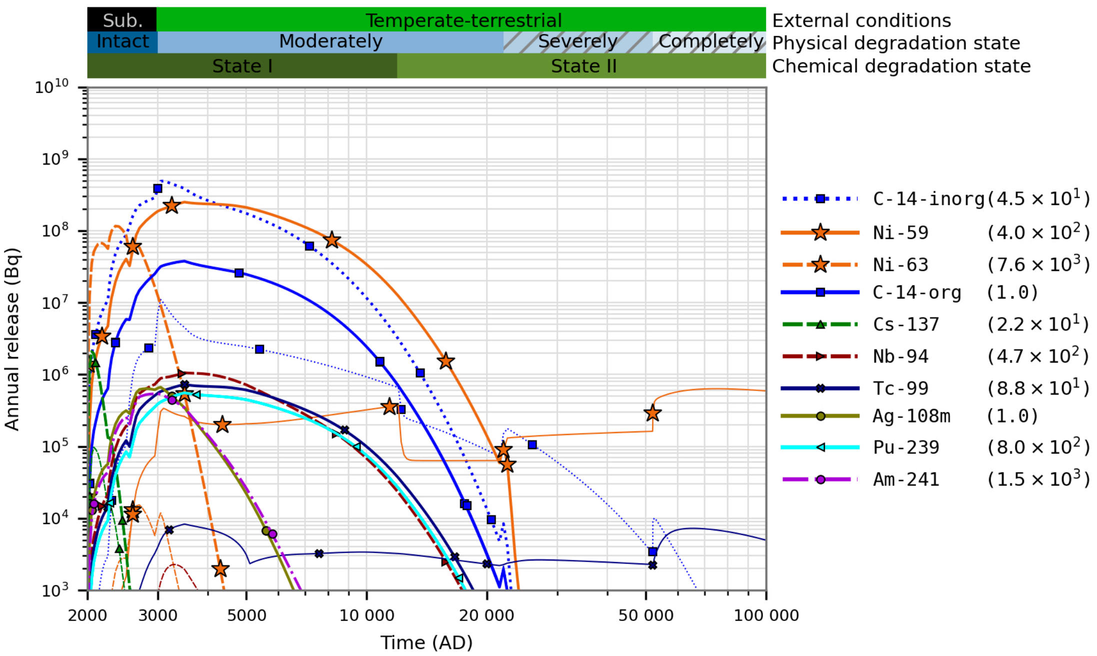

Figure C-2. *Comparison of the releases from 1BMA without sorption (thick lines) and for the base case (thin lines). The values in parentheses show the ratio between the maximum release in the present case and the base case.*

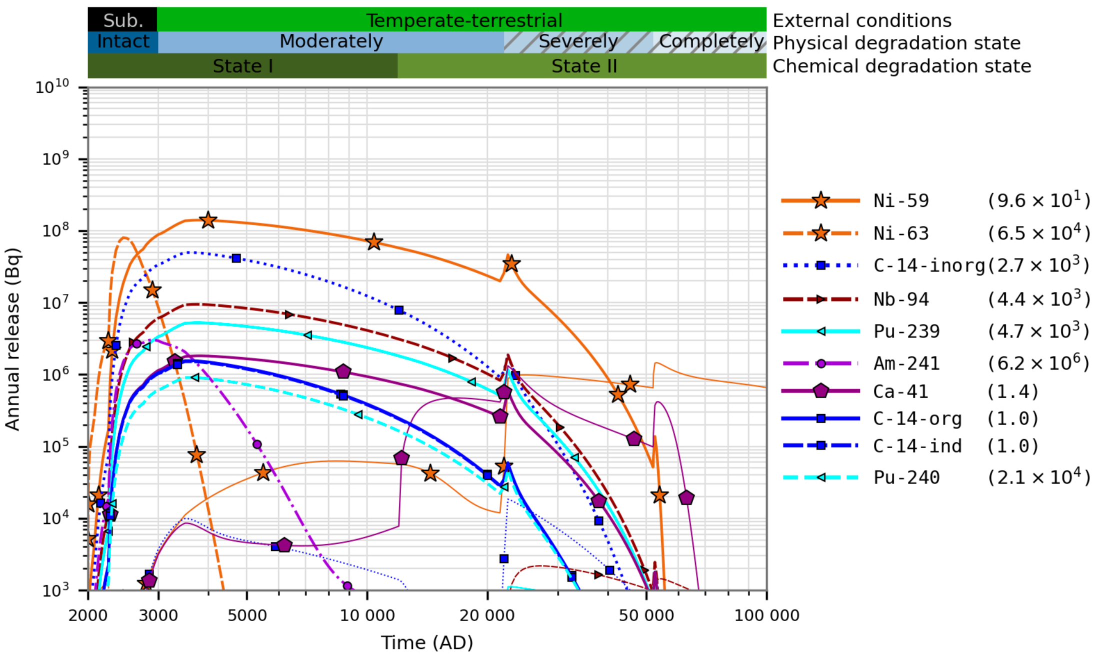

Figure C-3. *Comparison of the releases from 2BMA without sorption (thick lines) and for the base case (thin lines). The values in parentheses show the ratio between the maximum release in the present case and the base case.*

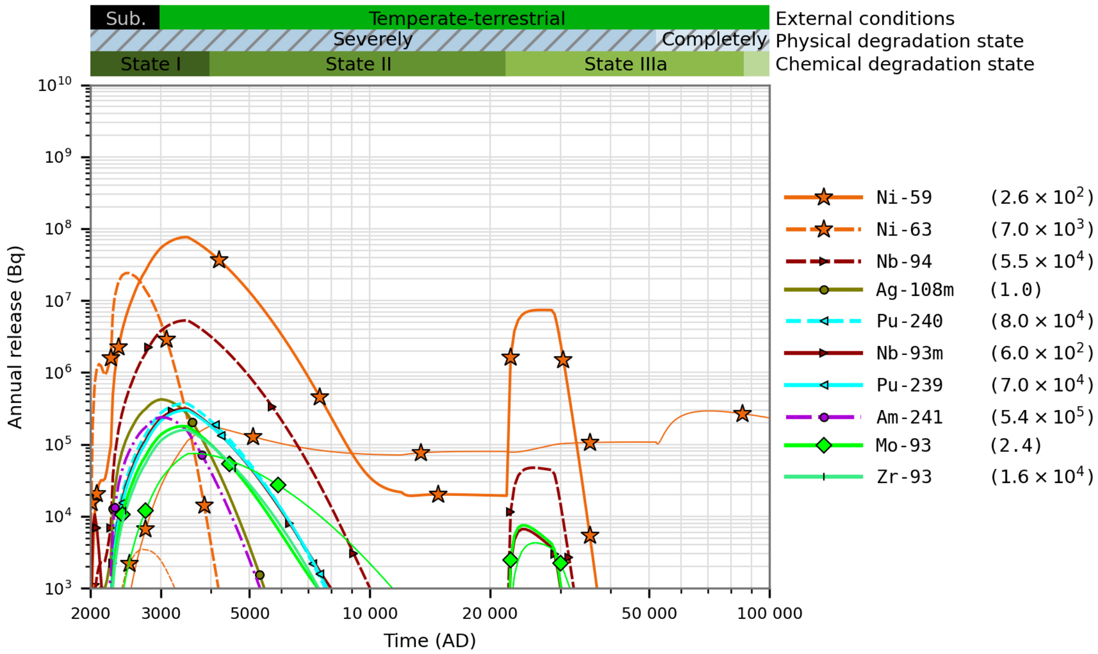

Figure C-4. *Comparison of the releases from 1BRT without sorption (thick lines) and for the base case (thin lines). The values in parentheses show the ratio between the maximum release in the present case and the base case.*

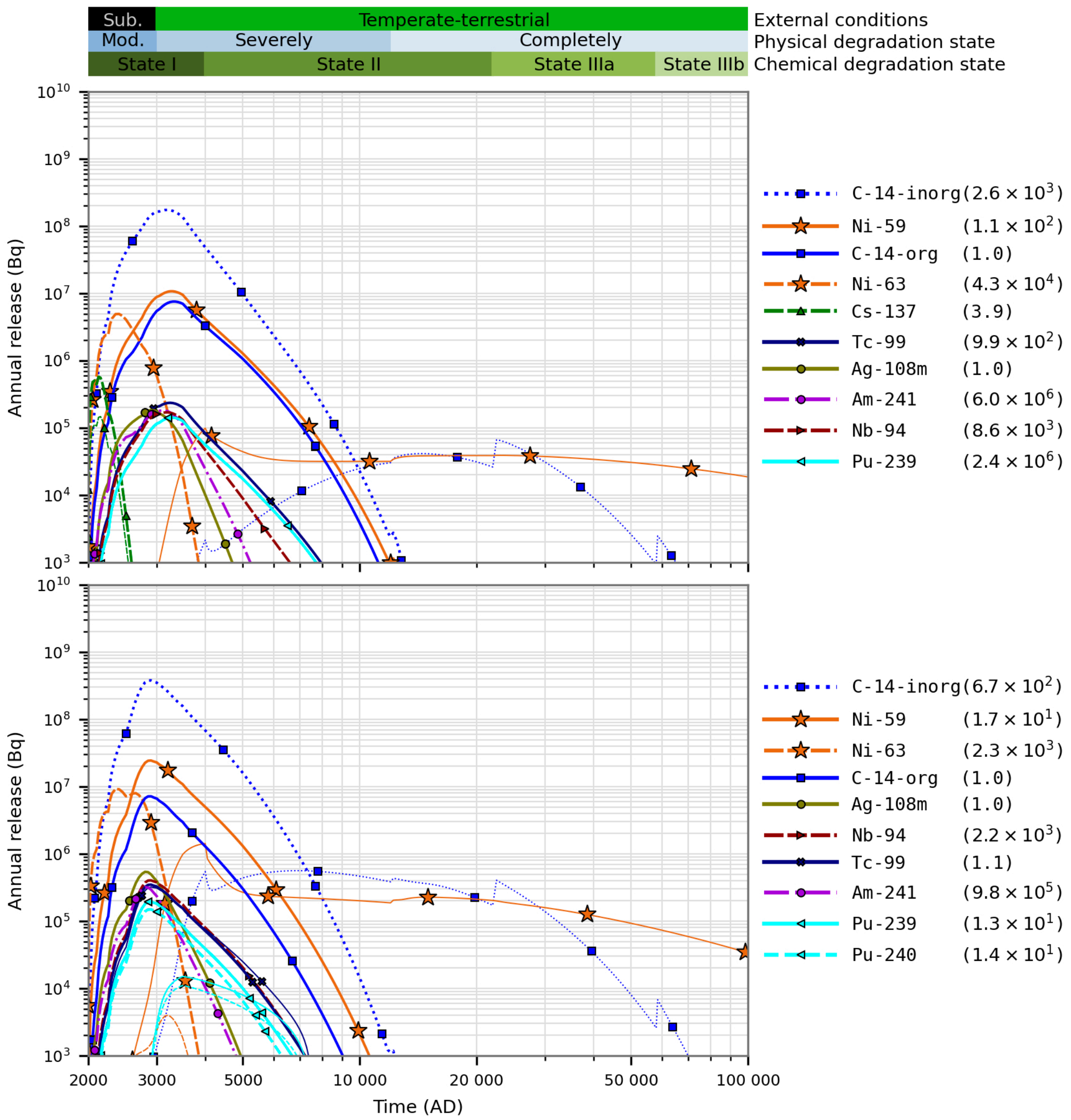

Figure C-5. *Comparison of the releases of radionuclides from 1BTF (upper panel) and 2BTF (lower panel) without sorption (thick lines) and for the base case (thin lines).*

C2 No sorption in waste and grout

This supporting calculation case is similar to the previous "No sorption" calculation case. However, here the effect of no sorption in waste and grout is investigated, while the barriers (concrete and bentonite) and backfill are assumed sorbing.

As can be seen in Figure C-6 to Figure C-10 the releases of Mo-93 and Ni-59 become significantly higher if sorption in the waste domain is not taken into account. However, the sorption in the barriers still limits the releases significantly compared with the previous calculation case, where no sorption at all is assumed.

Note that for 1BMA (Figure C-7) most of the inventory of inorganic C-14 is in bitumen-solidified waste with no sorption (also in the *base case*), hence the effect on the release is minor in this calculation case.

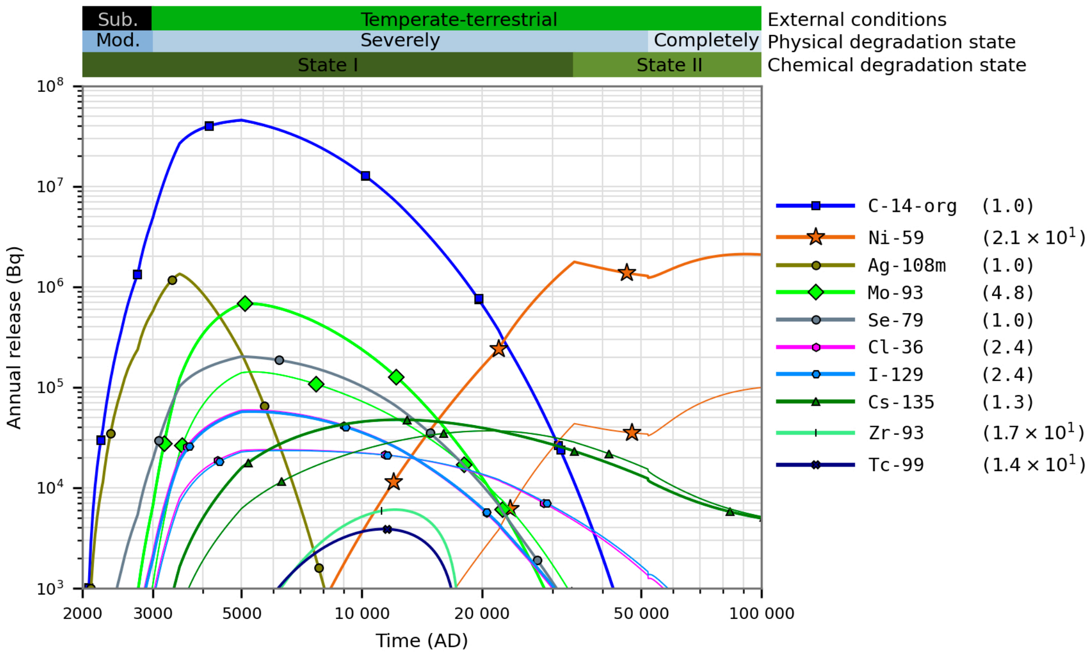

Figure C-6. *Comparison of the releases of from the silo with no sorption in waste and grout (thick lines) and for the base case (thin lines). The values in parentheses show the ratio between the maximum release in the present case and the base case.*

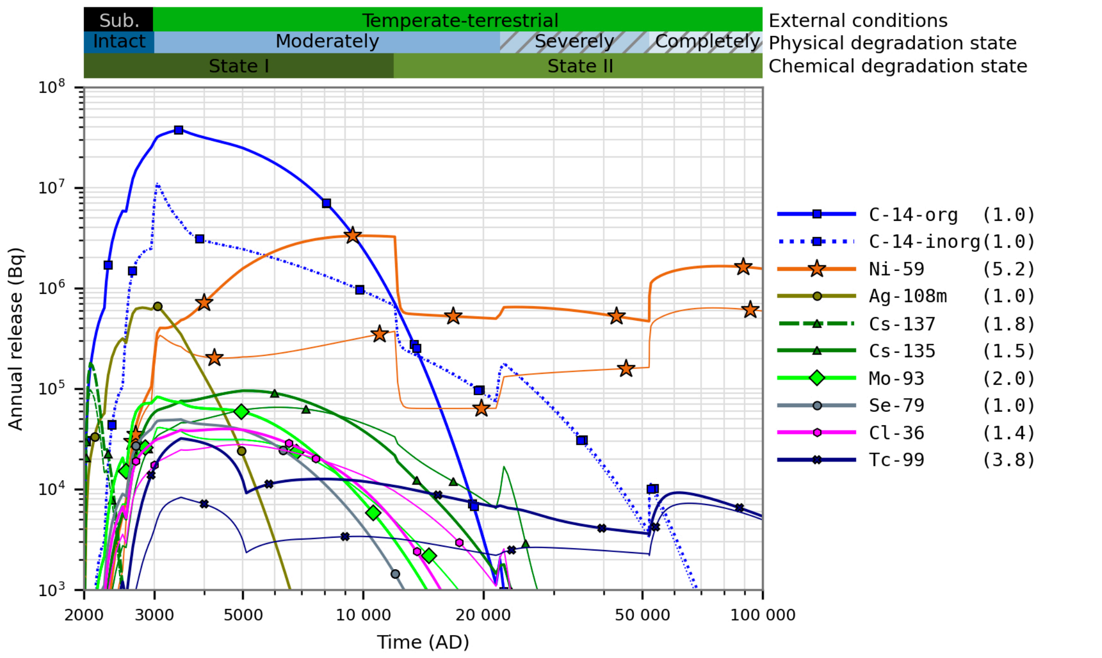

Figure C-7. *Comparison of the releases from 1BMA with no sorption in waste and grout (thick lines) and for the base case (thin lines). The values in parentheses show the ratio between the maximum release in the present case and the base case.*

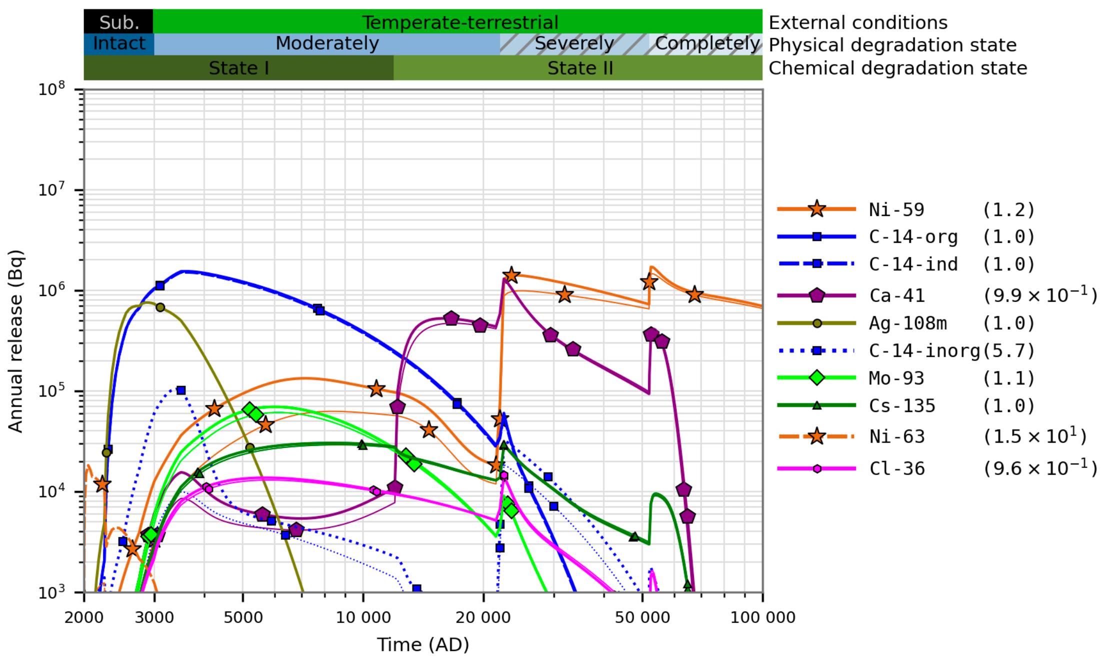

Figure C-8. *Comparison of the releases from 2BMA with no sorption in waste and grout (thick lines) and for the base case (thin lines). The values in parentheses show the ratio between the maximum release in the present case and the base case.*

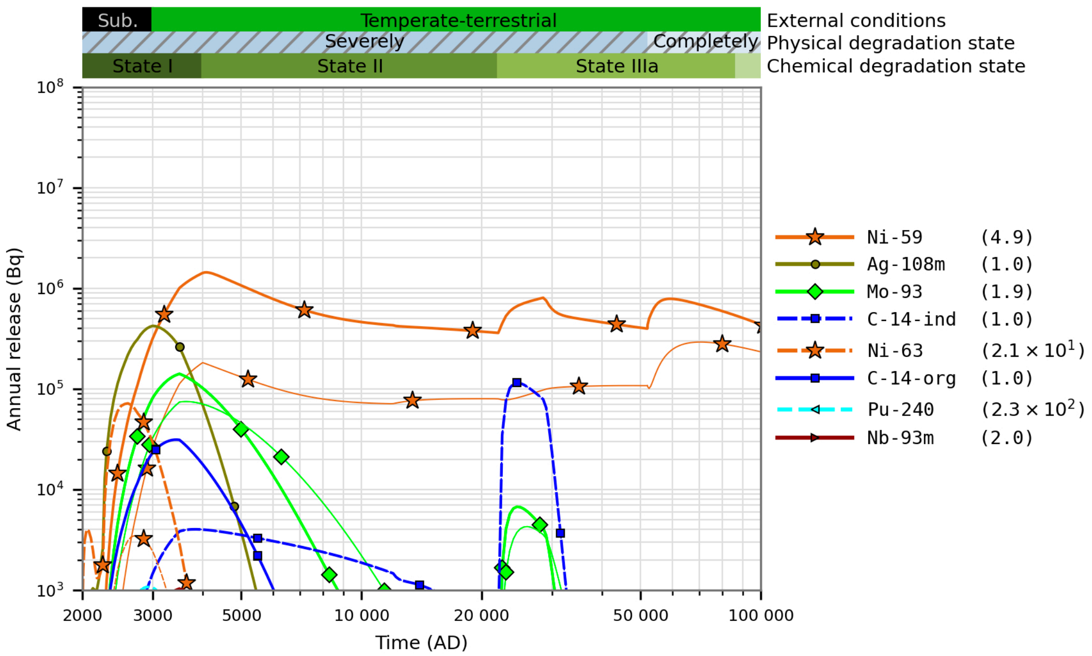

Figure C-9. *Comparison of the releases of radionuclides from 1BRT with no sorption in waste and grout (thick lines) and for the base case (thin lines). The values in parentheses show the ratio between the maximum release in the present case and the base case.*

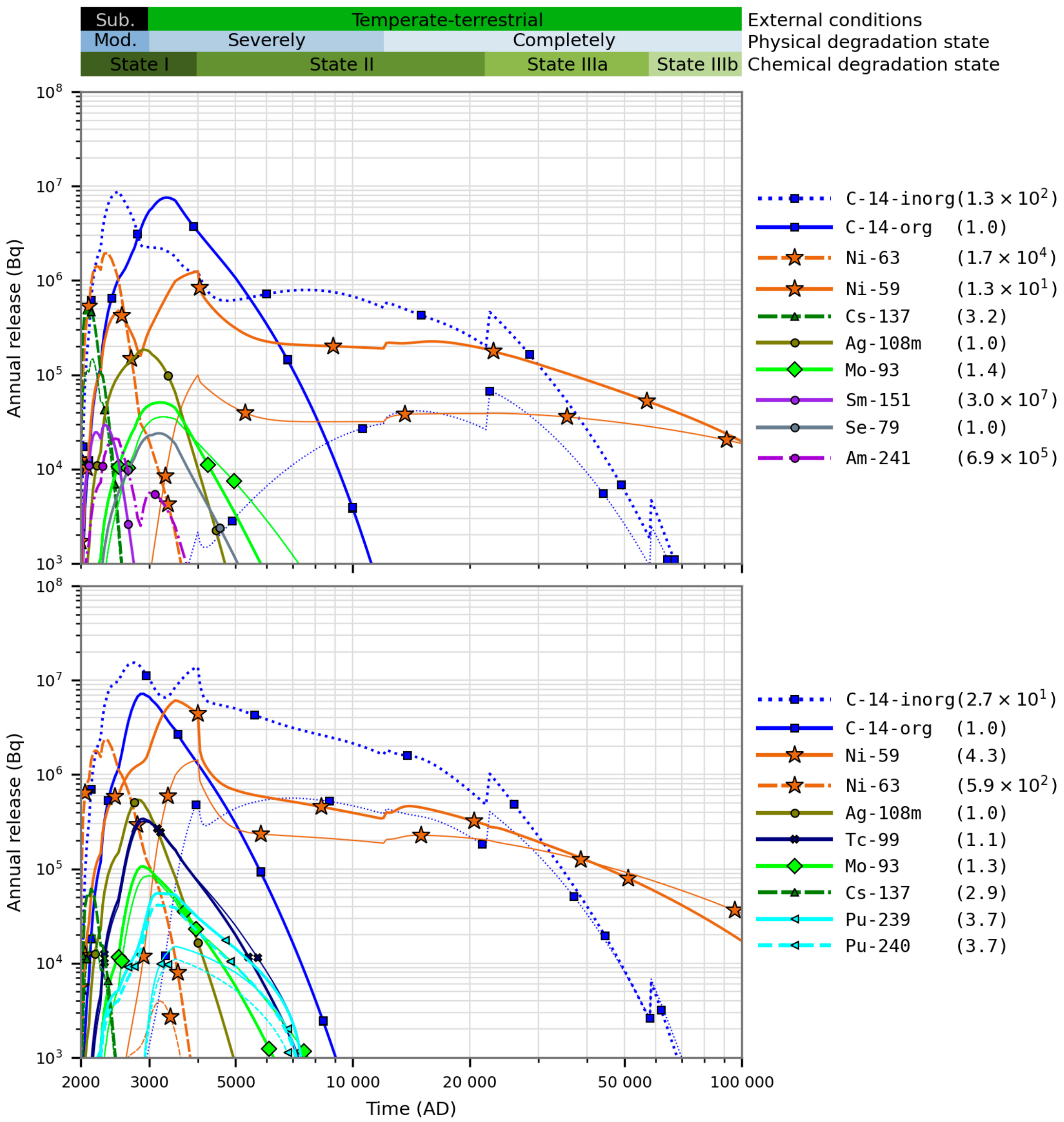

Figure C-10. *Comparison of the releases from 1BTF (upper) and 2BTF (lower) with no sorption in waste and grout (thick lines) and for the base case (thin lines). The values in parentheses show the ratio between the maximum release in the present case and the base case.*

C3 No sorption on cementitious materials in the silo

This is a calculation case that applies only to the silo. In this calculation case the bentonite and backfill are assumed sorbing, whereas all cementitious materials are assumed non-sorbing. The results from the calculation (Figure C-11) show that the sorption on cementitious materials is crucial to the performance of the silo. This is due to the large amounts of C-14-inorg in the silo and C-14-inorg is not expected to sorb on bentonite. The releases of Ni-59 are somewhat limited due to the sorption on bentonite.

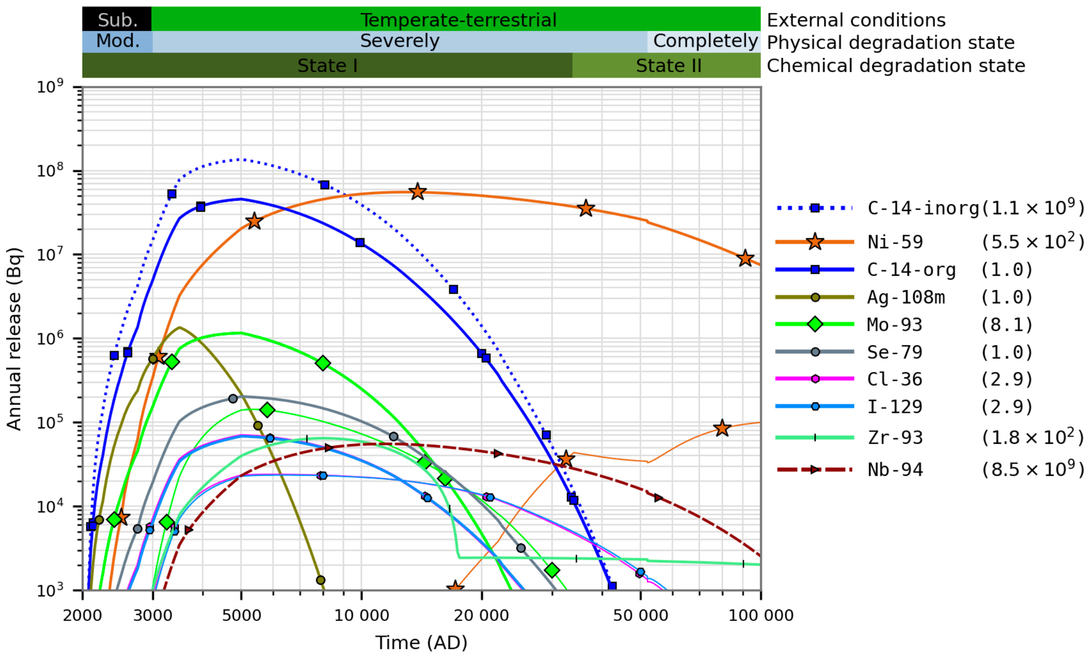

Figure C-11. *Comparison of the releases from the silo with no sorption on cementitious materials (thick lines) and for the base case (thin lines). The values in parentheses show the ratio between the maximum release in the present case and the base case.*

C4 No sorption on bentonite in the silo

In this calculation case the effect of sorption on bentonite is investigated. The calculation is done with K_d for all radionuclides set to zero in bentonite.

The results from the calculation (Figure C-12) show that the sorption on bentonite is not critical for the performance of the silo, however for Ni-59, Cs-135 and Tc-99 a significant increase in releases is shown. The extremely high increase of the release of Nb-93m is due to the fact that it is a daughter of Mo-93 (and Zr-93) and has a very short half-live (16 years). Thus, in the *base case* Nb-93m is delayed by sorption in the bentonite and hence has a longer time to decay and its release is very low. However, in this calculation case it leaves the bentonite in a very short time before it has had time to decay.

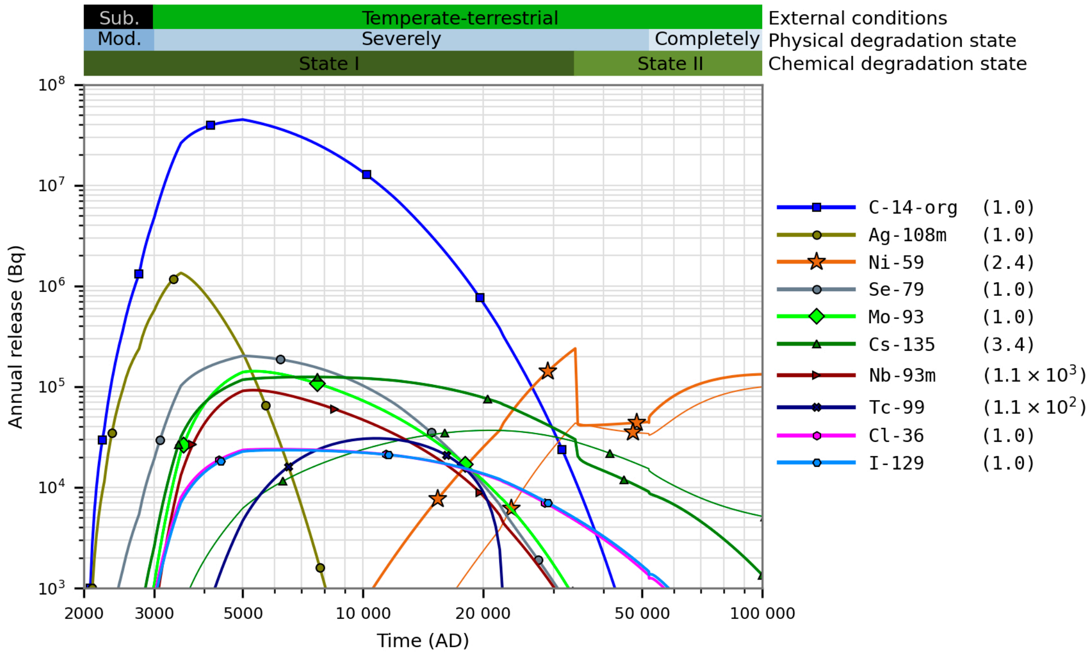

Figure C-12. *Comparison of the releases from the silo without sorption on bentonite (thick lines) and for the base case (thin lines). The values in parentheses show the ratio between the maximum release in the present case and the base case.*

C5 No sorption on crushed rock

In this calculation case the effect of modelling sorption on the crushed rock backfill is investigated. The calculation is done with K_d for all radionuclides set to zero in crushed rock.

As can be seen in Figure C-13 to Figure C-17 the releases are not significantly affected by the crushed rock sorption except for small differences for Cs-135, Cs-137, Ni-59, Ni-63, Nb-93m, Nb-94 and Tc-99. The sorption on crushed rock cannot be expected to have a large effect as the K_d values for crushed rock in general are very small compared to the K_d values for cement (Figure 4-4 and Figure 4-6). In the silo the releases are mainly directed downwards so the radionuclides are mostly not affected by sorption in the crushed rock backfill in the top of the silo. The effect on Nb-93m can be described by the same mechanism as discussed in the previous section.

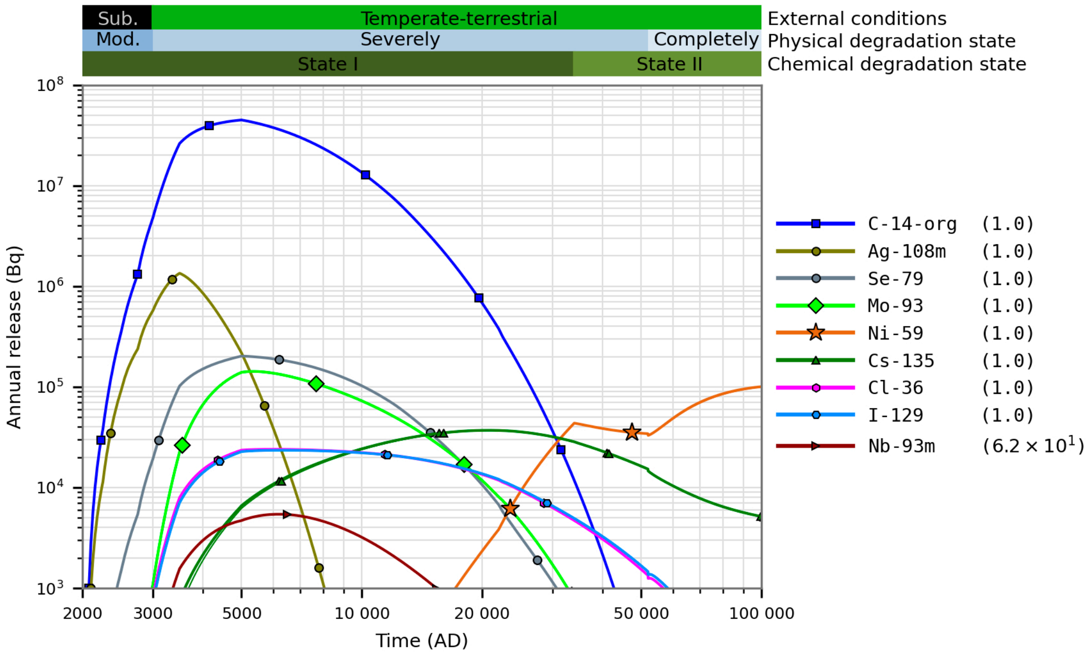

Figure C-13. *Comparison of the releases from the silo with no sorption on crushed rock (thick lines) and for the base case (thin lines). The values in parentheses show the ratio between the maximum release in the present case and the base case.*

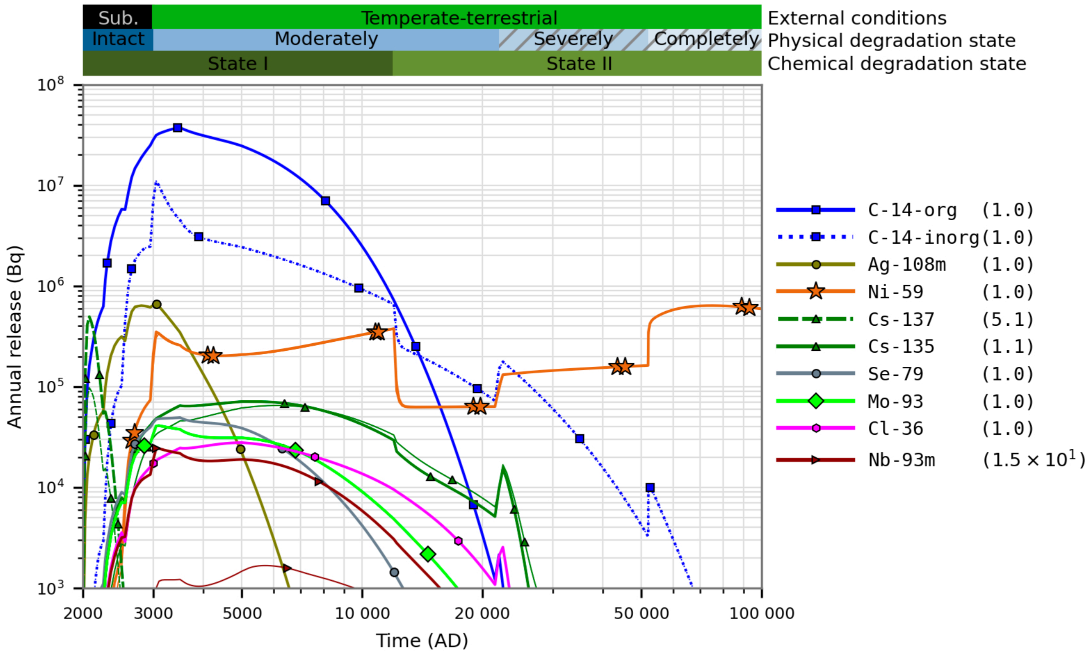

Figure C-14. *Comparison of the releases from 1BMA with no sorption on crushed rock (thick lines) and for the base case (thin lines). The values in parentheses show the ratio between the maximum release in the present case and the base case.*

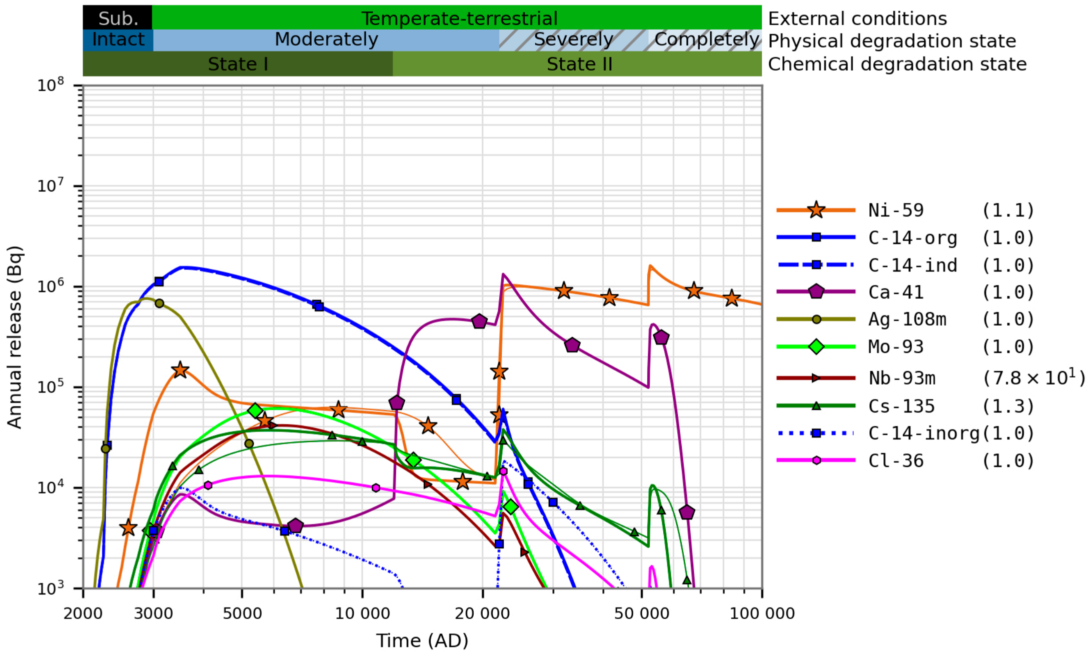

Figure C-15. *Comparison of the releases of radionuclides from 2BMA with no sorption on crushed rock (thick lines) and for the base case (thin lines). The values in parentheses show the ratio between the maximum release in the present case and the base case.*

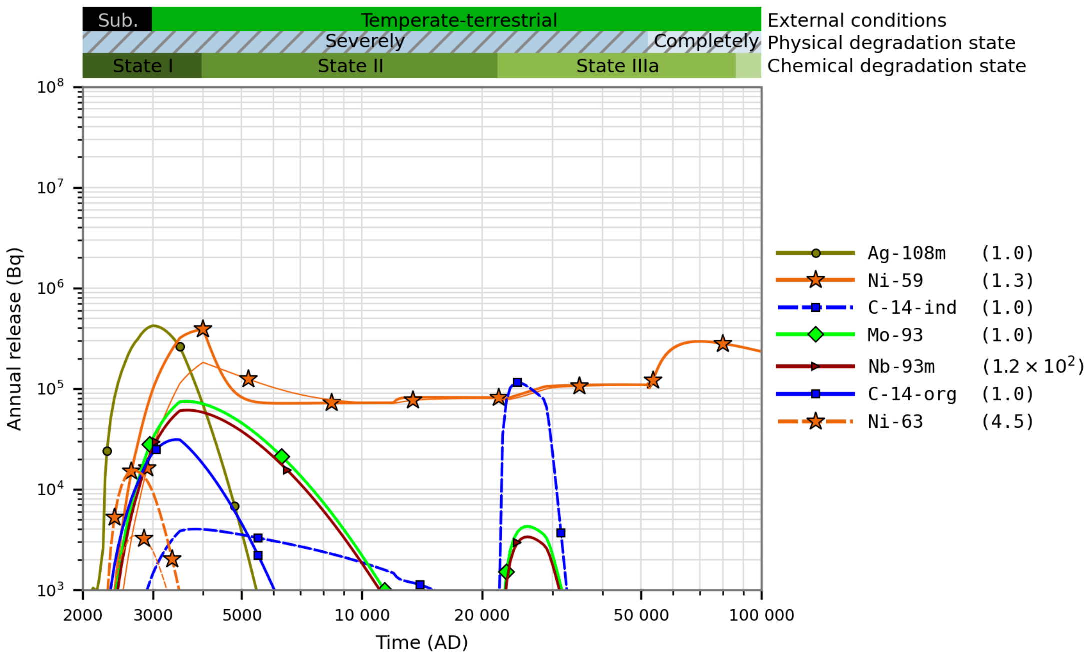

Figure C-16. *Comparison of the releases of radionuclides from 1BRT with no sorption on crushed rock (thick lines) and for the base case (thin lines). The values in parentheses show the ratio between the maximum release in the present case and the base case.*

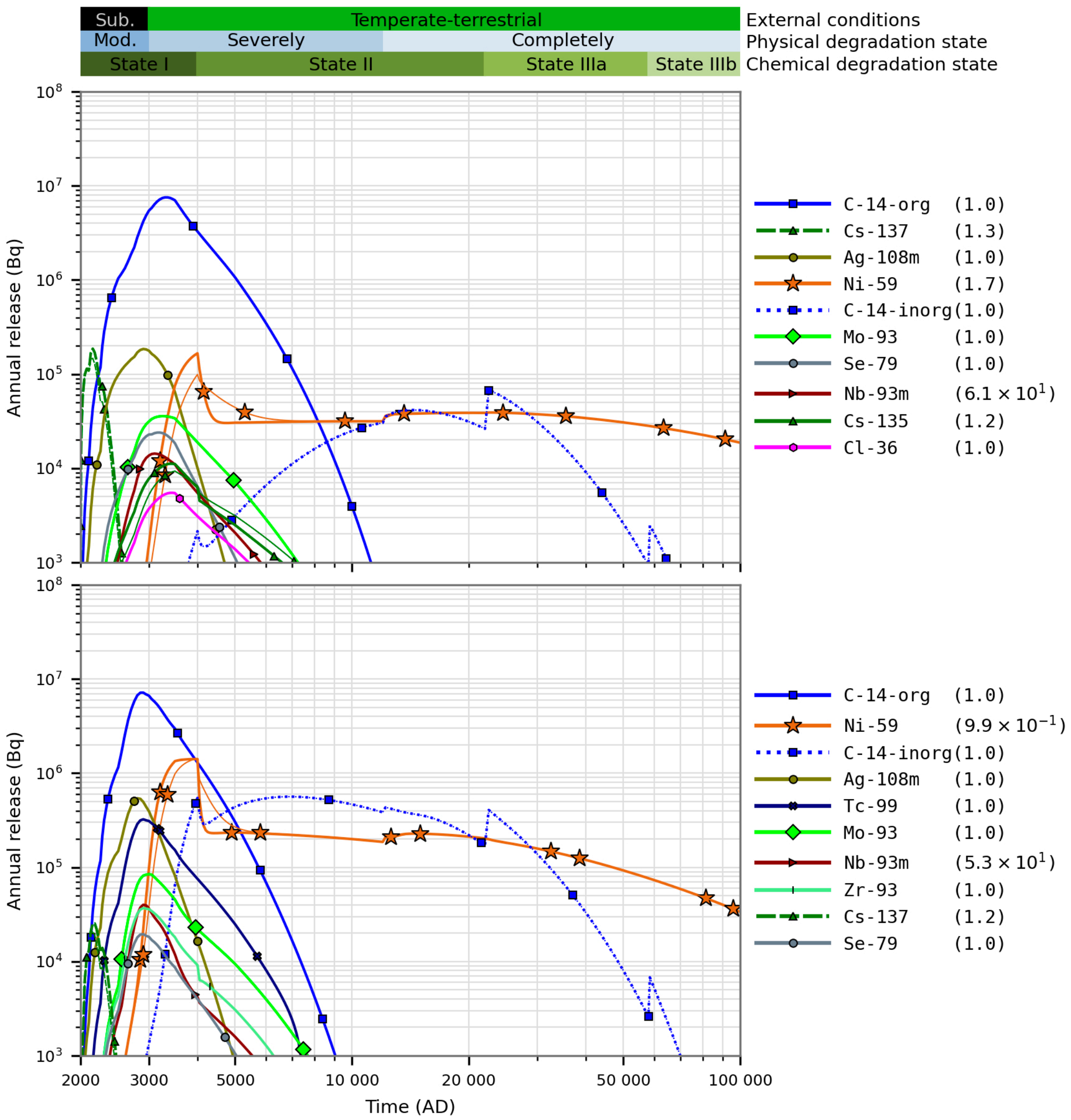

Figure C-17. *Comparison of the releases of radionuclides from 1BTF (upper panel) and 2BTF (lower panel) with no sorption on crushed rock (thick lines) and for the base case (thin lines). The values in parentheses show the ratio between the maximum release in the present case and the base case.*

C6 Hydraulic barrier functions

This calculation case investigates the effect of the hydraulic barrier functions.

In this calculation case, the near-field water-flows from the "no barriers" case in the hydrological calculations (Abarca et al. 2020) are used during the whole assessment period. The groundwater flow is calculated assuming no resistance to flow in the concrete and bentonite barriers in the vault structures. Furthermore, the effect of vault closure plugs is neglected. Other internal and external conditions are assumed to be the same as in the *base case*. These conditions are clearly hypothetical, and the objective of the calculation case is to investigate the effect of the hydraulic barrier and thus the sorption properties of the concrete and bentonite are kept unchanged.

As can be seen in Figure C-18 to Figure C-23 the hydraulic barrier is of great importance for the releases. However, for sorbing radionuclides the chemical barrier function still limits the releases significantly. As can be seen in Figure C-21 the hydraulic barrier is of less importance to 1BRT, than for e.g. the silo and 1–2BMA. The release of radionuclides from 1BRT is largely limited by the corrosion rate. As the BLA vaults have no internal barriers, only the effect of the plugs affects this calculation for the BLA vaults. As can be seen in Figure C-23 the plugs are of some importance to BLA. However, most peak releases increase less than a factor of two.

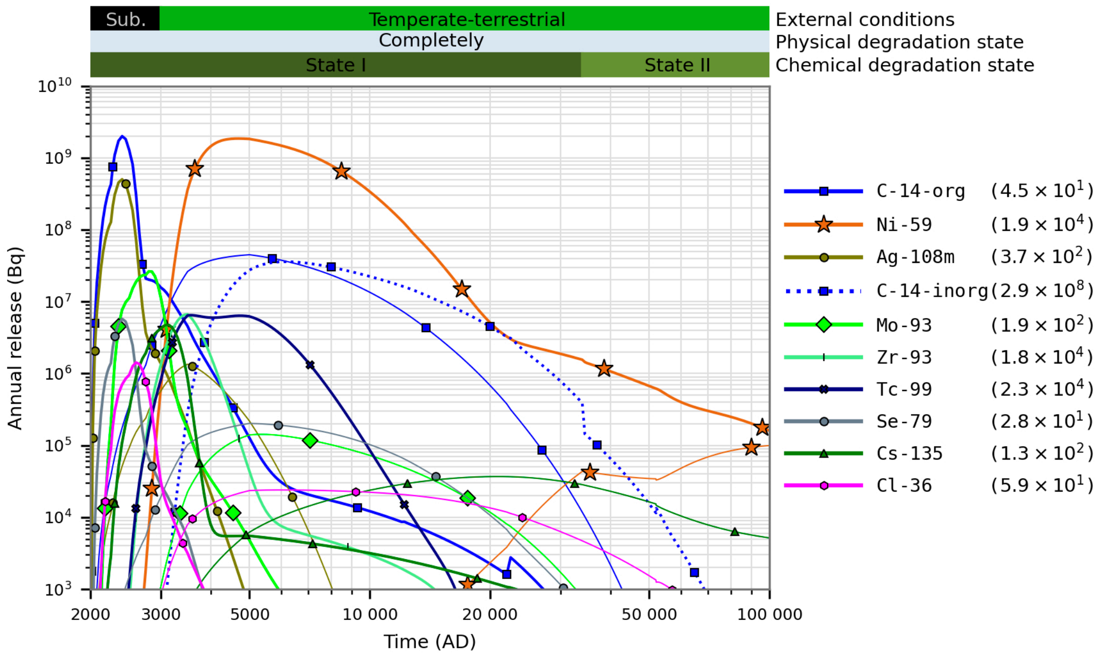

Figure C-18. *Comparison of the releases from the silo with no hydraulic barriers (thick lines) and for the base case (thin lines). The values in parentheses show the ratio between the maximum release in the present case and the base case.*

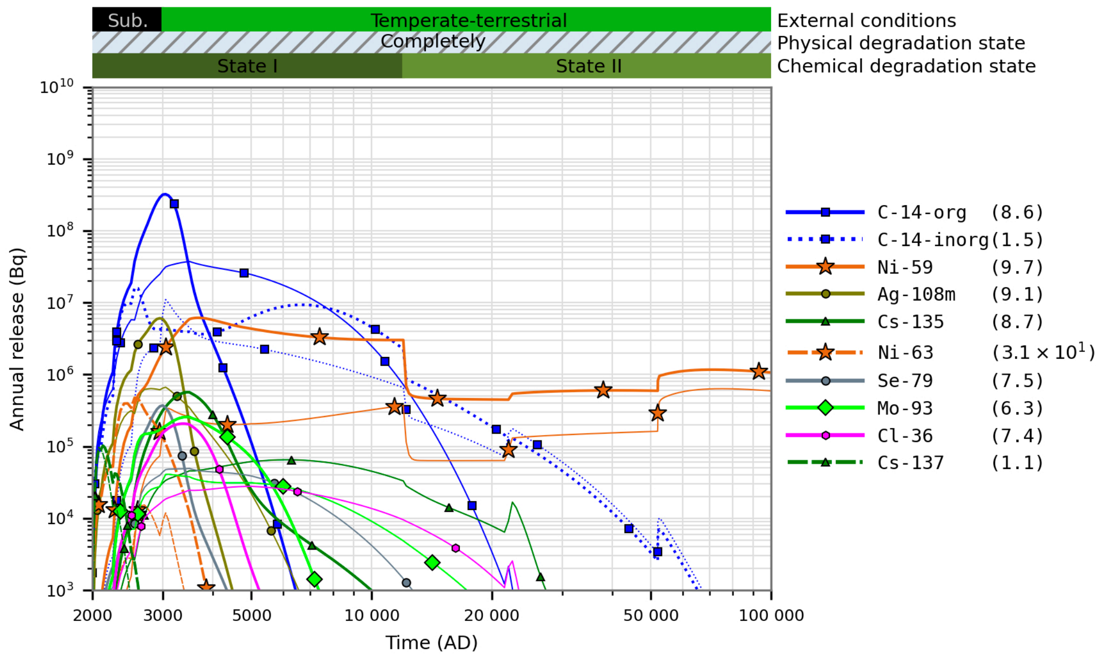

Figure C-19. *Comparison of the releases from 1BMA with no hydraulic barriers (thick lines) and for the base case (thin lines).*

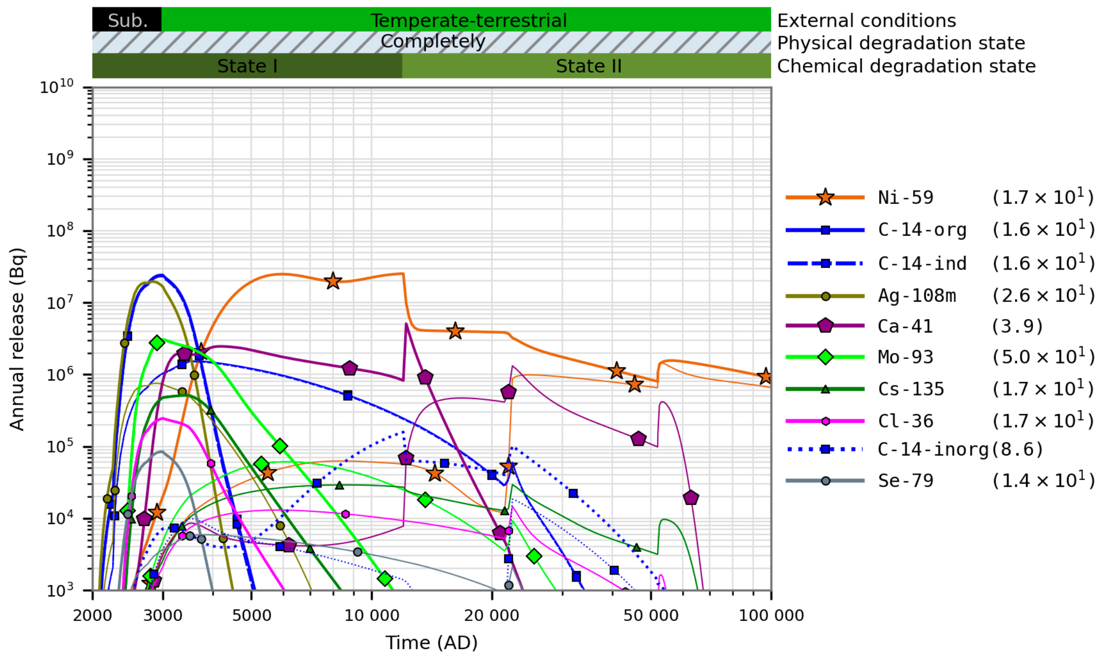

Figure C-20. *Comparison of the releases of radionuclides from 2BMA with no hydraulic barriers (thick lines) and for the base case (thin lines).*

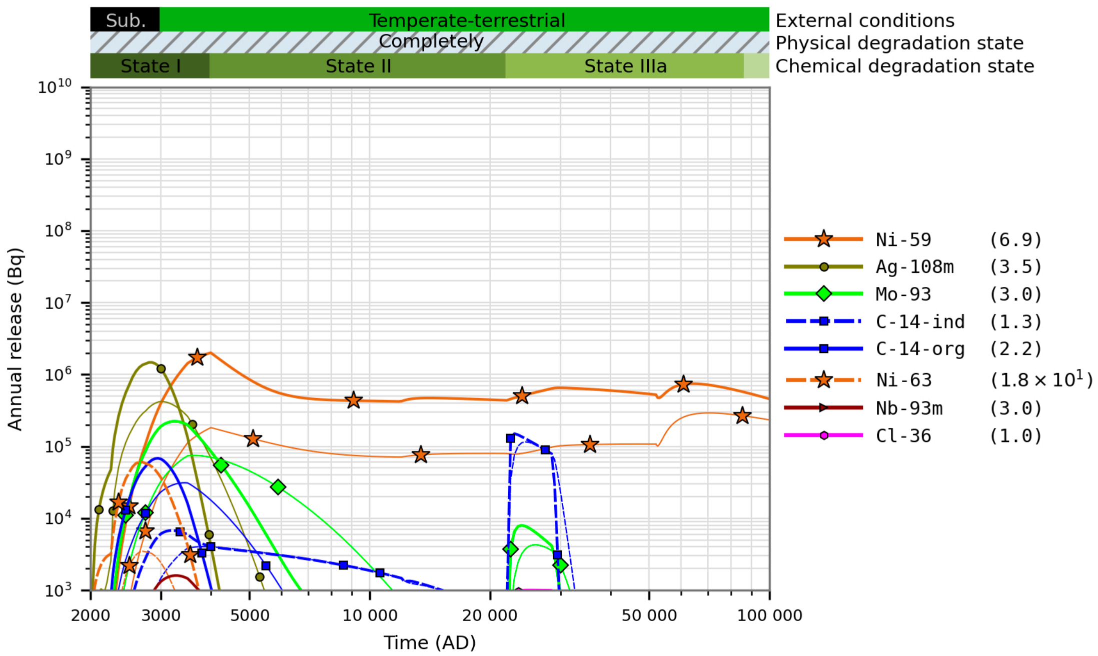

Figure C-21. *Comparison of the releases of radionuclides from 1BRT with no hydraulic barriers (thick lines) and for the base case (thin lines).*

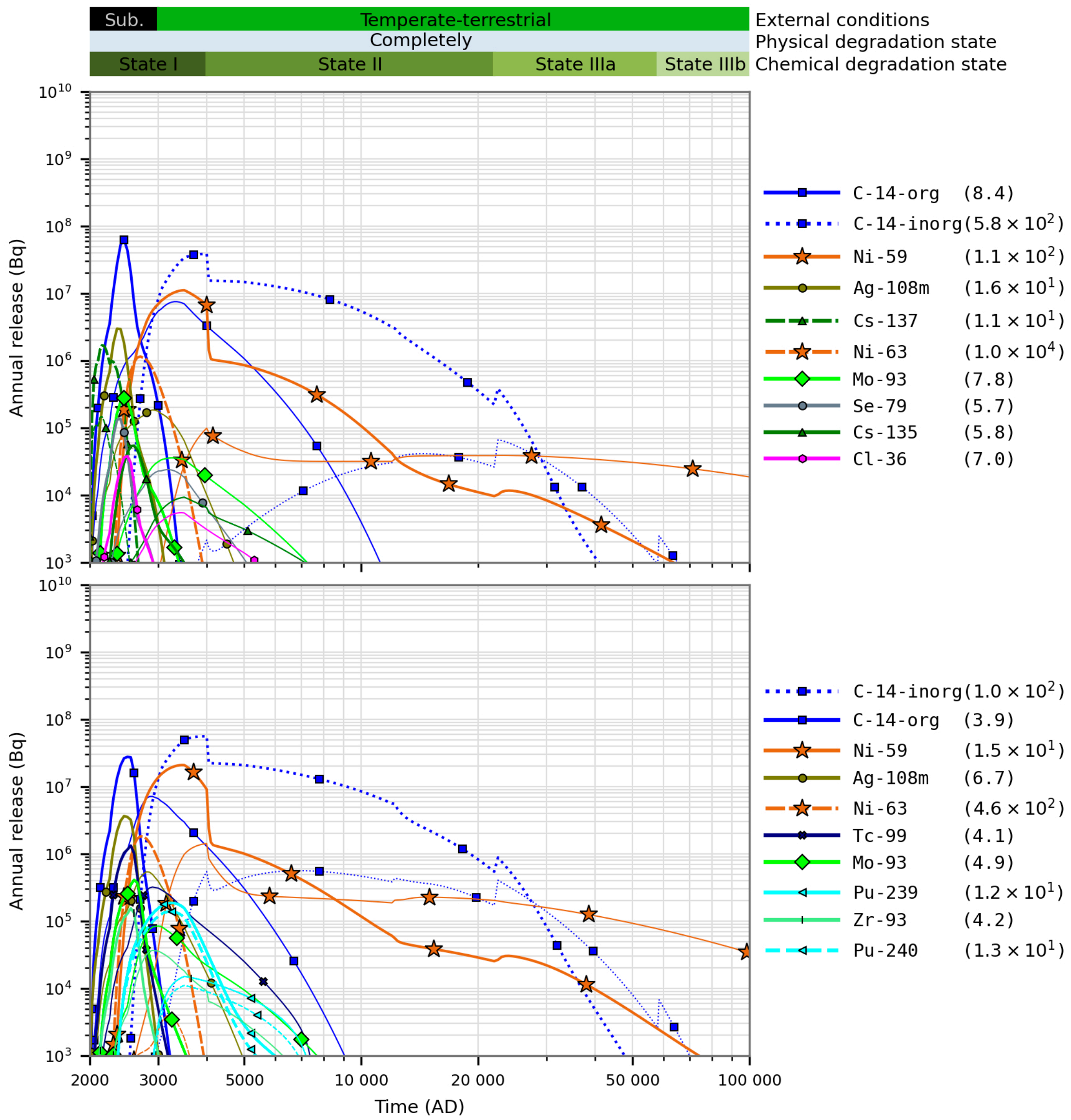

Figure C-22. *Comparison of the releases of radionuclides from 1BTF (upper panel) and 2BTF (lower panel) with no hydraulic barriers (thick lines) and for the base case (thin lines).*

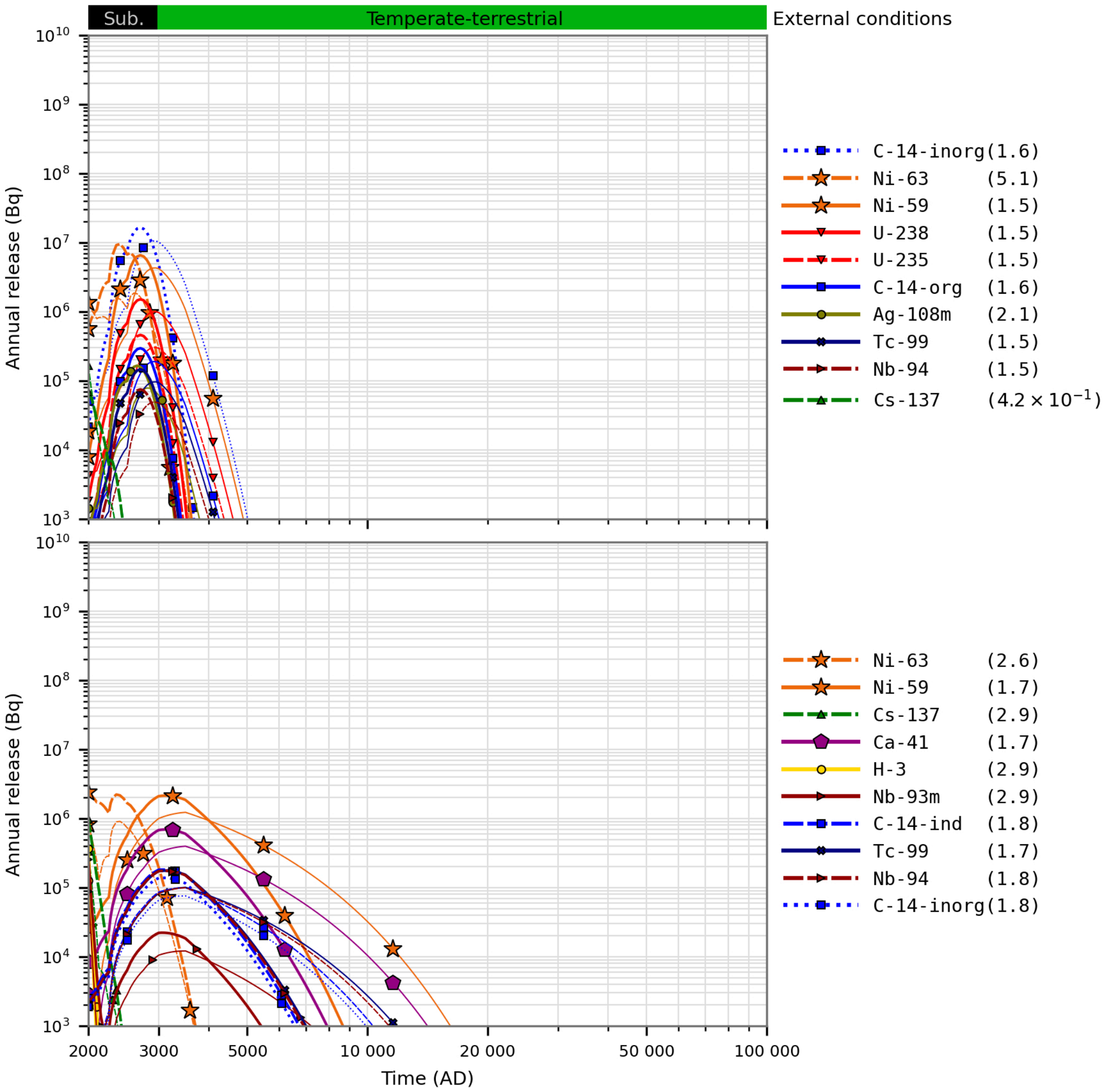

Figure C-23. *Comparison of the releases of radionuclides from 1BLA (upper panel) and 2BLA (lower panel) with no hydraulic barriers (thick lines) and for the base case (thin lines).*

C7 Sensitivity to diffusivity

This calculation case investigates the effect of the diffusion barrier function in the near-field. The calculation is done with scale factors (0.5, 2, 10) for the effective diffusivities in all parts of the system. In addition, the calculation for the *base case* is presented for reference (scale factor 1.0).

As can be seen in Figure C-24 to Figure C-28 the release of radionuclides from the silo is largely affected by diffusion during the initial submerged period, while at later timepoints the effect of higher diffusivities can be seen mainly on the more sorbing radionuclide Ni-59.

As can be seen in Figure C-25 the release of radionuclides from 1BMA is to large extent affected by diffusion, but due to the crack in the slab the more sorbing radionuclide Ni-59 gets higher release initially with lower diffusivities, before a concentration equilibrium has been reached between waste and concrete barriers. As can be seen in Figure C-26 the release from 2BMA is largely affected by diffusion during the initial period (up to ca 22 000 AD) when the water flow through the waste domain is very low and thus diffusion is the dominating transport process.

As can be seen in Figure C-27 the release from 1BRT is relatively unsensitive to the varying diffusivities. This is due to the high waterflows assumed for 1BRT.

As can be seen in Figure C-28 the release from BTF is relatively insensitive to the varying diffusivities. This is due to the high waterflows assumed for the 1–2BTF waste-domain already in the *base case* ($K = 1 \times 10^{-5}$ already at 3000 AD).

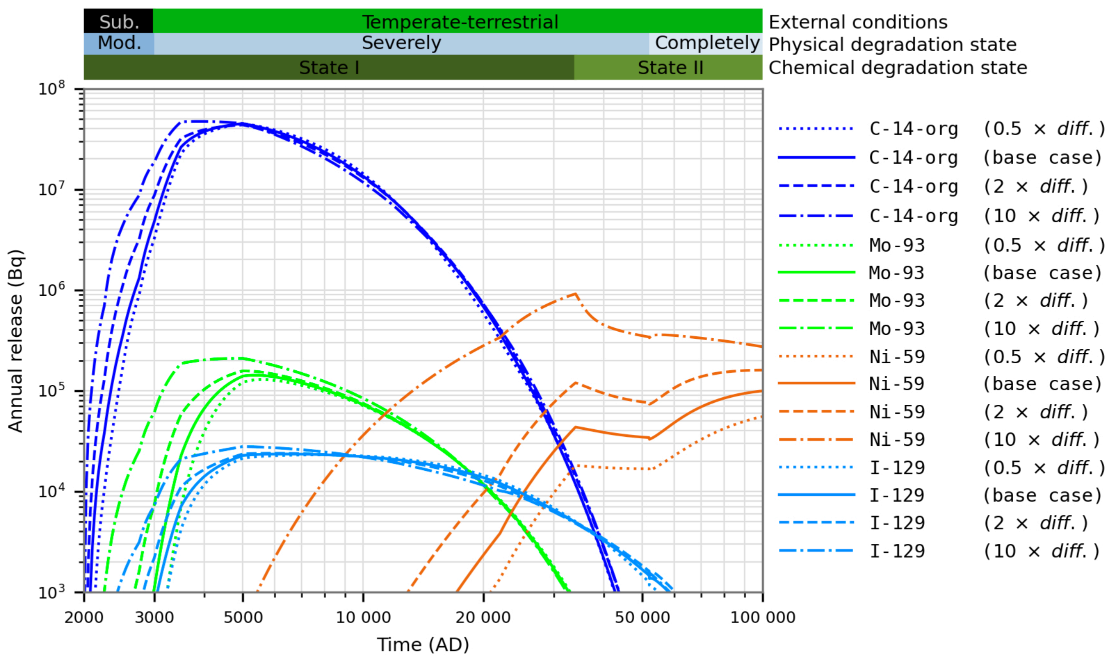

Figure C-24. *Comparison of the releases from the silo with various diffusivities.*

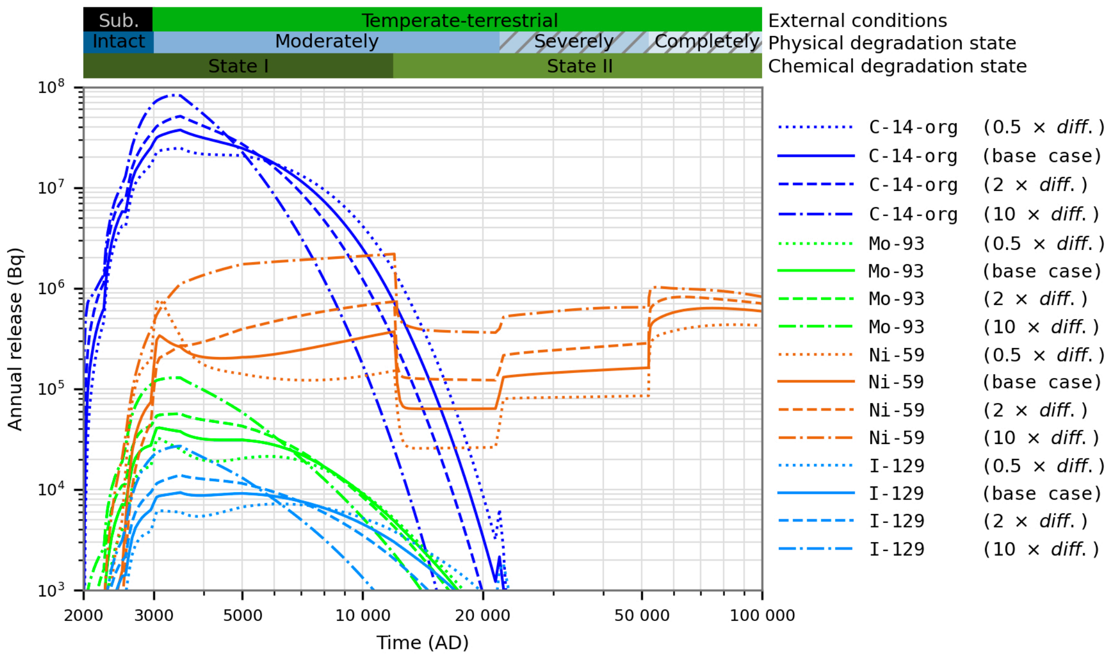

***Figure C-25.** Comparison of the releases of radionuclides from 1BMA with various diffusivities.*

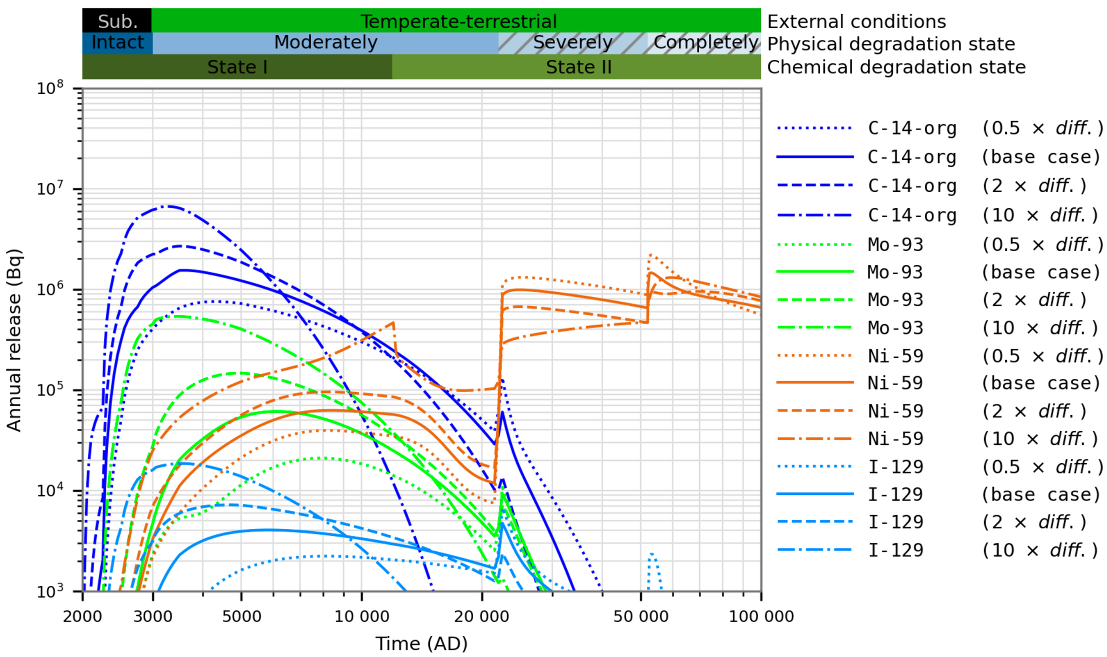

***Figure C-26.** Comparison of the releases of radionuclides from 2BMA with various diffusivities.*

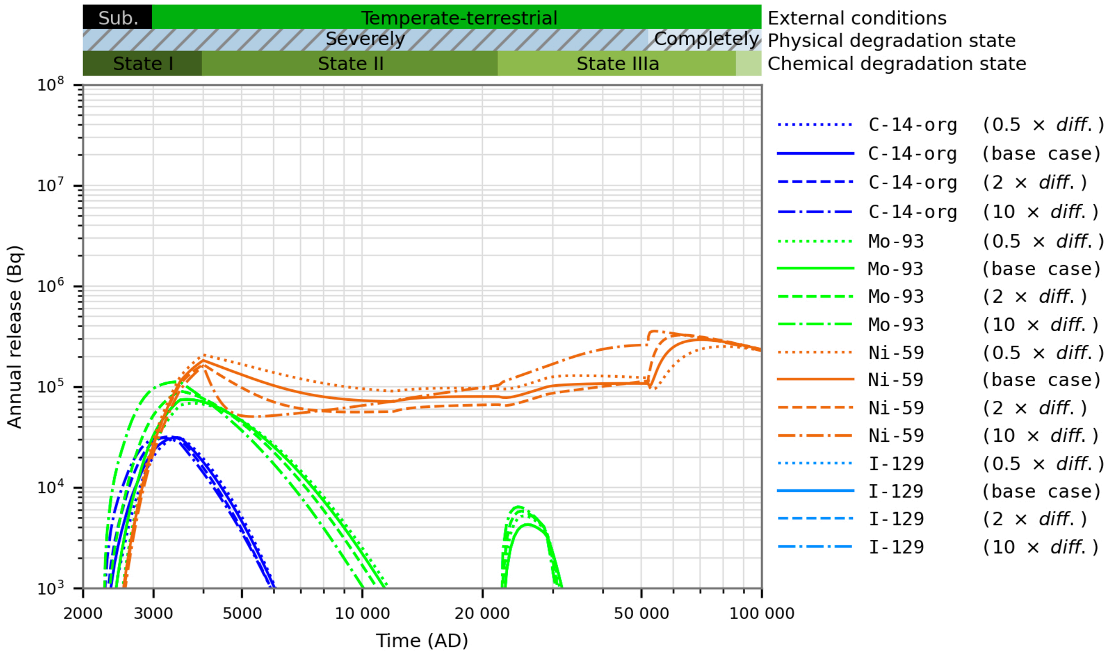

Figure C-27. *Comparison of the releases of radionuclides from 1BRT with various diffusivities.*

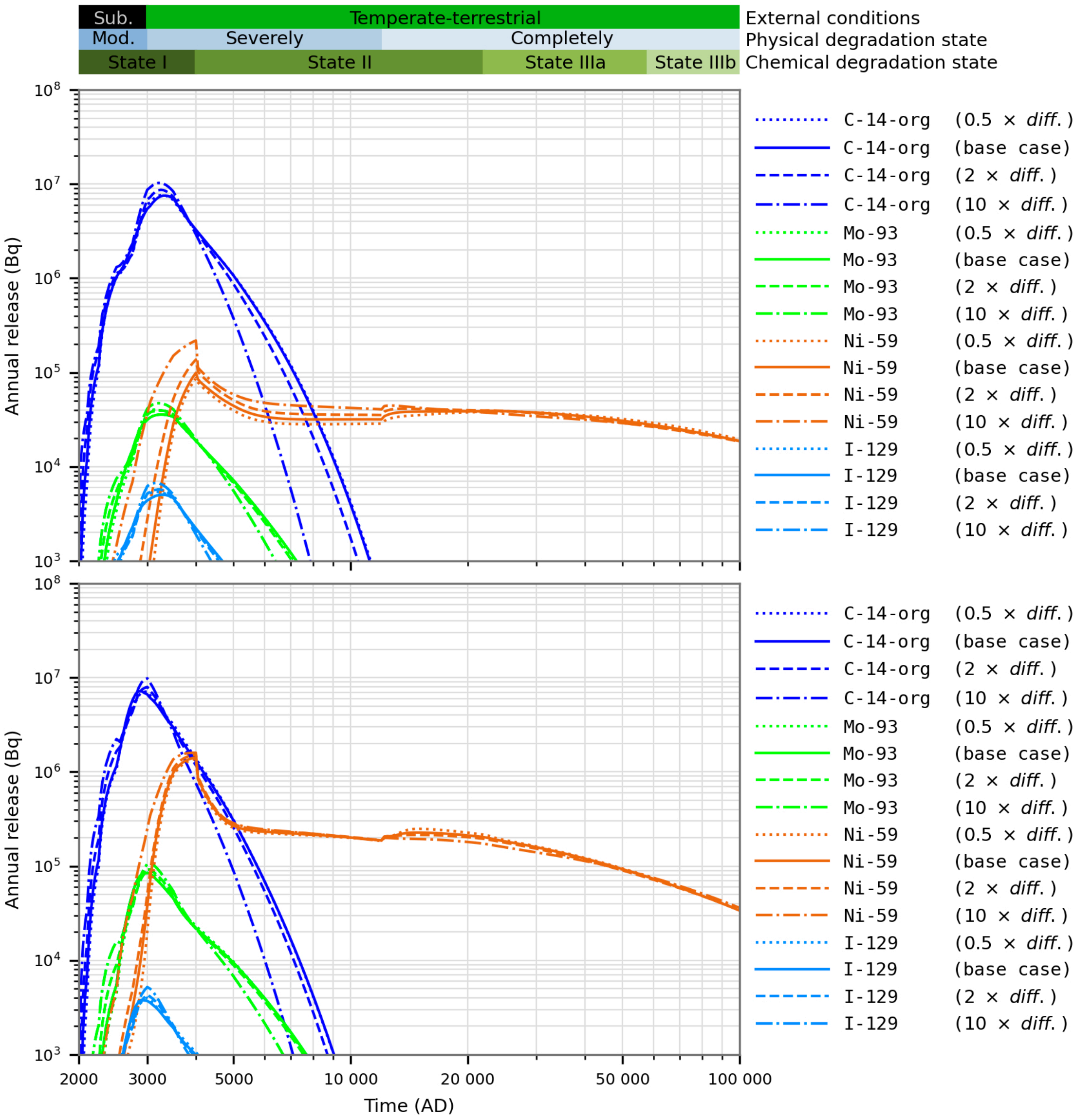

Figure C-28. Comparison of the releases of radionuclides from 1BTF (upper panel) and 2BTF (lower panel) with various diffusivities.

C8 Initial cracks in concrete structures

In this calculation case the effect of hypothetical initial cracks in the concrete structures is investigated. These calculations are done with modified models where cracks (as described in Section 2.3) are introduced in the concrete barriers. In addition to this a higher hydraulic conductivity ($K = 1 \times 10^{-5}$ m/s) is assumed already from start in the calculations.

Figure C-29 to Figure C-32 show that cracks and higher initial conductivity in concrete have a significant effect on the releases of C-14-inorg and Ni-59. Also other more weakly-sorbing radionuclides such as C-14-org and Mo-93 are significantly affected in 1–2BMA, in the silo these radionuclides are not significantly affected due to the bentonite that is the main flow barrier in the silo. It should be noted that for 1BMA the assumption is that cracks are present in the slab from start already in the *base case*, this explains the relatively moderate effect in 1BMA in this calculation case compared with e.g. 2BMA. In 1–2BTF the effect is also limited to mainly C-14-inorg and Ni-59 as the releases of weakly-sorbing radionuclides are limited largely by the vault flow (due to the less efficient concrete barriers in 1–2BTF compared to 1–2BMA).

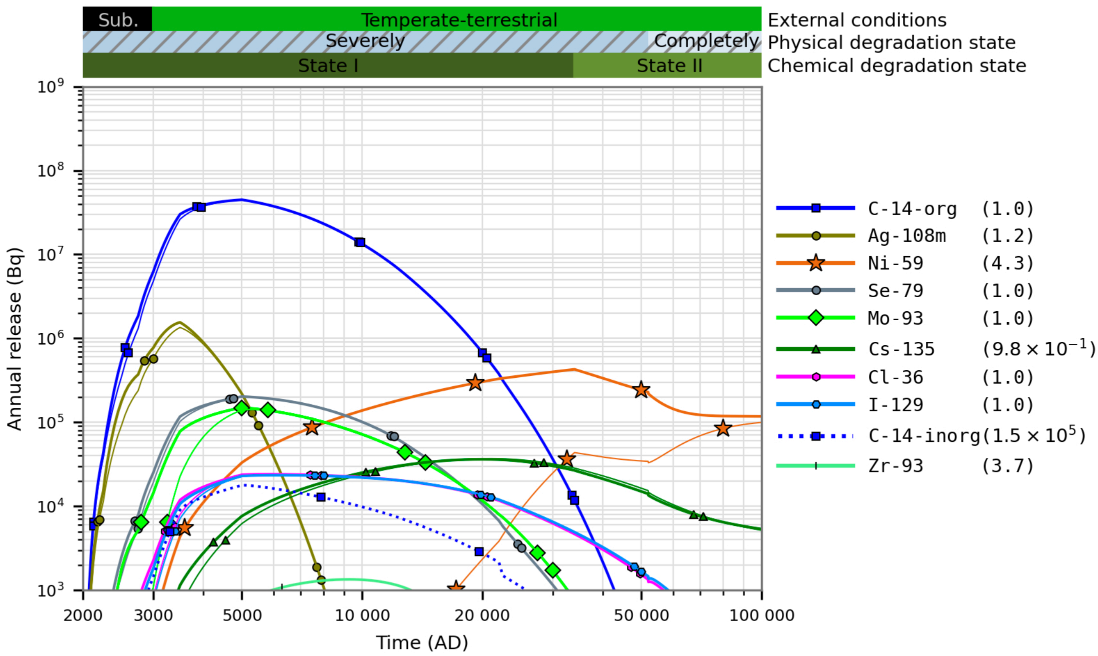

Figure C-29. *Comparison of the releases from the silo with initial cracks (thick lines) and for the base case (thin lines). The values in parentheses show the ratio between the maximum release in the present case and the base case.*

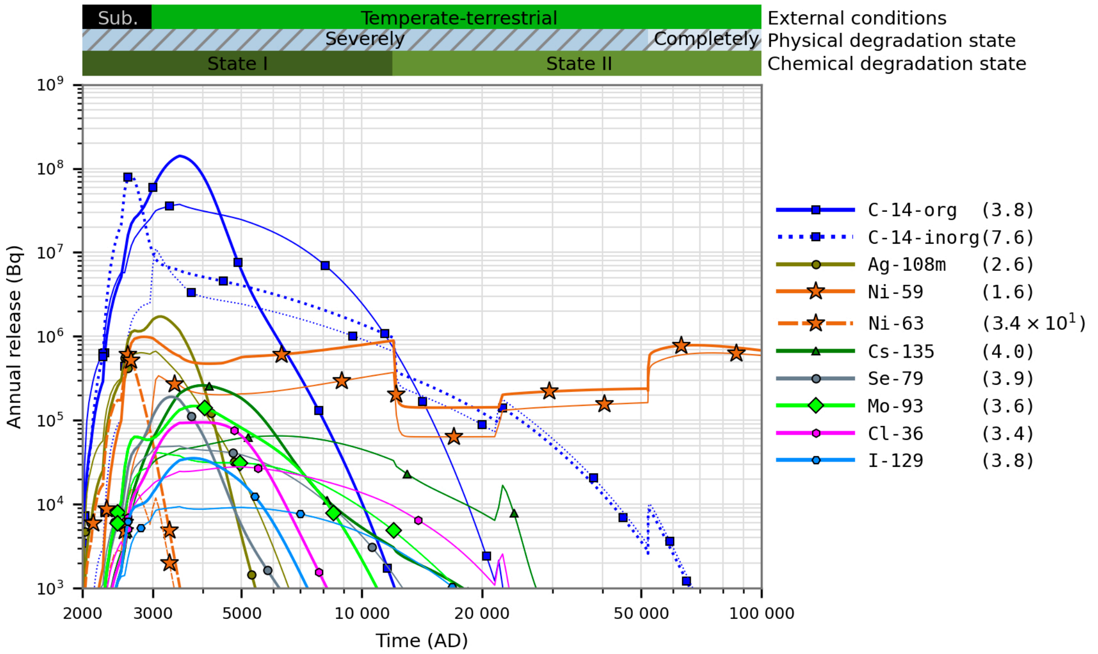

Figure C-30. *Comparison of the releases of radionuclides from 1BMA with initial cracks (thick lines) and for the base case (thin lines). The values in parentheses show the ratio between the maximum release in the present case and the base case.*

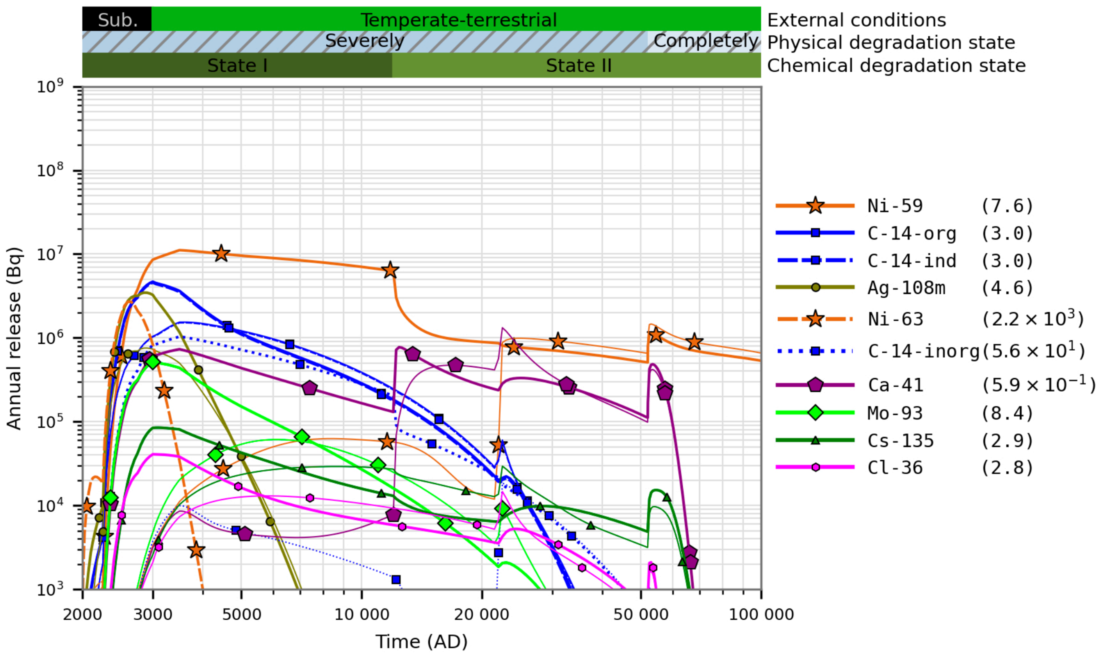

Figure C-31. *Comparison of the releases of radionuclides from 2BMA with initial cracks (thick lines) and for the base case (thin lines). The values in parentheses show the ratio between the maximum release in the present case and the base case.*

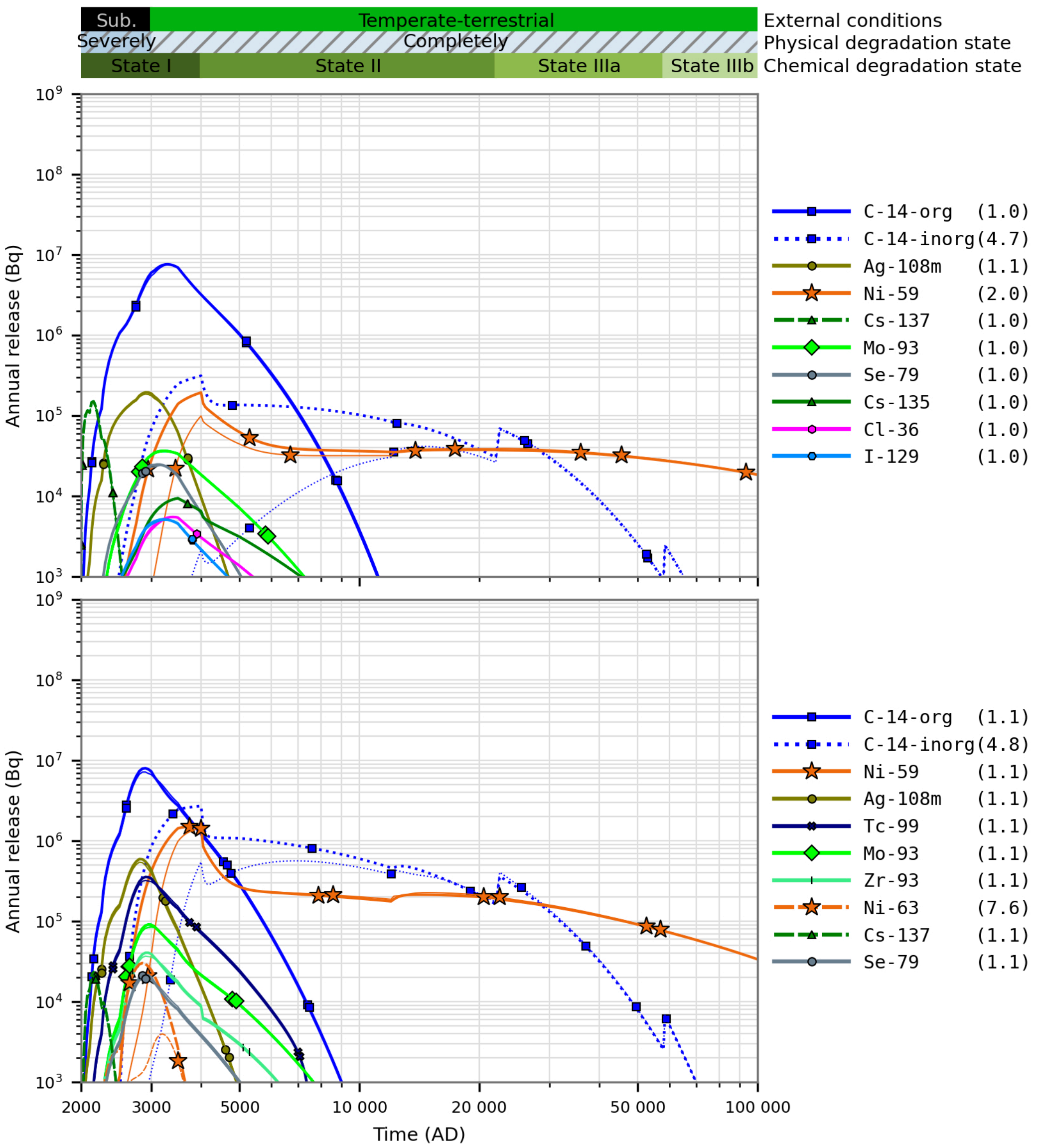

Figure C-32. *Comparison of the releases from 1BTF (upper) and 2BTF (lower) with initial cracks (thick lines) and for the base case (thin lines). The values in parentheses show the ratio between the maximum release in the present case and the base case.*

C9 Effect of gas evacuation channels in 2BMA

This supporting calculation case investigates the effect of the dimension of the gas evacuation channels on the release of radionuclides. In Figure C-33 a comparison is shown between results from calculations conducted assuming different lengths of gas evacuation channels, 0.1 m and 0.64 m (the *base case*). It can be noted that the releases of, in particular, the sorbing radionuclides Ni-59, Ca-41 and C-14-inorg are sensitive to the length of the gas evacuation channels.

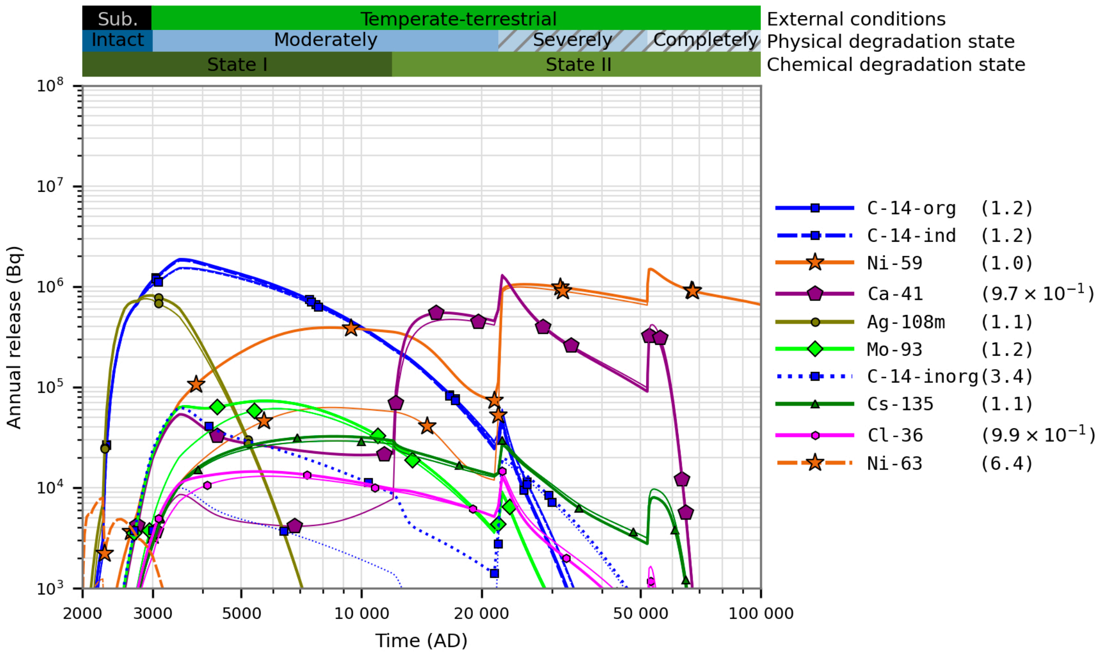

Figure C-33. *Releases from 2BMA using shorter gas evacuation channels (0.1 m – thick lines) compared to the base case (0.64 m – thin lines). The values in parentheses show the ratio between the maximum release in the present case and the base case.*

C10 Instant release from steel in 1BRT

The metallic wastes in 1BRT will release induced radioactivity at the same rate as the metal corrodes. This calculation case illustrates the importance of the limited corrosion rate. In the model this is handled by assigning the whole inventory of surface contamination as well as the induced activity to the grout compartment at the start of the simulation. Table C-1 shows the partition between induced activity and surface contamination for the radionuclides most important to the safety assessment. The results of the instant release calculation are shown in Figure C-34. All the C-14-ind is released very rapidly as no sorption for this radionuclide is taken into account. Also, a large increase in the early releases of Mo-93 is shown. Mo is weakly sorbing and a large fraction of the Mo-93 inventory is induced in the steel. The increased release of Ni-59 is moderate as Ni is more strongly sorbing and a large fraction of the inventory is surface contamination.

Table C-1. Surface and induced radionuclide inventory in 1BRT for key radionuclides.

Radionuclide	Surface (Bq)	Induced (Bq)	Total (Bq)
C-14-org	5.72×10^7	0.0	5.72×10^7
C-14-ind	0.0	1.33×10^{10}	1.33×10^{10}
Cl-36	2.83×10^5	7.1×10^6	7.38×10^6
Ni-59	1.19×10^{11}	5.94×10^{10}	1.78×10^{11}
Ni-63	1.1×10^{13}	4.16×10^{12}	1.52×10^{13}
Nb-93m	9.76×10^{11}	8.99×10^{10}	1.07×10^{12}
Mo-93	3.51×10^8	2.75×10^9	3.1×10^9
Ag-108m	4.81×10^9	0.0	4.81×10^9

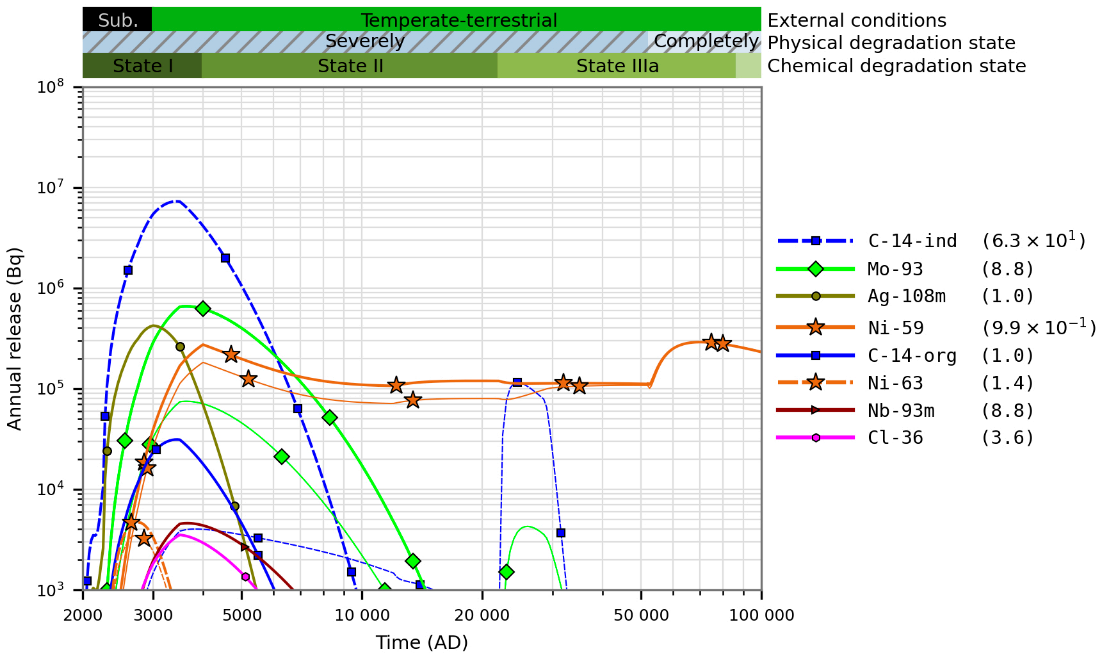

Figure C-34. *Comparison of the releases of radionuclides from 1BRT for instant release of induced activity (thick lines) and for the base case (thin lines). The values in parentheses show the ratio between the maximum release in the present case and the base case.*

C11 Solubility limited release

This calculation case investigates the effect of solubility limited release from the BLA vaults. As the relatively high amounts of U-238 and U-235 in these vaults can be expected to be subject to solubility limitations. Precise solubility limits have not been determined instead an illustrative calculation has been made with an arbitrarily low but reasonable solubility limit for uranium 9.5×10^{-7} mol m^{-3} (SKB TR-10-50). The calculations are performed as described in Section 2.4.

As can be seen in Figure C-35 the releases of U-235 and U-238 becomes insignificant with solubility represented, while releases of their decay products last throughout the whole simulation. It should be noted that, if solubility is taken into account, ingrowth of radiotoxic decay products may lead to high doses from intrusion wells at later time points (**FHA report**). However, the dose contribution from decay products of uranium will not exceed that from radionuclides in the initial inventory as shown in Figure C-36.

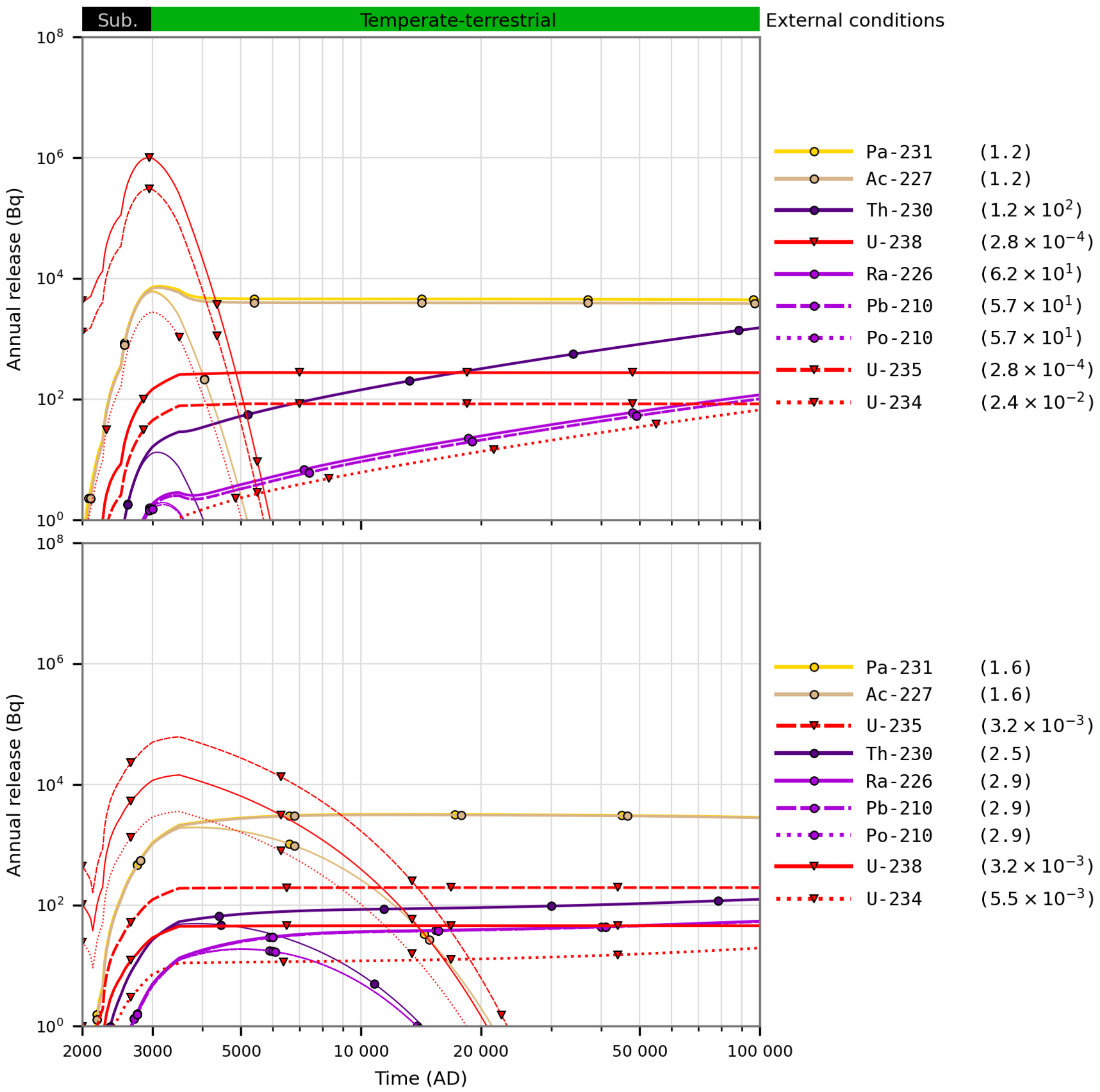

***Figure C-35.** Comparison of releases from 1BLA (upper) and 2BLA (lower) with solubility limits (thick lines) and for the base case (thin lines). Only U-238 and U-235 with their decay products are shown.*

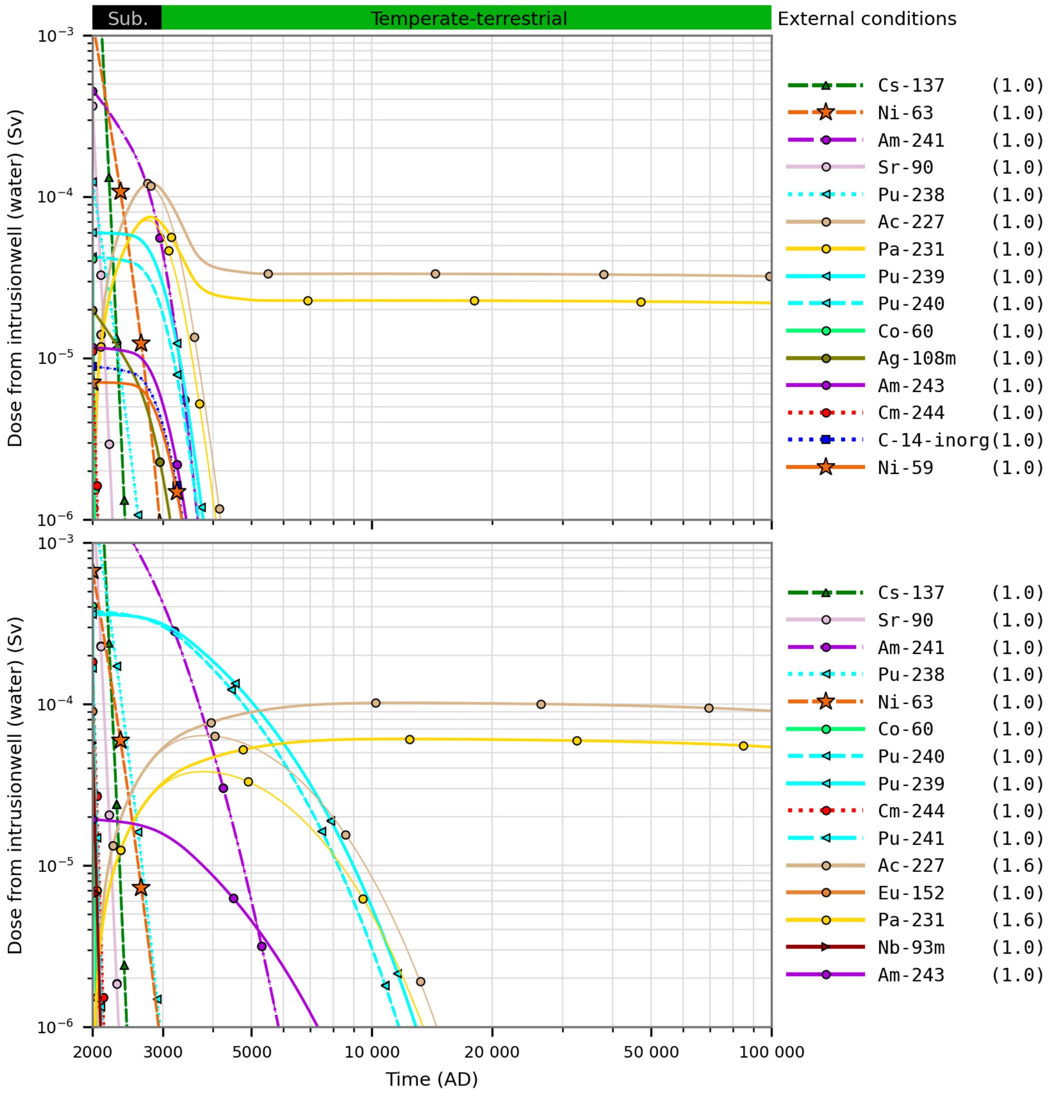

Figure C-36. *Comparison of hypothetical doses from ingestion of water from 1BLA (upper) and 2BLA (lower) with solubility limits (thick lines) and for the base case (thin lines).*

C12 Simplified models

Simplified versions of 1BMA, 2BMA and the silo models are implemented for comparison with and verification of the assessment models (these more detailed models are used in all other calculations). The character of the barriers and the expected relative importance of the other waste vaults (1BRT, 1–2BTF and 1–5BLA) implies that it is sufficient to carry out the assessment calculations with rather simple models as is already done in the assessment models, hence no simplified variant of these models has been considered.

The simplified models are implemented with only one compartment for the waste domain, i.e., the whole waste domain is modelled as a stirred tank as shown in Figure C-37. The simplified versions of the BMA models are implemented as one-dimensional models with one compartment each for the waste domain, concrete barrier and backfill. The total water flow through the waste domain and the total vault flow are used to assess the flow from waste to crushed rock and from crushed rock to bed-rock, respectively. The simplified silo model has compartments in two directions (radially and axially).

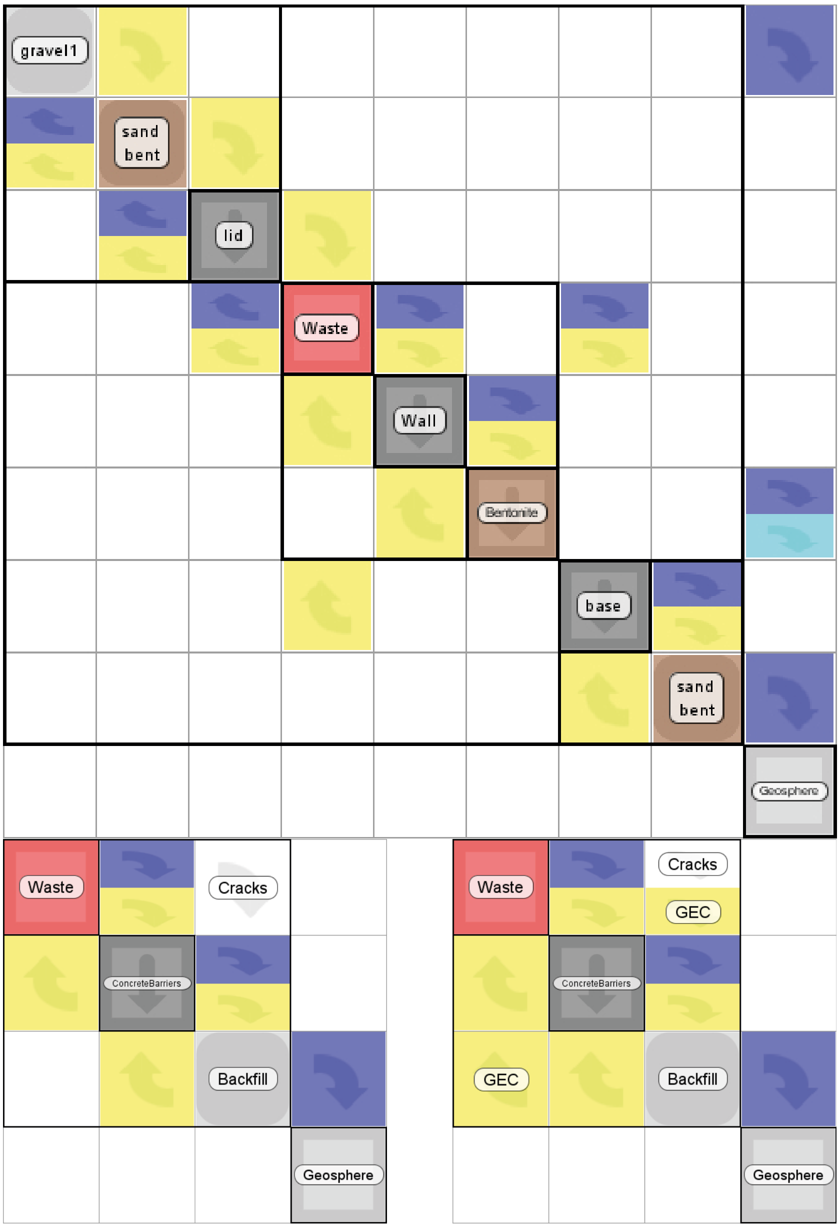

***Figure C-37.** Simplified models of the silo (top), 1BMA (lower left) and 2BMA (lower right). The yellow and blue arrows represent diffusion and advection, the cyan arrow represents Qeq (silo) and the white arrows represent flow through cracks in the concrete barriers (1BMA and 2BMA). Note also the diffusive transfer through the gas evacuation channels (GEC) in 2BMA.*

As can be seen in Figure C-38 the difference in releases between the simplified silo model and the assessment model are small for significant radionuclides.

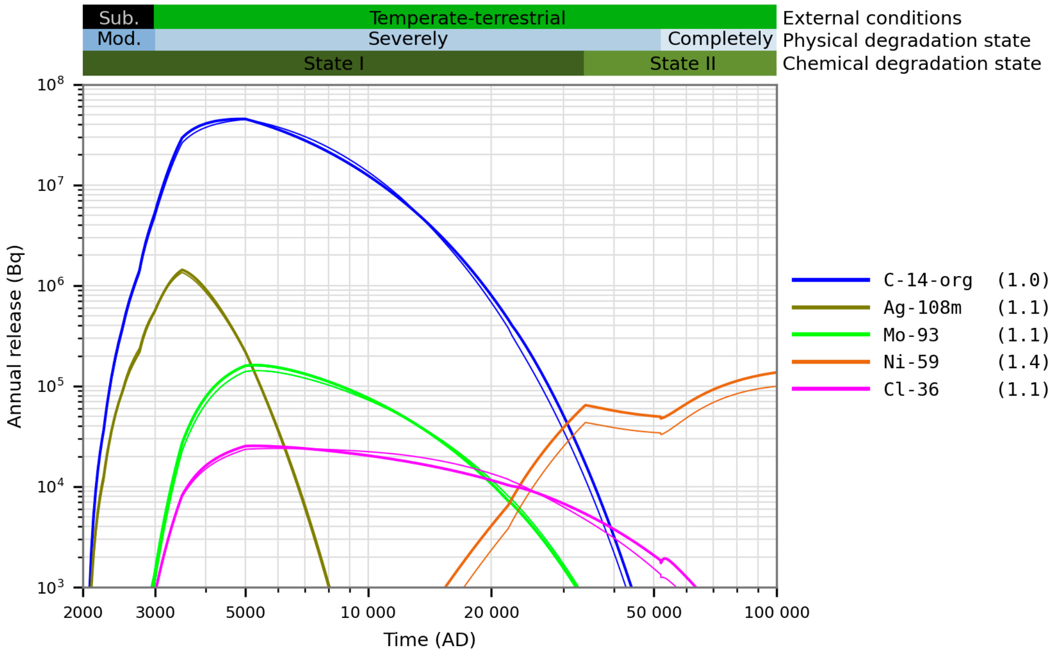

Figure C-38. *Comparison of releases calculated with the simplified silo model (thick lines) and the assessment model (thin lines)). The values in parentheses show the ratio between the maximum releases from the simplified model and the assessment model.*

Figure C-39 shows a comparison of radionuclide release from the simplified 1BMA model and the assessment model. The simplified model shows a larger early release of mobile radionuclides e.g. C-14-org, Ag-108m and Mo-93. For sorbing radionuclides e.g. C-14-inorg and Tc-99 early releases are lower and late releases are higher. This is likely due to the coarser discretisation of the simple model, i.e., different sections of 1BMA are not modelled separately. Some of the sections have little cement content, whereas other sections have more, thus the releases of sorbing radionuclides occur at very different rates. This phenomenon is not captured by the simple model where all waste is represented by one compartment.

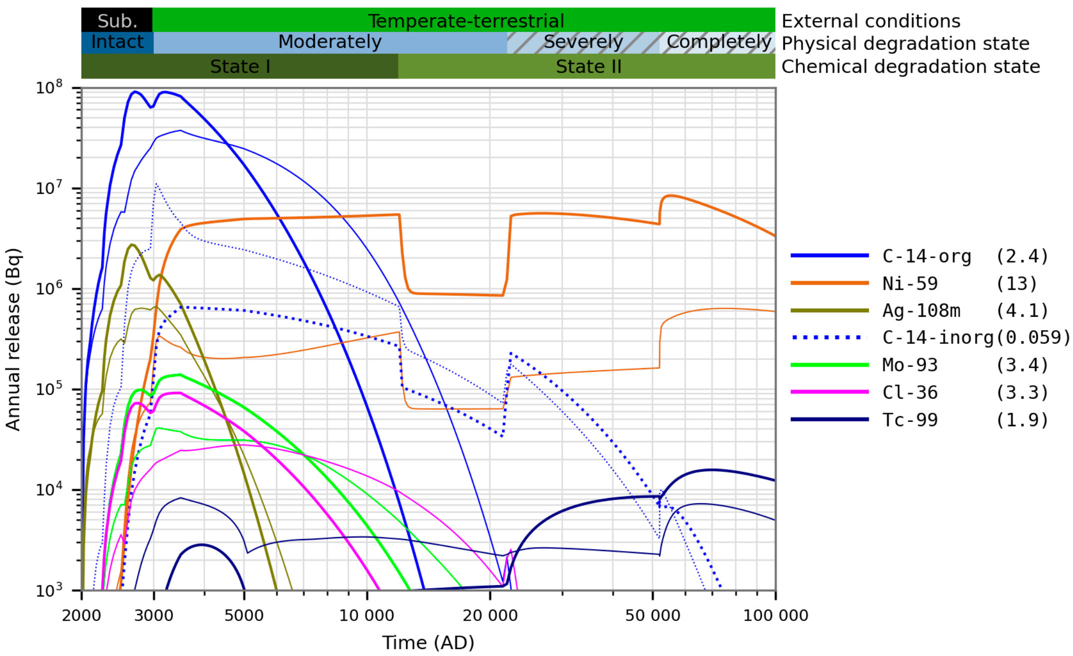

Figure C-39. *Comparison of releases calculated with the simplified 1BMA model (thick lines) and the assessment model (thin lines). The values in parentheses show the ratio between the maximum releases from the simplified model and the assessment model.*

Figure C-40 shows a comparison of radionuclide release from the simplified 2BMA model and the assessment model. The simplified 2BMA model represents the assessment model better (than the corresponding models for 1BMA), this can be expected as all the caissons in the 2BMA vault are identical. The tendency for higher initial releases can be partly explained by the omission of waste packaging in the simple model. Further, the representation as a one-dimensional model gives a higher release as no storage capacity beside the flow path is considered.

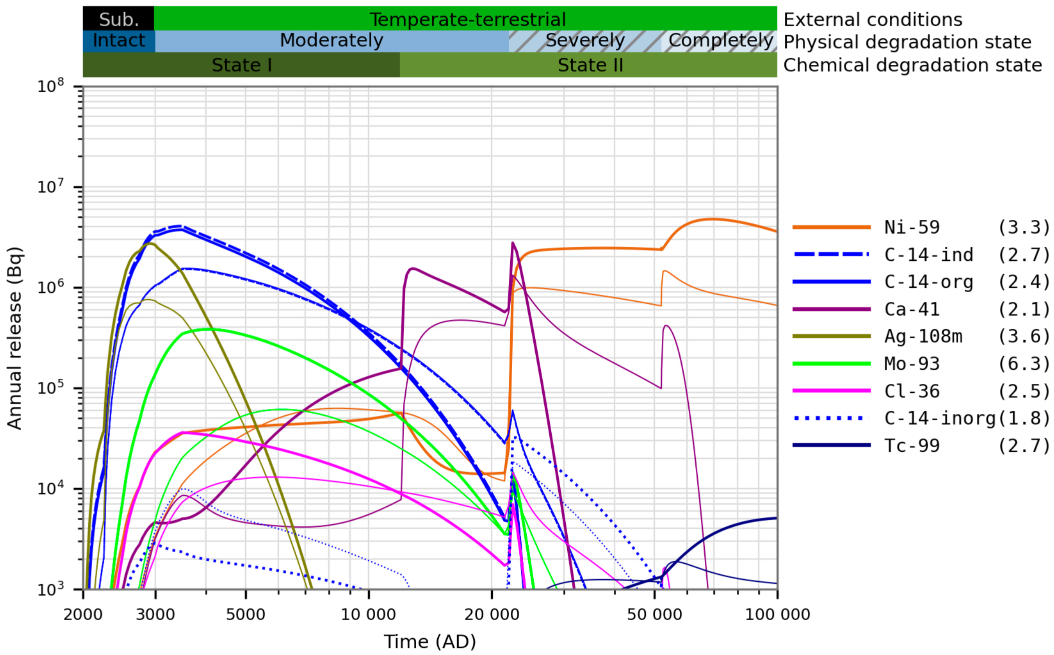

Figure C-40. *Comparison of releases calculated with the simplified 2BMA model (thick lines) and the assessment model (thin lines). The values in parentheses show the ratio between the maximum releases from the simplified model and the assessment model.*

Appendix D

Comparison with SR-PSU

Updates to the near-field transport calculations in the PSAR compared with SR-PSU involve both changes in input data and the modelling approach. The main updates and a comparison of results from the RNT models are discussed in this appendix.

D1 Updates of data in the PSAR

D1.1 Radionuclide inventory

Figure D-1 shows the ratio between the updated radionuclide inventory used in the PSAR and the inventory used in SR-PSU (for a selection of radionuclides with significant releases).

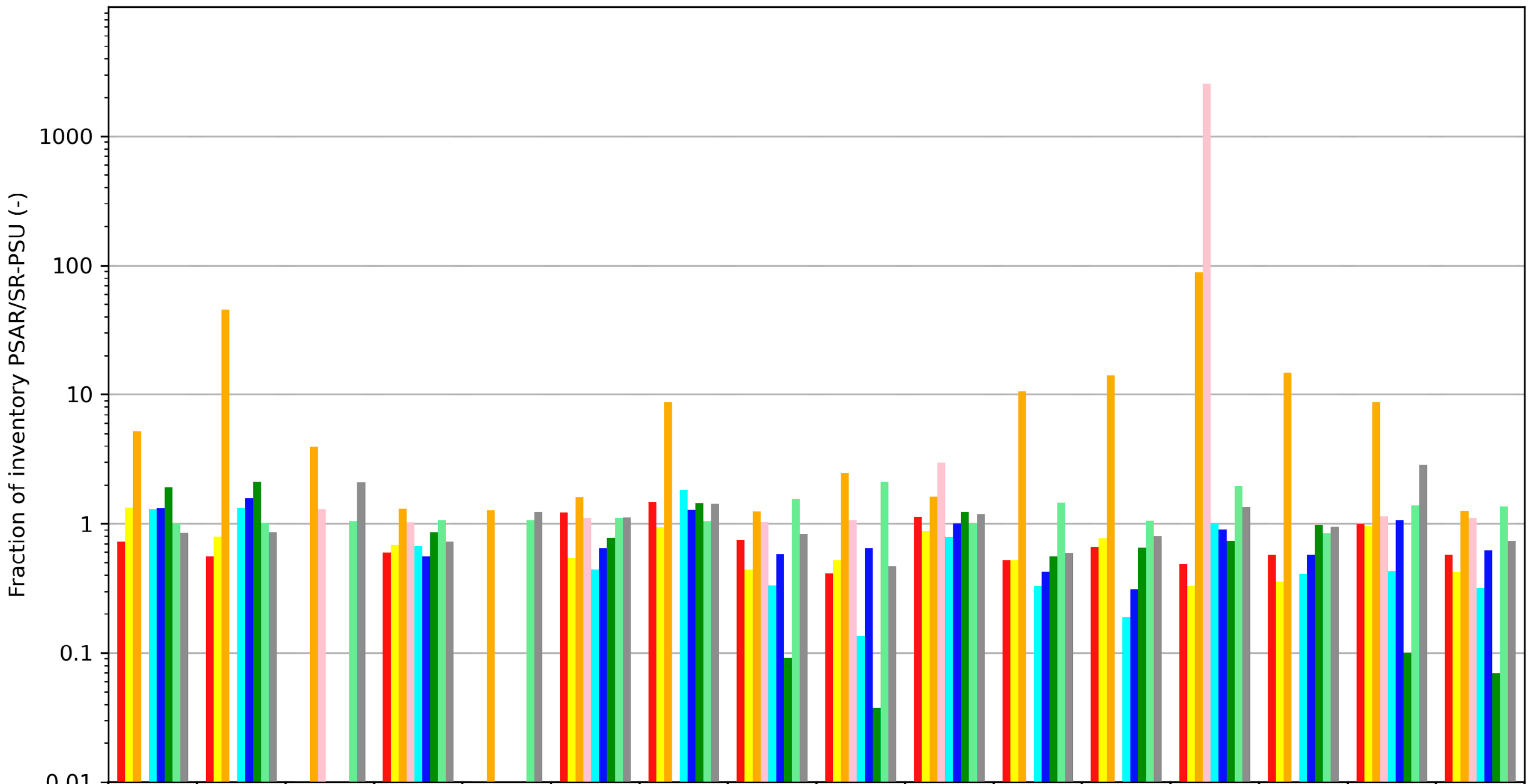

	C-14-org	C-14-inorg	C-14-ind	Cl-36	Ca-41	Ni-59	Se-79	Mo-93	Tc-99	Ag-108m	I-129	Cs-135	U-235	U-238	Pu-239	Pu-240
Silo	0.724	0.56	nan	0.595	nan	1.22	1.47	0.752	0.409	1.13	0.524	0.659	0.487	0.572	0.997	0.571
1BMA	1.34	0.795	nan	0.683	nan	0.541	0.943	0.44	0.523	0.872	0.521	0.776	0.328	0.356	0.955	0.421
2BMA	5.2	45.6	3.91	1.31	1.27	1.61	8.73	1.24	2.46	1.63	10.7	14.0	88.5	14.6	8.74	1.26
1BRT	inf	inf	1.3	1.02	nan	1.11	nan	1.03	1.07	2.97	nan	nan	2.55e+03	inf	1.14	1.11
1BTF	1.3	1.32	nan	0.67	nan	0.444	1.81	0.332	0.135	0.788	0.328	0.189	1.0	0.405	0.431	0.317
2BTF	1.33	1.58	nan	0.558	nan	0.646	1.27	0.58	0.646	1.0	0.427	0.312	0.904	0.575	1.06	0.623
1BLA	1.93	2.1	nan	0.856	nan	0.779	1.44	0.0913	0.0376	1.23	0.558	0.652	0.731	0.977	0.1	0.0697
2-5BLA	0.998	1.01	1.04	1.06	1.06	1.11	1.04	1.55	2.1	1.02	1.45	1.05	1.96	0.837	1.38	1.36
Total SFR	0.852	0.858	2.09	0.726	1.23	1.12	1.42	0.836	0.466	1.19	0.589	0.804	1.35	0.95	2.86	0.73

Figure D-1. *Ratio between radionuclide inventory in the PSAR and SR-PSU.*

D1.2 Updates in design

The evaluation in SR-PSU was done assuming grouting in both 1BMA and 2BMA. In the updated design for the PSAR both 1BMA and 2BMA are assumed to be left without grouting. The lid and side walls of 1BMA are assumed to be enhanced with an extra layer of cast concrete. In 2BMA several interior shaft walls are assumed to be risen inside the caissons (**Initial state report**, Chapters 5 and 6).

In SR-PSU the assumption was that whole BWR pressure vessels were to be placed in 1BRT. In the PSAR the pressure vessels are assumed to be cut into segments, placed in double moulds and stabilised with concrete (**Initial state report**, Chapter 7) and in addition three reactor-tank lids are assumed to be placed in 1BRT.

D1.3 Updates in water flow data

Higher early water flow was assumed in SR-PSU (due to interpolation between the very low water flow at 2000 AD and a significantly higher water flow at 3000 AD). The near-field hydrological calculations are made at 2000, 2500, 3500 and 5000 AD, in SR-PSU calculations were made at 2000, 3000 and 5000 AD, which results in a less steep increase in early water flow during shore line regression for the PSAR. In addition to this extra interpolation points are included based on the geosphere hydrological calculations as described in the **Radionuclide transport report.**

Figure D-2 to Figure D-5 show a comparison of water flow calculated in the PSAR and SR-PSU for different times and degradation states of the concrete (Abarca et al. 2013, 2014, 2020).

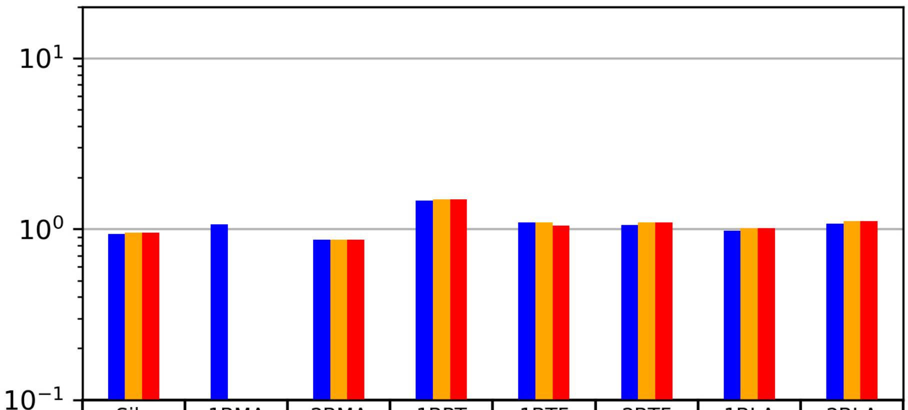

	Silo	1BMA	2BMA	1BRT	1BTF	2BTF	1BLA	2BLA
MD	0.935	1.06	0.867	1.47	1.1	1.06	0.977	1.07
SD	0.952	N/A	0.867	1.49	1.1	1.1	1.01	1.11
CD	0.953	N/A	0.867	1.49	1.05	1.09	1.01	1.11

Figure D-2. *Comparison (PSAR/SR-PSU) of water flow through vaults at 2000 AD based on data from Abarca et al. (2013, 2014, 2020). The row headers in the table at the bottom denotes; moderately degraded concrete (MD), severely degraded concrete (SD) and completely degraded concrete (CD).*

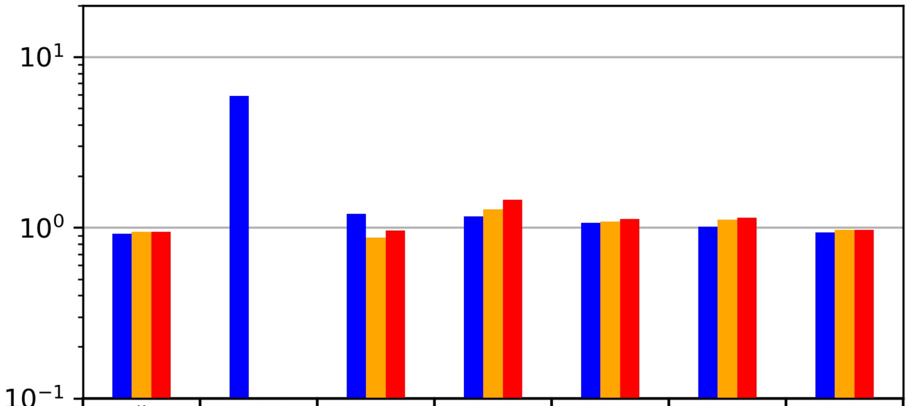

	Silo	1BMA	2BMA	1BRT	1BTF	2BTF	1BLA
MD	0.92	5.88	1.2	1.16	1.06	1.01	0.938
SD	0.942	N/A	0.874	1.28	1.08	1.11	0.969
CD	0.942	N/A	0.96	1.45	1.12	1.15	0.969

Figure D-3. *Comparison (PSAR/SR-PSU) of water flow through waste at 2000 AD based on data from Abarca et al. (2013, 2014, 2020). The row headers in the table at the bottom denotes; moderately degraded concrete (MD), severely degraded concrete (SD) and completely degraded concrete (CD). (Note that vault flow and waste flow are identical for 2BLA and thus not presented in this table).*

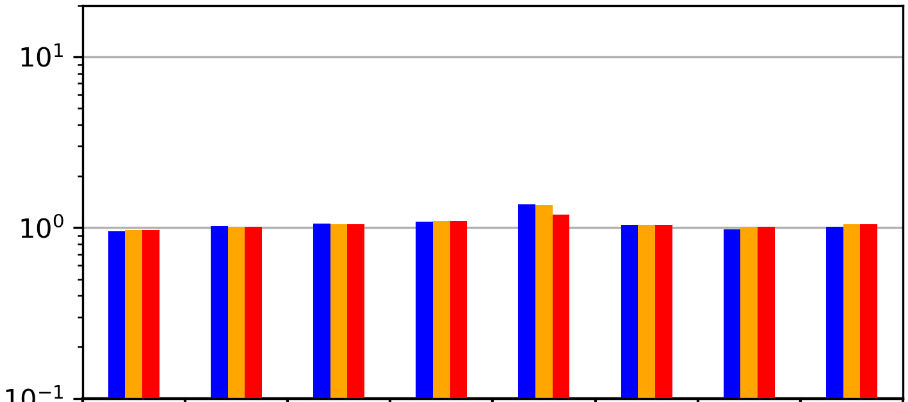

	Silo	1BMA	2BMA	1BRT	1BTF	2BTF	1BLA	2BLA
MD	0.956	1.02	1.05	1.09	1.38	1.04	0.973	1.02
SD	0.972	1.01	1.05	1.09	1.36	1.04	1.01	1.05
CD	0.972	1.01	1.05	1.1	1.19	1.04	1.01	1.05

Figure D-4. *Comparison (PSAR/SR-PSU) of water flow through vaults at 5000 AD based on data from Abarca et al. (2013, 2014, 2020). The row headers in the table at the bottom denotes; moderately degraded concrete (MD), severely degraded concrete (SD) and completely degraded concrete (CD).*

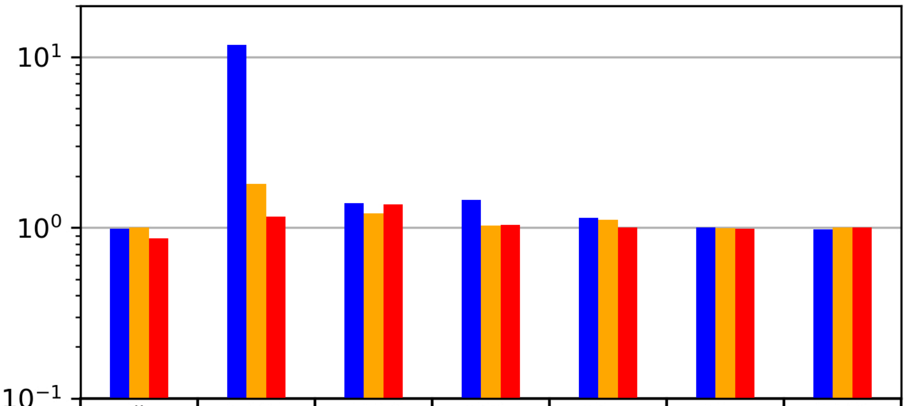

	Silo	1BMA	2BMA	1BRT	1BTF	2BTF	1BLA
MD	0.983	11.8	1.4	1.45	1.14	1.0	0.981
SD	1.0	1.8	1.21	1.03	1.12	0.992	1.0
CD	0.869	1.16	1.36	1.04	1.0	0.983	1.0

Figure D-5. *Comparison (PSAR/SR-PSU) of water flow through waste at 5000 AD based on data from Abarca et al. (2013, 2014, 2020). The row headers in the table at the bottom denotes; moderately degraded concrete (MD), severely degraded concrete (SD) and completely degraded concrete (CD). (Note that vault flow and waste flow are identical for 2BLA and thus not presented in this table).*

D1.4 Updates in sorption data

Figure D-6 shows the ratio between K_d values used in the PSAR (**Data report**) and SR-PSU (SKB TR-14-10). Missing in the figure are Ag, Se, C-ind and H that are considered non sorbing in both the PSAR and SR-PSU. C-14-org was considered non sorbing in SR-PSU but has a small K_d (1×10^{-5} m^3 kg^{-1}) in the PSAR. Mo is considered non sorbing for degradation state IIIb. It should be noted that the change in K_d for U is because in the PSAR it has been assumed that U is present in oxidation state (IV) whereas in SR-PSU it was assumed to be present in oxidation state (VI); this update is based on resent research presented in Bruno et al. (2018). In addition to the K_d values the sorption reduction factors have been updated, these are specific to each vault and discussed in Sections D2 to D6. Furthermore, the transition from chemical degradation state I to state II has been set to 12 000 AD is the PSAR while in SR-PSU this transition was set to occur at 7000 AD (**Post-closure safety report**, Chapter 6).

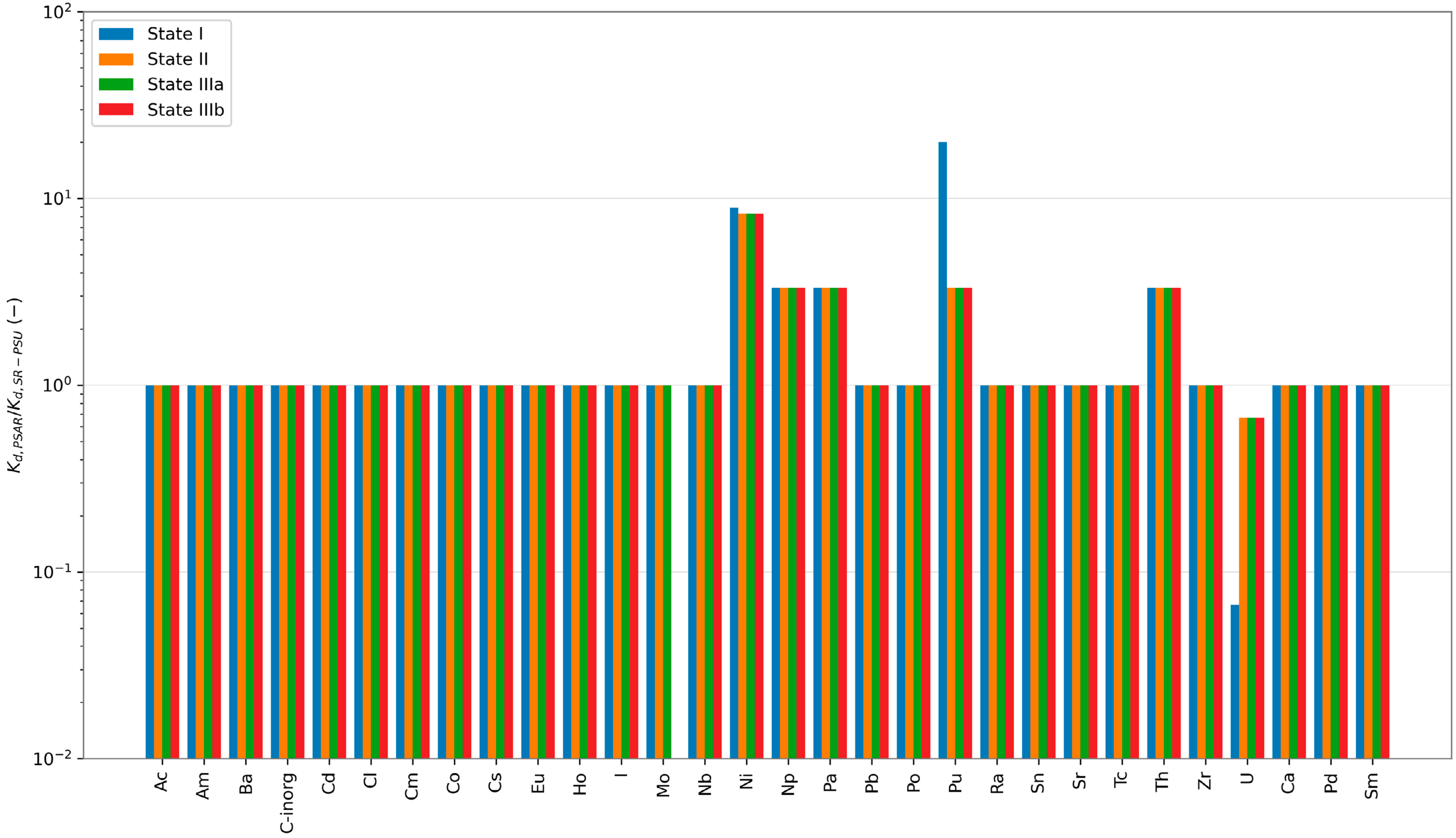

Figure D-6. *Comparison of K_d values used in the PSAR/SR-PSU.*

D2 The silo model

The discretisation of the RNT model for the silo is simplified in the PSAR compared with SR-PSU (SKB TR-14-09), this can be expected to affect the strongly sorbing radionuclides to a larger extent than the non or weakly sorbing radionuclides. However, the silo has only insignificant releases of strongly sorbing radionuclides. Hence, small differences can be expected due to the simplification of the model.

With an exception for Ni-59 the calculated releases in the PSAR agree well with those in SR-PSU, for significant radionuclides, as can be seen in Figure D-7. The large difference for Ni-59 can be explained by the higher K_d for nickel used in the PSAR (see Figure D-6).

A number of radionuclides also have a lower initial inventory in the PSAR e.g. C-14-org and Mo-93 (Figure D-1), which partly explains the decrease in releases for these radionuclides.

Higher early water flow was assumed in SR-PSU (due to interpolation as explained in Section D1.3). This affects the early releases of e.g. C-14-org, Ag-108m, Mo-93 and Se-79.

The calculated water flows through the silo are very similar in the PSAR and SR-PSU (Section D1.3), thus no significant differences in radionuclide release are due to this. However, the updated approach to handling of the uncertainties of water flow includes a scaling of the silo water flow rates in the PSAR with the scaling factors shown in Table 4-1. The scaling factor of about 0.7 (from 2750 AD and later) contributes to the general trend for lower releases in the PSAR.

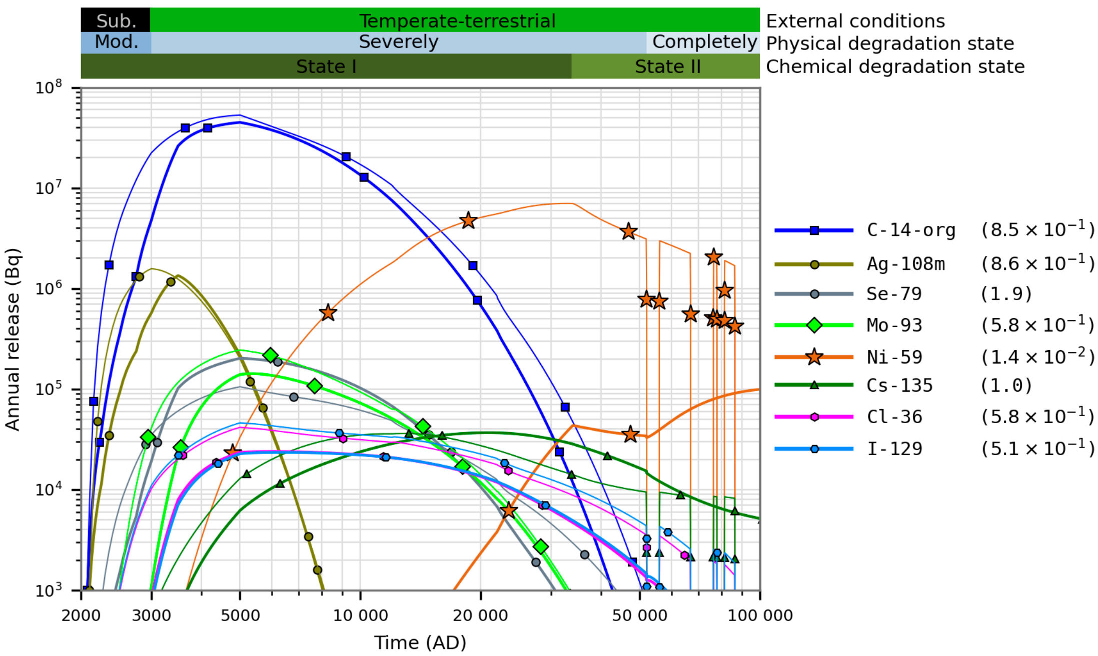

Figure D-7. *Releases from the silo calculated in the PSAR (thick lines) and SR-PSU (thin lines). The values in parentheses show the ratio between the maximum release in the PSAR and SR-PSU. The colour bars refer to the PSAR calculation, in the SR-PSU calculation moderately degraded concrete was assumed only up to 2500 AD.*

D3 The 1BMA model

The releases of several radionuclides differ significantly between the PSAR and SR-PSU (SKB TR-14-09) calculations (Figure D-8). As for the silo the large difference for Ni-59 can be explained by the larger K_d value for Nickel used for cementitious materials in the PSAR assessment (see Figure D-6). In addition, the characteristic decrease in Ni-59 (at 7000 AD) in the SR-PSU model has been shifted to 12 000 AD in the PSAR model as the estimated shift in chemical degradation state of the cementitious materials has been set to this later time point in the PSAR.

Early releases of e.g. C-14-org and Mo-93 are affected in 1BMA by the added time points in the interpolation of water flow rates as described in Section D1.3. Early release of sorbing radionuclides e.g. Cs-137 is more affected by the higher diffusive resistance due to the assumed intact concrete during the first 1 000 years in the PSAR and thus releases are lower.

A significantly lower release of Tc-99, for later time points can be seen due to the lower sorption reduction factors. In SR-PSU the SRF for Tc was constant over the whole simulation period (Keith Roach et al. 2014) whereas in the PSAR the SRF for Tc (Group 3) has a time-dependent value specific to each section in the 1BMA model shown in Table 7-6. The effect of the time dependent SRF (highest at the start) can be seen on the release of Tc-99, which has a peak release at about 4000 AD in the PSAR calculation.

There is a significant increase in the release of the highly sorbing radionuclide C-14-inorg in the PSAR. This is likely to be ascribed to the lack of grouting (sorbing material) in the waste domain and the initial presence of cracks in the concrete bottom plate in the PSAR model. This is of particular importance to the large fraction (ca 63 % Figure 7-5) of C-14-inorg in 1BMA that is conditioned with bitumen, as bitumenised wastes are assumed to provide no sorption.

The calculated water flow through the waste domain differs significantly (tenfold higher in the PSAR) between the SR-PSU and the PSAR for moderately degraded concrete during the inland period (Figure D-5), in addition to this an uncertainty factor of 1.27 is applied to the 1BMA water flow during the inland period in the PSAR (Table 4-1). This may contribute to the higher release of C-14-org in the period 5000 AD to 20 000 AD. However, during this period also diffusion contributes significantly to the release. The inventory of C-14-org is also slightly higher in the PSAR calculation (Figure D-1).

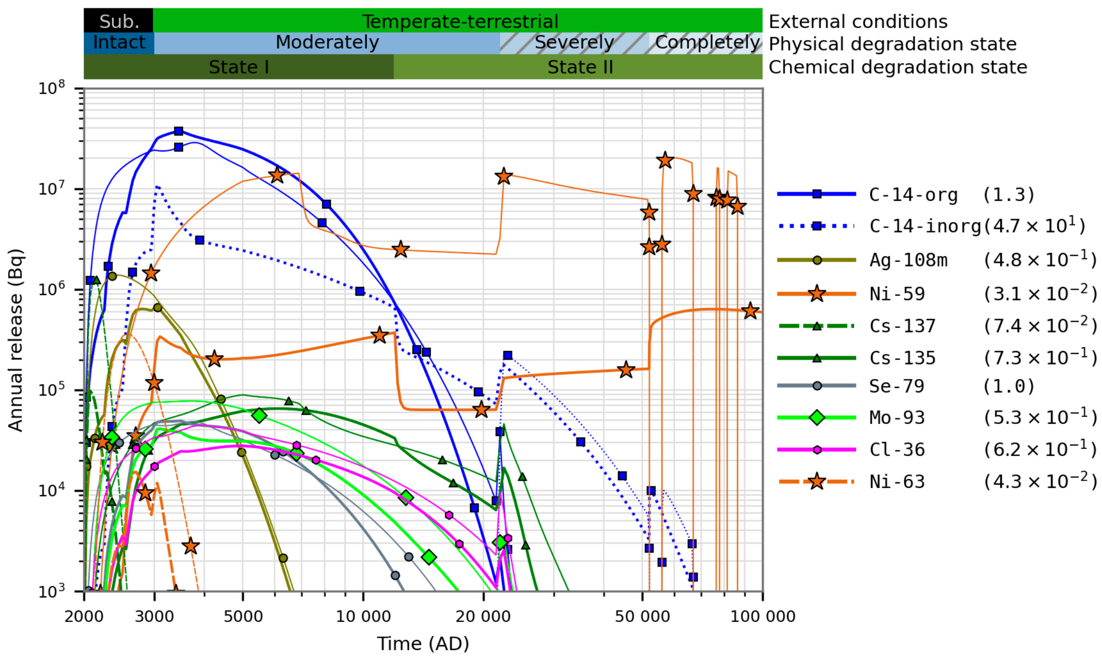

Figure D-8. *Releases from 1BMA calculated in the PSAR (thick lines) and SR-PSU (thin lines). The colour bars in the upper part of the figure show the evolution of the external conditions and of the concrete physical and chemical degradation, respectively. The colour bars refer to the PSAR calculation, in the SR-PSU calculation moderately degraded concrete was assumed already from the beginning and the transition from chemical degradation state I to state II occurred at 7000 AD.*

A small K_d (1×10^{-5} m^3 kg^{-1}) is assumed for C-14-org in the PSAR. However, this has a minor counter-acting effect compared with the higher water flow.

D4 The 2BMA model

The release of several radionuclides differs significantly between the 2BMA calculations in the PSAR and SR-PSU (Figure D-9). As for the silo and 1BMA the large difference in nickel release can be explained by the larger K_d value for Nickel used in the PSAR (Figure D-6). The characteristic decrease in Ni-59 and increase in Ca-41 release (at 7000 AD) in the SR-PSU model has shifted to 12 000 AD in the PSAR model along with the estimated shift in the chemical degradation state of the cementitious materials.

The later onset of releases of Ag-108m and Mo-93 can be explained by the added time points in the interpolation of water flows as described in Section D1.3.

The increased releases of Cs-135 and C-14-inorg in the PSAR are mainly due to the increased inventory (Figure D-1). Also, C-14-org and C-14-ind have a significantly higher inventory in the PSAR. A trend for higher early releases of sorbing radionuclides (e.g. Ca-41, C-14-inorg and Ni-59) in the PSAR can be attributed to the gas evacuation channels introduced in the PSAR models.

The calculated water flow (at 5000 AD) through the 2BMA vault is slightly higher in the PSAR (Figure D-5) calculations, in addition to this an uncertainty factor of about 1.6 (Table 4-1) during the inland period has been applied. However, diffusion is the dominating transport mechanism until 22 000 AD.

Palladium (Pd-107) is affected by sorption reduction factors. The SRF with value 100 (-) (Keith-Roach et al. 2014, 2021). applied in SR-PSU has not been applied in the PSAR and hence the releases of Pd-107 are significantly lower in the PSAR.

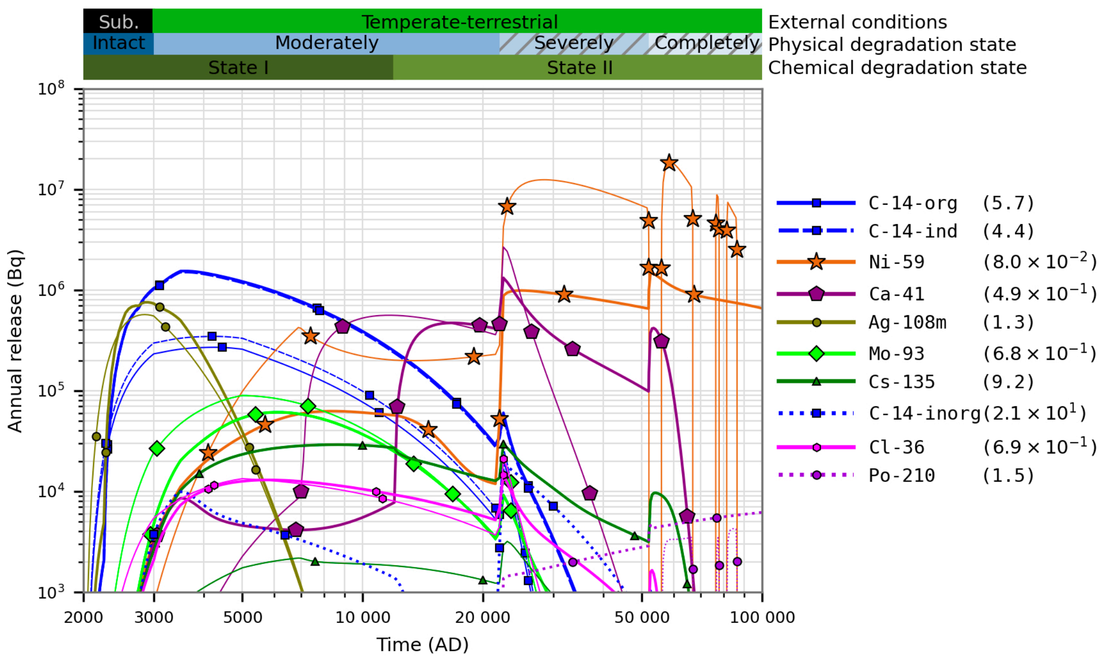

Figure D-9. *Releases from 2BMA calculated in the PSAR (thick lines) and SR-PSU (thin lines). The colour bars in the upper part of the figure show the evolution of the external conditions and of the concrete physical and chemical degradation, respectively. The colour bars refer to the PSAR calculation, in the SR-PSU calculation moderately degraded concrete was assumed already from the beginning and the transition from chemical degradation state I to state II occurred at 7000 AD.*

Further, the discretisation of the 2BMA model has been updated to represent radionuclide transport in three dimensions in the PSAR, while the 2BMA model used in SR-PSU had a simplified representation as a one-dimensional model, this explains the higher release at later time points (notable for Ca-41) as storage capacity beside the flow path is considered more inventory remains at later time points and the peak release of Ca-41 is lower.

D5 The 1BRT model

In Figure D-10 a comparison of radionuclide releases calculated within the PSAR and SR-PSU is shown. As for silo and 1–2BMA the large difference for Ni-59 and Ni-63 releases can be explained by the larger K_d value used for nickel in the PSAR (Figure D-6). The release of C-14-org in the PSAR can be explained by the added inventory of this radionuclide (Figure D-1).

The later onset of releases of Ni-63, Ag-108m and Mo-93 can be explained by the added time points in the interpolation of water flow rates as described in Section D1.3.

The release of C-14-ind is controlled entirely by the corrosion rate which is lower during the initial period and higher during the later period in the PSAR compared with SR-PSU (Table D-1). C-14-org can only be seen in the PSAR results as this radionuclide was not present in the SR-PSU inventory (Figure D-1).

The calculated water flow (at 5000 AD) through the 1BRT vault is slightly higher in the PSAR (Figure D-4) calculations, the uncertainty factor of about 0.9 (Table 4-1) during the inland period cancels this out and thus there should be no significant effect of changes in water flow.

Table D-1. Corrosion related parameters in SR-PSU and the PSAR.

	Assumed thickness of steel waste (m)	Time of start of corrosion rate 2 (AD)	Corrosion rate 1 ($m\ a^{-1}$)	Corrosion rate 2 ($m\ a^{-1}$)
SR-PSU	0.14	22000	5.0×10^{-8}	2.8×10^{-6}
PSAR	0.134	22000	2.5×10^{-8}	1.0×10^{-5}

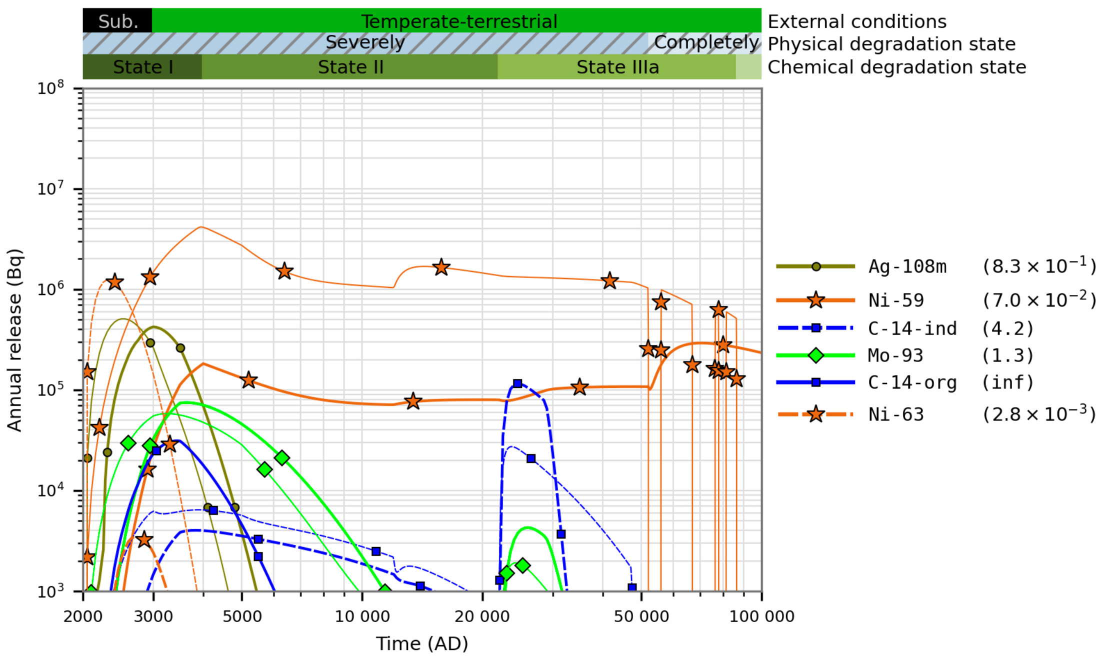

__Figure D-10.__ Releases from 1BRT calculated in the PSAR (thick lines) and SR-PSU (thin lines). The colour bars refer to the PSAR calculation, in the SR-PSU calculation completely degraded concrete was assumed already from 12 000 AD.

D6 The BTF models

Figure D-11 shows a comparison of radionuclide releases calculated with the PSAR 1–2BTF models and the SR-PSU models. As for the silo and 1–2BMA the large difference in nickel release can be explained by the larger K_d value for nickel used in the PSAR assessment (Figure D-6). The later onset of releases of C-14-org, Ag-108m and Mo-93 can be explained by the added time points in the interpolation of water flow rates as described in Section D1.3. The much larger and earlier release of Tc-99 (2BTF) in the PSAR can be explained by the much larger SRF used for Tc (SRF Group3) in the PSAR. In SR-PSU the SRF used was 100 (-) whereas the SRF used in the PSAR is 6 673 (-) (Keith-Roach et al. 2014, 2021).

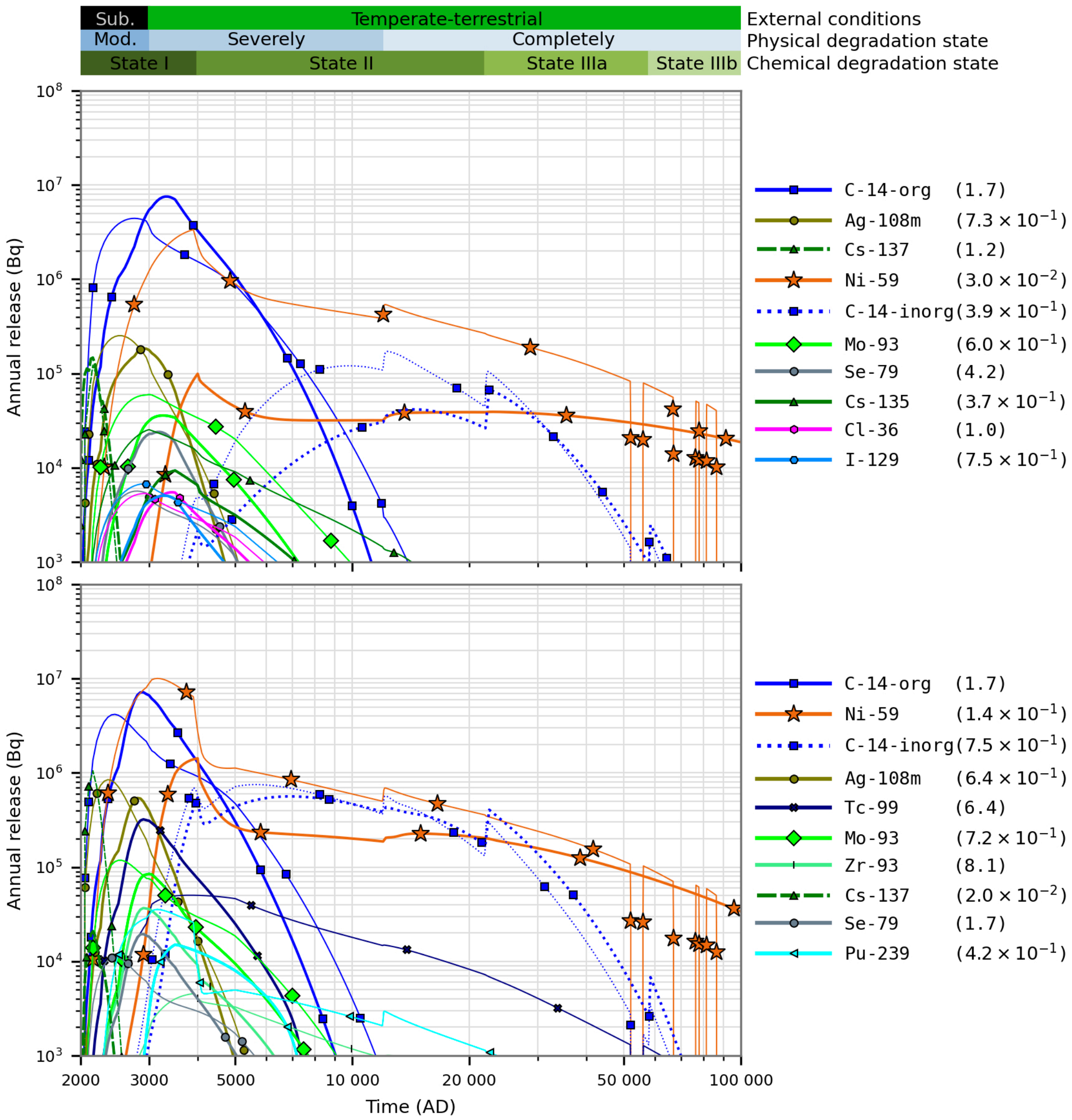

Figure D-11. Releases from 1BTF (upper panel) and 2BTF (lower panel) calculated with the PSAR model (thick lines) and the SR-PSU model (thin lines).

D7 The BLA models

Figure D-12 shows a comparison of releases from 1BLA (upper panel) and 2BLA (bottom panel) calculated within the PSAR and SR-PSU. The main differences from SR-PSU can be explained by the added time points in the interpolation of water flow rates as described in Section D1.3. In addition, for Tc-99 and Mo-93 a significantly lower inventory is assumed for 1BLA in the PSAR (Figure D-1), for 2BLA a notable higher inventory is assumed for Tc-99, U-234 and U-235 in the PSAR.

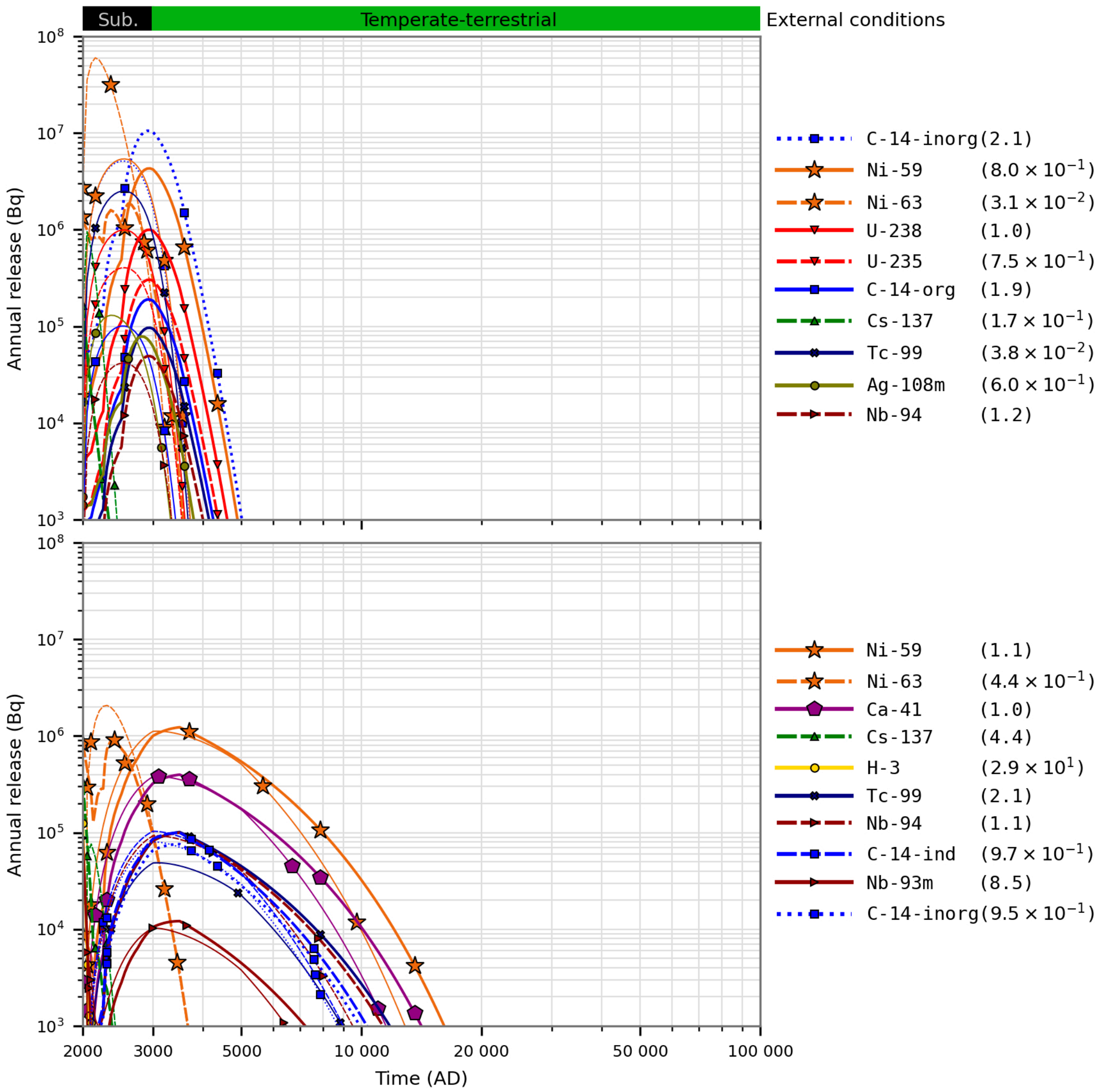

Figure D-12. *Releases from 1BLA (upper panel) and 2BLA (lower panel) calculated with the PSAR model (thick lines) and the SR-PSU model (thin lines).*

Arkitektkopia AB, Bromma, 2022

SKB is responsible for managing spent nuclear fuel and radioactive waste produced by the Swedish nuclear power plants such that man and the environment are protected in the near and distant future.

skb.se